# On the in-situ manufacture of thermoplastic sandwich structures with continuous fibre reinforced facesheets and integral foam cores

Zur In-Situ Herstellung thermoplastischer Sandwichstrukturen mit endlosfaserverstärkten Decklagen und Integralschaumkernen

Dissertation

zur Erlangung des Doktorgrades

der Ingenieurwissenschaften

vorgelegt von

**Felix Christian Weidmann**

aus Weinheim

genehmigt von der

Fakultät für Natur- und Materialwissenschaften

der Technischen Universität Clausthal

Tag der mündlichen Prüfung

16.12.2019

**Dekan**
Prof. Dr.-Ing. Karl-Heinz Spitzer

**Vorsitzender der Promotionskommission**
Prof. Dr.-Ing. Heinz Palkowski

**Betreuer**
Prof. Dr.-Ing. Gerhard Ziegmann

**Gutachter**
Prof. Dr.-Ing. Jürgen Wieser

# Abstract

Novel hybrid processes for the manufacture of continuous fibre reinforced thermoplastic (CFRTP) components have been emerging, due to increasing requirements regarding cost-efficient lightweight design especially in the automotive sector. A promising example is the in-situ CFRTP sandwich process, which combines overmoulding of thermoplastic composites with foam injection moulding. This hybrid process enables function-integrated components with high weight specific mechanical properties and complex geometry at low cycle times. However, methods for the pre-design of in-situ CFRTP sandwich components are required for the application of this process in industrial component manufacture. Therefore, several challenges must be met especially with respect to the critical aspect of interfacial bonding between CFRTP facesheets and injection moulded core as well as to the resulting weight specific mechanical behaviour depending on the material and process parameters.

In this context, the present work aims to clarify the mechanisms behind the interfacial bonding development during the in-situ manufacture of CFRTP sandwich specimens. Furthermore, the relationship between process as well as material parameters and the resulting weight specific flexural behaviour of sandwich components is evaluated. This shall lay the foundation for the development of methods, which enable the mechanical modelling of in-situ CFRTP sandwich structures and thereby facilitate the pre-design of new components.

For the quantitative evaluation of the interfacial bonding of in-situ CFRTP sandwich structures, suitable test methods need to be established at first. Subsequently, experimental campaigns are conducted in order to evaluate the mechanisms responsible for the development of interfacial bonding during the in-situ process. Therefore, polypropylene-based in-situ CFRTP sandwich specimens are manufactured and subsequently object of mechanical testing and analysis. After focusing on an investigation of the polymer specific bonding mechanisms, the effect of chemical and physical blowing agents on the interfacial bonding of facesheet and core is determined.

In addition, the inherent lightweight design potential of in-situ CFRTP sandwich structures is evaluated, represented by the weight specific flexural rigidity. For this purpose, the foam morphology that is induced by material and process parameters as well as the corresponding weight specific flexural properties of sandwich specimens are assessed via micro computer tomography and four-point bending tests respectively.

Based on these studies, model based predictive characterisations of the interfacial bonding as well as of the weight specific flexural behaviour of in-situ CFRTP sandwich structures are developed and evaluated using experimental data.

In order to demonstrate the applicability of the developed models in the pre-design of in-situ sandwich components, they are used for the substitution of a steel reference component. This shall further highlight the promising potential regarding cost-efficient lightweight design of in-situ CFRTP sandwich structures.

# Glossaries

## Abbreviations

### General

| | |
|---|---|
| ASTM | American Society for Testing and Materials |
| BEV | battery electric vehicle |
| CC | cross composite |
| DIN | Deutsche Industrie Norm |
| EV | electrified vehicles |
| ICE | internal combustion engine |
| ISO | International Organization for Standardization |
| VDI | Verein Deutscher Ingenieure |
| UD | undirectional |
| VOC | volatile organic compounds |

### Symbols

| | |
|---|---|
| $\Delta$ | difference |
| $\mu$ | friction coefficient |
| $A$ | area |
| $A_i$ | area at solid-liquid interface |
| $a$ | crack length |
| $a_0$ | the initial uniform asperity height |
| $B_c$ | Hobbs specific width |
| $\chi$ | diffusion distance |
| $\chi_\infty$ | equilibrium diffusion distance |
| $C$ | gas concentration coefficient |
| $d$ | midspan deflection |
| $d/dt$ | time derivative |
| $d_0$ | initial uniform width |
| $D_b$ | degree of bonding |
| $D_{diff}$ | diffusion coefficient |
| $D_h$ | degree of healing |
| $D_{ic}$ | degree of intimate contact |
| $d\Pi$ | potential energy |
| $\delta$ | delta |
| $\delta$ | traverse stroke |
| $\delta$ | load deflection |
| $E$ | Young's modulus |
| $E_0$ | longitudinal tensile modulus of UD layer |
| $E_{90}$ | transversal tensile modulus of UD layer |
| $E_c$ | tensile modulus core |
| $E_{f,i}$ | tensile modulus of facesheet with spec. layup |
| $E_{f,II}$ | longitudinal tensile modulus |

| | |
|---|---|
| $E_{f\perp}$ | transversal tensile modulus |
| $E_H$ | Hobbs homogenised modulus |
| $F_a$ | alignment load |
| $F_p$ | applied load |
| $\bar{F}_p$ | mean applied load |
| $f_b$ | dimensionless fusion bonding number |
| $\eta$ | viscosity |
| $\eta_0$ | zero shear viscosity |
| $g$ | gravitational acceleration |
| $G$ | fracture toughness |
| $G'$ | storage modulus |
| $G''$ | dissipative modulus |
| $G_C$ | critical fracture toughness |
| $G_\infty$ | equilibrium fracture toughness |
| $G_{co}$ | cross-over modulus |
| $G_N^0$ | plateau modulus |
| $G_D$ | activation energy of diffusion |
| $G$ | free energy |
| $\Delta G_\eta$ | threshold energy for polymer chain transport |
| $\Delta \bar{G}_{*,2}$ | critical nucleation energy for secondary nucleation |
| $\Delta G_{hom}$ | free energy change during homogenous nucleation |
| $\gamma_i$ | tension at interface contact |
| $\Gamma$ | phase shift |
| $h$ | core height |
| $h_N$ | notch height |
| $H$ | total height |
| $\Delta H_m$ | polymer melt enthalpy |
| $\Delta H_{cr}^0$ | melt enthalpy of 100% crystalline material |
| $\Delta H_L$ | solution enthalpy |
| $I$ | second moment of inertia |
| $I(T)$ | temperature dependent growth rate |
| $I_0$ | growth rate factor |
| $I_H$ | Hobbs second moment of inertia |
| $k$ | Boltzmann constant |
| $\lambda$ | wavelength |
| $l$ | minor chain length |
| $L$ | polymer chain length |
| $L$ | total specimen length |
| $l$ | support span length |
| $l'$ | load span length |
| $LD$ | lightweight design |
| $m$ | mass |
| $m_{Gas}$ | mass of gas |
| $m_{polymer}$ | mass of polymer |
| $M$ | molecular weight |
| $M_c$ | critical molecular weight |
| $M_e$ | molecular weight of entanglement |

| | |
|---|---|
| $\Delta n$ | birefringence |
| $\Omega$ | parameter for of intimate contact or healing dominance evaluation |
| $\psi$ | mass fraction |
| $p_{app}$ | applied pressure |
| $p_c$ | critical pressure |
| $p_{in}$ | inner pressure |
| $r$ | radius |
| $R$ | ideal gas constant |
| $R^*$ | relative density parameter |
| $r_c$ | critical radius |
| $r_{cell}$ | cell radius |
| $\rho$ | density |
| $\rho_s$ | density of solid polymer |
| $S$ | solubility coefficient |
| $S_0$ | solubility extrapolated to an infinite temperature |
| $\sigma$ | stress |
| $\sigma_\infty$ | equilibrium strength |
| $T$ | temperature |
| $\dot{T}$ | cooling rate |
| $T_c$ | critical temperature |
| $t_f$ | final bonding time |
| $T_m$ | melt temperature |
| $T_{melt}$ | melting temperature |
| $t_p$ | process time |
| $t_R$ | reptation time |
| $t_s$ | thickness of solid foam core-skin |
| $T_w$ | mould temperature |
| $t_w$ | welding time |
| $\tau$ | shear stress |
| $\tau_{NLS}$ | notched lap shear strength |
| $\theta$ | tilt angle |
| $V$ | volume fraction total |
| $V_s$ | volume fraction of solid material |
| $v_a$ | specific volume fraction |
| $v_{diff}$ | diffusion velocity |
| $VOC$ | volatile organic compound |
| $vol.$ | volume |
| $\nu_{yx}$ | Poission's ratio |
| $W$ | width |
| $w_0$ | initial uniform distance between the asperities |
| $W_N$ | width of notch |
| $wt.$ | weight |
| $x$ | x-axis variable |
| $\xi$ | degree of crystallinity |
| $y$ | y-axis variable |
| $z$ | z-axis variable |

## Materials

| | |
|---|---|
| 1UD | UD tape layer |
| 2UD | two consolidated UD tape layers |
| aPP | atactic polypropylene |
| AS4 | HexTow™ carbon fibre |
| CBA | chemical blowing agent |
| CC | cross-ply composite |
| CF | carbon fibre |
| CF-CC | cross-ply composite carbon fibre layup |
| CF-PP | carbon fibre reinforced polypropylene |
| CF-UD | unidirectional carbon fibre layup |
| CFRP | continuous fibre reinforced polymer |
| CFRTP | continuous fibre reinforced thermoplastic |
| EPP | expanded PP |
| FRP | fibre reinforced plastic |
| FRTP | fibre reinforced thermoplastic |
| GF | glass fibres |
| GF-CC | cross-ply composite glass fibre layup |
| GF-PP | glass fibre reinforced polypropylene |
| GF-UD | unidirectional glass fibre layup |
| HC | high crystalline |
| iPP | isotactic polypropylene |
| PBA | physical blowing agent |
| PBT | polybutylene terephthalate |
| PEEK | polyether ether ketone |
| PEI | polyetherimide |
| PET | polyethylene terephthalate |
| PI | polyimide |
| PMI | polymethacrylimide |
| PP | polypropylene |
| PP-H | polypropylene homopolymer |
| PP-T20 | 20 wt.-% talcum reinforced polypropylene |
| SFRTP | short fibre reinforced thermoplastics |
| sPP | syndiotactic polypropylene |
| TPU | thermoplastic polyurethane |

## Methods

| | |
|---|---|
| 4 PB | four-point bending |
| CAD | computer aided design |
| CDP | climbing drum peel |
| CLT | classical laminate theory |
| CNT | classical nucleation theory |
| CT | computer tomography |
| DCB | double cantilever beam |
| DSC | differential scanning calorimetry |
| FEG | field emission gun |

| | |
|---|---|
| GMR | general mixing rule |
| IR | infrared radiation |
| LEFM | linear elastic fracture mechanics |
| MBT | modified beam theory |
| NLS | notched lap shear |
| PLM | polarised light microscopy |
| RPT | roller peel test |
| SAXS | small angle X-ray spectrography |
| SCB | single cantilever beam |
| SEI | secondary electron imaging |
| SEM | scanning electron microscopy |
| TSD | tilted sandwich debond |
| TTL | thermoplastic tape laying |
| WAXS | wide angle X-ray spectrography |
| µCT | micro computer tomography |
| µFTIR | infrared microscopy |

# Table of Contents

# 1. Introduction

In recent years, lightweight design has gained new interest resulting from the rise of electric vehicles (EVs). Due to increasingly vigorous emission regulations on car fleets, vehicles with conventional internal combustion engine (ICE) approach the limit of economic feasibility considering the large development cost which is necessary to achieve the emission targets [1]. However, the battery as energy storage results in an increased car weight of EVs, though several components for ICE vehicles can be spared or simplified such as the gearing [1, 2]. The considerably high weight of EVs leads to a higher traction energy consumption, resulting in lower traction energy efficiencies despite energy recuperation measures [3, 4].

Hence, in the automotive sector and especially with respect to EVs, an enhanced cost-efficient lightweight design is necessary. In order to achieve this, an intensified use of fibre reinforced plastics (FRP) needs to be considered. Accordingly, BMW (Bayerische Motoren Werke AG) launched with the BMW i3 a battery electric vehicle (BEV) with a strong focus on lightweight design based on thermoset composites [5–7]. However, the cycle time of continuous fibre reinforced polymer (CFRP) components based on thermoset matrices still does not match time and cost requirements especially in the high volume segments of the automotive industry [5].

Fibre reinforced thermoplastics (FRTP) represent a promising alternative to conventional thermoset composites. Thermoplastic composites offer advantages like almost unlimited shelf life, recyclability, simplified work space hygiene and increased freedom of design [8, 9]. Most importantly however, thermoplastic composites enable shorter cycle times compared to composites with thermoset matrix, as the manufacture does not involve a curing time but a comparatively short cooling time [10, 11]. Consequently, FRTP denote a promising lightweight design material for cost-sensitive high volume applications.

The mechanical properties of FRTP components depend on the fibre volume or mass fraction, fibre length as well as fibre orientation and structure within the polymer matrix [8, 12, 13]. Generally, the weight specific mechanical properties and hence the lightweight design potential increase with growing fibre length and fibre volume within the composite. Unfortunately, the cost efficiency of manufacture as well as the freedom of design as yardstick for the achievable geometric complexity decreases simultaneously, see Figure 1. Injection moulding of short and long glass fibre reinforced thermoplastics for example denotes a manufacturing method for the cost-efficient production of complex shaped components and thus high freedom of design with moderate mechanical properties. Structural lightweight design components with highest demands regarding weight specific mechanical strength and stiffness however require continuous fibre reinforced thermoplastics (CFRTP) [8], yet at the disadvantage of a reduced freedom of design. Current processing technologies for the manufacture of CFRTP components are based on impregnated and mostly consolidated semi-finished thermoplastic composites, such as unidirectional tapes (UD tapes) or organo sheets. The production of CFRTP structures from UD tapes or organo sheets is often based on thermoforming. This process involves the heating of the CFRTP above the polymer matrix melting temperature and the subsequent forming and shaping in a cooled compression mould [12]. This process enables the manufacture of CFRTP components only with moderate geometrical complexity, due to the limited drapability and flow behaviour during compression moulding of the CFRTP material. Contrary to organo sheets, UD tapes can also be automatically placed and stacked using thermoplastic tape

laying (TTL) in order to build a CFRTP component with defined fibre orientation [14–16]. This makes TTL superior with respect to lightweight design [11], yet, the freedom of design is similarly limited and cost efficiency is a challenge. The latter is due to the high cost for the complex robotic tape placement systems and the need for post-processing via autoclaves in order to provide sufficient consolidation between the UD tape layers [17].

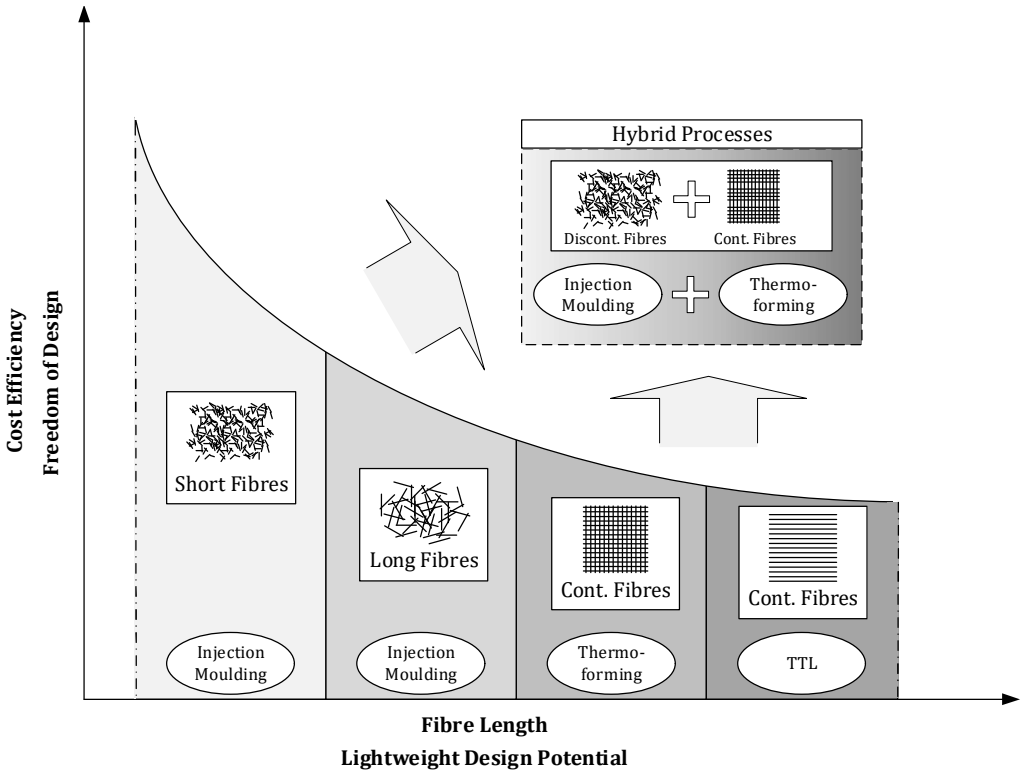


Figure 1: Schematic relationship of cost efficiency, freedom of design, fibre length and lightweight potential of fibre reinforced thermoplastic materials and corresponding processing routes: hybrid moulding processes combine benefits of conventional techniques and enable new potentials.

It can be summarised that cost efficiency, freedom of design and the lightweight design potential of FRTP components is limited by the inherent relationship between fibre length and resulting manufacturability. Therefore, hybrid processing technologies for FRTP materials and structures have been emerging, which combine processing variants for different fibre lengths. The hybrid overmoulding method e.g. represents a fusion of injection moulding with CFRTP structures that may be thermoformed beforehand. The overmoulding technique originates from the combination of metals with injection-overmoulded polymer structures [10, 18, 19]. This principle has been enhanced with the use of CFRTP as base material, providing increased weight specific mechanical properties and bonding strength between overmoulded polymer structures and the CFRTP substrate compared to their metal based counterparts. This is because during overmoulding of CFRTP with thermoplastic melt, both structures are welded together [18, 19]. The “Erlanger Träger”, developed and published by the Institute of Polymer Technology (LKT Erlangen) in the early 2000s, is one of the most well-known examples of hybrid moulding components [10]. Since then, a variety of different hybrid moulding technologies and composite components has been developed and published [11, 18, 20–27]. Hybrid moulding techniques such as overmoulding thus enable the use of CFRTP and their

promising lightweight design potential with the freedom of design and cost efficiency of short and long fibre reinforced thermoplastics.

## 1.1. Motivation

Although the classical overmoulding of CFRTP substrate structures has been object to large research efforts which succeeded in several industrial applications [28–34], the full potential of the combination of injection moulding technologies and CFRTP materials is not yet utilised with respect to lightweight design and cost.

Most hybrid thermoplastic composite structures and components consist of considerably thick CFRTP structures combined with e.g. overmoulded ribs and screw bosses [18, 27]. Especially when considering the frequent case of flexural loads, the extensive use of CFRTP material as base layer is often not associated to the actual stress field in the component. Hence, the lightweight design potential is not fully utilised resulting in low weight reductions compared to isotropic lightweight materials e.g. aluminium. Furthermore, the component cost is unnecessarily high because more costly CFRTP material is used than actually needed [11]. Finally, the function integration of current hybrid composites is limited to the modification of mechanical properties, especially with respect to torsional and bending properties, while polymers offer the possibility of additional functionalities e.g. thermal and acoustic insulation properties [35].

In this respect, process variants for the in-situ manufacture of full thermoplastic sandwich components with CFRTP facesheets and integral polymeric foam cores are promising candidates to provide cost-efficient lightweight design components [36]. The process is based on a combination of foam injection moulding and overmoulding of CFRTP, see Figure 2.

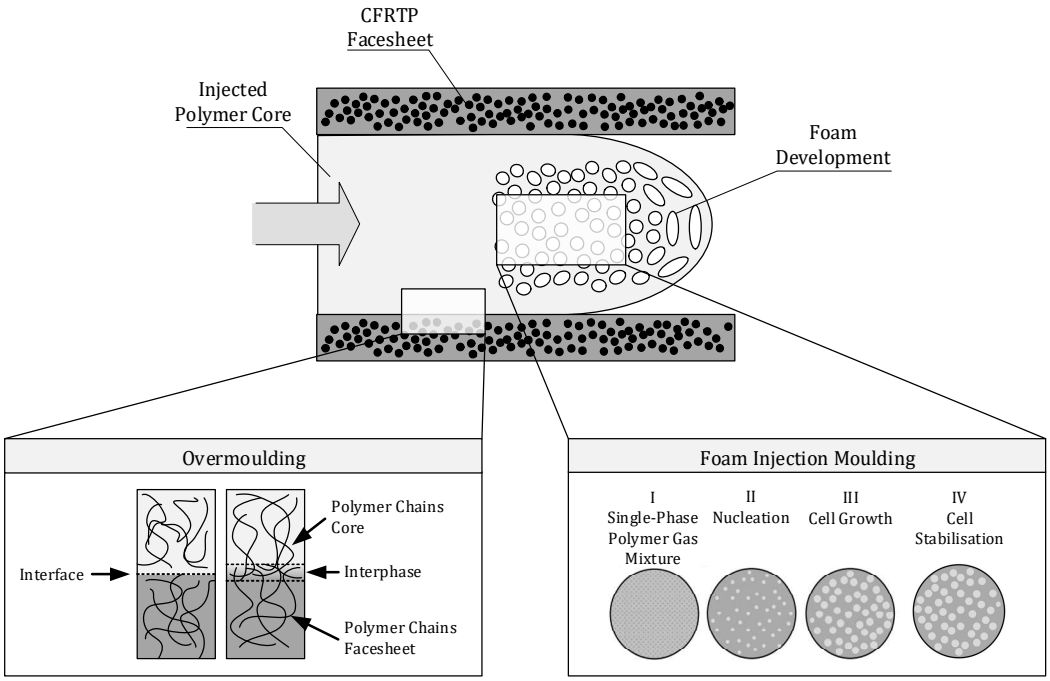


Figure 2: Schematic illustration of the incorporated processes in the in-situ manufacture of CFRTP sandwich components and its inherent challenges: overmoulding requires a proper interfacial bonding between the miscible thermoplastic adherents whereas foam injection moulding rises the challenge of foam morphology development and its induced weight specific mechanical behaviour.

During the manufacture, an integral foam core is injection moulded between thin CFRTP facesheets resulting in a full thermoplastic sandwich composite structure. Similar with thermoset based sandwich composites, the CFRTP sandwich structures exhibit high flexural properties at low weight [37]. This combinatory processing method has been developed by different institutes and researchers in recent years [35, 38–42].

The in-situ technique aims to increase weight specific mechanical properties and freedom of design while at the same time to reduce component cost by an efficient material application and production process. However, several challenges still need to be met in order to make this hybrid processing technique applicable for industrial scale component manufacture. These challenges are presented and discussed in the following, hence defining the objectives of the present work.

## 1.2. Objectives

The present work aims at a contribution to the diversification of manufacturing methods for hybrid CFRTP based lightweight structures. Therefore, it is necessary to gain insight into the phenomena governing the in-situ manufacture and the mechanical properties of CFRTP sandwich structures. This shall subsequently allow for a model-based prediction of the skin-core interfacial bonding and flexural behaviour of the resulting sandwich components. These models shall ultimately lead to a simplification of the pre-design of in-situ CFRTP sandwich structures. In order to achieve this, three main objectives are consequently pursued:

1. Development of Interfacial Bonding
2. Lightweight Design Potential and Optimisation
3. Predictive Models for Pre-Design

Initially, the bonding behaviour between injection moulded core and CFRTP facesheets plays a major role in order to use the full mechanical potential of in-situ CFRTP sandwich structures [37]. Hence, a profound understanding of the relationship between material and process parameters with respect to the resulting bonding between CFRTP facesheets and injection moulded polymer core is necessary. For this purpose, test methods are required that quantitatively describe the core-skin bonding thus enabling an evaluation and optimisation of the in-situ CFRTP process. After the selection of best-suited testing methods, it shall be analysed which material and process parameter combinations lead to high or low interfacial bonding of the injection moulded core to the CFRTP facesheets. The evaluation of the skin-core interface area as well as the fracture behaviour shall give insight into the phenomena governing the in-situ bonding of injection moulded core and CFRTP facesheets.

The second main objective of this work is the optimisation of the lightweight design of in-situ CFRTP sandwich structures represented by their weight specific flexural properties. Therefore, it is necessary to evaluate in a first step the effect of the use of different blowing agents on the interfacial bonding development of facesheet and core compared to sandwich specimens with unfoamed cores. In a second step, the effects of physical and chemical blowing agents as well as process parameters on the resulting weight specific flexural properties of in-situ CFRTP sandwich components are evaluated.

The third main objective focuses on the prediction of the structural behaviour of in-situ CFRTP sandwich structures in order to simplify the pre-design process for new components using this manufacturing technique. Different models shall therefore be developed and evaluated for the prediction of the interfacial bonding between CFRTP facesheets and injection moulded foam cores as well as of the flexural rigidity of the resulting in-situ sandwich structures. The models shall be validated and hence enable a specific optimisation of in-situ sandwich structures during a pre-design process.

## 1.3. Approach

The structure of the present work is schematically depicted in Figure 3. It comprises eight chapters.

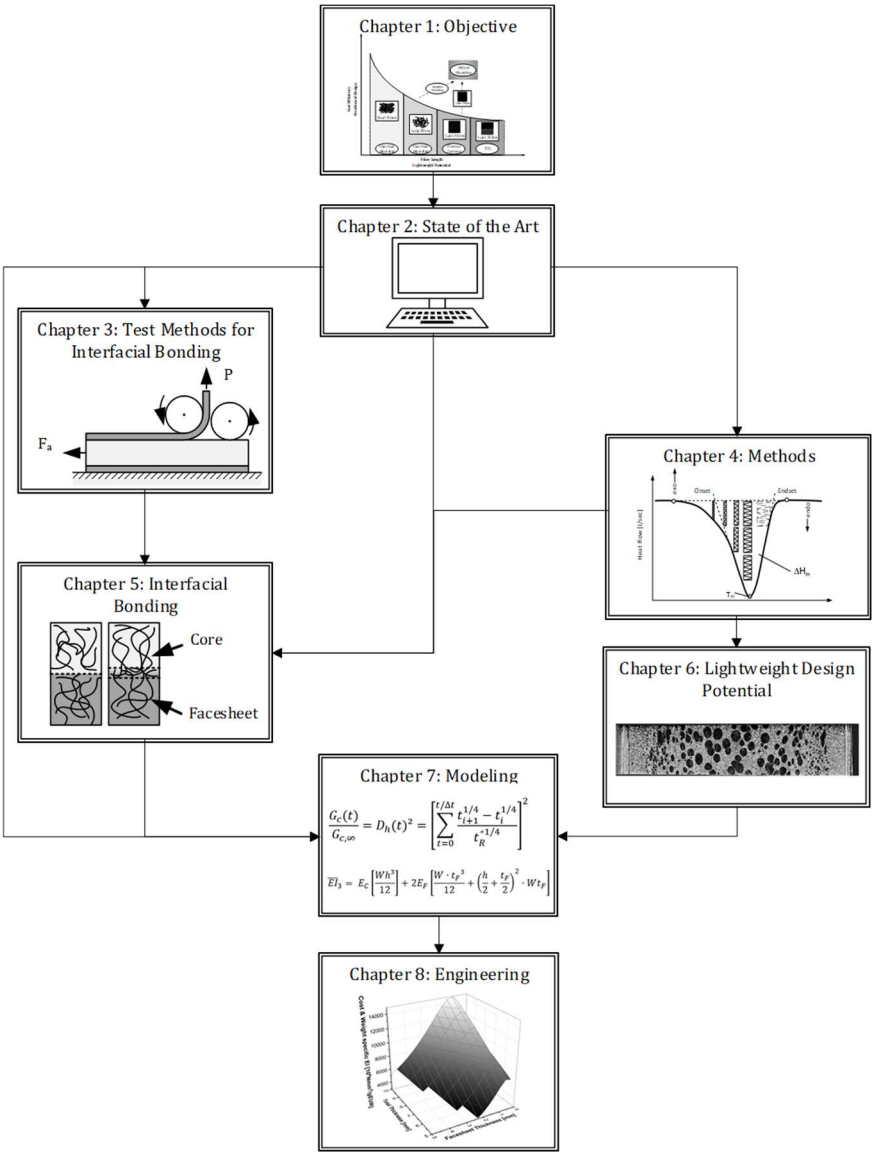


Figure 3: Schematic overview of the approach of the present work which is divided into 8 main chapters.

According to the objectives defined in chapter 1.2, a profound literature study in chapter 2 builds the basis for the subsequent chapters.

Chapter 3 focuses on the investigation and evaluation of mechanical testing procedures for the quantification of the bonding behaviour between injection moulded cores to CFRTP facesheets of in-situ CFRTP sandwich components. Therefore, different test methods are evaluated based on a thorough literature study and the most promising methods are selected based on the standardised rating procedure according to VDI 2225 [43].

Aside test methods for the assessment of interfacial bonding, other methods used in this work are presented in chapter 4. They include a four-point bending (4PB) test set-up in order to evaluate the flexural properties and lightweight design, as well as polarised light microscopy, computer tomography and scanning electron microscopy for the structural and fractographic characterisation of in-situ CFRTP sandwich components.

In chapter 5 the object of study is the investigation of the interfacial bonding of injection moulded core and CFRTP facesheets. Therefore, in-situ CFRTP sandwich specimens will be manufactured using different material and process parameters. Fracture analysis and polymer analytic methods shall give indication, how material and process parameters influence the in-situ interfacial bonding of injected core and CFRTP facesheets. In a second step, the skin-core bonding of in-situ CFRTP sandwich specimens with integral foam core is compared to those with solid polymer cores.

The focus of chapter 6 lies on the lightweight design potential of the in-situ process. High weight specific flexural properties of CFRTP sandwich structures with thin facesheets are targeted. This shall be achieved by an optimisation of the integral foam core with respect to the foam morphology and integral structure using different blowing agents and core materials. For the analysis of the resulting foam morphology, methods based on computer tomographic (CT) scans shall be used.

For the dimensioning and design of new components using the in-situ CFRTP sandwich process, a prediction of the resulting bonding between CFRTP facesheets and integral foam core as well as the flexural properties is necessary. Therefore, two models are evaluated in chapter 7 that shall enable this predictive characterisation. First, a fusion bonding model for the prediction of the interfacial strength development between CFRTP facesheet and integral foam core during the in-situ manufacture is presented. In addition, the weight specific flexural properties are characterised using different predictive models. A comparison with experimental results shall validate the models.

Chapter 8 demonstrates the applicability of the developed models at the exemplarily substitution of a reference component. The use of the models for the targeted optimisation of in-situ CFRTP sandwich structures is presented based on defined requirements and constraints. After the optimisation of lightweight design, suitable processing parameters are predicted using the interfacial bonding model. The optimised sandwich structures are compared to the reference steel structure with respect to weight specific flexural rigidity, packaging and cost, demonstrating the lightweight design potential of in-situ CFRTP sandwich structures.

# 2. State of the Art: Thermoplastic Sandwich Structures

In this chapter, the state of the art of thermoplastic sandwich structures is presented, see Figure 4.

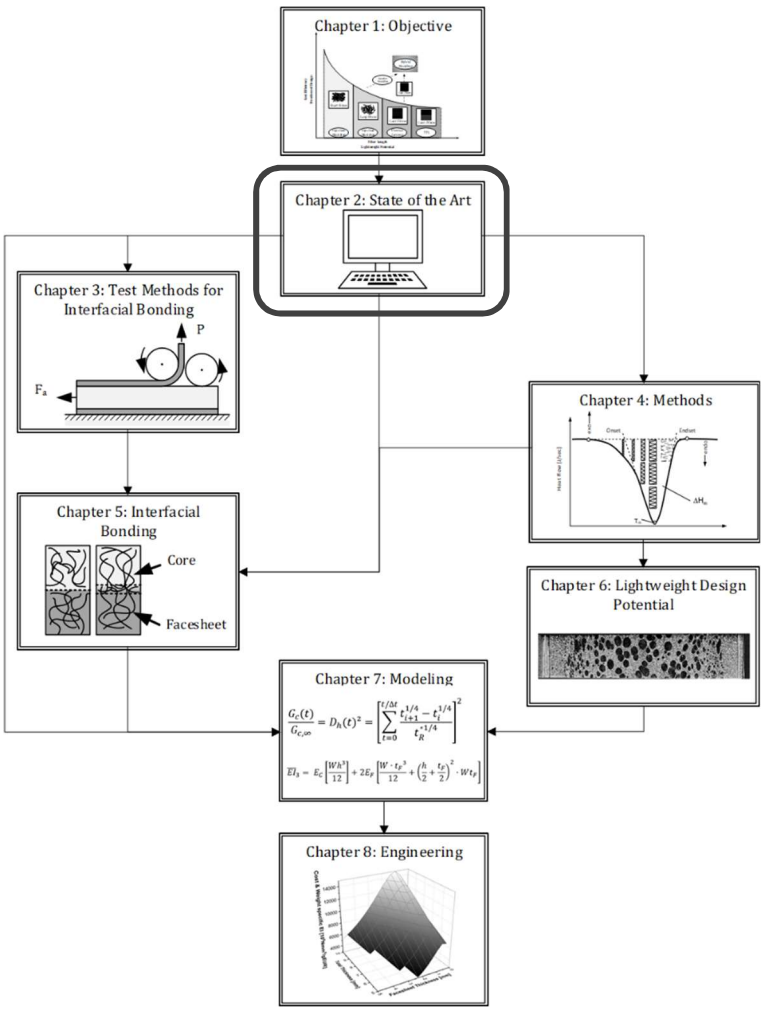


Figure 4: Systematic approach of this work: chapter 2 presents an overview of the state of the art and critically discusses its applicability on the present work.

This chapter is divided into the following sub-chapters:

2.1. Motivation for Sandwich Structure Architectures
2.2. Materials for Thermoplastic Sandwich Structures
2.3. Manufacturing Processes for Thermoplastic Sandwich Structures
2.4. Manufacture of In-Situ CFRTP Sandwich Structures
2.5. Flexural Behaviour of Thermoplastic Sandwich Structures with Integral Foam Core
2.6. Conclusion

At first, the potential of sandwich constructions regarding lightweight design is demonstrated, justifying the motivation for their use in a large spectrum of applications.

Subsequently, materials for thermoplastic sandwich structures are presented. The focus is set on polypropylene based components, since this is used in this work.

Due to the different processing methods compared to thermosets, the state of the art of the relatively young field of thermoplastic sandwich structure manufacturing is presented in the following sub-chapter, highlighting the high potential of in-situ CFRTP sandwich processes for cost-efficient production of lightweight design components.

As the in-situ process is a hybrid manufacture technique combining foam injection moulding with overmoulding of CFRTP, an overview of the foam injection moulding and foam cell development is given. Here, the foam development largely influences the lightweight design potential of the in-situ sandwich structures. However, the successful manufacture of in-situ CFRTP sandwich components largely depends on the proper bonding between injected core and CFRTP facesheet during the process. Therefore, an overview of the mechanisms of interfacial strength development and the relationship between material and process parameters is discussed in sub-chapter 2.4.

This builds the foundation for the development of model-based predictions of the interfacial bonding during in-situ moulding, which does not exist to this date. This model is required for the pre-design of new CFRTP sandwich components using the in-situ process. In addition, the development of models for the prediction of the flexural behaviour of in-situ CFRTP sandwich structures is targeted in this work. A challenge is the integral foam core, since the process and material induced foam core morphology needs to be validly represented by these models. Hence, an overview of the state of the art of model-based predictions of mechanical properties of integral foams is presented.

The last sub-chapter summarises the most important findings of the state of the art review and their effect on this work. Based on these findings, the necessity of the research conducted in this work is underlined.

## 2.1. Motivation for Sandwich Structure Architectures

Within the scope of lightweight design, the term sandwich structure describes a three layer construction consisting of a low density core and facesheets with high mechanical properties [44, 45]. The resulting composition is similar to an I-beam structure with a clear division of tasks between facesheets and core [46, 47]. The facesheets bear most of the tensile and compression stresses resulting from the bending load and are therefore often chosen to be continuous fibre reinforced polymer (CFRP) laminates or metal sheets [37]. The core bears the transverse shear stresses and serves as spacer that enhances the second moment of area without a significant mass increase of the total sandwich structure due to its low density [48]. Resulting from the arrangement of a material with low density at the low stressed core area and high strength and stiffness materials at the highly stressed skin areas, sandwich structures exhibit high weight specific mechanical properties especially with respect to flexural strength and stiffness [44, 48–50].

This is exemplarily demonstrated based on a unidirectional CFRTP reference structure consisting of a 34 volume percent (vol.-%) continuous glass fibre reinforced polypropylene with total thickness $H$, see Figure 5. The flexural rigidity of this reference structure is compared with different sandwich structures, using the same type of composite only in their facesheets. The thickness of the facesheets yields each $0.25\ H$, which results in the application of only 50 % of the composite compared to the reference monolithic structure. The resulting flexural rigidity of these sandwich constructions is enhanced by factor 4.8 and 44.4 respectively, see Table 1.

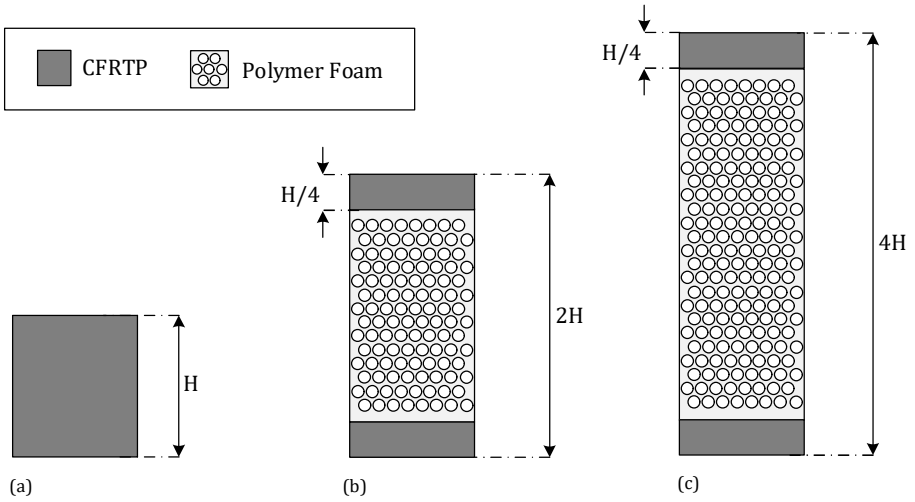


Figure 5: A monolithic CFRTP beam of height H (a) is substituted by an in-situ sandwich beam with equal amount of CFRTP split into two facesheets divided by a foam core (b). This increases the flexural and weight specific flexural rigidity with increasing core thickness (c).

Assuming a mean density of the polymeric foam of 0.65 g/cm³ and considering a density of the CFRTP material of 1.55 g/cm³, the density specific flexural rigidity can be even increased by factor 8.5 to 90.2. This clearly demonstrates the lightweight design potential of sandwich structures, especially when it comes to components, which are subject to bending.

Table 1: Overview of the resulting properties of monolithic as well as of CFRTP sandwich structures. All values are normalised with respect to the monolithic reference.

| | Monolithic (a) | Sandwich (b) | Sandwich (c) | Dimension |
|---|---|---|---|---|
| Composite Thickness (norm.) | 1 | 0.5 | 0.5 | - |
| Total Thickness (norm.) | 1 | 2 | 4 | - |
| Flexural Rigidity (norm.) | 1 | 4.8 | 44.4 | - |
| Specific Flexural Rigidity (norm.) | 1 | 8.5 | 90.2 | - |
| Density (norm) | 1 | 0.71 | 0.56 | - |

In the following, CFRTP based sandwich structures are presented including sandwich materials, manufacture and mechanical characterisation.

## 2.2. Materials for Thermoplastic Sandwich Structures

Within the last decades, a variety of different materials and processes has been established for the manufacture of polymer based sandwich composites. Since the beginning of its development and application, sandwich composite structures are mostly based on thermoset composites. Bonding between core and facesheets is achieved using adhesives which are also based on thermosets [48, 51]. Aside high weight specific flexural stiffness, the resulting sandwich structure exhibits high resistance against compression and fatigue.

However, thermoset composite sandwich structures have a list of disadvantages. Brittle mechanical behaviour and low debonding resistance of facesheets are major challenges, as debonding can lead to failure of the whole structure [52, 53]. Furthermore, the production of thermoset sandwich

composites is time- and cost-intensive, as the curing time of the thermoset adds to the cycle time. This makes thermoset sandwich composites little attractive for cost-sensitive high volume applications [44, 48]. Also, thermosets consist of possibly hazardous and toxic raw components, especially the curing agents and the highly reactive monomers, which collides with increasing sustainability requirements [8].

Thermoplastic composites in contrast can be considered superior with respect to the aforementioned issues, and add largely improved recyclability properties [44, 54–56]. Therefore, a number of different thermoplastic based sandwich composite structures and processing techniques have been developed in recent years [44, 46, 48, 55, 57–62]. Since both the materials as well as the manufacturing process define the resulting properties of the component, thermoplastic sandwich composite materials as well as manufacturing methods will be presented in the following, with special focus on polypropylene as polymer material for the CFRTP facesheet matrix and as core material.

### 2.2.1. Polypropylene as Semi-Crystalline Thermoplastic Polymer

Thermoplastic polymers can be divided according to the thermoplastics pyramid in commodity, engineering and high performance thermoplastics regarding their material cost and thermomechanical properties, see Figure 6 [63].

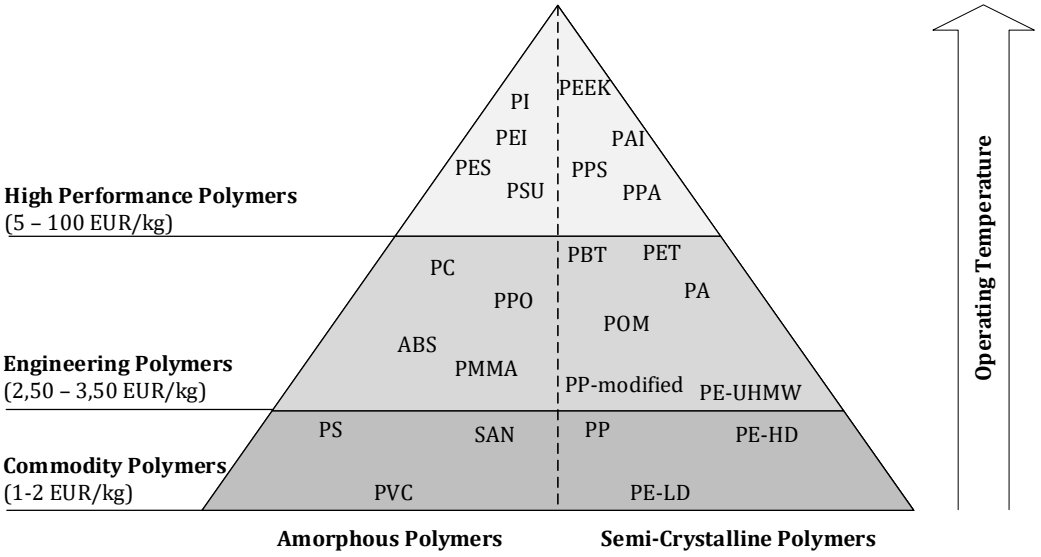


Figure 6: Classification of thermoplastic polymers according to the thermoplastics pyramid into commodity, engineering and high performance polymers (based on [63]).

Commodity polymers represent by far the largest fraction of the thermoplastics demand, with polyolefins representing more than 60 % of annually produced polymers [64]. In the group of polyolefins, polypropylene is frequently used for industrial applications for example in the cost-sensitive automotive segment. Polypropylene owes its popularity to the advantageous combination of properties such as chemical resistance, low volatile organic compounds (VOC) and high weight specific mechanical properties at moderate cost [65–69]. The degree of crystallinity has a major effect on the mechanical properties of polypropylene. Neglecting transition areas, the structure of

semi-crystalline plastics in general and hence also of polypropylene can be represented as a 2-phase model including an amorphous and a crystalline phase, see Figure 7. In this simplified scheme, crystalline regions alternate with amorphous regions. The random amorphous structure represents entropically the most favourable condition. Following the second law of thermodynamics, polymeric macromolecules always seek this condition [70]. Semi-crystalline thermoplastics however have a certain fraction of ordered crystalline areas. The crystalline fraction depends on the cooling process and largely influences the properties of the polymer [71, 72].

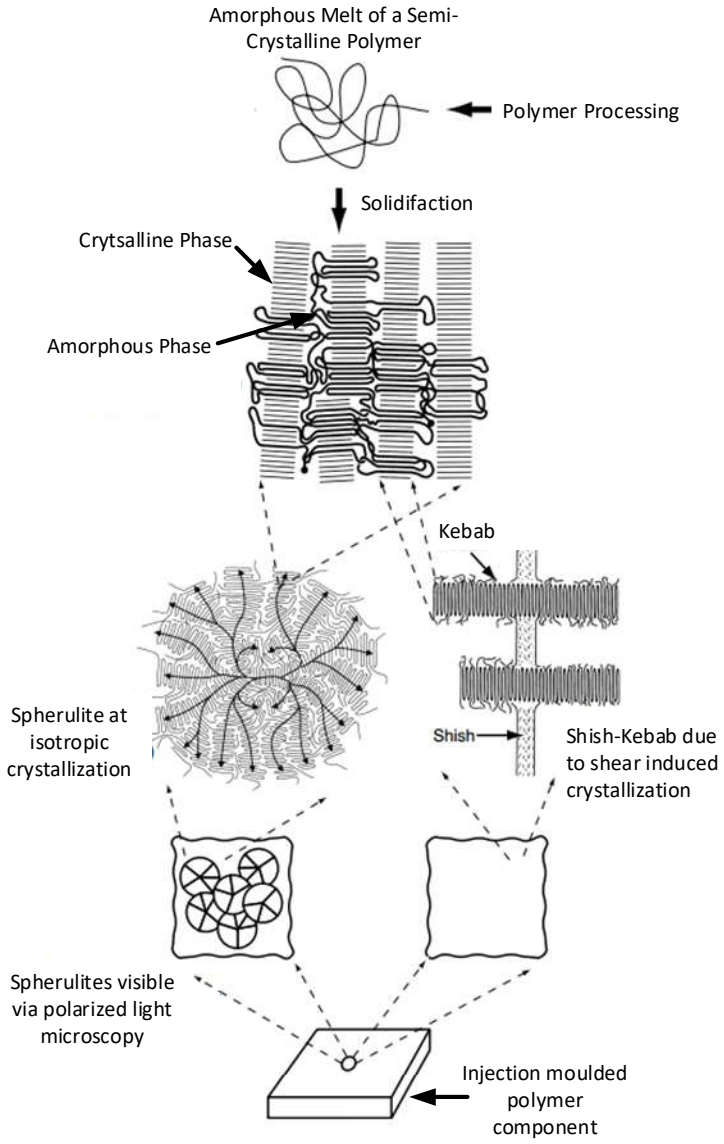


Figure 7: From the melt of a semi-crystalline polymer at microscopic scale to the injection moulded component at macroscopic scale (based on [73]).

The proportion of crystalline and amorphous material in a volume can be described by the degree of crystallinity $\xi$. As polymers do not crystallise completely, even in the presence of perfect crystallisation conditions, the degree of crystallinity is defined as the maximum achievable fraction of crystalline structures in the respective polymer [64]. The degree of crystallinity is hence defined as

the ratio of the crystalline volume fraction $V_c$ to the polymer-specific maximum achievable volume fraction of crystalline phase $V_\infty$ after an infinitely long time [74] leading to

$$\xi = \frac{V_c}{V_\infty}. \tag{1}$$

The experimental determination of the degree of crystallinity can be conducted by means of various methods, the most popular being differential scanning calorimetry (DSC) as well as wide and small angle X-ray spectrography (WAXS and SAXS) respectively, but also micro Fourier-transform infrared spectroscopy can be used (µFTIR) [64, 75].

***Crystallisation of Semi-Crystalline Thermoplastic Polymers: Nucleation and Growth***

According to the works of Hoffmann and Lauritzen [76–78] the crystallisation of semi-crystalline polymers can be divided into two steps. The initial step of the crystallisation of a molten, semi-crystalline polymer is the primary nucleation, which results in stable nuclei. Subsequently, these stable nuclei serve themselves as nucleus, inducing the accretion of back-folding polymer molecules which leads to the growth of a lamellae [79]. Stochastic processes dominate primary nucleation, which can be mathematically described using probability calculus [64]. The primary nucleation according to the classical nucleation theory (CNT) can be furthermore divided into homogeneous and heterogeneous nucleation [80, 81]. Homogeneous nucleation describes the nucleation of crystalline structures in a polymer melt due to localised stochastic density fluctuations [70, 79]. The heterogeneous nucleation on the other hand takes place at the transition to another phase, which acts as a nucleating agent [82–84]. These may be fillers or solid substrates such as polymer films or CFRTP in the case of hybrid injection moulding processes [63]. The development of nuclei can be described using the free energy $G$ in the system. For primary nucleation, the change of the free energy of a system per volume $\delta G$ during the development of solid phases from a liquid phase can be described as [70, 85–87]

$$\delta G = V_s \Delta G + A_i \gamma_i. \tag{2}$$

Here, $V_s$ denotes the volume of the solid phase, $\gamma_i$ is the free energy at the interface between solid and liquid, $A_i$ is the interface area at the contact of solid and liquid and $\Delta G$ denotes the difference of free energy per volume of solid $G_s$ and liquid $G_l$ as

$$\Delta G = G_s - G_l. \tag{3}$$

The free energy difference $\Delta G$ for the development of ball shaped nuclei with radius $r$ can be described as

$$\delta G = \frac{4}{3}\pi r^3 \Delta G + 4\pi r^2 \gamma_i. \tag{4}$$

In order to achieve a stable nucleus that sets the basis for subsequent crystal growth, a critical nucleus radius $r_c$ must be exceeded which initiates the growth of nuclei. Stable nuclei are achieved if their radius $r_0$ leads to $\delta G = 0$, see Figure 8.

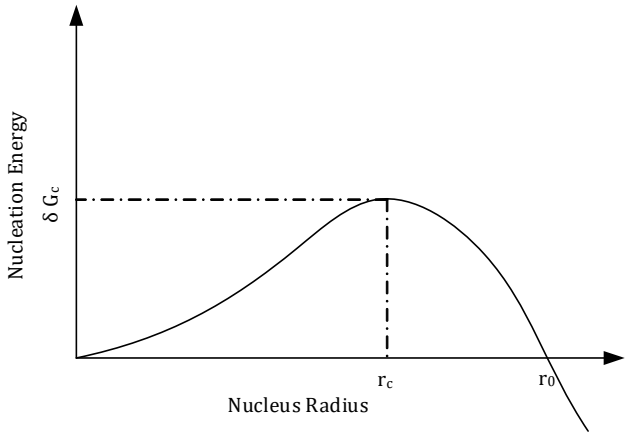


Figure 8: Qualitative relationship of nucleation energy and nucleus radii. At $r_c$ the critical nucleus radius is reached at which the nucleus growth initiates. At $r_0$ stable nuclei are achieved (based on [70]).

Thus, the critical nucleus radius $r_c$ can be assessed by setting the derivative of Equation 4 equal to zero, leading to

$$r_c = -\frac{2\gamma_i}{\Delta G}. \tag{5}$$

If at radii equal or larger than $r_0$ stable nuclei are achieved, crystal growth as the second step of polymer crystallisation takes place at the positions of stable nuclei. During the growth of crystalline polymer structures, random oriented polymer chains convert into an arranged structure corresponding to a lower state of entropy. For the description of this growth of crystalline structures, different models can be used. Often the two-stage model according to Hoffmann and Lauritzen [78] is applied which describes a back-folding of chains, see Figure 9. This model comprises the deposition of secondary nuclei on already stable primary nuclei via back-folding, which leads to the formation of oriented lamellae [70].

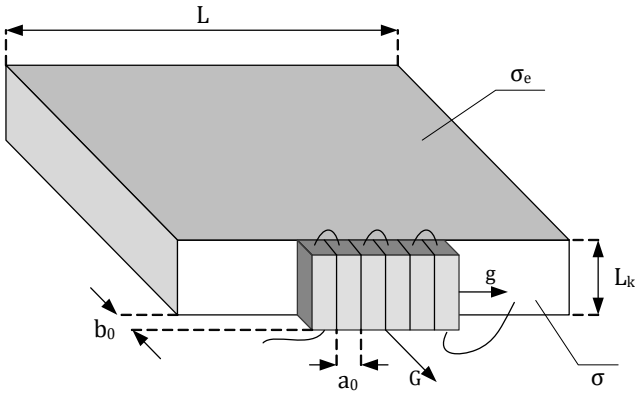


Figure 9: Schematic model for crystal growth induced by chain-folded surface nuclei according to Lauritzen and Hoffmann (based on [78]).

According to Turnbull and Fisher [81] the temperature dependent growth rate $I(T)$ of the lamellae can be described as

$$I(T) = I_0 \cdot exp\left(\frac{\Delta G_{*,2}}{kT}\right) exp\left(\frac{\Delta G_\eta}{RT}\right). \tag{6}$$

The factor $I_0$ is depending on the temperature and the molecular weight, however in case of polypropylene the effect of the molecular weight is small [88] and the temperature dependency is negligible compared to the exponential terms [89]. The first exponential term describes the growth of a two-dimensional nucleus on the lamellar surface via the critical nucleation energy for secondary nucleation $\Delta G_{*,2}$, the Boltzmann constant $k$ and the temperature $T$. The second term controls the transport of a molecule to the phase boundary between amorphous and crystalline areas based on the threshold energy $\Delta G_\eta$, the ideal gas constant $R$ and the temperature $T$ [70, 79]. In general, the linear growth rate $I(T)$ is proportional to the secondary nucleation rate, i.e. mostly the molecule transport is faster than their installation into crystalline structures. Thus the first term in Equation 6 dominates the growth rate [63, 70].

This growth proceeds radially under isotropic conditions, starting from a stable primary nucleus, so that due to the lamellae growth, a ball-shaped spherulite with sizes of 1 µm to a few mm is formed [63, 90]. At certain conditions however, an oriented lamellar growth can occur resulting in an oriented spherulite. This columnar growth of spherulites is called trans-crystalline growth and was first described by Jenckel et al. [91]. It is often observed in fibre-reinforced semi-crystalline thermoplastic polymers, at which the fibre acts as a heterogeneous nucleus, see Figure 10 [84, 92, 93]. If the nucleation density at the vicinity of the heterogeneous nuclei significantly exceeds the nucleation density in other locations of the polymer volume, transcrystalline growth can result [94]. In the case of hybrid processes such as overmoulding, the solid surfaces of the CFRTP substrates can also largely increase the nucleation density of the semi-crystalline polymer melt and lead to the development of transcrystalline layers [63, 95].

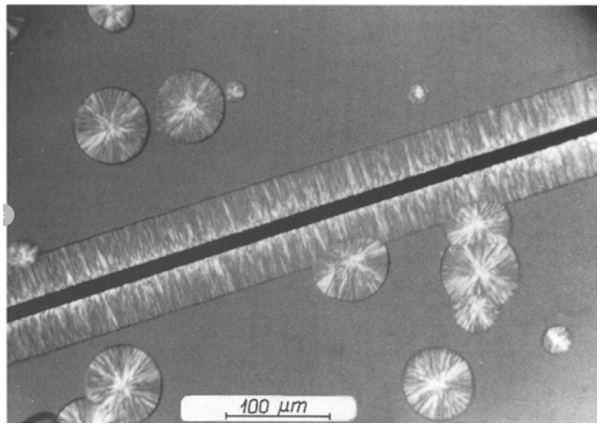


Figure 10: Different crystalline morphologies of iPP: radial spherulite growth as well as transcrystalline structures induced by an embedded carbon fibre at $T$ = 135 °C [93].

Whether and how strong a transcrystalline zone is formed depends on several parameters, such as the surface roughness of the solid phase, physical, chemical as well as thermal properties [96]. An increased roughness of various substrates has a strong effect on the likelihood of forming transcrystalline layers of the polymer, as it increases the nucleus density [97, 98]. In addition, when a strong thermal gradient exists, the spherulite and its lamellae grow along the direction of the gradient [79, 99]. Raimo [90] even assumes that the thermal properties of the materials as well as the process are essential for the development of a transcrystalline phase and refers to early studies on this topic [100–102]. Along with its different morphology, transcrystalline structures can be

accompanied by increased mechanical properties. Yan et al. [83] ascertains that overmoulding of a solid PP substrate with a PP melt leads to increased interfacial strength due to thermally induced transcrystalline contact zones. Lebsack [95] finds in the overmoulding of continuous fibre reinforced polyamide 6 (PA6) substrates with PA6 melt a correlation between increased interfacial strength as well as interfacial fracture toughness and the size of the transcrystalline zone originating from the CFRTP surface.

### 2.2.2. Continuous Fibre Reinforced Thermoplastics as Sandwich Facesheet

Continuous fibre reinforced and fully consolidated thermoplastic composites as semi-finished product are usually used as facesheet when thermoplastic sandwich structures with high mechanical properties are required [103]. These consolidated composites offer a high reproducible laminate quality and are available in a large variety of matrices ranging from commodity polymers such as polypropylene (PP) to aviation grade high performance polymers such as polyetherimide (PEI) and polyether ether ketone (PEEK) [48]. The continuous fibre reinforcement can be based on carbon (CF) or glass fibres (GF), whereas their orientation and structure can be classified into unidirectional fibre orientation and fabric structures. The type of fibre reinforcement structure divides the consolidated thermoplastic composites into two groups:

- unidirectionally reinforced tapes (UD tapes)
- fabric reinforced sheets (organo sheets)

Organo sheets are based on a fabric reinforcement, usually twill, with a fibre volume fraction of up to 47 vol.-% [104]. As with UD tapes, the fibre type can be chosen to be glass or carbon. Commercial organo sheets are manufactured by compression moulding based on the film stacking process using double belt presses providing high output rates [18]. As the first process step, a fabric is unwound from a coil and both faces are covered with thin layers of polymer becoming the composite matrix. These stacked films are inserted into a double belt press, where they are heated above their melt temperature. Then, pressure is applied which leads to the flow of the polymer melt through the space between the filaments until the fabric is fully impregnated. Thereafter, the newly formed composite is cooled down in a pressure controlled way in order to compensate for the shrinkage due to crystallisation and thermal contraction of the mostly semi-crystalline matrix thus receiving fully consolidated organo sheets [7].

Compared to organo sheets, UD tapes provide higher mechanical properties, as reinforcing continuous fibres do not exhibit undulations contrary to the fabric reinforcement of organo sheets [8]. In addition, the fibres can be precisely oriented along load directions within the component during its manufacture, e.g. using TTL [11]. UD tapes usually consist of glass or carbon fibres and the fibre volume fraction may be as high as 45 vol.-% [105]. Different manufacturing methods for UD tapes have been developed based on polymer powder (slurry), polymer melt impregnation and film stacking, see Figure 11 [106–109]. Commercially available UD tapes however, which are used within this work, are cost-efficiently produced by melt impregnation, which is based on an extrusion process. In this process, the reinforcing fibres in form of rovings are unwinded of coils. Rovings consist of several hundreds to thousands of filaments that are combined after their manufacture using a coating that reduces abrasive damage of the fibres during processing and improves fibre matrix adhesion [8]. Since the high viscosity of the thermoplastic melt makes full impregnation of all

filaments challenging, the single filaments within the roving are separated and spread flatwise by breaking up the sizing. By doing this, the impregnation flow length is reduced which is a major factor influencing impregnation time [12, 107]. This consequently allows for faster and better impregnation with polymer melt [8, 12].

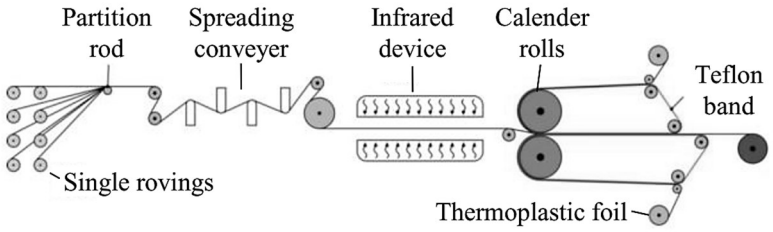


Figure 11: Continuous manufacture of UD tapes based on the film stacking technique [107].

The full and proper impregnation of all filaments, also termed micro-impregnation, and the subsequent consolidation into a laminate with very low porosity poses generally one of the main challenges of the manufacture of thermoplastic composites [7]. The spread filaments are heated e.g. by an infrared radiation (IR) system and introduced in an extrusion mould, where they are impregnated with hot thermoplastic melt. A pressure gradient in thickness direction of the filament layer leads to a polymer melt flow between the filaments. Subsequently, the melt impregnated filament layer is consolidated using chill rolls that apply a compaction force while cooling the UD tape. Manufacturing speeds of up to 20 m/min can be achieved by using this method making UD tapes a very cost-efficient CFRTP material [110].

### 2.2.3. Thermoplastic Sandwich Core Structures

Thermoplastic sandwich structures can be composed of homogeneous and non-homogeneous cores, based on their structural architecture, see Figure 12 [37].

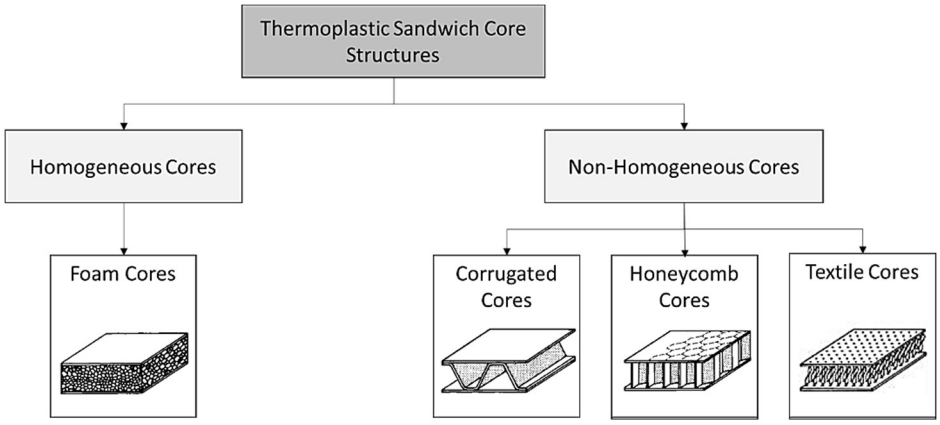


Figure 12: Core structures for thermoplastic sandwich composites divided according to their composition [37].

Most thermoplastic sandwich composites use foam and honeycomb cores. Corrugated cores are used in special applications since they offer lower mechanical properties in transverse direction of

the corrugated profile. Thermoplastic honeycomb structures can be manufactured by the production of co-extruded tubes and subsequent welding (fusion bonding) thereof to create a planar layer of honeycombs [48]. Honeycomb core structures provide high mechanical properties, however they used to be costly [51]. A recently developed process largely simplifies thermoplastic honeycomb manufacture by directly extruding a line of honeycomb profiles which are subsequently back-folded in order to receive a planar honeycomb structure [111].

Foam cores are also widely applied, as they combine high mechanical properties with high temperature resistance, good thermoforming properties and high acoustic and thermal insulation [48, 51]. Polymeric foams are usually manufactured by polymer foam extrusion providing foamed plates of different materials and sizes. Contrary to other polymer core architectures, polymeric foam cores can also be manufactured by foam injection moulding. A major advantage of injection moulding of polymeric foams is that the process provides ready-made foam components within seconds that do not require time and cost intensive post-processing steps such as milling or thermoforming [112].

## 2.3. Manufacturing Processes for Thermoplastic Sandwich Structures

Different processing methods can be utilised in order to receive thermoplastic sandwich composites. The choice of a specific processing method mainly depends on the core material and structure as well as the applied polymer types respectively. These methods can be divided into 2 groups, i.e. adhesive bonding as well as fusion bonding of core and facesheet, see Figure 13.

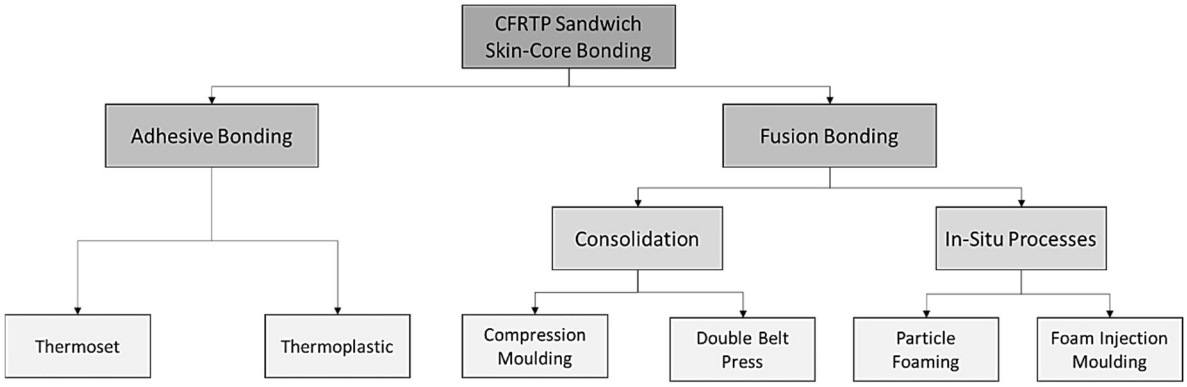


Figure 13: Different manufacturing routes for continuous fibre reinforced thermoplastic sandwich structures [48].

For several decades, composite sandwich structures have been based mostly on thermoset polymers, which were manufactured by the adhesive joining of cores and facesheets. This method can similarly be applied at thermoplastics. In order to join core and facesheets, a coupling agent is placed between the core and the facesheets hence improving interfacial bonding, e.g. a hot melt film. This film exhibits a lower melting temperature than core and skin, bonding of core and skin is thus based on physical mechanisms [48]. The hot melt film also allows for the combination of different core and facesheet polymers, which leads in turn to a reduced recyclability. Moreover, the temperature resistance of the sandwich structure is limited by the low melting hot melt film. The consolidation process variants include compression moulding of CFRTP facesheets and rigid foam cores using a double belt press or a discontinuous laboratory press. Here, the interfacial bonding between foamed

core and facesheets is usually achieved by melting only the facesheet matrix, which flows in the porous surface of the unmelted rigid foam core, thus creating a lock of both interfaces after cooling. During this process, the foam core temperature must be kept sufficiently below its melting temperature in order to avoid a collapse of the foam structure [54]. Consequently, the rigid foam cores should consist of polymers with higher melting temperatures as the facesheet polymer, such as polymethacrylimide (PMI) or polyethylene terephthalate (PET) [54, 113]. Other consolidation methods to manufacture thermoplastic sandwich structures are based on fusion bonding of facesheet and core. For this, the applied core and facesheet polymer are required to be miscible.

In terms of a targeted reduction of the resulting component cost, it is desirable to use commodity thermoplastics such as PP. Moreover, with respect to recyclability and high compatibility of foam core and facesheets, it is advantageous to use the same polymer for the core and facesheet matrix [44]. Using the same or miscible polymers for both the core and the facesheet matrix, it is possible to apply so called in-situ processes for the manufacture of thermoplastic sandwich structures [58]. The in-situ processes are characterised by the fact that during the manufacture of the foam core, bonding between core and the reinforcing CFRTP facesheets and hence the creation of a sandwich structure develops simultaneously [46, 58, 114]. The foaming process technology can be either particle foaming or foam injection moulding. Using particle foaming, the foam core consists of pre-foamed expanded beads, which are processed to the later foam core in several steps. First, the CFRTP facesheets are thermoformed to the required geometry (preforms) if necessary. The CFRTP preforms are then heated e.g. via IR radiators before they are inserted into the cooled mould. After closing the mould, the cavity between the preform facesheets is filled with the expanded beads that are subsequently sintered together using hot water fume [113, 115]. The heat induced by hot water fume leads to a bonding of particle foam beads and facesheets [58]. However, only a limited spectrum of materials can be used for this process, including expanded PP foams (EPP) although recent developments enable the use of expanded thermoplastic polyurethane (TPU), PET and polybutylene terephthalate (PBT) as particle foams [116].

Another in-situ process for the manufacture of thermoplastic sandwich structures is based on the combination of foam injection moulding and CFRTP facesheets. Using this combination of manufacturing processes, polymer sandwich composites can be manufactured in very short cycle times with high weight specific mechanical properties using a large spectrum of possible thermoplastics [45, 117]. This process is object of study of the present work. Consequently, the term “in-situ process” denotes solely the manufacture of CFRTP sandwich structures with foam injection moulded core henceforth. The in-situ CFRTP sandwich process will be presented in detail in the following.

## 2.4. Manufacture of In-Situ CFRTP Sandwich Structures

The idea behind the in-situ CFRTP sandwich processes is a consequent utilisation of the potentials that come along with advanced injection moulding technologies such as the direct integration of functionalities in the component and the high mechanical properties of CFRTP materials. However, the in-situ manufacture of CFRTP sandwich structures is a complex process due to the combination of overmoulding and foam injection moulding, each imposing their own challenges for a successful application at the manufacture of a component and possibly adding new issues due to their combination.

The successful manufacture of in-situ CFRTP sandwich structures consequently requires the proper control of the foam injection moulding process as well as the fusion bonding during the overmoulding process of the CFRTP facesheets, see Figure 2. This makes a control of the in-situ technique considerably complex. The respective sub-processes thus need to be fully understood and are therefore presented in the following.

### 2.4.1. Foam Injection Moulding

Using the foam injection moulding process, polymer components with integral foam structure can be manufactured [112]. An integral foam exhibits a varying density distribution $\rho$ in thickness dimension $z$ of the part, see Figure 14.

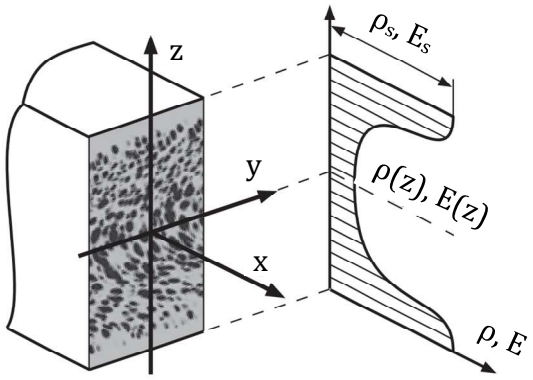


Figure 14: Integral foam structure of a foam injection moulded component shows high density reductions in the center whereas solid skins develop near the mould. The resulting mechanical properties correlate with the density distribution [112].

In the center of the integral foam core, the density reduction is largest, while it sharply increases near the surface. There the density of the solid polymer $\rho_s$ as well as its mechanical properties are reached, e.g. the Young's modulus $E_s$. The cell sizes, their distribution as well as the total integral foam structure strongly depends on the material and process parameters used during foam injection moulding [47]. Material parameters include the foamed polymer, additives serving as nucleation agent and foam stabiliser. The polymer melt can be foamed using physical (PBA) or chemical blowing agents (CBA) leading to the creation of a single-phase polymer-gas solution. CBA are endothermal chemicals that release mostly water ($H_2O$) and carbon dioxide ($CO_2$) during temperature induced decomposition. Typical types of CBA are sodium hydrogen carbonate ($NaHCO_3$) and citric acid ($C_8H_6O_7$) derivatives [112]. Commercial master batches often contain a mixture of both. These pellet master batches consist of a polymer carrier material, e.g. polyethylene, added with 20 to 70 % effective constituents of the blowing agent. The manufacture of chemically foamed thermoplastic components is achieved by adding 1 to 3 weight percent (wt.-%) of the master batch to the polymer pellets, depending on the type of master batch and the manufacturer recommendation. Due to the temperature during plasticisation of the pellets in the barrel, the CBA decomposes and releases $H_2O$ and $CO_2$. The latter is dissolving in the polymer melt until a single-phase polymer-gas solution is achieved [112]. Machinery requirements for chemical foam injection moulding are low, a regular

machine with a 3-zone screw is sufficient. However, an increased corrosion resistance due to the released water and possible citric acid residues is recommended [112].
The use of physical blowing agents in contrast requires sophisticated industrial manufacturing equipment. Several process variants have been developed differing with respect to the gas introduction and the type of gas used. PBA are mostly inert gases such as $N_2$ or $CO_2$, that are usually dissolved in the polymer as supercritical fluid which enhances the dissolving behaviour [47]. The introduction of gas in the polymer melt can be achieved in the barrel (MuCell®) as well as in the feed hopper (ProFoam) for example. For both, a modified injection moulding machine is necessary.

In this work the ProFoam process is used as physical blowing agent technology. The machine modifications include a modified pressurised hopper for the introduction of the physical blowing agent, see Figure 15.

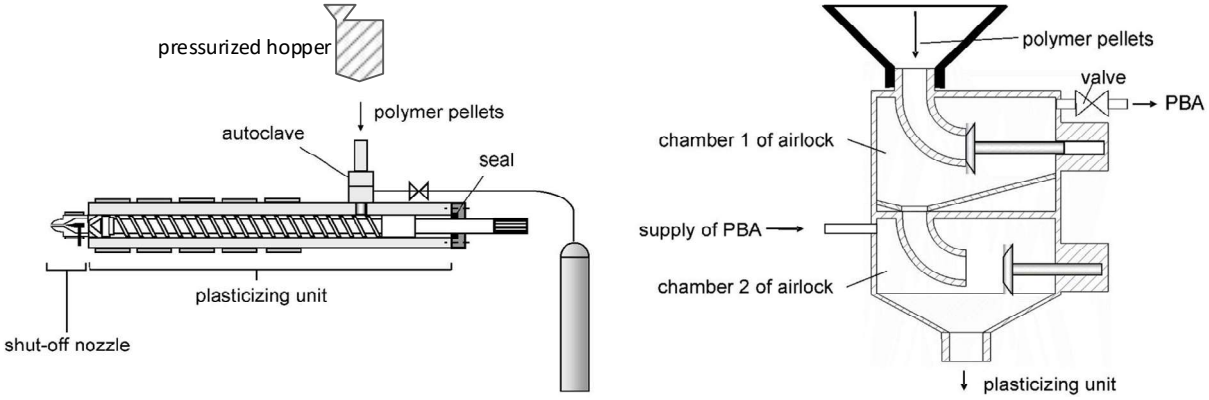


Figure 15: Foam injection moulding with physical blowing agent (PBA) based on the ProFoam Technology [118]: plasticising unit (left) with the pressurised hopper (right).

An additional seal prevents a leakage of gas from the barrel [118, 119]. In this special hopper, the unpressurised pellets are mixed with the gas in the second chamber at a defined pressure of 50 bar and subsequently fed to the plasticising unit [120]. The system is equipped with a shut-off nozzle, which keeps the melt and as such the polymer-gas-solution constantly under pressure until its injection into the cavity.

### *Foam Morphology Development*

The foam morphology results from the combination of materials and process parameters used during foam injection moulding. The development of the polymeric foam structure can be divided into four steps:

I. Creation of a single-phase polymer-gas mixture
II. Cell nucleation
III. Cell growth
IV. Cell stabilisation

These four steps of foam development based on a single-phase polymer-gas mixture are schematically depicted in Figure 16 [112].

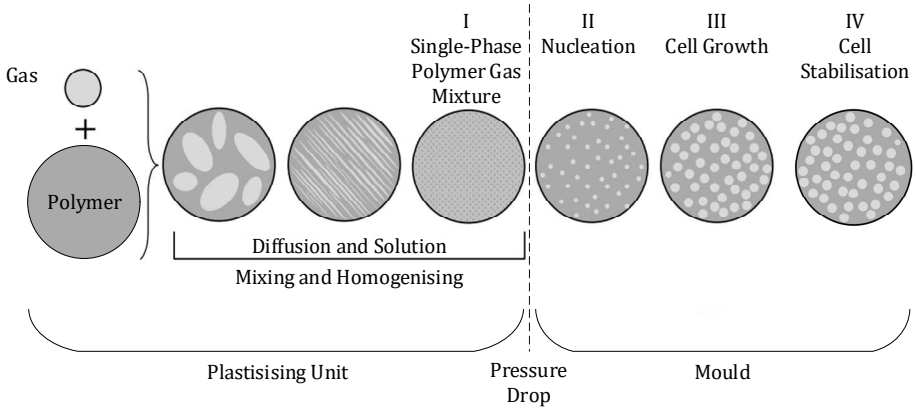


Figure 16: Foam morphology development schematically illustrated with its four phases: after the diffusion and solution of gas in the polymer melt, a single-phase polymer-gas solution is achieved in the barrel of the plasticising unit (step I). Subsequent injection into the mould cavity induces a pressure drop leading to the nucleation of foam cells (step II) and subsequent cell growth (step III). The foam morphology is finally stabilised after freezing of the melt (step IV) (modified from [47] and [112]).

In order to achieve a single-phase polymer-gas mixture, the gas needs to be dissolved in the molten polymer. The chemically or physically induced solution of gas in a polymer melt can be described by the saturation concentration $C$ as the ratio of gas mass $m_{Gas}$ to polymer mass $m_m$, see Equation 7 [121]. If the saturation limit is approached, the concentration $C$ of the gas dissolved in the polymer can be determined on the basis of the relationship between the solubility coefficient $S$ and the partial pressure following Henry's law [112, 121]. According to this, the gas concentration $C$ is proportional to the partial pressure $p$ of the gas leading to

$$C = \frac{m_{Gas}}{m_m} = S. \tag{7}$$

Hence, the amount of gas, which is dissolved in the polymer, increases as the pressure growths. However, the solubility coefficient $S$ furthermore depends on the prevailing melt temperature. This can be expressed using an Arrhenius approach [121]:

$$S = S_0 e^{-\frac{\Delta H_L}{RT}}. \tag{8}$$

$S_0$ denotes the solubility extrapolated to an infinite temperature with $\Delta H_L$ as the solution enthalpy, $R$ is the ideal gas constant and $T$ is the temperature. The solution of the gas begins at the interface between gas and polymer. The gas must subsequently diffuse through the polymer melt in order to obtain a uniform solution of the gas in the polymer [122]. The diffusion is based on concentration differences and can be described by the first Fick's law assuming a one-dimensional diffusive mass flow [112] as

$$\frac{dm}{dt} = -D_{diff} A \rho \frac{dC}{dx}. \tag{9}$$

According to Equation 9, the diffusive mass flow $dm/dt$ in x-direction depends on the diffusion coefficient $D_{diff}$, the diffusion cross section $A$, the density $\rho$ and on the concentration gradient $dC/dx$. If the saturation limit is approached, the concentration gradient decline leads to a decrease of the diffusive mass flow. Similar to the solution coefficient $S$, the diffusion coefficient $D_{diff}$ is temperature dependent and can be described by an Arrhenius equation [112, 123, 124]:

$$D_{diff} = D_{diff,0} e^{-\frac{G_D}{RT}}. \tag{10}$$

$D_{diff,0}$ corresponds to the diffusion coefficient at infinite temperature while $G_D$, $R$ and $T$ correspond to the activation energy of the diffusion, the general gas constant and the temperature. According to Equation 10, the diffusion coefficient increases with growing temperature due to Brownian motion of both the gas and the polymer [112]. Thus, a high pressure and melt temperature favours the solution of gas in the polymer melt. However solution and diffusion are opposing mechanisms that may lead to different resulting gas concentrations depending on the type of gas used [47]. For instance, an increase of temperature leads to growing solubility of $N_2$ in polypropylene whereas the solution of $CO_2$ decreases [125]. The diffusion and solution of gas in polymer melts can be further improved if the gas is added in supercritical state which requires the gas to surpass both the critical temperature $T_c$ and critical pressure $p_c$ [47]. The temperature and pressure dependent phases of a gas, including the critical point (CP), are schematically depicted in Figure 17.

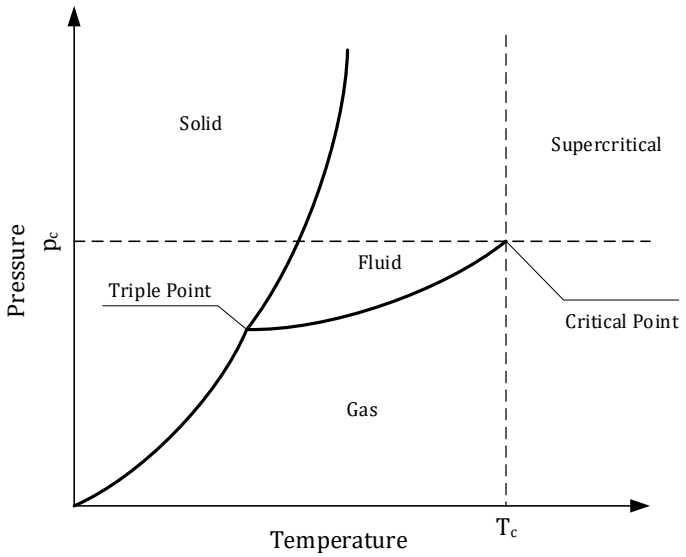


| Properties at critical point | $N_2$ | $CO_2$ | Dimension |
|---|---|---|---|
| Temperature | -147 | 31 | °C |
| Pressure | 34 | 74 | bar |
| Density | 0.31 | 0.47 | g/cm³ |

Figure 17: Schematical representation of a pressure-temperature (p-T) phase diagram of a gas [126] (left) with an overview of critical point properties of $CO_2$ and $N_2$ (right).

These requirements are usually satisfied during injection moulding with $N_2$ since the typical pressures and temperatures during processing usually exceed the critical values, see Figure 17 (right) [112]. Foam injection moulding technologies based on physical blowing agents utilise this effect [126].

After achieving a single-phase polymer-gas mixture, the latter is injected into the mould initiating the foaming process. Therefore, the melt must generally be subject to a temperature increase, a

pressure drop or a combination of both and subsequently be able to increase its volume during foaming [127, 128]. In foam injection moulding practice, usually the pressure drop in the mould cavity leads to the nucleation of foam cells [112, 129]. The pressure drop induces a change of the thermodynamic equilibrium of the saturated polymer gas solution leading to a decrease of solubility of the gas within the melt [121]. A fraction of the gas is released building nuclei for foam cells.

The foam cell nucleation can be divided into homogenous and heterogeneous nucleation according to the classical nucleation theory [130, 131]. Heterogeneous nucleation characterises the development of nuclei in a single-phase polymer-gas mixture induced by separate phases such as fillers or residues of the decomposition of chemical blowing agents. Homogenous nucleation during foam injection moulding thus only occurs using physical blowing agents with unfilled polymers [112]. According to the classical nucleation theory, stable nuclei require a reduction of free energy $\delta G$ [121, 122]. The free energy change in the system can be described in accordance with the nucleation of crystalline structures, see Equation 4, as

$$\delta G = V\Delta G + A_i\gamma_i. \tag{11}$$

The foam cell with volume $V$ and surface $A_i$ is subject to a pressure gradient $\Delta p$ between the pressure inside the cell and the surrounding polymer-gas solution and exhibits a surface tension $\gamma_i$. Considering that during the development of the foam structure the creation of ball shaped cells is most probable due to the resulting minimal surface tension [121], Equation 11 can be written with $\Delta G = \Delta p$ as

$$\delta G = \frac{4}{3}\pi r^3 \Delta p + 4\pi r^2 \gamma_i. \tag{12}$$

After nucleation, growth of existing nuclei occurs if the developing cells exceed a critical cell size [123, 132]. According to Leung and Vieth [123, 124], the precondition of successful cell growth is attributed to the free energy barrier for heterogeneous as well as homogenous nucleation, for which the critical cell radius $r_c$ can be determined based on the derivative of Equation 12 [112] as

$$r_c = -\frac{2\gamma_i}{\Delta p}. \tag{13}$$

If the size of a foam pore exceeds the critical radius, it is nucleated followed by cell growth. If it is smaller, the nucleus collapses, see Figure 8. The critical cell radius is identical for homogenous and heterogeneous nucleation, whereas the free energy barrier is smaller for heterogeneous nucleation [121, 123]. Hence, the probability of reaching the critical cell radius is higher in case of heterogeneous nucleation, which leads to an increased number of nuclei. The cell growth continues until an equilibrium of forces developed between the gas pressure within the cell and its surface tension [122]. The equilibrium of forces leads to Equation 14, combining the cell surface tension $\gamma_i$, the inner pressure $p_{in}$ as well as the radius of the cell $r_{cell}$ [112] to

$$p_{in} = \frac{2\gamma_i}{r_{cell}}. \tag{14}$$

Assuming an equal surface tension, this results in a larger inner pressure $p_{in}$ of smaller pores compared to larger pores, resulting in the diffusion of gas from small into large pores. This leads to the growth of the large pores and to an increase in the size imbalance of cells in a foam. Since the diffusion is time-dependent, a very rapid pressure drop can inhibit the diffusion of gas to existing nuclei and favourably induce the development of new cell nuclei which results in a more fine and homogenous foam morphology [119]. Furthermore, a rapid cooling of the foam melt is beneficial, since the viscosity $\eta$ is an important factor. According to Stoke's law, the diffusion velocity $v_{diff}$ increases with low viscosity, so that especially at high melt temperatures the gas exchange between cells is enhanced [112]. With the gravitational acceleration $g$, this leads to:

$$v_{diff} = \frac{g \cdot (2r_{cell})^2}{18\eta} \Delta\rho. \tag{15}$$

After the nucleation and growth of the foam cells, the cooling of the polymeric foam finally leads to a solidification and stabilisation of the foam morphology [133, 134]. The foam injection moulding process is completed with this last step and the component can be demoulded.

The initiation of the aforementioned mechanisms requires a pressure drop, wich can be achieved using two different methods. The conventional foam injection moulding is based on a partial filling of the cavity volume with gas-loaded melt leading to low cavity pressures, see Figure 18. Hence, this method is called low-pressure foam injection moulding process. The cavity is only filled resulting from the growth of foam cells initiated by the pressure drop of the single-phase polymer-gas mixture after injection into the cavity. This method does neither pose specific requirements to the injection moulding machine nor tool, except for a shut-off nozzle. However, the resulting foam structure varies with the flow length.

In recent years, the high pressure foam injection moulding method has emerged, leading to disctinctly higher cavity pressures, see Figure 18. Here, the gas-loaded polymer melt fills the mould completely during injection moulding. An increase of cavity volume shortly after its complete filling induces the required pressure drop followed by the growth of cells and the creation of the foam.

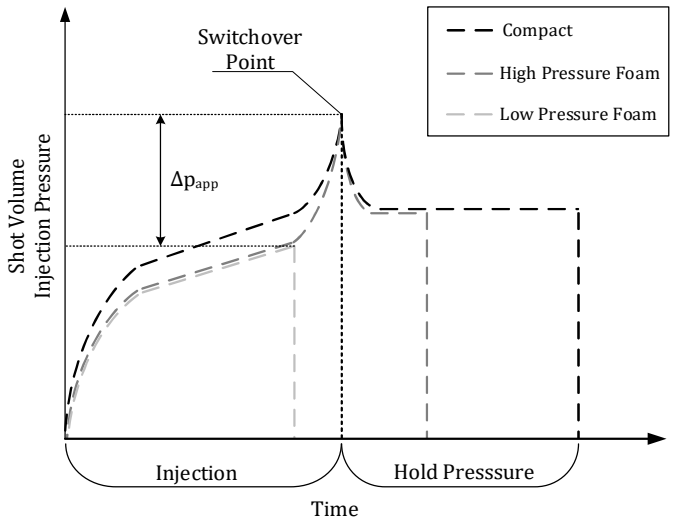


Figure 18: Qualitative pressure profile during injection moulding of compact components, foam injection moulding using the high pressure and low pressure process variant (based on [47]).

This foam injection moulding variant enables higher density reductions compared to the low-pressure process and it avoids flow length dependencies of the foam morphology [47]. However, high requirements regarding the machine and the mould are imposed in order to enable a controlled cavity increase during manufacturing of the foamed component. Due to these constraints, the low-pressure method is used for the manufacture of in-situ CFRTP sandwich components in this work.

### 2.4.2. Fusion Bonding of Miscible Thermoplastic Interfaces

The second process included in the in-situ manufacture of CFRTP sandwich components is the overmoulding technique of CFRTP material, which involves fusion bonding between the overmoulded structures and the CFRTP substrate. Fusion bonding of two polymeric surfaces and the resulting stress transfer at the interfaces is generally described by the intimate contact of the polymer surfaces and the subsequent diffusion of polymer chains across the interface, also known as autohesion or healing, see Figure 19 [135–155].

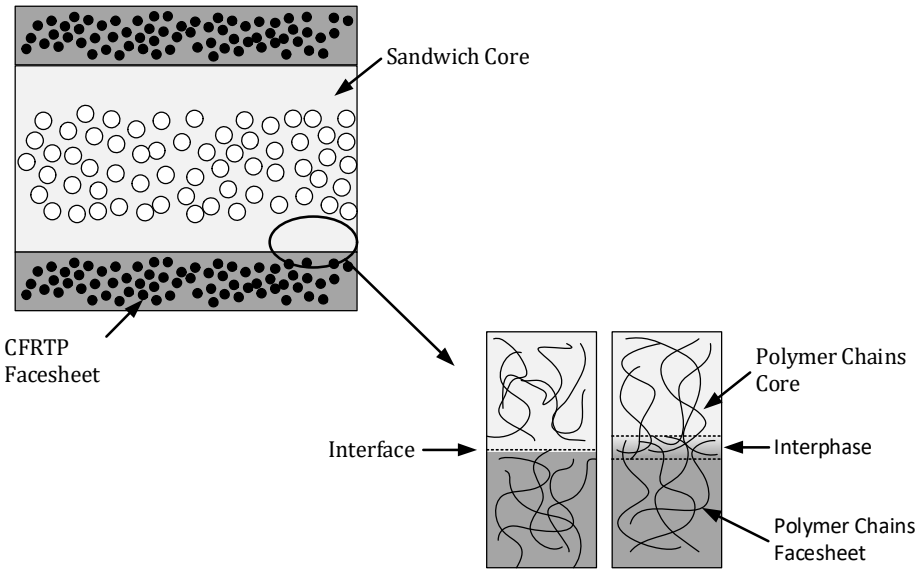


Figure 19: Process of diffusion based bonding of miscible thermoplastics. After two thermoplastic surfaces achieved intimate contact, polymer chains can diffuse across the interface and entangle. As a result, an interphase is formed that affects the interfacial strength (modified from [15]).

These steps during fusion bonding as well as a phenomenological overview of the process and the effects of material and process parameters on the resulting interfacial bonding between the adherents is presented in the following sub-chapters.

#### *Intimate Contact*

The generation of intimate contact is a prerequisite for diffusion processes between the polymer interfaces [15, 16, 156, 157]. Intimate contact is achieved if two polymer interfaces are in direct and perfect contact to each other. The fraction of the area in perfect contact in relation to the total interface area is defined as the degree of intimate contact $D_{ic}$ [147, 158]. As solid polymeric interfaces do not have perfectly flat surfaces, the initial intimate contact is incomplete. One of the

most important parameters for the generation of intimate contact is thus the initial surface roughness of the interfaces [14, 159]. With increasing heat and pressure, the polymer interface asperities are flattened due to the viscous flow of the polymer, thus increasing the degree of intimate contact [145]. Modelling approaches for the intimate contact generation during processing consequently consider the surface asperity geometry. While the first model of Dara and Loos [158] incorporates the surface geometry via a statistical distribution of rectangles with different width and height, Lee and Springer [160] simplify the model considering all surface asperities as uniform rectangles, see Figure 20.

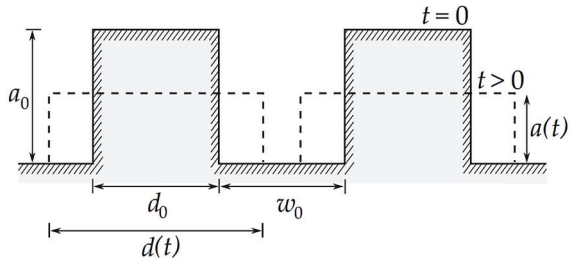


Figure 20: Simplified model of surface asperities of an initially solid fusion bonding adherent [16]: the initial surface asperity (indicated by grey rectangles) is flattened (indicated by dotted lines) due to the applied pressure and temperature during the bonding process.

These are described via the initial uniform width $d_0$, the initial uniform distance between the asperities $w_0$ and the initial uniform asperity height $a_0$. The degree of intimate contact at times $t > 0$ yields

$$D_{ic}(t) = \frac{d(t)}{d_0 + w_0}. \tag{16}$$

Using confocal microscopy, it is possible to determine the initial surface roughness of the interface and thus to use measured surface data for the modelling of the development of intimate contact [16]. Considering one-dimensional laminar flow of the rectangles and the conservation of mass, the evolution of intimate contact can be modelled according to Mantell and Springer [145] as

$$D_{ic}(t) = D_{ic,0}\left[1 + 5\left(1 + \frac{w_0}{d_0}\right)\left(\frac{a_0}{d_0}\right)^2 \int_0^{t_c} \frac{p_{app}(t)}{\eta_0(T(t))} dt\right]^{1/5}. \tag{17}$$

According to Equation 17, the material and process parameters which significantly influence the intimate contact development are the surface geometry of the interfaces denoted by the geometry parameters $w_0$, $d_0$and $a_0$ as well as the process paramters temperature $T$, contact pressure $p_{app}$, zero shear viscosity $\eta_0$ and time $t$ [145, 159–162]. In the case of overmoulding of a solid polymer based substrate with a hot polymer melt however, it is commonly assumed that intimate contact is achieved almost instantly due to the high pressure and low viscosity of the polymer melt combined with high melt temperatures [14, 159, 163].

### *Healing of Miscible Interfaces*

When two amorphous thermoplastic interfaces are brought in intimate contact, polymer chains diffuse across the interfaces due to Brownian motion [16, 164]. This diffusion process of amorphous polymer chains is generally described by the reptation theory according to de Gennes [165] based on an earlier work of Edwards [166]. According to Edwards, polymer molecules are constraint within a tube surrounded by other macromolecules. The reptation theory of de Gennes further introduces the reptative movement of the polymer chain of total length $L$ within and along the tube based on Brownian movement surrounded by an amorphous polymer bulk under isothermal conditions, see Figure 21 [14, 138].

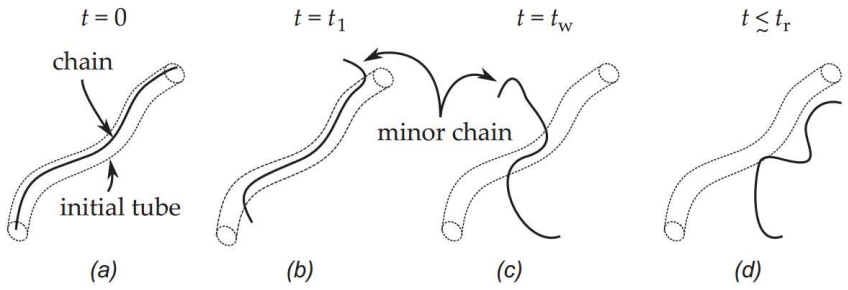


Figure 21: Polymer chain movement resulting from Brownian motion based on the reptation theory [16]: at times greater than $t_0$, the minor chains begin to emigrate from the tubes (b and c) until they completely escaped the original tube at the reptation time $t_r$ accompanied with losing the memory of its initial alignment (d).

With proceeding time, the chain ends can partially escape the tube, forming the minor chains. The length of the minor chains $l$ growths with increasing time until the whole chain escaped the tube at the reptation time $t_R$, also losing memory of its original tube [167]. Kim and Wool [148] extended the reptation model to the minor chain model describing the diffusion of polymer chains at interfaces between amorphous polymers. According to an earlier work of Wool and O'Connor [150], this process can be divided into 5 steps:

1. Rearrangement
2. Surface approach
3. Wetting
4. Diffusion to a distance $\chi$
5. Diffusion to an equilibrium distance $\chi_\infty$ and randomisation

The minor chains can diffuse across the interface resulting in the interpenetration depth $\chi$, which contributes to the creation of a load path across the polymer interface [167]. The former polymer interfaces gradually disappear and finally become indistinguishable from the bulk polymers [168]. The strength across the interface thus created is proportional to the interpenetration distance $\chi$, which is also proportional to the minor chain length $l$ [113]. Consequently, the interface strength increases with growing interpenetration depth and minor chain length, reaching a maximum at reptation time $t_R$ at which an equilibrium interpenetration depth $\chi_\infty$ is achieved, see Figure 22 [167, 169].

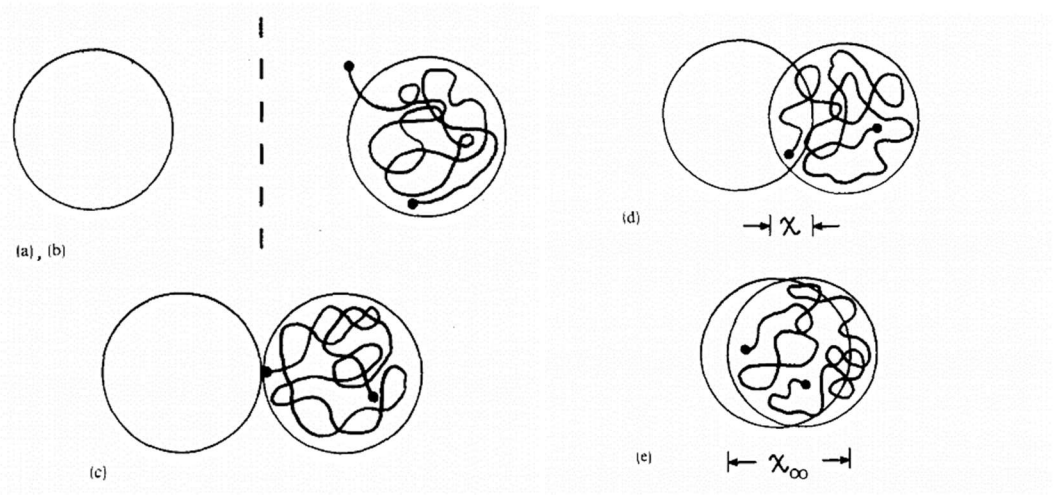


Figure 22: 5 steps of interfacial strength development during fusion bonding of polymeric interfaces according to Wool and O'Connor [150]: (a) rearrangement and surface approach followed by wetting of the surfaces (c). Subsequent diffusion of polymer chains (d and e) and randomisation (e) enables interfacial bonding.

The healing process can be described as the ratio of current to maximum interface strength and fracture toughness via the degree of healing. This ratio is correlated to the relation of current to maximum interpenetration depth $\chi(t)$ and $\chi_\infty$, minor chain length $l(t)$ to polymer chain length $L$ and process time $t$ to reptation time $t_R$ [149, 165, 167]. Considering healing as mechanism enabling the development of stress transfer across an interface, the isothermal development of interfacial strength $\sigma(t)$ and fracture toughness $G(t)$ can be described as

$$D_h(t) = \frac{\chi(t)}{\chi_\infty} = \left(\frac{l(t)}{L}\right)^{1/2} = \left(\frac{t}{t_R}\right)^{1/4} = \frac{\sigma(t)}{\sigma_\infty} = \left(\frac{G(t)}{G_\infty}\right)^{1/2}. \tag{18}$$

As most polymer processing techniques exhibit temperature changes during processing, Bastien and Gillespie adapted this model for non-isothermal healing of amorphous polymer interfaces [146]. They divided the process into $q$ time intervals with $q = t/\Delta t$ at which the process temperature is approximated as the isothermal mean temperature $T^*$ during the respective time steps $t_i$ and $t_{i+1}$. The development of interfacial strength $\sigma(t)$ and the degree of healing $D_h(t)$ thus calculates as

$$\frac{\sigma(t)}{\sigma_\infty} = D_h(t) = \sum_{t=0}^{t/\Delta t}\left[\frac{t_{i+1}^{1/4} - t_i^{1/4}}{t_R^{*1/4}}\right]. \tag{19}$$

The fracture toughness development $G_c(t)$ of an interface during non-isothermal fusion bonding yields

$$\frac{G_c(t)}{G_{c,\infty}} = D_h(t)^2 = \sum_{t=0}^{t/\Delta t}\left[\frac{t_{i+1}^{1/4} - t_i^{1/4}}{t_R^{*1/4}}\right]^2. \tag{20}$$

According to Equations 19 and 20, the thermal history as well as the temperature dependent reptation time are required for the calculation of $D_h$. The reptation time can be assessed using different methods. A first route is based on mechanical experiments and Arrhenius relationships, which was followed by Bastien and Gillespie [146] for the fusion bonding of AS4/PEEK composites. The assessment of the reptation time using mechanical experiments however is complex and the determined reptation time curves can be considered comparatively sensitive to the experimental set-up. The reproduction of results is therefore a challenge. Other authors determine the reptation time by rheological experiments using a parallel plate rheometer (frequency sweep test), neglecting the polydispersity of the polymer material. Here, the critical angular frequency i.e. the critical shear rate is determined, which is the onset of non-linear melt viscosity [105, 153].

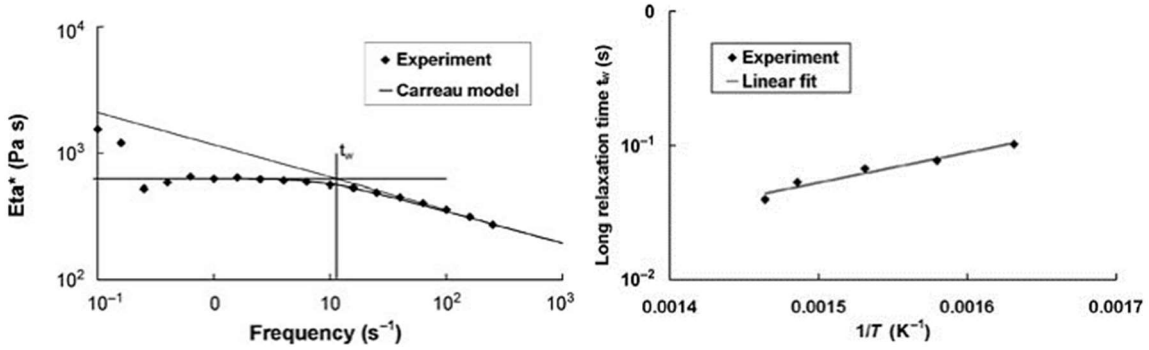


Figure 23: Reptation time assessment for PEEK based materials based on rheological experiments according to the Carreau Model (left) and subsequent fitting using an Arrhenius approach (right) [153].

At low shear rates, the melt behaves like a Newtonian fluid. At the critical shear rate, the shear properties of the melt become nonlinear, shear-thinning occurs [170]. The point of change from Newtonian to nonlinear viscosity behaviour of the polymer melt denotes the relaxation time or reptation time respectively [153]. After determining the reptation time for different temperatures, an Arrhenius equation provides a continuous description of the temperature dependent reptation time, see Figure 23. However, the rheological assessment of the reptation time is limited to the temperature range in which the thermoplastic is in a molten state. In solid state, the temperature dependent reptation time $t_R(T)$ can be assessed according to Graessley [171] using

$$t_R(T) = \frac{45}{\pi^2}\left(\frac{G_N^0}{cR_GT}\right)^2 \frac{M^3\eta_0(M_c)}{G_N^0 M_c}. \tag{21}$$

Here, the reptation time can be assessed by the plateau modulus $G_N^0$, the molecular weight $M$, the critical molecular weight $M_c$, and the zero shear viscosity $\eta_0$ associated with the critical molecular weight. For the assessment of the aforementioned parameters, it is referred to the relevant literature [172–177].

Considering that intimate contact is a prerequisite for the healing process to take place, authors developed combined intimate contact and healing models. Butler developed a coupled bonding model that predicts the resulting degree of bonding $D_B$ based on the combination of the degree of intimate contact and degree of healing for isothermal processes [143]. A dimensionless parameter $\Omega$

allows for the evaluation of intimate contact or healing dominance of the resulting bonding properties. Yang and Pitchumani [167] extended this degree of bonding model using a non-isothermal degree of healing. The degree of bonding can be calculated with the final bonding time $t_f$ as

$$D_b(t_f) = D_{ic}(0) \cdot D_h(t_f) + \int_0^{t_f} D_h(t_f - t) \frac{dD_{ic}(t)}{dt} dt. \quad (22)$$

At any time $t_f$ during the process, the respective intimate contact at this time $dD_{ic}(t)/dt$ enables the diffusion of chains characterised via the degree of healing depending on the available healing time $D_h(t_f - t)$. The time for healing $(t_f - t)$ is hence reduced by the time at which intimate contact is achieved during the process. This non-isothermal degree of bonding can also be evaluated with respect to the intimate contact or healing dominance by means of a dimensionless fusion bonding number $f_B$. If intimate contact is immediately achieved during processing of polymer interfaces, the degree of bonding equals the degree of healing [178].

According to Wool and co-authors [144, 147] the presented models are only valid for amorphous polymer interfaces. Several authors observed that a direct transfer of the presented fusion bonding models from their original application at amorphous melts to semi-crystalline polymer interfaces does not yield high correlations between model predictions and experimental results [141, 151]. Thus, fusion bonding of semi-crystalline polymer interfaces must also include other phenomena, which are influencing the interfacial strength development. A phenomenological literature overview shall give insight in the non-isothermal fusion bonding behaviour of semi-crystalline polymer interfaces.

### *Influence of Process Parameters on Fusion Bonding of Semi-Crystalline Thermoplastics*

During overmoulding, the CFRTP layers in the mould come in physical contact with the polymer melts. The heat transfer of the hot polymer melt leads to the melting of the CFRTP surface. During this process step, interfacial adhesion is achieved by the diffusion of polymer chains across the interface between injected polymer core and the CFRTP surface. Due to the cooled mould, the melt and thus the interface temperature rapidly decreases leading to the crystallisation of the interface and the solidification of the complete sandwich structure. Contrary to the fusion bonding of amorphous polymers, a distinguishable zone develops during healing of semi-crystalline polymer interfaces which is sometimes called interphase, indicating that this zone exhibits a different morphology [95, 168, 179].

The interphase morphology and the corresponding mechanical properties of fusion bonded semi-crystalline interfaces result from material and process parameters during the bonding process. Here, the time for fusion bonding of semi-crystalline interfaces is of major importance. This is not only the case regarding interfacial strength but also regarding cost efficiency, as the time for manufacture is directly linked to the cost it comes to industrial production. Considering injection moulding based processes, production cycles can be as short as seconds, depending on material, cooling rate and geometry aside others. This is also valid for hybrid injection moulding processes such as overmoulding of CFRTP substrates and in-situ thermoplastic sandwich composite manufacturing methods. It is of major interest, whether the time needed for diffusion of polymer chains is within

these typical processing times in order to provide sufficient interfacial strength of overmoulded structure and solid substrate. According to experimental studies by Lamèthe [154] full healing of PEEK interfaces can be achieved within less than a second. Furthermore, Grouve [16] found that full healing was achieved in less than one millisecond (ms) for thermoplastic tape laying processes with PPS matrix polymer according to calculations using the non-isothermal degree of bonding model of Yang and Pitchumani [140, 167]. Thus, the time needed for bonding should clearly deceed the cycle time of in-situ sandwich composite processing.

The effect of temperature on fusion bonding of two semi-crystalline polymer interfaces includes the interface-temperature that develops during the process as well as the thermal gradient between the adherents. Healing models of polymer interfaces are based on the chain mobility of amorphous polymer structures, which able to move across the interface based on Brownian motion above the glass transition temperature ($T_g$) [167]. $T_g$ represents per definition a singular quantity of an effect that actually spreads along a wider temperature range of amorphous thermoplastics or generally fractions of amorphous structures in polymers. It is denoted by the transfer from brittle energy-elastic to rubbery entropy-elastic mechanical behaviour of the respective polymer when $T_g$ is exceeded [180]. Yang and Pitchumani [140] as well as Awaja [181] assume that healing of semi-crystalline polymer interfaces only occurs if the melting temperature is reached or surpassed and most of the crystalline structures are molten.

However, fusion bond between two thermoplastic surfaces is also possible below their melting temperature. If the melting temperature is considered as threshold of diffusive strength development of semi-crystalline interfaces, this is found to result in an underestimation of bonding when compared with experimental results [136]. Grouve [16] determined, that laser assisted tape laying of UD tapes with polyphenylene sulfide (PPS) matrix on organo sheets with PPS matrix yielded very high interfacial fracture toughness although the melting temperature at the interface was not reached according to thermal simulations. He assumes that the amorphous fraction of the polymer enables sufficient polymer chain mobility for interfacial fusion bonding below the melting temperature $T_{melt}$ of the crystalline fractions. Similar results were found by Stokes-Griffin and Compston [156]. They argue that $T_{melt}$ only denotes the peak endotherm of the melting behaviour, meaning that also between $T_{melt}$ and $T_g$ fractions of the crystal structure with lower melting temperature melt, which can be observed in differential calorimetry (DSC) measurements. This enables a diffusive chain movement of parts of the crystalline fractions of semi-crystalline polymers below the nominal melting temperature. Even below the glass transition temperature, healing of amorphous polymer interfaces was found, however with low bonding strength and necessary bonding times of up to several months [151].

Aside the interface temperature that dominates interfacial bonding development during fusion bonding of polymers, the temperature difference of the adherents has a contributing or detrimental influence on the interfacial bond. Several studies have shown that during fusion bonding of semi-crystalline polymer interfaces, significantly higher interfacial bonding could be achieved if the adherent surfaces do not exhibit the same temperature and thus the presence of a thermal gradient. Aurrekoetxea [182] found higher interlaminar shear strengths of overmoulded thermoplastic composites with increasing thermal gradient between composite and melt. Similar results were yielded by other authors who found that given the same interface temperature, an increasing thermal gradient between the adherents leads to an increase of interface strength [183, 184]. An example for the healing of semi-crystalline interfaces with large thermal gradient is the overmoulding

of a solid polymer-based component, e.g. a non-heated CFRTP base structure with hot polymer melt. During overmoulding, the solid substrate surface melts if the heat energy of the overmoulded polymer melt is sufficient. If both adherent interfaces are in molten state, healing begins followed by co-crystallisation across the former interface. This is induced by the thermal gradient, as the solid substrate serves as nucleation aid and the crystalline structure grows in direction of the thermal gradient in thickness direction creating a strong interfacial bond [139, 168, 182–184]. The assumed mechanism behind the advantageous effect of the thermal gradient on the fusion bonding behaviour is depicted in Figure 24.

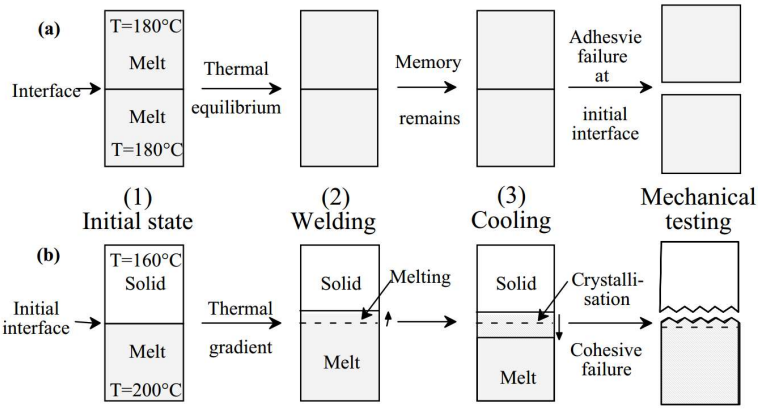


Figure 24: Differences between interfacial bonding resulting from different thermal gradients: both adherents are molten and have the same temperature (a). Their interfacial strength is limited as the molecular memory of the former interfaces is preserved. Solid and molten adherents with high thermal gradient result in the melting of interface near areas of the solid adherent and subsequent crystallisation leading to a new interphase morphology with increased interfacial bonding [168] (b).

Kausch et al. [168] argue that when two semi-crystalline polymer interfaces are brought into contact at the same temperature above their melting temperature, the crystalline structure of the adherent interfaces remains similar due to a morphological memory effect. This leads to a reduced interfacial strength when the thermal gradient is small or non-existent although both adherents exhibit temperatures above $T_{melt}$. If in contrast two semi-crystalline polymer interfaces with high thermal gradient are subject to fusion bonding, the resulting interface strength is higher compared to the one with a low thermal gradient of adherents although the same interface temperature prevails.

In conjunction with the temperature, the crystallinity of the polymer interfaces must be considered with respect to the fusion bonding process due to involvement of the Brownian motion. This is because diffusive movement of polymer chains across the interface and their subsequent entanglement is necessary for interfacial strength development. The diffusion however is inhibited by the presence of crystalline fractions at the interfaces of the adherents [16, 136, 141, 178]. Boiko et al. [141] found that for the same processing conditions, the interface strength of fusion bonded amorphous/amorphous as well as amorphous/crystalline adherents is one order of magnitude higher compared with semi-crystalline/semi-crystalline adherents. Similar results were found by Grouve [16] who observed that interfacial strength development decreased with increasing degree of crystallinity. In case of overmoulding of a solid semi-crystalline polymer interface or a CFRTP with an amorphous melt, the crystalline fractions consequently denote a bottleneck for fusion bonding since they reduce the chain mobility across the interface, see Figure 25. If the heat energy of the

overmoulding polymer mass is insufficient to melt the crystalline fractions of the solid adherent, the bonding strength is reduced [141].

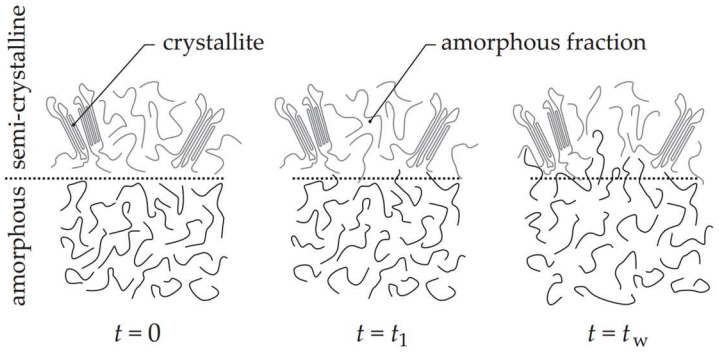


Figure 25: Crystalline fractions hinder diffusive molecular movement during healing of two semi-crystalline polymer interfaces [16].

Consequently, dominant factors for the successful fusion bonding of miscible polymer interfaces are found to be the resulting interface temperature and the temperature gradient between the polymer adherents as well as the crystallinity of the polymer matrix, especially at the very surface [139].

## 2.5. Flexural Behaviour of Thermoplastic Sandwich Structures with Integral Foam Core

The mechanical characterisation of heterogeneous structures is based on their constituents, their distribution within the structure and their geometry. Considering polymeric integral foams as two-phase-systems comprising the polymer and the foam cells, the mechanical characterisation focuses on the incorporated voids reflected by a variety of parameters. According to Tissandier et al. [185] these parameters mainly include:

- Cell diameter
- Cell density
- Density reduction

Regarding integral foams, these parameters are location-dependent since the integral foam exhibits a variable morphology in thickness direction [112]. It is assumed that for mechanical modelling, especially with respect to moduli, the density or the density distribution is sufficient and the microscopic foam morphology parameters such as cell diameter, cell size distribution and cell shape play a minor role [185–187]. In the following sections, the simplified modelling of integral foams and hence of the core of in-situ sandwich structures is presented. It is divided into the modelling of the structural composition and flexural rigidity of integral foams based on their density profile as well as the determination of the Young's modulus of integral foams.

### 2.5.1. Simplified Modelling of Integral Foams: Flexural Rigidity

Different models can be used to describe the structural composition and the resulting flexrual rigidity of integral foams according to their density distribution in thickness direction, see Figure 26. The

density profile model of Rodrigue [187, 188] denotes a continuous model, which includes the actual density of integral foams into the calculation of the flexural rigidity. Here, the modulus $E(z)$ is not constant but dependent of the $z$ location. This model was found to yield high correlations with experimental results [188], however the density profile must be known and the accuracy of the density measurement is directly correlated with the prediction accuracy of the model. The density assessment is usually achieved using X-ray density profilers or µCT analysis after the manufacture of the integral foam component [185, 189]. A precise determination of the local density is necessary for the density profile models, which makes this characterisation of integral polymeric foams complex and time-consuming.

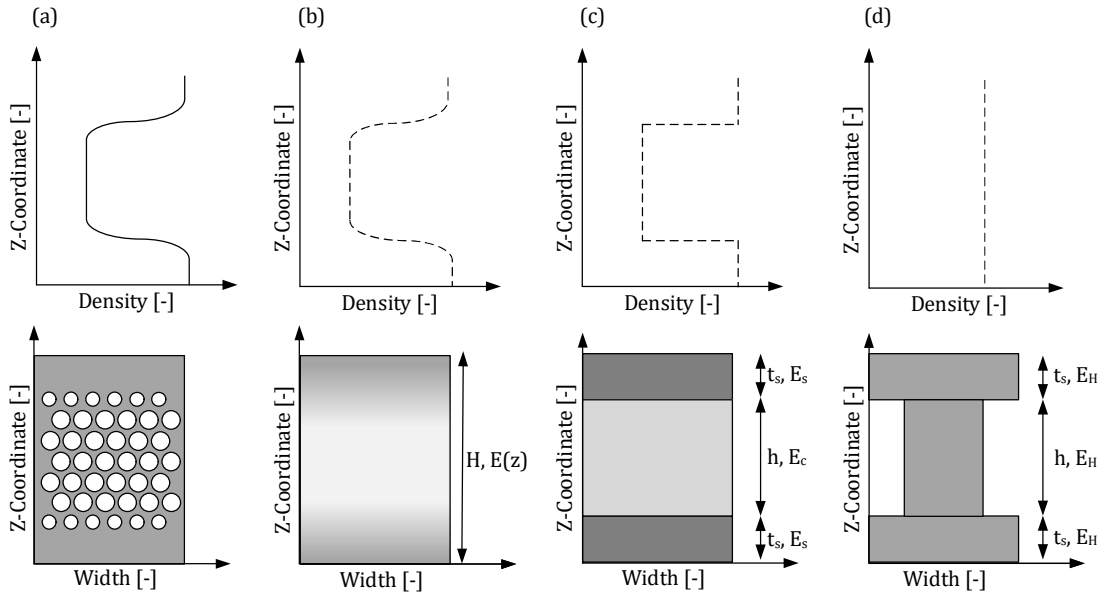


Figure 26: Real density distribution and structural composition of an integral foam (a) and different simplifying approaches for the modelling of its mechanical behaviour. Continuous modelling of the density according to Rodrigue [187, 188] (b) is complex and hence models with simplified structural composition are often used, such as the layered composition with layer-specific constant moduli [190] (c) or the equivalent one-beam model which assumes constant moduli yet different widths of the layers [191] (d).

In order to reduce this complexity, different models exist which apply simplifying assumptions. The equivalent one-component beam model of Hobbs [191] approximates the sandwich structure of integral foams using equivalent beams with constant modulus $E_H$ and varying width. Different equivalent beam geometries attribute to the respective density profile. Contrary to the Hobbs approach, the I-beam model of Gonzales [190] approximates the integral foam density profile based on a three-layer model with different moduli in each layer. Here the integral foam skin is assumed solid whereas the core is homogenised resulting in an average core density and modulus. The calculation of resulting flexural rigidities according to the model is based on the Euler-Bernoulli beam theory, including the corresponding simplifying assumptions. For a detailed discussion of the Euler-Bernoulli beam theory it is referred to relevant literature [192]. Using constant moduli of the foamed core $E_c$ and the solid core-skin $E_s$, this leads to the flexural rigidity of the integral foam as

$$\overline{EI} = E_c I_c + 2 \cdot E_s I_s. \tag{23}$$

If the width $W$ of the core and the facesheet is equal, the second moment of inertia of core $I_c$ and solid skin respectively $I_s$ is calculated as

$$I_c = \left[\frac{Wh^3}{12}\right], \tag{24}$$

$$I_s = 2\left[\frac{W{t_s}^3}{12} + \left(\frac{h}{2} + \frac{t_s}{2}\right)^2 W t_s\right]. \tag{25}$$

The I-beam model is frequently used for the simplified modelling of integral foams and yields high correlations with experimental results in other studies [47, 112]. Therefore, it builds the foundation for the modelling of the integral foam cores of in-situ CFRTP sandwich structures in chapter 7.2.

### 2.5.2. Simplified Modelling of Integral Foams: Assessment of Moduli

For the characterisation of an integral foam according to Equation 23, the determination of the modulus of the foam core $E_c$ is necessary. The assessment of mechanical properties and specifically of different moduli of foam structures is based on the general mixing rule (GMR) [47, 112, 187]. It enables the assessment of Young's moduli of heterogeneous materials and structures $E_h$ based on the specific moduli of the constituents $E_1$ and $E_2$ as well as the volume fraction of the second constituent $\varphi$ [187]:

$$(E_h)^p = \varphi(E_2)^p + (1-\varphi)(E_1)^p. \tag{26}$$

Here, the exponent $p$ can result from various parameters, such as Poisson's ratio, geometrical properties or orientations [193, 194]. Based on the GMR, foams can be characterised as a 2-part composite consisting of the polymer matrix with modulus $E_m$ and the incorporated pores with modulus $E_{cell}$ equal to zero [187]. This leads to the Young's modulus of a polymer foam $E_c$ as

$$(E_c)^p = \varphi(E_{cell})^p + (1-\varphi)(E_m)^p \approx (1-\varphi)(E_m)^p. \tag{27}$$

Here, $\varphi$ denotes the void fraction $v$ of the foam. Furthermore, the void fraction equals the total density reduction $\Delta\rho$ defined as the ratio of foam density $\rho_f$ and compact polymer density $\rho_m$ [112, 187] leading to

$$\varphi = v, \qquad v = \left(1 - \frac{\rho_f}{\rho_m}\right) = \Delta\rho. \tag{28}$$

Combining Equations 27 and 28 yields

$$E_c = E_m(1-\Delta\rho)^n, \tag{29}$$

$$n = \frac{1}{p}. \tag{30}$$

The variation of the exponent $n$ enables an adaptation of the model to experimentally determined moduli of different foam structures, as well as the introduction of additional structural parameters to the model other than the void content [187, 195, 196]. Hobbs [191] applied an exponent value of $n = 1$, whereas for spherical cells Moore et al. [197] proposed $n = 2$. According to Altstädt [112], a value of $n = 2$ is recommended for very thick foam structures whereas for very thin structures a value of $n = 1.5$ yields high correlations with experimental results.

Based on the presented models for the prediction of elastic moduli of integral foam structures, models for the prediction of the flexural rigidity of in-situ CFRTP sandwich structures shall be developed and validated in this work.

## 2.6. Conclusion

This chapter presented an overview of the in-situ manufacture of full thermoplastic sandwich structures with integral foam core and CFRTP facesheets, based on polypropylene as core and facesheet matrix polymer respectively. After a first review of materials and processes for the manufacture of full thermoplastic sandwich structures, the in-situ process was introduced in detail. Two aspects of the process and of the manufactured in-situ sandwich structures were taken into focus:

- Development of integral foam morphology
- Development of interfacial bonding

A literature review was presented to give insight into the main mechanisms behind these critical aspects of in-situ CFRTP sandwich manufacture. According to the classical nucleation theory, the development of the foam morphology was found to result from the nucleation of foam cells from a single-phase polymer gas mixture, which can be achieved using chemical or physical blowing agents. The second aspect of interfacial strength development between facesheet and injected foam core was found to be based on the diffusive polymer chain movements across their interface and relevant material and process parameters were identified.

Furthermore, different model-based approaches to predict the interfacial bonding as well as the resulting mechanical properties of an integral foam core were presented. The interfacial bonding can be described using the reptation theory, which allows for the prediction of bonding development in dependency of the material and process parameters. The continuous integral foam structure and its mechanical behaviour can be characterised via its density profile in thickness direction.

Based on the presented state of the art, it can be concluded that neither do studies exist which focus on the bonding development during the manufacture of in-situ CFRTP sandwich components nor do allow for a model-based prediction of the interfacial bonding. Furthermore, the lightweight design as well as mechanical characterisation methods of in-situ sandwich structures need to be evaluated and developed, respectively.

Hence, the necessity for a fundamental study of mechanisms and relationships during the manufacture of in-situ sandwich structures is demonstrated. The findings of these chapters will be combined and thus enable the development the targeted methodology for the prediction of interfacial bonding and flexural properties of in-situ sandwich structures based on material and

process parameters. This shall facilitate the pre-design of new CFRTP sandwich components based on the in-situ process.

# 3. Interfacial Bonding Test Methods for Thermoplastic Sandwich Structures

The interfacial bonding of facesheet and core in sandwich structures is fundamental in order to enable the use of their full mechanical and lightweight design potential. However, the manufacture and the evaluation of the interfacial bonding poses a major challenge for any sandwich structure. Wiedemann [37] points out:

> *„The most difficult task of the sandwich technology lies in the proper manufacture and testing of the bonding between core and facesheets".*

The evaluation of the interfacial bonding between CFRTP facesheets and injected core is essential for the analysis of the in-situ CFRTP sandwich process and optimisation thereof with respect to the mechanical properties of the manufactured components.

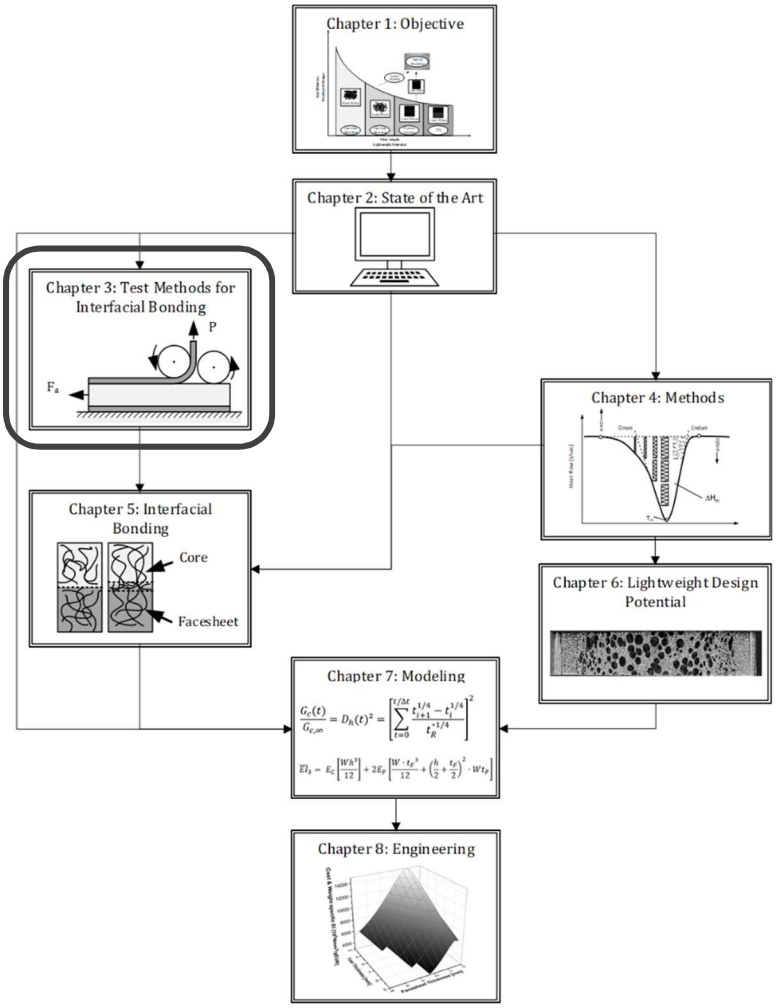


Figure 27: Systematic approach of this work: chapter 3 gives an overview of interfacial bonding test methods and discusses their valid applicability on in-situ sandwich structures.

Testing the interfacial bonding of composite sandwich structures involves a large spectrum of possible methods and set-ups [198–215]. They can be divided into test methods for the assessment of interfacial fracture toughness as resistance to debonding and interfacial strength as resistance to

failure due to interlaminar stresses. Contrary to monolithic structures however, no specific variants have yet been established for sandwich structures [216, 217], especially with integral foam structure. Thus, the specific requirements on a valid test method, which shall be used in the present work, are first presented in chapter 3.1. Subsequently, an overview of current methods to test and evaluate the interfacial bonding between facesheet and core of sandwich structures is presented. The following chapter 3.2 and chapter 3.3 focus on the assessment of interfacial fracture toughness and interfacial strength, respectively. In chapter 3.4, the test methods are evaluated with respect to the requirements and the best-rated testing procedures are selected for use in this work.

## 3.1. Requirements and Constraints

Test methods used in this work for the assessment of interfacial bonding between CFRTP facesheets and injection moulded cores of in-situ CFRTP sandwich structures are required to fulfil the following requirements:

1. Generation of related test values
2. Avoidance of high peel angles
3. Avoidance of high point or line loads
4. Ease of preparation, execution and evaluation

The first requirement attributes to the need of a valid comparison of results between different sandwich geometries as well as material combinations in order to enable a detailed investigation of the interfacial bonding mechanisms. In addition, a comparison with literature results is beneficial. For this purpose, related properties such as stresses and toughnesses are therefore required as testing result.

The second requirement is imposed due to the thin CFRTP facesheets of the in-situ sandwich structures. The use of thin facesheets for sandwich structures may lead to high peel angles. If the interfacial bonding exceeds a certain value, the peel angle becomes large enough to induce severe strain on the facesheets material due to the low intrinsic flexural rigidity of thin facesheets. This may result in fibre kinking and fibre damage of the CFRTP facesheets. In combination with the tensile load during peel-off, this ultimately leads to facesheet failure instead of face to core failure [16, 95].

Similarly, the load application by compressive or bending loads may result in invalid failure of the sandwich structure due to high line loads (requirement 3). The load application with stamp devices for bending based test procedures may lead to indentation of the load application and the support respectively into the facesheets and the sandwich structure in general. Superimposed with compressive stresses resulting from the bending load, this can lead to a micro stability failure of the fibres in the facesheets, consequently leading to strength failure resulting from the imposed shear [8, 218]. This issue is well known for testing of bending behaviour of thermoplastic composites with low modulus matrix material, such as polypropylene. Indentation of load applications in a sandwich structure with foam core foundation is expected to be even more critical due to the compliance of the core. Thus, it must be ensured that the failure occurs within the face to core interfacial region.

At last, the testing procedures should be time-efficient with respect to specimen manufacture, test preparation and execution, which is reflected in requirement 4. The manufacture based on the in-situ process should optimally lead to ready-to-use test specimens. The test preparation should avoid

adhesives, as this is critical with polyolefin polymers such as polypropylene. Complex geometrical fixations instead of adhesives should also be avoided due to the induced preparation effort.

In the following chapters 3.2 and 3.3, a critical discussion is presented of the applicability of state of the art testing methods on the study of interfacial bonding of thermoplastic in-situ sandwich structures with CFRTP facesheets and integral foam core. This is followed by an evaluation of the methods with respect to the requirements and the selection of the best rated testing procedures in chapter 3.4.

## 3.2. Interfacial Fracture Toughness Test Methods

The fracture toughness of a homogenous or heterogeneous material can be quantified based on linear elastic fracture mechanics (LEFM). The LEFM assumes that the fractured material deforms in accordance with linear elasticity and plastic deformations are considered negligibly small [219]. The fracture of structures can be divided into three modes according to the type of crack opening, see Figure 28 [219, 220], into:

- Mode I (opening of crack faces)
- Mode II (shearing of crack faces)
- Mode III (tearing of crack faces)

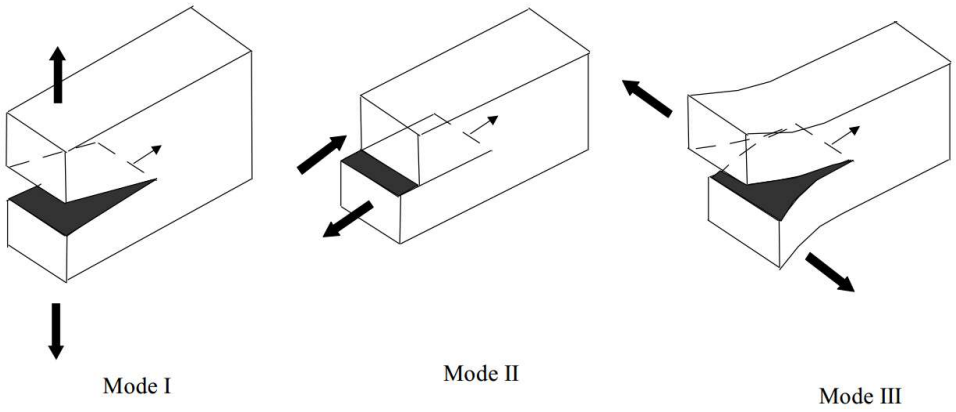


Figure 28: Types of fracture depending on the crack opening mechanism: opening of crack faces is attributed to Mode I, while shearing and tearing is assigned to Mode II and Mode III respectively [154].

The crack growth can be described based on the strain energy release rate $G$. The strain energy release rate is calculated from the released potential energy $d\Pi$ referred to the infinitesimal crack surface area $dA$ or to the crack length $da$ [219]:

$$G = -\frac{d\Pi}{dA}, \qquad G = -\frac{d\Pi}{da}. \tag{31}$$

An interpretation of the strain energy release rate is given by Griffith [221], assuming that crack propagation occurs, if the energy required for this equals the released energy at break [219].

In literature, several test methods have been proposed and studied to quantify the skin-core interfacial fracture toughness of sandwich structures. They usually examine the fracture toughness

via the critical strain energy release rate in Mode I, Mode II or combined in mixed mode. Without raising claims to completeness, they include:

- Mode I:
    - Climbing drum [212, 222]
    - Double cantilever beam [223–226]
    - Single cantilever beam [202, 227–230]
- Mode II & Mixed Mode:
    - End notch flexure [198, 216, 231]
    - Modified three point bending [232–234]
    - Tilted sandwich [203, 235–238]
    - Cracked sandwich beam [198, 199, 201, 229, 233, 239]

Pure Mode I behaviour on the crack tip is considered as the most critical due to its crack-opening effect [211, 240, 241]. Furthermore, Mode II test methods often include load applications by bending of the specimen and thus possibly result in high line loads. This shall be avoided as thermoplastic polymers often exhibit low Moduli, leading to indentation of the load application and micro kinking of the facesheets at simultaneous compression stresses which originate from the bending load [8]. Hence, Mode I fracture toughness test procedures appear most promising and are therefore subject to further evaluation.

### 3.2.1. Climbing Drum Peel Test

The climbing drum peel test (CDP) was first standardised in the 1960s [242]. Since then, several variants have been established [243, 244]. The test method is often applied for testing the delamination resistance and face-to-core bonding of sandwich structures respectively [211]. The testing starts with the fixation of the facesheet on a rotating drum, which exhibits a diameter of more than 100 mm, see Figure 29.

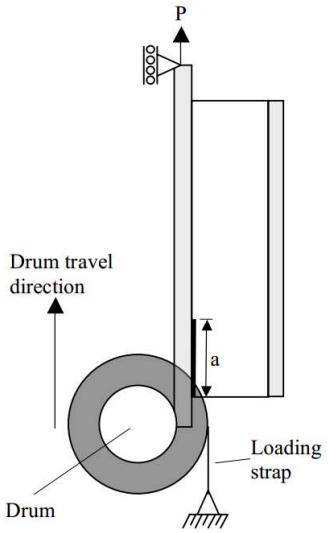


Figure 29: The climbing drum peel test set-up: a rotating “climbing” drum induces the continuous debonding of the facesheet [211].

During testing, the drum rolls along the sandwich length while peeling off the facesheet. Here, the peeling angle is defined by the drum radius, which avoids extensive bending of the facesheets during the test. An unfavourable characteristic of the CDP is that the testing apparatus and the necessary specimen are both considerably large. The specimen length is usually larger than 300 mm, making specimen preparation with injection moulding based processes complicated with respect to the therefore required size of the injection moulding machine and mould. Moreover, the applicability of the method is difficult if sandwich structures with thick facesheets need to be tested [211, 222]. However, the results are independent of the facesheets thickness which enables a comparison of sandwich structures with varying thickness [216]. A major drawback is that the results can hardly be compared to other sandwich variants, as the result is a peeling force which does not relate to a peel area [223]. A recently published study however presents the determination of the strain energy release rate $G_I$ based on the CDP [212].

### 3.2.2. Double Cantilever Beam

The double cantilever beam (DCB) is a standardised testing procedure [245] to evaluate the strain energy release rate of unidirectional continuous fibre reinforced plastics with the pre-crack and crack propagation in the middle of the specimen thickness. Used for the testing of a sandwich specimen, the pre-crack and propagation is located at the core-facesheet interface, see Figure 30. The load is applied e.g. by a piano hinge which is attached to the upper facesheets by adhesives or mechanical fixation. The application of transverse loads leads to a Mode I loading of the crack tip with the initial crack length $a$. After exceeding a critical load, the crack propagates yielding the strain energy release rate for the crack onset $G_{I,onset}$ and propagation $G_{I,prop}$. In this work, the fracture toughness during crack propagation is subject of study, therefore $G_{I,prop}$ is denoted $G_I$ henceforth.

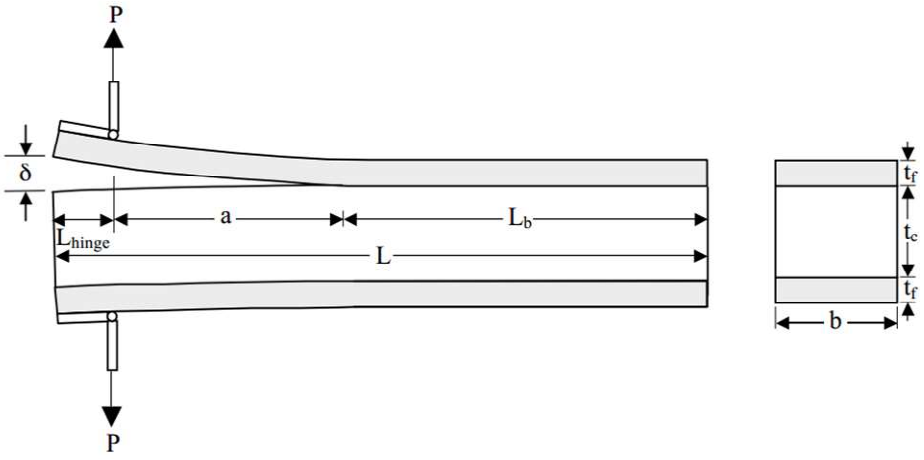


Figure 30: The double cantilever beam used for interfacial testing of sandwich structures: the asymmetric crack location in thickness direction and load application using piano hinges (based on [211]).

Different approaches can be applied for the assessment of strain energy release rates. Most require the specimen width $b$, the applied load $P$, the load point deflection $\delta$ and the crack length $a$ continuously during the test.

The strain energy release rate is calculated e.g. based on the modified beam theory (MBT) as [227]

$$G_I = \frac{3P\delta}{2Wa}. \tag{32}$$

According to Ural et al. [246], the use of the standardised load application fixtures, eg. piano hinges and end blocks may lead to invalid test results due to poor alignment of the load applications on the specimen, local stiffening of the latter due to the additional structure on the specimen and rotation of the specimens. Due to the crack, propagation during testing, the peel angle decreases and the specimen rotates around the axis of the bottom hinge. Also, DCB specimens are subject to bending moments in the core due to the thickness asymmetry of the crack and hence load application [211]. The resulting tensile stresses in the core can lead to crack kinking into the latter during testing [233]. Furthermore, Ural et al. [246] found that the strain energy release rate depends on the facesheet thickness, making a comparison of different sandwich geometries questionable.

### 3.2.3. Single Cantilever Beam

As a consequence to the difficulties of the double cantilever beam, the single cantilever beam (SCB) test method for sandwich structures includes additional fixations e.g. at the bottom of the specimen, see Figure 31. The single cantilever beam is considered a promising procedure for the examination of the interfacial fracture toughness of sandwich components [211, 241]. The testing procedure and $G_I$ assessment is equivalent to the double cantilever test method.

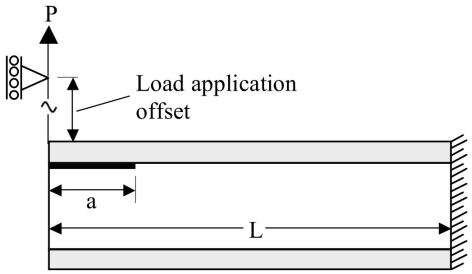


Figure 31: The single cantilever beam variant with a clamp at the specimen end [209].

Several variants have been developed specialising on Mode I and Mixed Mode testing of sandwich interfacial adhesion that may be classified as SCB methods [211].

During the interfacial fracture toughness testing of sandwich specimens, it is possible that the crack kinks towards the core leading to a sub-interface crack [201, 236]. If this is the case, the test does not reflect a mechanical evaluation of the interfacial bonding between facesheet and core anymore [236]. According to He and Hutchinson [247] this is due to a positive shear stress at the crack tip, see Figure 32 [228]. First proposed by Grenestedt [235], the tilted sandwich debond test (TSD) allows for the control of the crack propagation orientation due to an adaption of the tilt angle $\theta$ [203, 236, 237]. If an empirically determined critical tilt angle $\theta_c$ is deceeded, kinking can be avoided.

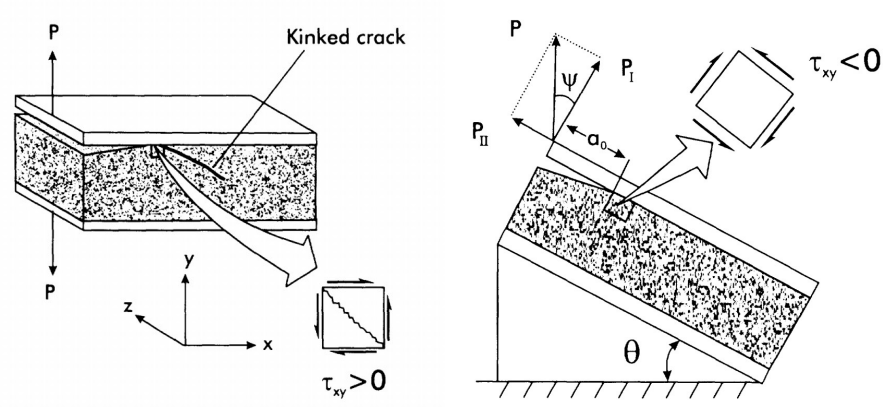


Figure 32: The tilted sandwich debond method allows for the variation of tilt angle and thus enables to modify the mixed mode ratio and to avoid crack kinking in the core [236].

The TSD can thus minimise possible kinking effects in a test set-up, however at the cost of introducing mixed Mode loading and varying tilting angles, which complicates comparison of different sandwich structures.

In order to reduce Mode mixture to a minimum and to receive a Mode I dominant failure, the SCB with rigid flat base plate is often used [211, 216, 230]. However, since during the testing procedure the crack tip moves constantly, the load application is equivalently moving during testing which results in a rotation thereof and a varying test angle. This leads to the development of shear stress in the core and a minor Mode II component at the crack tip depending on the angle at the crack tip [223, 230, 236, 248]. Another approach is to enable a constant location of the crack tip with respect to the testing machine axis during the test. Cantwell and Davies [202, 223] developed a single cantilever beam with a sliding carriage base on which the specimen can be attached to, see Figure 33. Similar methods have been developed by other authors [117, 248].

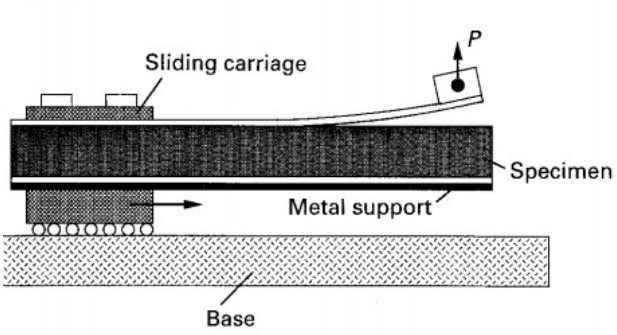


Figure 33: Single cantilever beam with sliding carriage base plate avoids the variation of the peel angle [223].

SCB methods with sliding carriage base plates exhibit Mode I dominant behaviour [216, 233]. However, the test procedure is considerably complicated, as the fixation of the specimens on the base plate requires either specimen compatible adhesives, which may be difficult for nonpolar polymer matrices. Moreover, the specimen preparation is subject to curing times if adhesives are used and a high number of base plates is necessary, which even might be only used once if the tested specimen cannot be removed after testing. Other variants involve geometrical fixations such as

undercuts, which again require a complex specimen preparation yet sparing the need of numerous base plates.

Nevertheless, the SCB test method needs to be modified if sandwich structures with thin facesheets need to be tested since the latter exhibit a very low intrinsic flexural rigidity. This leads to the development of a very high peel angle of the facesheet at the crack tip during the test. This results in a damage of the facesheets that is followed by tensile failure during testing making it impossible to quantify the interfacial bonding [95, 249]. The addition of doublers increases the flexural rigidity of the facesheets and reduces the peel angle However, Adams et al. [216] found that this leads to an increase of $G_I$ values. In addition, the doublers and their fixation on the facesheets requires adhesive bonding, which increases specimen preparation complexity. Also, the adhesive strength of doublers and specimen may be challenging.

### 3.2.4. Mandrel Peel Test

In order to avoid high peel angels during SCB testing of sandwich structures with thin facesheets, which induce invalid failure as discussed in chapter 3.1, the bending radius should be large enough. Therefore, the introduction of a defined bending radius is a promising approach. For this purpose, the SCB concept was modified and the mandrel peel test was developed, see Figure 34. The mandrel peel test was originally developed for the testing of hybrid metal-plastic components [205, 206, 250]. Here, the test specimen is fixed to a sliding table e.g. by use of adhesives or by using an undercut. The specimen consists of a UD tape, which is welded on a CFRTP base structure. During testing, the UD tape is peeled off the base structure by applying a tensile load $F_p$. An alignment force $F_a$ resulting from a dead weight [205] or pneumatic cylinder [251] is used to ensure an radial alignment of the tape to the mandrel. This provides a constant peel radius and angle respectively improving reproducibility and avoiding extensive bending of the facesheets that may ultimately lead to facesheet failure [249].

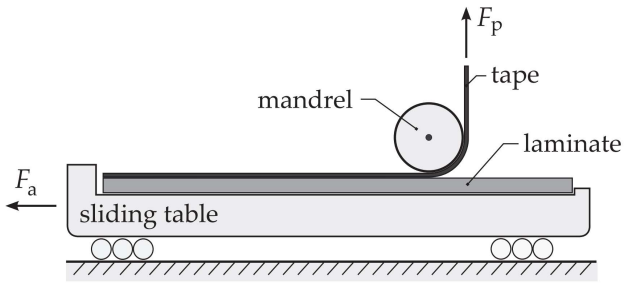


Figure 34: The mandrel peel test enables the interfacial testing of structures with low intrinsic flexural rigidity. The mandrel defines the bending radius and hence avoids extensive compressive strains due to small bending radii of the debonding structure [16].

The assessment of the strain energy release rate during testing is based on Equation 31 and considers the external energy $U_{ext}$, the energy dissipated during peeling $U_d$ and the strain energy stored in the peel arm $U_s$ with the specimen width $b$ and incremental crack length $da$ leading to

$$G = \frac{1}{b}\left(\frac{dU_{ext}}{da} - \frac{dU_d}{da} - \frac{dU_s}{da}\right) \tag{33}$$

According to [249] the residual stresses and the elastic strain in the peel structure are small compared to the external work introduced by the peeling load $F_p$ and alignment load $F_a$ as well as to the dissipated energy by friction. This leads to the simplified equation for the determination of interfacial fracture toughness:

$$G = \frac{1}{b}\left[F_p(1-\mu) - F_a\right]. \tag{34}$$

The friction coefficient attributes to the friction in the test set-up and was found for the set-up of Grouve et al. [251] to be as low as $\mu = 0.02$. The test procedure provides a high reproducibility of results and avoids kinking of the crack into one of the adherents [249]. However, the fixation of the specimens on a sliding table as base plate requires adhesive bonding of specimen and base plate or geometrical fixations.

### 3.2.5. Roller Peel Test

The fixation of the mandrel peel test specimen on a base plate carrier system according to Grouve and co-workers [16, 249, 251, 252] poses a critical issue, when using nonpolar polymers such as polypropylene. Pre-trials have shown that at moderate peel forces, the specimen can detach from the base fixation thus making the test invalid. Surface pre-treatment such as roughening and flame treatment did not yield in satisfactory results.

Lebsack [95] developed a Mode I test method based on a combination of the mandrel peel test according to the work of Grouve and co-workers [16, 249, 251, 252], the sliding carrier SCB method based on Weidmann [117] as well as the test standards DIN 53494 [253] and DIN EN 1372 [254]. The test procedure is similar to the mandrel peel test, with the benefit to avoid the base plate fixation on a movable sliding carriage since the specimen itself moves during the test on a flat surface with low friction, see Figure 35.

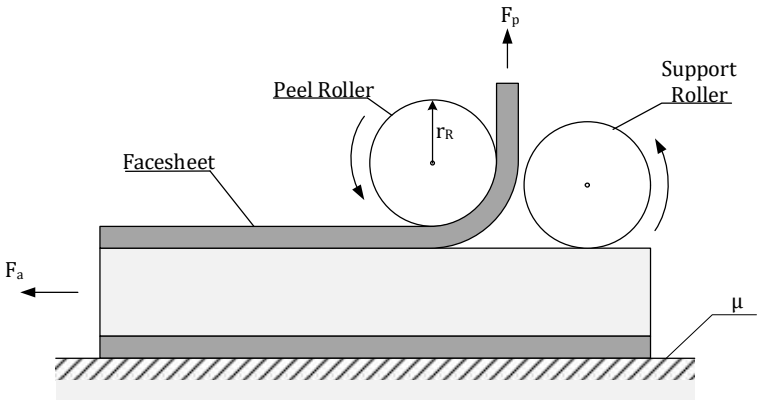


Figure 35: The roller peel test enables the testing of the facesheet-core interfacial fracture toughness of in-situ CFRTP sandwich structures. A peel roller similar to the mandrel peel test avoids an extensive bending of the thin debonding facesheets with low intrinsic flexural rigidity. The set-up significantly simplifies the specimen preparation.

First, the top facesheet is pulled around the peel roller and clamped by chuck jaws, another roller serves as rotating support during peel-off. During testing, the peel angle of the crack tip is defined by the peel roller and by the alignment force, pulling the facesheet radially on the peel roller [16, 249, 252]. The calculation of the interfacial fracture toughness $G_I$ is conducted according to Equation 34. The induced friction due to the direct contact of the specimen with the base plate needs to be included in the assessment of the effective peel load equivalent with the mandrel peel test. The effective friction coefficient was measured to yield a value of $\mu = 0.18$.

The test method can be used for the testing of various sandwich structures of varying geometry and materials. Originally developed for interfacial fracture toughness evaluation of sandwich structures with thin facesheets and low intrinsic bending stiffness, the roller peel test can be adapted to thicker facesheets by increasing the peel roller radius $r_R$. In preliminary tests, specimens with equal facesheet thickness were subject to roller peel testing with varying peel roller diameter. No effect on the resulting $G_I$ values was be observed, hence the effect of changing peel roller radii on the measured $G_I$ value is assumed negligible.

## 3.3. Interfacial Strength Test Methods

In addition to the interfacial fracture toughness, which is of special interest regarding the propagation of face-core debonding, the strength of the interface shall be quantified using a quasi-static testing method. Test procedures for the assessment of skin-core interfacial strength of sandwich structures can be based on tensile tests at which a tensile load is applied on the sandwich facesheets, which pulls in direction of the surface normal vector [38, 255]. However, this test set-up requires an adhesive fixation of the load application on the sandwich structure that is effortful and challenging when it comes to nonpolar matrix polymers such as polypropylene. Hence, the focus was set on other test methods avoiding this kind of critical load application. These methods for the evaluation of an interface strength can be divided into two groups:

- Short beam shear [215, 218, 256–259]
- Lap shear [213, 214, 240, 260–262]

Test methods for the evaluation of interfacial strength of a joint often include lap shear test set-ups. However, interlaminar failure of two joined components can also be induced by beam shear testing methods, which are frequently used for FRP. The applicability of these test methods for the evaluation of core to face interfacial strength of CFRTP sandwich components with integral foam core will be evaluated in the following.

### 3.3.1. Short Beam Shear

Short beam shear tests are often used to study the interlaminar strength of composites [218]. Several test standards have been developed, the most well known and most accepted being ASTM D2344 [217]. The test standard is based on short beam specimens, which are usually subject to three-point bending inducing high shear stresses while the resulting flexural stresses are comparatively low. The dominance of shear stresses is defined by the test set-up and specimen geometry [218]. Although the load is usually applied in a three point bending test set-up, see Figure 36, also four-point-bending set-ups can be applied [258].

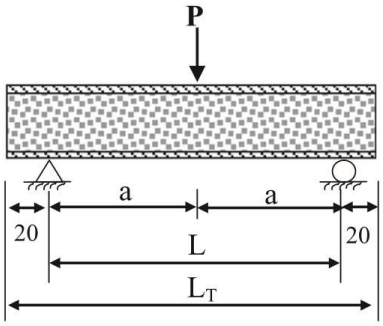


Figure 36: The short beam shear test set-up based on three-point bending for interlaminar testing of a sandwich structure [215].

Despite its low complexity and convenient test procedure, this test exhibits major drawbacks, especially when using thermoplastic matrices [258, 263, 264]. Since the latter often exhibit comparatively low elastic moduli, the high line loads introduced by the load application roller often result in indentations at the compressive specimen side, which ultimately leads to micro-buckling of fibres and invalid specimen failure [218, 264]. Adapted methods based on four-point bending with reduced line loads may level but not fully avoid this issue [217].

The main other challenge is the inhomogeneous stress state, as the short beam shear tests do not solely introduce shear stresses in the specimen but also stresses resulting by the applied bending moment. Failure consequently results from a complex stress state and a clear assignment of the cause is challenging [217, 218]. In addition, the test results and the failure modes are sensitive to the geometrical parameters of the test specimen and the test set-up. Small variations of span length and component thickness ratios may lead to different results due to variations of the induced stress state [217].

A quantitative assessment of face to core interfacial strength of foam core CFRTP sandwich structures with varying geometrical and material parameters based on short beam shear methods is therefore questionable [218, 264]. Qualitative assessment of the interfacial strength however is possible [258, 265], yet this requires geometrical and material parameters to be kept constant.

### 3.3.2. Lap Shear

Lap shear test methods have been subject to extensive scientific research and numerous variants have emerged. Standards have been developed specifically for metal-metal lap joints [266], lap joints with plastic [267] as well as FRP adherents [268]. Mostly, their focus lies on testing the strength of an adhesive joint, however they can also be applied on welded joints of polymer based adherents [269, 270]. Several types of lap geometries have been developed, see Figure 37 [271].

The single-lap shear is the most frequently used variant due to its ease of specimen preparation and is widely applied for the assessment of the bonding strength of a joint. This includes adhesively bonded joints [262] as well as fusion bonded joints of thermoplastics and thermoplastic composites [260]. Several derivatives exist based on the single-lap shear test, each with the target of improving the resulting stress field (bevelled lap) or the specimen preparation (notched lap).

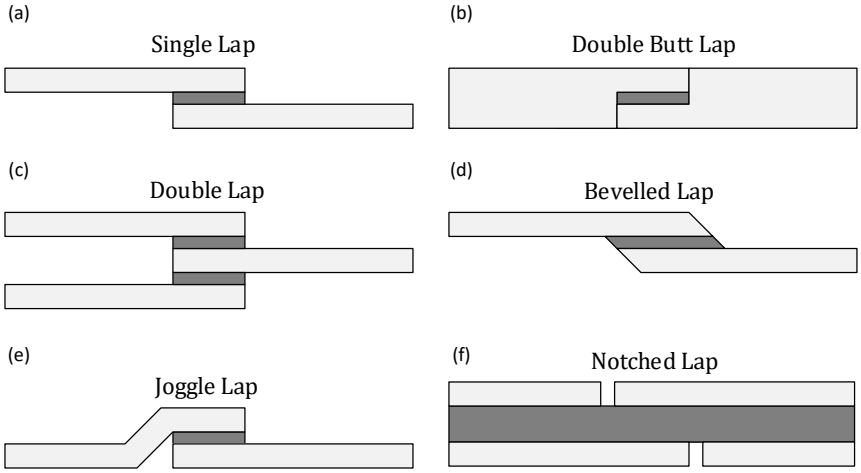


Figure 37: Schematic overview of lap shear test variants: the single-lap shear test is the most frequently used variant, yet its derivatives may be more suitable for specific applications, e.g. the notched lap shear test for sandwich structures.

In recent years, the lap shear test was often used to characterise interfacial strength of a bonded joint due to its often stated simplicity [262]. The application of the singe-lap shear test method for interfacial testing of sandwich structures is possible, if the sandwich core is considered as adhesive bond with very large thickness whereas the adherents exhibit comparatively low thicknesses.

However, the single-lap joint denotes a very complex test method, despite its constructive simplicity. The adhesive between the adherents, or in case of sandwich structures the core between the facesheets, is subject to an inhomogeneous stress field including a shear and a peel portion which makes testing and especially analysis of testing results very complex [213, 240, 251]. Volkersen [272] introduced the differential straining analysis of the single-lap joint, providing an explanation for shear stress peaks at the ends of the adhesive length. However, he disregarded the bending moment and the induced peel stresses that are superimposed to the shear stress, see Figure 38. Especially the peel stress is subject to large variation within the lap length and exhibits high stress peaks at the ends of the lap joint, resulting from the bending behaviour of the specimen induced by the off-axis of both adherents [8, 213, 262, 273].

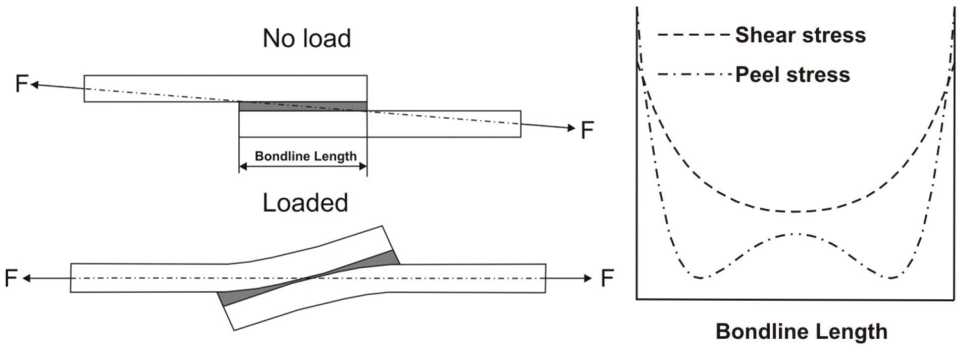


Figure 38: The stress distribution in the overlap length including peel as well as shear stresses: significant stress inhomogenities can be determined [274].

The single-lap test is thus very sensitive to changes of adhesive and adherent materials and geometry [240, 261]. An increasing adhesive thickness decreases the measured strength induced by an increased bending moment [214]. The measured strength is proportional to the overlap, until a maximum lap length is achieved at which the adherents fail [213]. The optimum overlap length moreover is dependent on the specimen length. Kafkalidis and Thouless [261] find that the specimen length should exceed the overlap length by factor 10. Also, the single-lap shear is sensitive to the material properties of adhesive and adherent [213, 262]. Consequently, the single-lap shear test and its results depend on the material properties but also on the specimen and bond geometry, including the specimen length, the thickness of the adherent or sandwich core, and the overlap length [261].

In conclusion, it becomes clear that the single-lap test method and its derivatives such as the notched lap shear benefit from simple test procedure and specimen preparation. The measured results however are often strongly dependent on geometric and material properties. Different structures and materials thus cannot be quantitatively compared to each other, nevertheless a qualitative comparison of bonded structures with identical geometry and materials is assumed valid.

## 3.4. Evaluation and Selection of Test Methods

Table 3 summarises the specific test method potentials and evaluates them based on the imposed requirements in chapter 3.1 according to VDI 2225 [43]. The evaluation scale is presented in Table 2.

Table 2: Evaluation rating scale according to VDI 2225.

| Evaluation | Points |
|---|---|
| Very Good (ideal) | 4 |
| Good | 3 |
| Satisfactory | 2 |
| Acceptable | 1 |
| Insufficient | 0 |

According to the results in Table 3, the roller peel test appears to be most suitable for the quantification of facesheet to core interfacial fracture toughness of thermoplastic composite sandwich structures. For the assessment of interfacial bonding strength, the notched lap shear method is most promising despite the discussed restrictions.

Table 3: Evaluation results of test methods for interfacial strength and interfacial fracture toughness. The notched lap shear (NLS) and the roller peel test (RPT) yield the highest rating and are hence selected.

| | Interfacial Strength | | | Interfacial Fracture Toughness | | | | | |
|---|---|---|---|---|---|---|---|---|---|
| Requirements | SBS | **NLS** | SLS | CDP | DCB | TSD | SCB | MPT | **RPT** |
| Generate Related Test Values | 1 | **1** | 1 | 2 | 4 | 4 | 4 | 4 | **4** |
| Avoid High Peel Angles | 4 | **4** | 4 | 4 | 0 | 1 | 0 | 4 | **4** |
| Avoid High Point or Line Loads | 0 | **2** | 2 | 4 | 4 | 4 | 4 | 4 | **4** |
| Easy to Prepare, Perform and Evaluate | 4 | **3** | 1 | 1 | 2 | 1 | 2 | 1 | **4** |
| ∑ | 9 | **10** | 8 | 11 | 10 | 10 | 10 | 13 | **16** |

Hence, these test methods are selected for the mechanical evaluation and subsequent optimisation of skin-core bonding during the in-situ manufacture of CFRTP sandwich structures.

# 4. Methods for the Characterisation of In-Situ CFRTP Sandwich Structures

This chapter presents the methods used in this work comprising mechanical test procedures, polymer analysis, as well as computer aided simulation methods, see Figure 39.

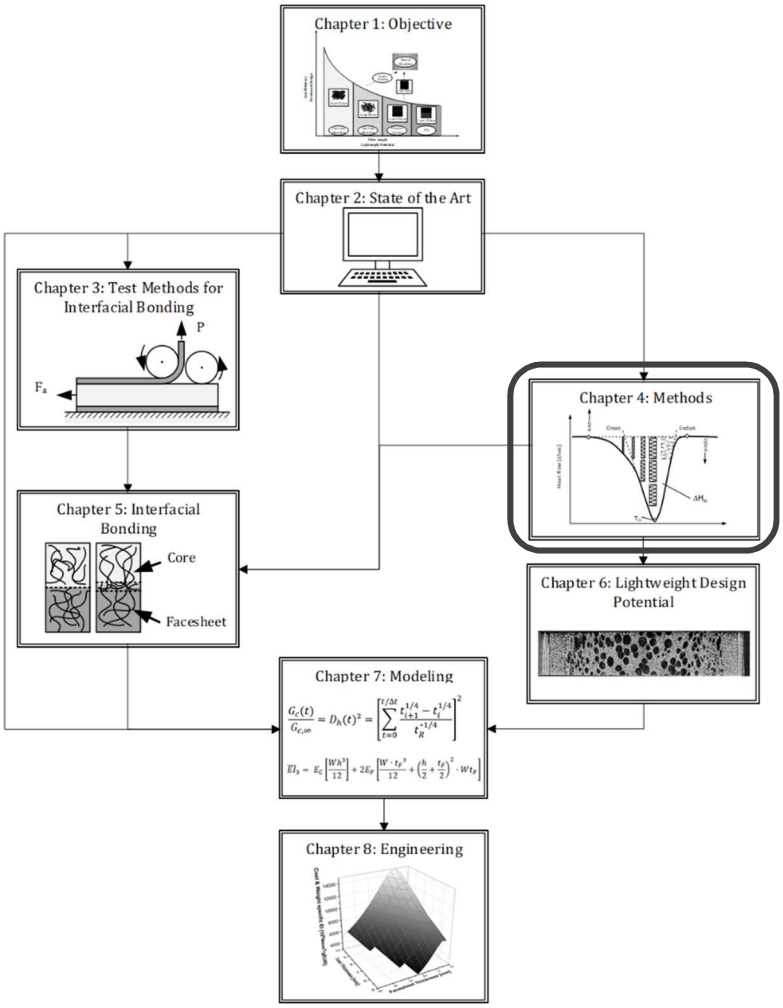


Figure 39: Systematic approach of this work: chapter 4 presents the methods used in this work for the characterisation of in-situ sandwich structures.

Following the evaluation and selection of suitable test methods in chapter 3, the interfacial bonding assessment by the roller peel test as well as the notched lap shear test is presented in detail. Moreover, the presented mechanical test procedures include the evaluation of the flexural behaviour of in-situ CFRTP sandwich structures via the four-point bending (4PB) test.

The fracture after interfacial testing as well as the process induced polymer morphology at the interface is evaluated by imaging techniques comprising scanning electron microscopy (SEM) and polarised light microscopy (PLM).

As the crystallinity of polymers plays an important role in the fusion bonding between CFRTP facesheet and injected foam core based on the results of chapter 2.4.2, differential scanning

calorimetry (DSC) is applied to evaluate the degree of crystallinity and to correlate it with the findings of the bonding tests.

Lastly, a simulation methodology is presented that allows for a prediction of the resulting temperature at the interface between CFRTP facesheets and the injected core during the in-situ manufacture of CFRTP sandwich specimens, since this denotes a major factor for the development of interfacial bonding.

## 4.1. Mechanical Characterisation

The mechanical test methods are presented in detail in the following sub-chapters, giving insight into the applied standards, testing parameters and specimen geometries.

### 4.1.1. Four-Point Bending

In order to assess the flexural rigidity of in-situ CFRTP sandwich specimens, a four-point bending (4PB) test is conducted. The 4PB test method is favourably used for fibre reinforced composite structures, due to the comparatively large area with constant bending moment in the mid-section of the test specimen. This reduces stochastic effects on the test results resulting from manufacture-induced defects such as fibre undulations and misalignments as well as fibre strength variation. Furthermore, the use of two load applications divides the locally induced load by two and reduces thus the probability of stamp indentation and following invalid failure at the load applications. The four-point bending procedure is conducted according to DIN EN ISO 14125 [275]. The test set-up is presented in Figure 40.

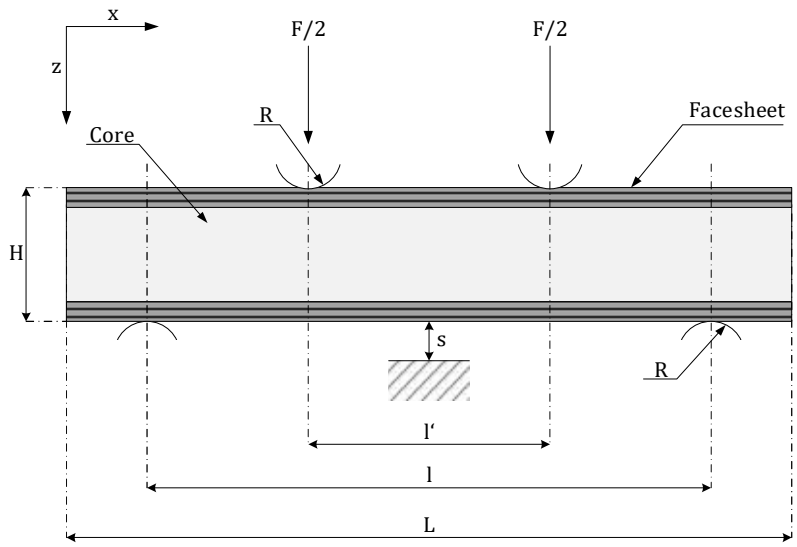


Figure 40: Schematic illustration of the four-point bending test set-up according to DIN EN ISO 14125 [275].

The load span length $l'$, the support span length $l$, and the total length of the specimen $L$ are listed in Table 4. The test is carried out on a hydraulic testing machine equipped with a 15 kN load cell in standard climatic conditions at a temperature of 23 °C and a relative humidity of 50 % (23/50). A

laser measures the specimen deflection $s$ in the middle of the load span length. Before the test, the sprue is removed and the specimen weighed. For each tested parameter setting, six specimens are tested, which were stored for 24 h under 23/50 standard climate conditions.

Table 4: Specimen geometry and test speed of the four-point bending test according to DIN EN ISO 14125 [275].

| Parameter | Value | Dimension |
|---|---|---|
| Load Span Length $l'$ | 90 | mm |
| Support Span Length $l$ | 180 | mm |
| Test Speed | 5 | mm/s |
| Specimen Length $L$ | 220 | mm |

The effective flexural modulus $E_f$ of the sandwich structure is evaluated according to [275] as

$$E_f = \frac{0.21 l^3}{W H^3}\left(\frac{\Delta F}{\Delta s}\right). \tag{35}$$

The flexural modulus $E_f$ depends on the support length $l$, the specimen width $W$, the specimen total thickness $H$, as well as the load and midspan deflection differences $\Delta F$ and $\Delta s$ at the outer-surface elongations $\varepsilon'$ = 0.0005 and $\varepsilon''$ = 0.0025 with

$$\Delta F = F(\varepsilon'') - F(\varepsilon') \tag{36}$$

and

$$\Delta s = s(\varepsilon'') - s(\varepsilon'). \tag{37}$$

The relationship of midspan deflection and outer-surface elongation is described as

$$s(\varepsilon) = \frac{\varepsilon L^2}{4.7h}. \tag{38}$$

The flexural rigidity $E_f I$, in this work indicated as $\overline{EI}$, is calculated as

$$E_f I = \frac{0.21 l^3}{W H^3}\left(\frac{\Delta F}{\Delta s}\right) I = \overline{EI}, \tag{39}$$

with

$$I = \frac{W H^3}{12}. \tag{40}$$

The second moment of inertia assumes the sandwich structure to be monolithic, since the evaluated flexural modulus $E_f$ refers to a homogenised monolithic structure.

### 4.1.2. Interfacial Fracture Toughness

The interfacial fracture toughness is assessed using the roller peel test (RPT). The test is conducted on a tensile test machine Zwick Z5.0 with a 5 kN load cell. Before testing, the specimens are stored at 23/50 standard climate for 24 h. The test is carried out using six specimens per test setting in a 23/50

standard climate. The traverse speed is set to 100 mm/min. The peel roller radius is adjusted with respect to the specific facesheet thickness. Facesheets with 0.33 mm thickness are tested with a peel roller diameter of $D_{0.33}$ = 15 mm. In order to avoid excessive strains in the facesheets, a peel roller with a larger diameter of $D_{0.66}$ = 30 mm is used for facesheets with a thickness of 0.6 mm. Experiments with 0.33 mm thick UD tape facesheets with both roller radii have shown that the determined $G_I$ values were unchanged with varying peel roller radius.

During the test, the effective peel force i.e. the applied load $F_p$ is measured. For evaluation, the middle part of the in-situ CFRTP sandwich specimen and the respective test data range is used, see Figure 41 (test length). Based on the specimen geometry and length, respectively, this results in a maximum test length of 100 mm.

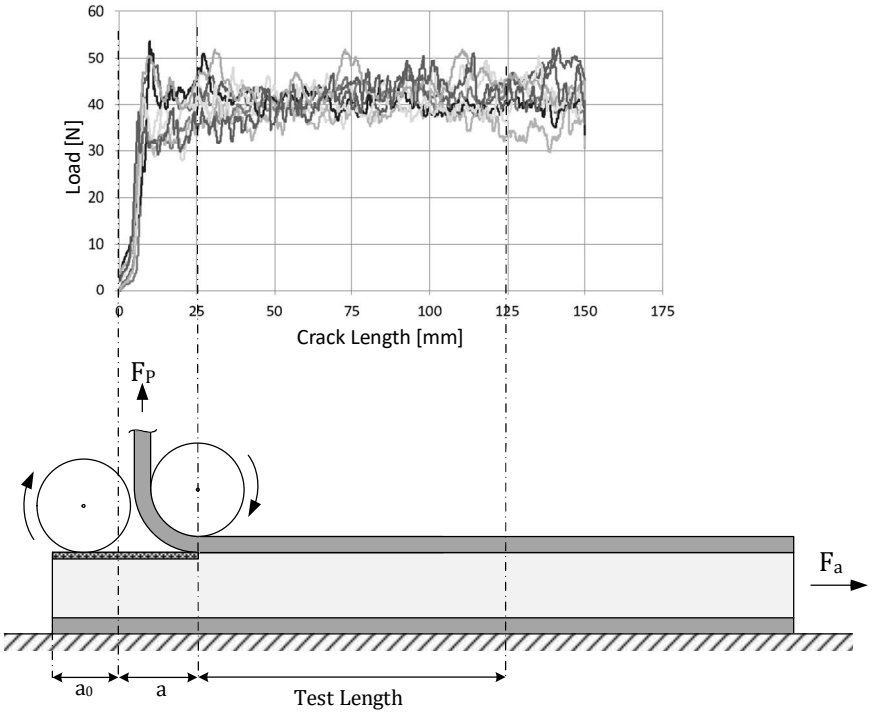


Figure 41: Determination of the debond load during the interfacial fracture toughness assessment using the roller peel test.

The calculation of $G_I$ is discussed in chapter 3.2.4 and 3.2.5. The interfacial fracture toughness is assessed via

$$G = \frac{1}{b}\left[\bar{F}_p(1-\mu) - F_a\right]. \tag{41}$$

with

$$\bar{F}_p = \frac{1}{n}\sum_{i=1}^{n} F_{P,i} \tag{42}$$

Here, $b$ is the specimen width, $F_P$ is the applied peeling load, μ is the experimentally assessed friction coefficient and $F_a$ is the alignment force. Based on preliminary experimental tests, a force of $F_a$ = 73.6 N is applied in order to enable a proper alignment of the facesheet to the roller surface. $\bar{F}_p$ marks the mean applied load within the specimen test length between 25 and 125 mm as depicted in Figure 41.

### 4.1.3. Notched Lap Shear

Notched lap shear testing is performed referring to ASTM D3846 and ASTM D3165 [276, 277]. Specimen preparation involves the in-situ manufacture of CFRTP sandwich specimens and subsequent integration of notches in order to achieve a single-lap specimen geometry as depicted in Figure 42.

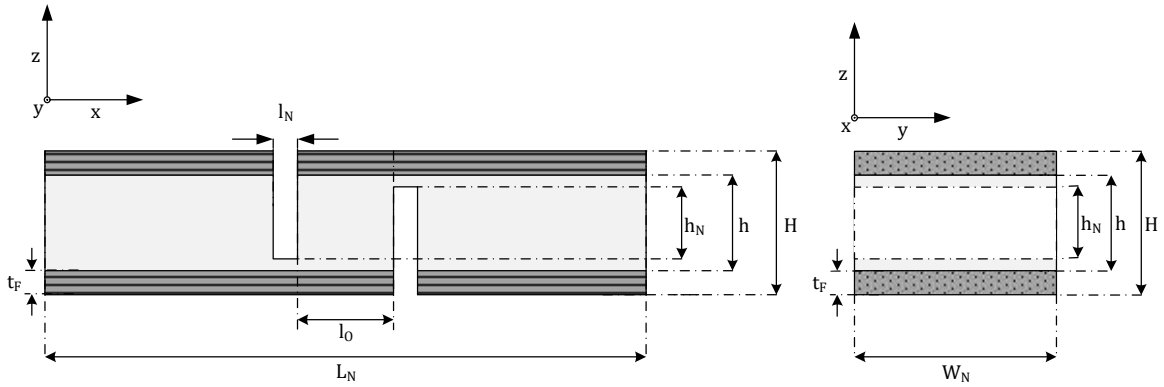


Figure 42: Notched lap shear test specimen.

The specimen length $L_N$ is 100 mm, the overlap length $l_O$ is 10 mm and the notch length $l_N$ is 3 mm. In order to avoid a damage of the UD tape facesheets, the notch does not spread along the entire core height resulting in a reduced notch height $h_N$. The difference of notch and core height $(h - h_N)$ yields 0.1 mm. The width $W_N$ of the specimen is 30 mm. The NLS is carried out on a hydraulic testing machine with a 15 kN load cell. The test specimens are stored for 24 h at 23/50 standard climate before testing. For each test setting, six specimens are subject to testing at 23/50 standard climate conditions. The traverse speed is set to 2.5 mm/min for compact CFRTP sandwich specimens. In-situ CFRTP sandwich specimens with integral foam core are tested at 5 mm/min due to the increased traverse stroke until failure of the specimens.

The notched lap shear strength calculates as the load at failure $F_{p,max}$ in relation to the shear cross-area $A$ in the *y*-*z*-plane according to Figure 43. Here, $W_N$ marks the specimen width and $h$ the sandwich core thickness. Based on the findings of chapter 3, it is acknowledged that the notched lap shear strength $\tau_{NLS}$ does not represent a distinct shear stress due to the inhomogeneous stress field. Nevertheless, it will be henceforth referred to as notched lap shear strength $\tau_{NLS}$.

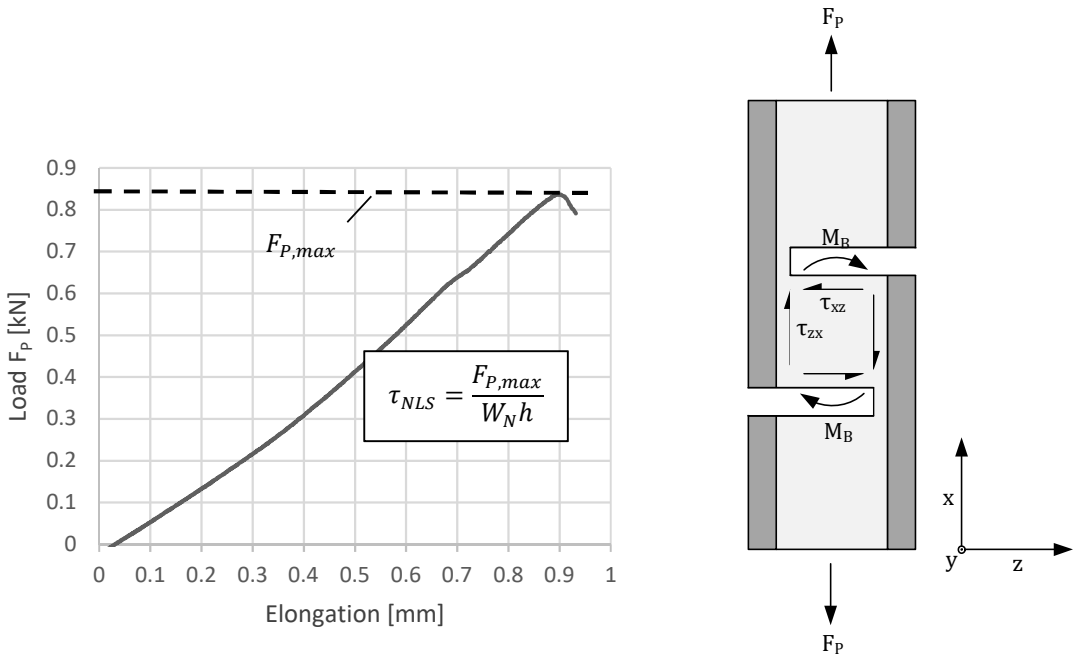


Figure 43: Determination of the notched lap shear strength: the maximum load is related to the cross section of the specimen core in the y-z-plane.

## 4.2. Polymer and Structural Analysis

The polymer analysis focuses on the bonding zone between polymer core and CFRTP facesheets after the manufacture of in-situ sandwich structures via polarised light microscopy (PLM) as well as on the characterisation of polymer crystallinity using differential scanning calorimetry (DSC). In order to evaluate the relationship of integral foam morphology and bending behaviour, micro computer tomography (µCT) based methods are applied.

### 4.2.1. Differential Scanning Calorimetry

For the assessment of the facesheet matrix polymer crystallinity, the differential scanning calorimetry is used. The DSC variant used in this work consists of an oven containing the sample material and the reference each in a metal pan. At a given temperature ramp program, the temperature of both pans is determined continuously by means of integrated thermocouples. A temperature difference of sample and reference during the test procedure indicates a change of the heat flux ϕ of the oven to the sample and reference, respectively [73]. The evaluation of the heat flux related to the time t or the reference temperature allows a series of inferences about the tested polymer and its properties, such as the polymer crystallisation behaviour and glass transition temperature [64]. In the case of semi-crystalline thermoplastics, the melting and crystallisation temperatures can be thus determined as endothermal and exothermal processes, respectively, as well as the glass transition temperature of amorphous polymer structures [64, 73]. The heating DSC curve gives an important insight into the melting behaviour of the material. Smaller crystallites with thinner lamellae melt at lower temperatures whereas larger crystallites melt at higher temperatures, see Figure 44 [73, 182]. Also, different polymorphs can be determined using the DSC [64]. The integral of the curve in Figure 44 corresponds to the enthalpy of fusion and indicates which amount

of heating energy must be applied in order to melt the specific crystalline portions of the sample. A higher fusion enthalpy is thus equivalent to a high degree of crystallinity [73].

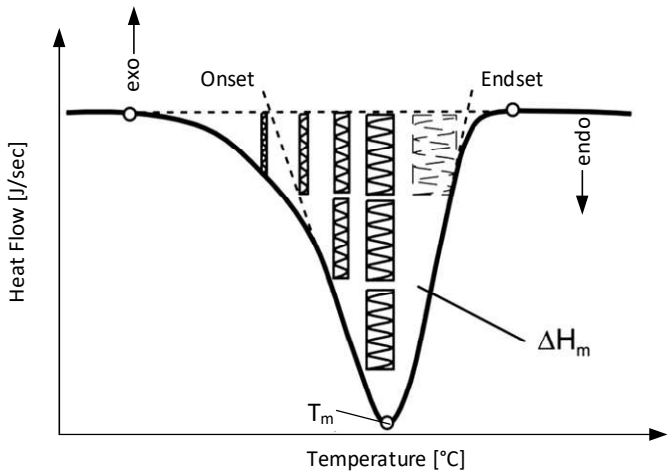


Figure 44: Schematic illustration of a DSC test curve as heat flow related to the test temperature. Smaller crystalline structures melt at lower temperatures whereas larger lamellae melt at higher temperatures [73].

In order to determine the degree of crystallinity of the tested polymer material, the measured melt enthalpy $\Delta H_m$ is related to the enthalpy of a 100 % crystalline sample $\Delta H_{cr}^0$ [278]. In order to determine the fusion enthalpy of reinforced thermoplastics such as UD tapes, the filler content $\varphi$ must be taken into account [75, 278]:

$$\xi = \frac{\Delta H_m}{(1-\varphi)\Delta H_m^0} \cdot 100. \tag{43}$$

According to Ehrenstein et al. [279] a theoretically completely crystallised polypropylene exhibits a fusion enthalpy $\Delta H_m^0$ of 207 J/g. Contrary to other materials that are able to crystallise, the degree of crystallinity of thermoplastics is substantially less than 100 %. This is because in addition to the crystalline structures, also amorphous fractions are included [74]. Furthermore, the temperature profile and the nucleation process have an effect on the resulting degree of crystallinity.

In this work, sample preparation and measurement are carried out in accordance with DIN EN ISO 11357-3 [280]. The temperature program is presented in Table 5.

Table 5: Temperature profile during DSC measurements.

| Program | Hold | Heating | Hold | Cooling | Heating | Cooling | Dimension |
|---|---|---|---|---|---|---|---|
| Time | 5 | - | 5 | - | - | - | s |
| Target Temperature | 25 | 220 | 220 | 70 | 220 | 25 | °C |
| Rate | - | +20 | - | -20 | +20 | -20 | °C/s |

The degree of crystallinity is assessed in the first heating cycle of the temperature program, since the cooling process after the first heating cycle alters the initial thermal history of the respective specimen.

### 4.2.2. Polarised Light Microscopy

In order to evaluate the fusion bonding zone near the interface of CFRTP facesheet and injected polymer core of in-situ sandwich structures, polarised light microscopy (PLM) is used. PLM represents a variant of the transmission light microscopy. The difference is the integration of a polariser and analyser as additional filters in the microscope set-up, which only transmit passing light along a specific plane. The polariser is located within the beam path between the light source and the sample whereas the analyser is placed between the eyepiece and the sample [281]. If the polarising planes of the polariser and the analyser are positioned perpendicular to each other, a polarisation dark field results because the transmitted linear-polarised light after the polariser is blocked by the analyser. This denotes the most frequent PLM set-up, called crossed polarisers. Morphological structures in semi-crystalline thermoplastics can be analysed by means of PLM due to their optical anisotropy. Objects with optical anisotropy (birefringence) split light into two orthogonal waves with different velocities, the extraordinary and the ordinary wave [281]. Consequently, these two partial waves with wavelength $\lambda$ undergo a path difference, the phase shift $\Gamma$, as a function of the birefringence $\Delta n$ and the thickness $d$ of the object:

$$\Gamma = \frac{2\pi}{\lambda} d \cdot \Delta n \,. \tag{44}$$

In particular, spherulites in semi-crystalline plastics represent optically anisotropic structures with birefringent optical behaviour due to the combination of amorphous and crystalline fractions [281]. Crystalline structures appear bright whereas amorphous or fine-spherulitic areas of thermoplastic samples are optically isotropic, and appear dark in PLM images, see Figure 45 [95, 282].

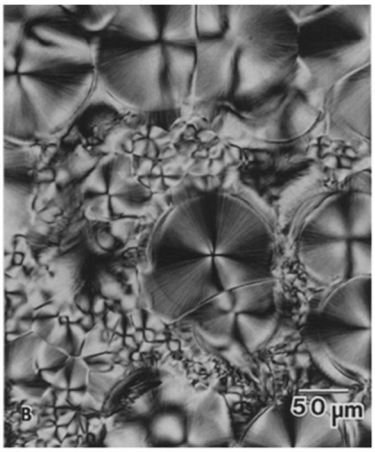


Figure 45: Image of birefringent thermoplastic spherulites using polarised microscopy [281].

For the evaluation of the interface polymer morphology using the PLM, thin cross sections with a thickness of approx. 10 µm must be manufactured by means of a microtome. With respect to FRP materials, the cutting quality is adversely affected by the reinforcing fibres because of their brittleness and hardness which results in the fact that contrary to the matrix polymer they are not cut but broken or torn out of the matrix [64]. Minimal cut thicknesses of 50 µm could therefore be achieved for the in-situ sandwich specimens with UD tape facesheets investigated in this work.

Photomicrographs with polarised light were performed using an Olympus BX50 microscope. The cross sectioning was carried out on a Leica RM2245 microtome.

### 4.2.3. Micro Computer Tomography

A foam morphology analysis based on micro computer tomography (µCT) is used in order to evaluate the cell size and cell density distribution in e.g. thickness direction of the in-situ CFRTP sandwich specimens. The µCT technique enables X-ray micrographs of objects with high resolution in the micrometre (µm) scale [189]. In the present work, a SkyScan 1072-100 micro computer tomograph is used for the analysis of structural foam morphologies including cell size distribution and local cell density. After placing the sample on a precisely rotary table, it is exposed to X-rays layer-wise from different directions by the micro-focused X-ray source during analysis. After each X-ray exposure, the precision table is rotated by a fixed angle until the object rotation yields 180 angular degrees (°). A detector records projection images whose resolution depends on the position of the sample to the X-ray source which can be adjusted accordingly. For the highest possible resolution, the sample thus must be positioned as close as possible to the radiation source. Using a special software, the recorded projection images are reconstructed into sectional images [283].

The measurements are carried out at a resolution of 1.7 µm. An acceleration voltage of 100 kV and a current of 98 µA is applied to the X-ray source. During the measurement, the specimen is rotated in total by 180° in increments of 0.45° at which a new projection image is taken. The recorded projection images exhibit a colour depth of 16 bit and are subsequently reconstructed into sectional images. After the µCT scan, the recorded projection images are reconstructed into sectional images, see Figure 46.

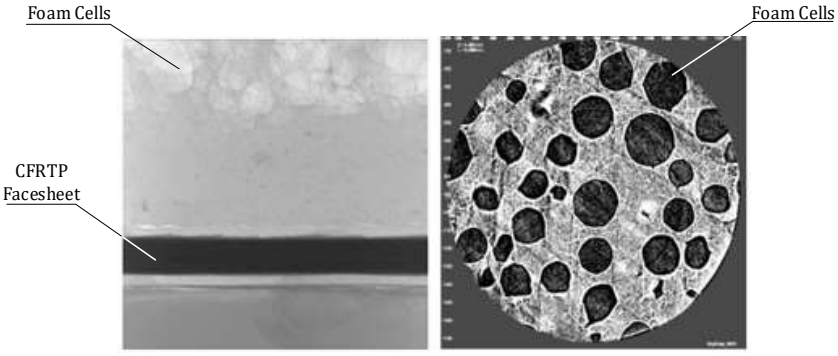


Figure 46: µCT scans of in-situ CFRTP sandwich structures with foam cores: projection image (left) and reconstructed sectional image (right) [189].

For the reconstruction of the cross-sectional images, the software CT-NRecon (Bruker microCT) is used. The reconstructed sectional images are observed via the software DataViewer (Bruker microCT). Three-dimensional models can be created based on the individual two-dimensional sectional images, which represent the complete sample volume at a resolution of 1.7 µm. For further information about this analysis procedure, it is referred to the work of Geiling [189].

### 4.2.4. Scanning Electron Microscopy

The fractured surface of the interface after testing the bonding between facesheet and core is evaluated by scanning electron microscopy (SEM). Using SEM it is possible to evaluate surface structures on micro scale with high depth of field [281]. This makes SEM predestined to analyse fracture surfaces in detail. The function principle is based on a directed electron beam, which scans the sample, see Figure 47. In order to create the electron beam, a tungsten wire can be used whereas newer methods are based on field emission gun (FEG) sources [281].

The Topcon SM-300 SEM used in the present work belongs to the thermionic emission sources with tungsten wire. By heating a tungsten wire (cathode) up to 2500 °K, a primary electron beam is generated, which is focused by a scattering cylinder. At the anode, the electron beam experiences an acceleration. This primary electron beam is bundled and focused by electromagnetic coils (condenser and end lens) and hits the surface of the target. After impacting on the target, different interactions take place. Three outgoing signals and evaluation modes are important for the SEM. These are the backscattered electrons, secondary electrons and X-rays [281]. Secondary electron imaging (SEI) is the most commonly used evaluation mode [281].

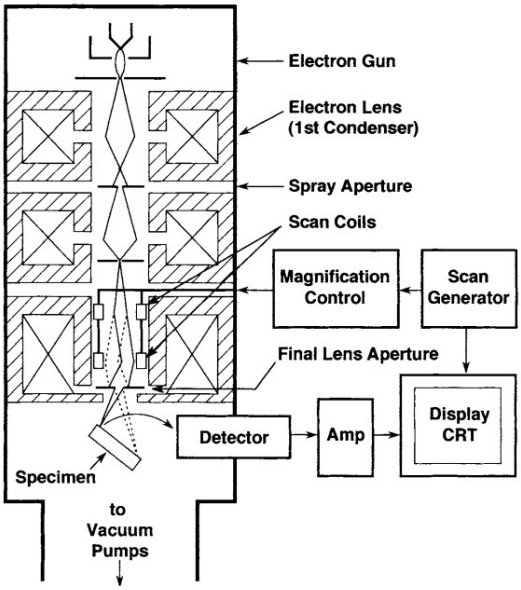


Figure 47: Schematic illustration of a scanning electron microscope and its components [281].

Secondary electrons are emitted by the specimen with low energy, so they can only originate from the surface of the target and a depth of merely a few nanometres (nm) [281]. The detector in the SEM used in this work is arranged obliquely to the object, this contributes to the depth-of-field perception of the scanned surfaces [281]. Electrically non-conductive specimens are usually coated with a thin film of conductive material. This sputtering process is mostly conducted with gold-palladium or platinum, which is applied in a vacuumed and argon flooded chamber using a plasma [281]. In the present work, the samples were sputtered with gold over a period of 360 s.

## 4.3. Interface Temperature Simulation

In order to determine the resulting interface temperature between CFRTP facesheet and polymer core depending on the applied process parameters during the in-situ manufacture, an injection moulding simulation based on Autodesk Moldflow Insight 2019 is used. The injection mould of the experimental campaigns in this work is modelled using a computer aided design (CAD) software (SolidWorks®, Dassault Systèmes SolidWorks Corp.). The 3D CAD model including the original cooling layout of the mould is implemented in the injection moulding simulation, see Figure 48.

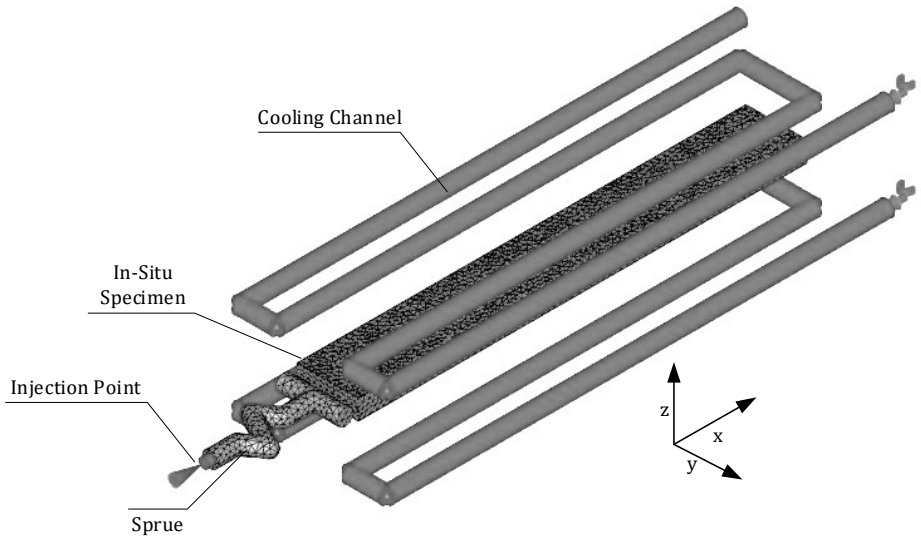


Figure 48: The CAD model used in the Moldflow Insight 2019 thermal simulation for the assessment of the interface temperature between UD tape facesheet and injection moulded core during the in-situ manufacture of sandwich specimens. The in-situ CFRTP sandwich specimen and the cooling channels are depicted. The mould is deliberately faded out for the sake of visibility.

The virtual specimen is modelled compliant with the injection moulded in-situ CFRTP sandwich specimens, see Figure 49. The facesheets are defined as inserts whereas the polymer core is injection moulded. The process parameters applied within the simulation are in accordance with the experimental manufacture of in-situ CFRTP sandwich specimens, which are described in the respective chapters in this work.

The foam injection moulding simulation with a chemical blowing agent assumes that the thermally induced decomposition of the CBA is fully completed in the barrel and furthermore neglects residues of the CBA decomposition aside the developing foaming gas. The foam injection moulding simulation uses the bubble nucleation model with a constant nucleation density of 25000 1/cm³ [285] and a blowing agent content of 3 % equal to the amount of blowing agent used in the experiments. The foam core material used in the simulation is Sabic® PP 576P and material properties are applied according to the Moldflow material database. Due to the lack of a material model for the UD tape facesheets, the inserts are defined as 50 wt.-% long glass fibre reinforced polypropylene (Celstran® PP-GF50-10) of the same material manufacturer, which is assumed a good approximation of the thermal behaviour of the 60 wt.-% continuous glass fibre reinforced polypropylene UD tapes. This is because the thermal behaviour is substantially characterised by the thermal conductivity and the specific heat capacity. The thermal conductivity of fibre reinforced plastics depends on the specific

conductivities of the reinforcing fibre as well as of the polymer matrix, weighted with the respective volume fraction according to the generalised mixing rule [8, 286]. As the material model in Moldflow does not include thermal anisotropies due to fibre orientations, fibre reinforced materials with similar fibre volume fraction and composite constituents are assumed to yield similar results in the thermal simulation [284].

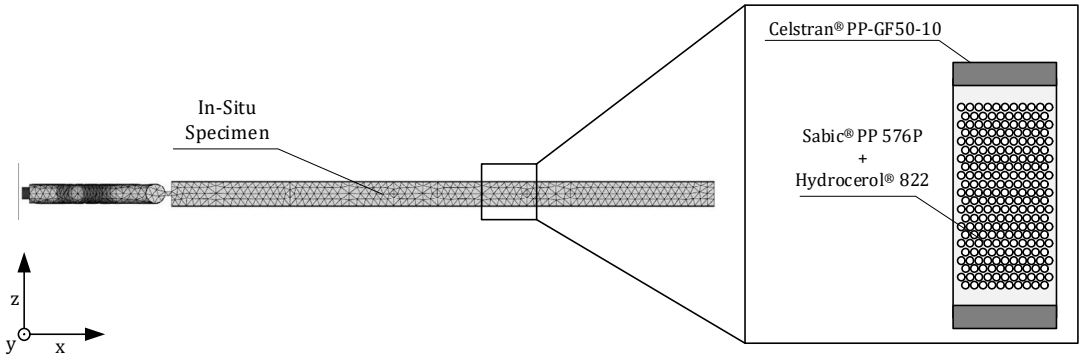


Figure 49: The meshed CAD model of the in-situ CFRTP sandwich specimen (left) with its attributed materials in the simulation (right). Considering the thermally isotropic thermal simulation of Moldflow [284], the polypropylene based UD tape facesheets with 60 wt.-% glass fibres (Celstran® CFR-TP PP GF60-13) are approximated with a 50 wt.-% glass fibre polypropylene of the same material manufacturer (Celstran® PP-GF50-10).

The resulting interface temperature is assessed on the facesheet at five symmetrical nodes. The middle of the RPT test length is chosen, attributing to a minor temperature decrease over the specimen length in x-direction due to the continuous cooling of the injected polymer melt as well as the test span during interfacial testing. A cross-shaped node layout is selected, in order to account for the small thermal variation in specimen width direction. Combining the temperature profiles of the five nodes, a mean temperature of the interface during the in-situ manufacture of the CFRTP sandwich specimens using CBA is determined, see Figure 50.

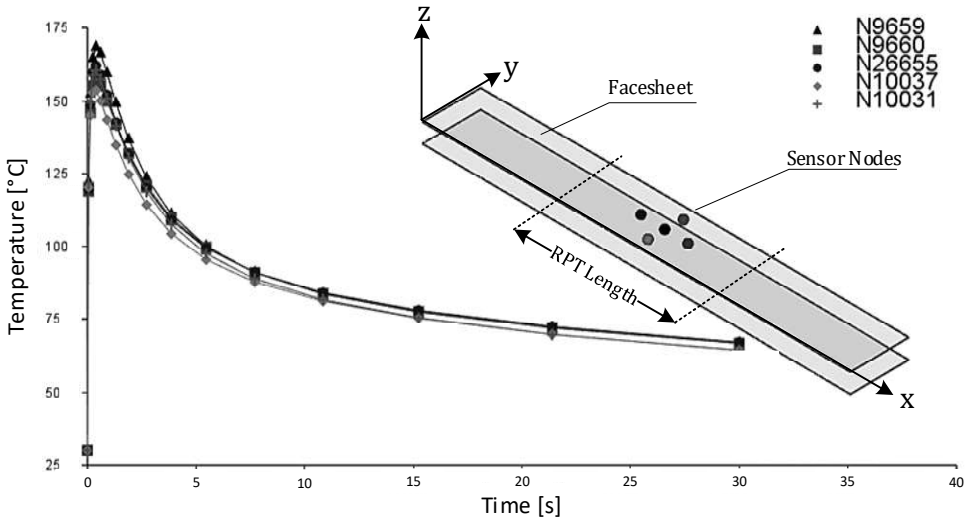


Figure 50: Simulated interface temperature development during the in-situ CFRTP sandwich manufacture based on Moldflow: in the centre of the facesheet surface and the roller peel test length, five nodes are used for the assessment of a mean temperature profile during the process.

The simulated temperature profiles on the CFRTP facesheet surfaces resulting from the injected polymer melt require experimentally assessed temperature profiles for validation. Trippel [132] developed a specific mould insert with an integrated thermocouple based on the mould and inserts used in this work. This mould-insert enables the in-situ measurement of temperature profiles on the surface of CFRTP facesheets overmoulded by an integral foam. The thermocouples exhibit a diameter of 0.25 mm and were specifically designed to provide a low thermal inertia in order to account for the high heating and cooling rates during the process. In the work of Trippel, the thermocouples were attached on UD tape facesheets equal to the ones used in the present work (Celstran® CFR-TP PP GF60-13). The campaign was conducted using the same material and process parameters as within the present work, including the injection moulding machine (Demag Multi 80 -310h/200v), the mould and the manufacturing process of specimens.

The experimentally assessed temperature profiles of the facesheet surfaces by Trippel [132] as well as the temperature profiles simulated within the present work are depicted exemplarily in Figure 51. It shows the resulting interface temperature at a melt temperature of $T_m$ = 270 °C and a mould temperature of $T_w$ = 30 °C. More simulation results can be found in Annex A.

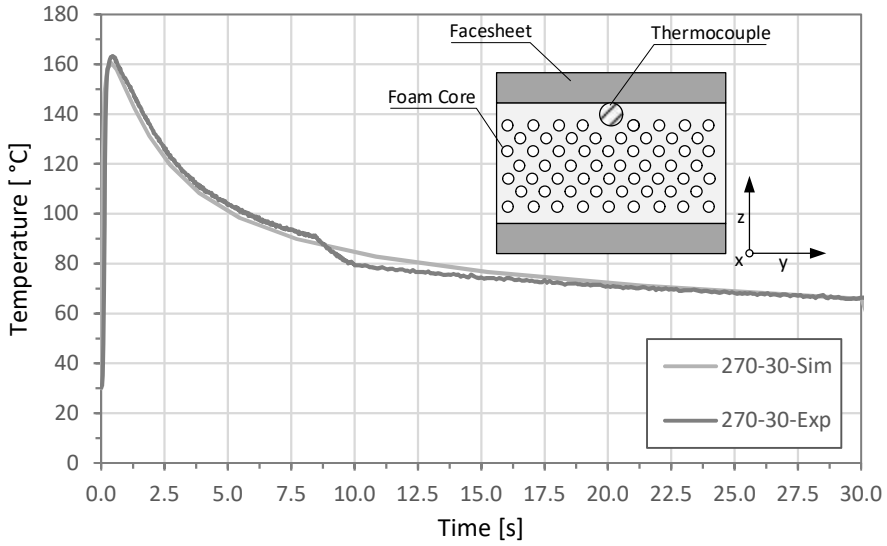


Figure 51: Comparison of simulated and experimentally assessed interface temperature development during the in-situ manufacture of CFRTP sandwich specimens at $T_m$ = 270 °C and $T_w$ = 30 °C. The simulation yields a high agreement with the measured temperature at the interface.

The simulation results and the experimentally assessed interface temperature correlate well for the evaluated process temperatures. The simulation with very low deviation from the experimental measurements precisely predicts the initial peak temperature as well as the cooling behaviour. This is necessary as the reptative movement of chains across an interface during fusion bonding is very temperature-sensitive, especially at the vicinity of the melting temperature, leading to variation interfacial bonding by several factors induced by only small temperature variations [139, 182].

# 5. Interfacial Bonding of In-Situ CFRTP Sandwich Structures

This chapter focuses on the interfacial bonding between UD tape facesheets and polymer cores during the in-situ manufacture of CFRTP sandwich components, see Figure 52. The goal of this study is to achieve a profound understanding about the mechanisms leading to high or low interfacial bonding between CFRTP facesheets and polymer cores during the process.

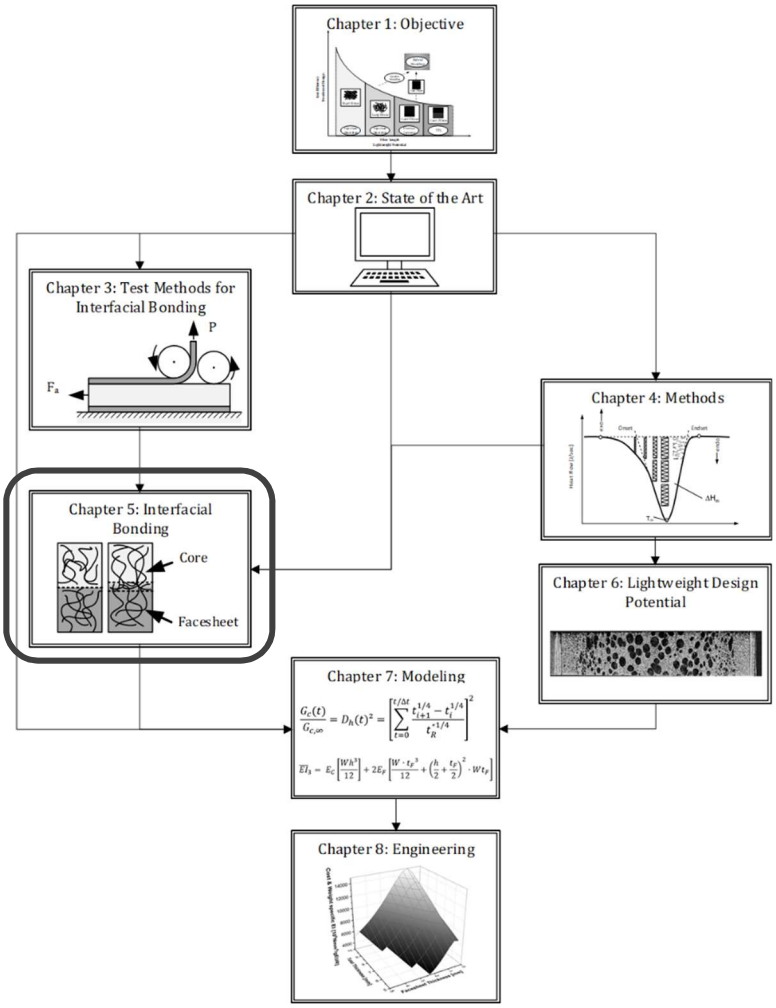


Figure 52: Systematic approach of this work: chapter 5 focuses on the evaluation of mechanisms behind the interfacial bonding development between facesheet and core during the manufacture of in-situ sandwich specimens.

Therefore, in-situ CFRTP sandwich specimens will be manufactured using a variation of process, material and structure parameters. The effect of these parameters on the interfacial bonding is assessed by mechanical testing, fracture as well as polymer analysis.

## 5.1. In-Situ CFRTP Sandwich Structures with Solid Core

In the first part of the study, the use of blowing agents as well as additional nucleating agents is deliberately omitted, in order to distinctly investigate only the fusion bonding of two miscible semi-crystalline polymer surfaces. The results of this study shall provide the foundation for the subsequent experimental campaign in which in-situ CFRTP sandwich structures with integral foam cores are subject to a detailed investigation.

### 5.1.1. Specimen and Materials

The CFRTP sandwich specimen is depicted in Figure 53. It exhibits a specimen length of $L$ = 220 mm, specimen width of $W$ = 30 mm and core thickness of $h$ = 2.34 mm. The total specimen thickness $H$ and the facesheet thickness $t_F$ are both subject to variation, according to the design of experiments, see Table 7. Specimens, which will be subject to roller peel testing, are modified: 30 mm of the facesheet surface facing the polymer core are covered with a polyimide (PI) foil, which generates the necessary initial crack length $a$.

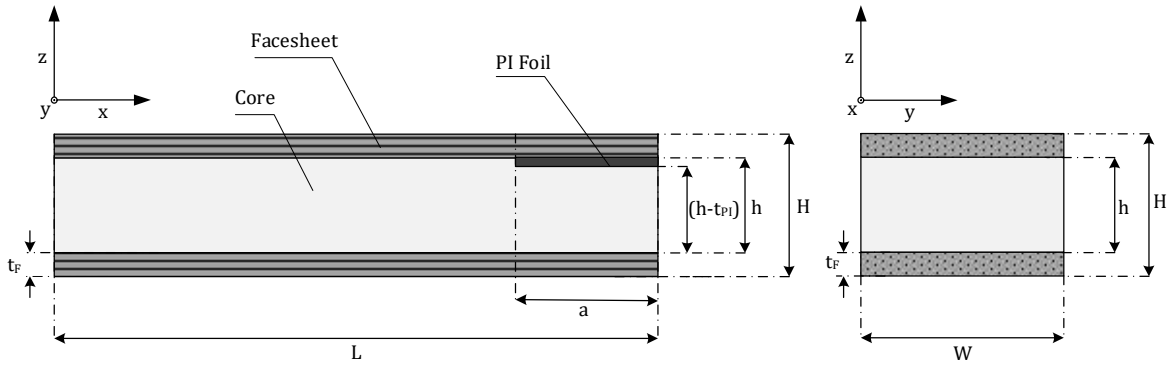


Figure 53: In-situ CFRTP sandwich specimen with solid polymer cores: specimen geometry in length (left) and cross direction (right). The glass fibres of the facesheets are oriented in x-direction.

The immiscibility of the PI tape with polypropylene and its much higher melting temperature ensures that no bonding develops between facesheet and the injected polypropylene core during in-situ sandwich manufacture. An initial crack length of 30 mm is necessary for the test, since the facesheet needs to be re-directed first around the peel rollers after which it is fastened with the help of the clamping jaws before the start of testing. The thickness of the PI foil was chosen to be as low as possible yielding $t_{PI}$ = 0.07 mm in order to ensure that the initial crack is near the bonding interface. In preliminary tests, RPT of specimens with different separating foil thicknesses have shown different resulting interfacial fracture toughness, thicker foils yielding significantly higher $G_I$ values.

The core and facesheet materials are presented in Table 6. The core material is a standard polypropylene homopolymer (Sabic® PP 576P) which will be used as the reference core material in this work. The facesheets consist of unidirectional continuous glass fibre reinforced polypropylene tapes with 60 wt.-% glass fibres (Celstran® CFR-TP PP GF60-13), which are oriented in x-direction (0°-direction).

Table 6: Overview of material paramters of the UD tape sandwich facesheet and the polymer core (*according to the datasheet [287], **according to DSC measurements in Annex B).

| | | Core | Facesheet | Dimension |
|---|---|---|---|---|
| Material | Name | Sabic® PP 576P | Celstran® CFR-TP PP GF60-13 | - |
| Polymer | Type | PP-H | PP-H | - |
| | Melting Temperature | 166 | 173*/163** | °C |
| Filler | Type | - | GF | - |
| | Content | - | 60 | wt.-% |
| | Structure | - | UD | - |
| | Orientation | - | 0 | ° |

As supplied, the UD tape is wound up on a roll. The thickness of the tape is 0.33 mm and the width is 330 mm. In this work, all UD tapes were cut from one roll, which reduces possible variations due to differences between lots to a minimum.

### 5.1.2. Design of Experiment

The experimental design focuses on the variation of process, material and structural parameters. The process parameter and values are depicted in Table 7. These values are based on simulations of the resulting interface temperature between UD tape facesheet and the injected core during the in-situ manufacture of sandwich specimens.

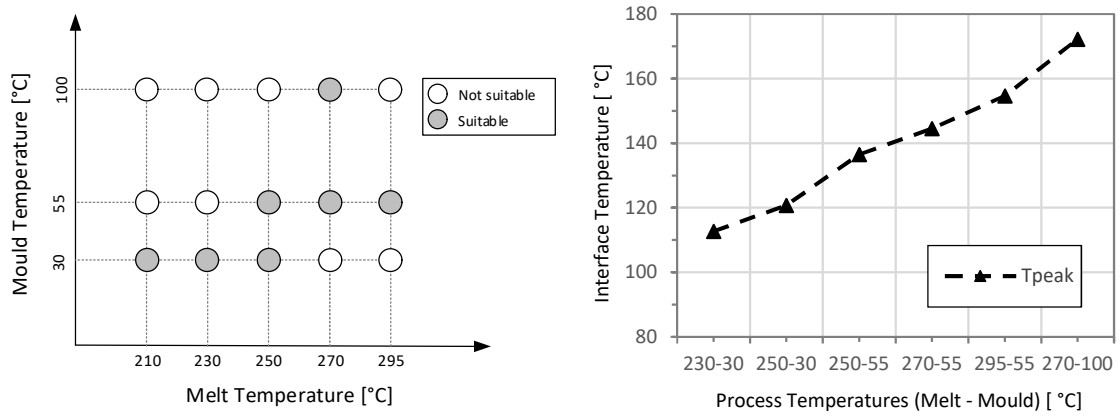


Figure 54: Schematical illustration of the DoE: decision for process parameters combinations (left) due to the resulting interface temperature (right). Process combinations combining high melt and low mould temperatures and vice versa lead to similar interface temperatures, which shall be avoided for the sake of a reduction of required tests settings.

Simulations of the interface temperature during in-situ manufacture have shown that these process parameter combinations yield in an almost linear increase of the peak temperature at the skin-core interface during the in-situ moulding of CFRTP sandwich specimens, see Figure 54. Therefore, process parameter combinations along the diagonal of the process parameter plane, see Figure 54 (left), were chosen for the experimental campaign.

Based on these considerations, the melt temperature $T_m$ is varied between 210 °C and 295 °C with 5 values in this experimental campaign, see Table 7. The mould temperature $T_w$ ranges from 30 to 100 °C with three values. The combination of melt and mould temperature is termed process temperatures henceforth.

Table 7: Overview of the process and material parameter variation.

| Parameters | Value 1 | Value 2 | Value 3 | Value 4 | Value 5 | Dimension |
|---|---|---|---|---|---|---|
| Melt Temperature | 210 | 230 | 250 | 270 | 295 | °C |
| Mould Temperature | 30 | 55 | 100 | - | - | °C |
| Facesheet Thickness | 0.33 | 0.6 | - | - | - | mm |

The facesheet thickness of in-situ CFRTP sandwich specimens is subject to variation between 0.33 mm and 0.6 mm according to the experimental design. The preparation of the 0.33 mm thick UD tape facesheets (1UD) for CFRTP sandwich manufacture requires cutting facesheet blanks from the

330 mm wide original tape by a hydraulic jar, see Figure 55. The edge areas of the UD tape are not used for the creation of facesheet blanks due to observed thickness differences compared to the middle part of the tape.

The 0.6 mm thick, facesheets (2UD) are manufactured by consolidation of two 1UD layers. A resulting average thickness of 0.6 mm of the 2UD laminate after the consolidation process was measured using a caliper. After demoulding of the 2UD laminates, they are cut equivalently to 1UD by means of a hydraulic jar receiving the final facesheet blanks. The consolidation process parameters are based on the processing guidelines provided by the tape manufacturer.

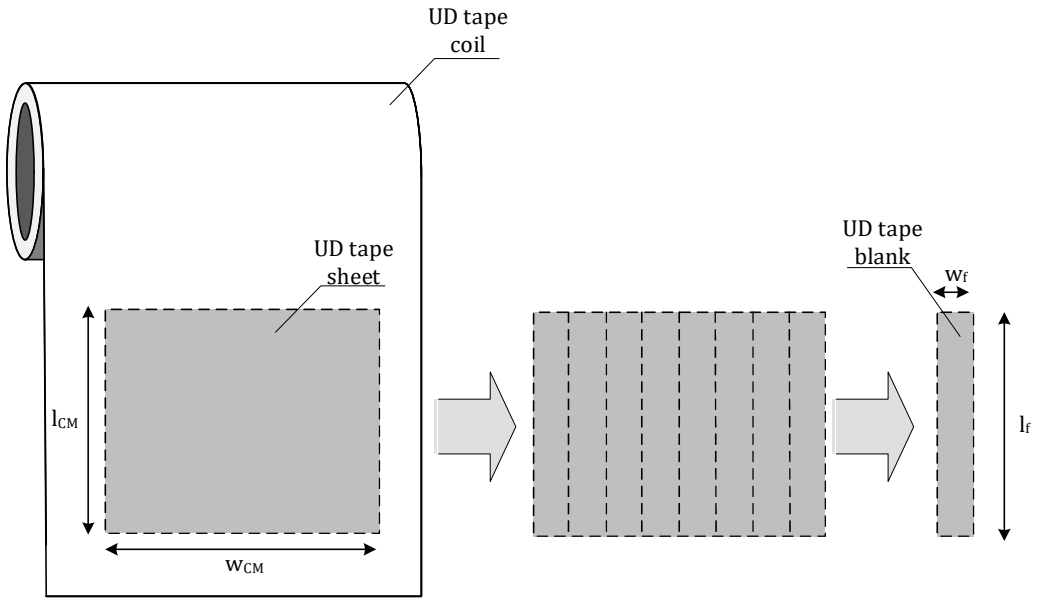


Figure 55: Preparation of 1UD facesheet blanks from the as-received UD tape roll: cutting a sheet from the roll and subsequent preparation of the UD tape facesheet blanks.

### 5.1.3. Manufacture of Specimens

The in-situ CFRTP sandwich test specimens are manufactured using a Demag Multi 80 -310h/200v injection moulding machine equipped with a standard 3-zone screw and a vertically mounted plasticizing unit with a needle shut-off nozzle.

The specimen is manufactured using a specific mould for the in-situ injection moulding of CFRTP sandwich components, which also allows a variation of component thickness $H$ by changing mould inserts, see Figure 56. The cavity thickness $H$ can be adjusted between 3.0, 3.6 and 10.0 mm. While the 10 mm cavity thickness is applied for foam injection moulding, 3 and 3.6 mm cavity thickness are used for CFRTP sandwich specimens with compact polymer core and 1UD and 2UD facesheets respectively. By adjusting the cavity thickness from 3 to 3.6 mm, the polymer core volume remains the same for 1UD and 2UD facesheet sandwich specimens. In order to generate a homogeneous flow of melt into the cavity and a uniform pressure development, a film gate is used. Both mould halves are each temperature controlled using a separate water circuit. The mould temperature is measured by two thermocouples, which are installed in both mould halves. To ensure a stable process temperature in the tool and plasticising unit, ten parts are manufactured before specimens are used for subsequent analysis.

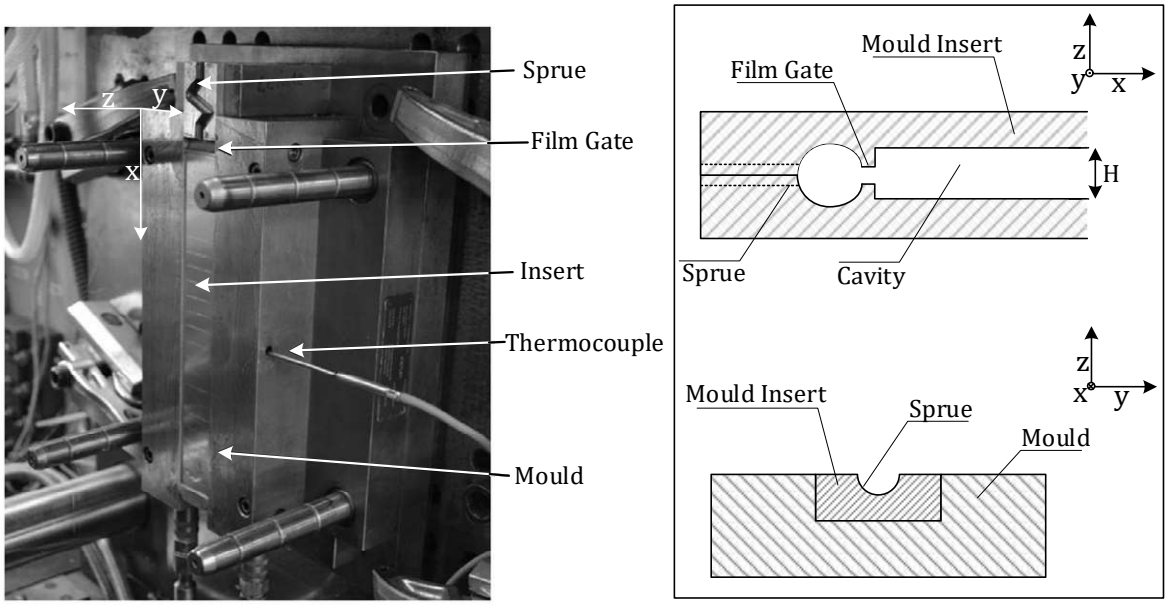


Figure 56: The mould for the manufacture of in-situ CFRTP sandwich specimens (left) includes a mould insert enabling the use of different cavities (right). This allows for the variation of component thickness using the same mould.

The manufacture of the specimens includes six process steps, which are schematically depicted in Figure 57.

After tailoring of the UD tape facesheets, they are cleaned with acetone in order to free the UD tape surfaces from any foreign substances that could have an effect on the bonding behaviour to the core. The polypropylene matrix of the UD tapes exhibits only a low solubility with acetone, thus the acetone cleaning treatment is assumed to have a negligible effect on the bonding behaviour [288]. The prepared and cleaned facesheets are placed and fixed manually in both mould sides. The UD tapes are always inserted with the same surface side up in the mould in order to avoid asymmetry effects induced by the UD tape production on the interfacial bonding. Since the tapes are delivered wound up on a roll, a slight curvature can still be observed after the facesheets have been tailored. It was made sure that the convex side is always pointing to the respective mould half after insertion. After closing the mould, the plasticised polypropylene melt is injected in the cavity between the two facesheets.

The injection moulding machine process parameters are presented in Table 8.

Table 8: Injection moulding machine parameters.

| Process Parameter | Value | Dimension |
|---|---|---|
| Injection Speed | 30 | ccm/s |
| Shot Volume | 34 | ccm |
| Switchover Point | 11 | ccm |
| Cooling Time | 30 | s |
| Hold Time | 20 | s |
| Hold Pressure | 300 | bar |

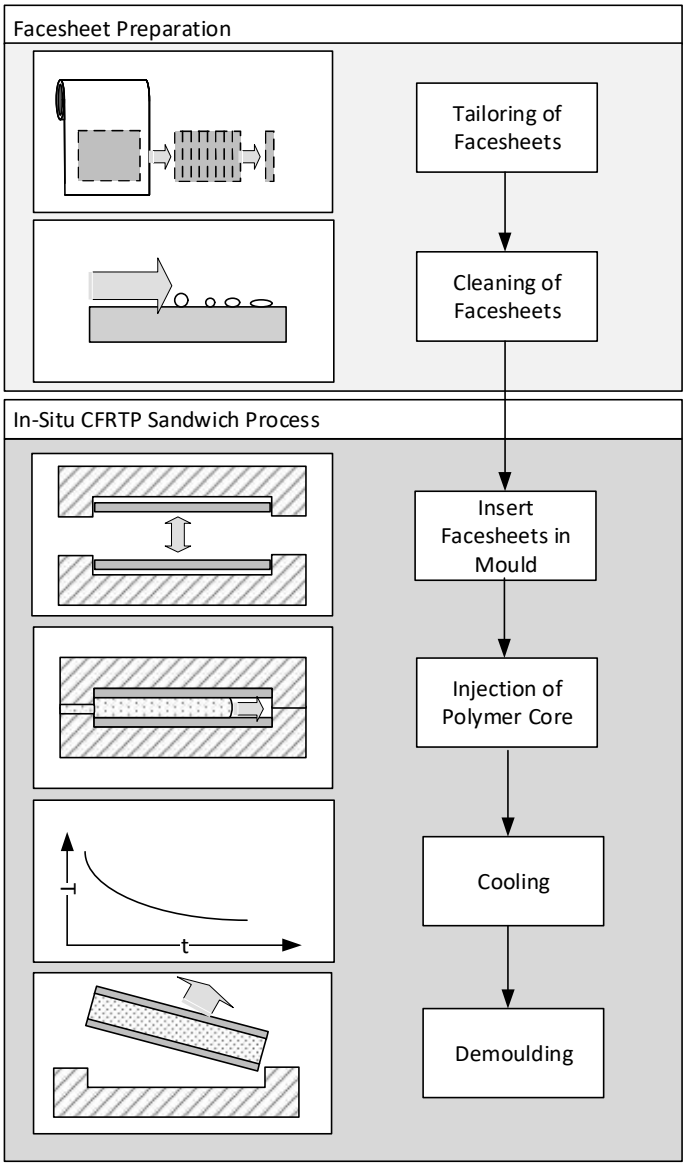


Figure 57: Schematic overview of the process steps of the in-situ manufacture of CFRTP sandwich structures, divided into the facesheet preparation and the actual in-situ manufacturing process.

After a cooling time of 30 s, the manufactured in-situ CFRTP sandwich component can be removed from the cavity and the next facesheets are placed in the moulds. Care is taken to keep the handling time for the placement of the facesheets in the moulds as constant as possible in order to minimise its influence on the resulting total cycle time.

### 5.1.4. Results

According to the design of experiments, the results of the process parameter variation on the interfacial fracture toughness and interfacial strength of compact injection moulded polymer cores to UD tape facesheets will be presented and discussed. Thereafter, the relationship between facesheet material parameters and the aforementioned sandwich properties are addressed.

***Process Parameter Variation***

The effect of the process parameter variation on the resulting interfacial bonding of 1UD tape facesheets to the injection moulded compact polypropylene core is presented in Figure 58. The process parameters comprise the polymer melt temperature and mould temperature. Roller peel test results show, that at the lowest process temperature combination of $T_m$ = 210 °C and $T_w$ = 30 °C no quantifiable fracture toughness of the interface between facesheets and polymer core could be assessed via RPT. Equally, the notched lap shear test yields no interfacial strength at this process temperature combination. However, a stress transfer of face to core could be measured with both testing methods at 20 °C higher melt temperature ($T_m$ = 230 °C) and unchanged mould temperature ($T_w$ = 30 °C). The NLS test as well as the RPT yield a comparatively abrupt increase of interfacial strength and interfacial fracture toughness respectively at this temperature combination, reaching $G_I$ = 0.99 kJ/m² and $\tau_{NLS}$ = 12.9 N/mm².

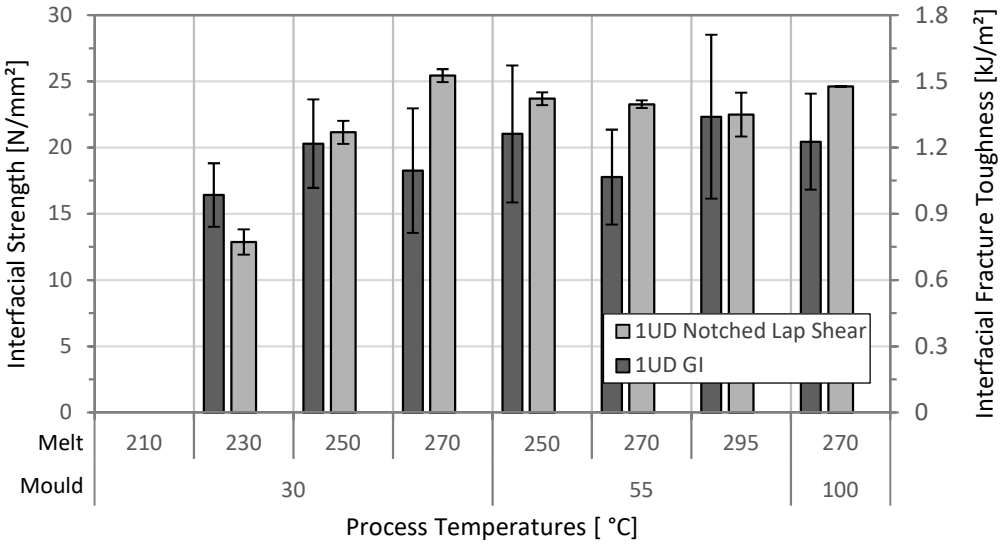


Figure 58: Results of interfacial fracture toughness and interfacial strength of in-situ sandwich specimens with UD tape facesheets and solid polymer core.

A further increase of the process temperature leads to growing interfacial strength and interfacial fracture toughness until both test methods yield a plateau value. The interfacial fracture toughness and interfacial strength plateau values are $G_I$ ≈ 1.5 kJ/m² and $\tau_{NLS}$ ≈ 25 N/mm². The interfacial fracture toughness plateau value is reached beginning at $T_w$ = 30 °C and $T_m$ = 250 °C whereas the interfacial strength plateau is reached at the same mould temperature yet 20 °C higher melt temperatures ($T_m$ = 270 °C). The plateau values are not exceeded even with the highest process temperature combinations. This indicates that already at moderate process temperatures the maximum interfacial skin-core bonding is achieved using 1UD facesheets.

Fracture Analysis

Images of the macroscopic fracture surfaces after roller peel testing were taken using a Nikon D300 digital reflex camera with a close-up lens. Figure 59 (left) shows the macroscopic fracture surface of an in-situ CFRTP sandwich specimen manufactured at $T_m$ = 230 °C and $T_w$ = 30 °C after roller peel

testing. The surface is heterogeneous and consists of two distinct fracture features. The fracture surface appears at most parts glassy and even. This surface fracture feature resembles the initial crack length $a$ of the specimen where the PI foil prevents fusion bonding of core and facesheet. Additionally, a second fracture surface feature can be observed on RPT specimens after testing: limited to specific locations on the specimen surface, rough and untransparent surface areas are found. This fracture feature dominates the surface of roller peel tested specimens which are manufactured at higher process temperatures with only little proportion or even complete absence of glassy surface areas, see Figure 59 (right).

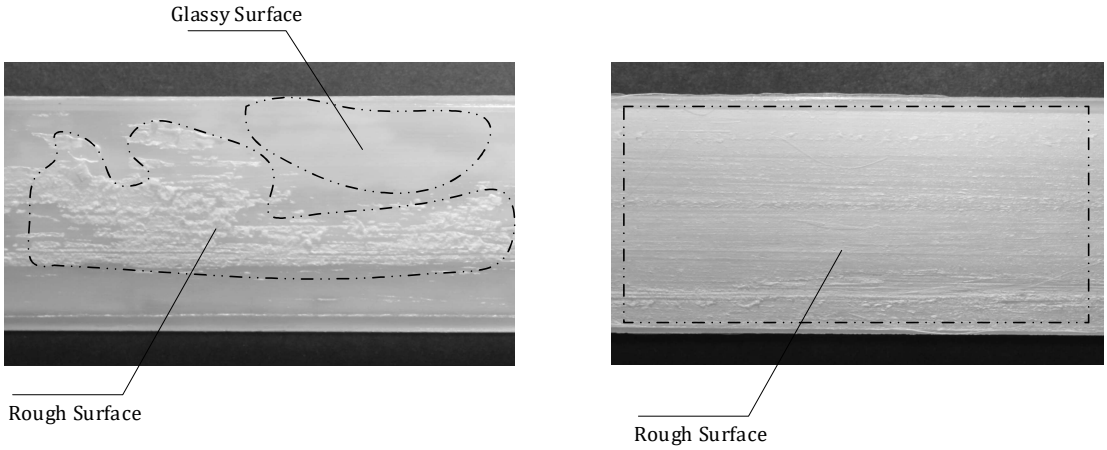


Figure 59: The image shows the core-sided fracture surface of in-situ CFRTP sandwich specimens after roller peel testing: incomplete fusion bonding of the interface characterised by a heterogeneous surface (left) at $T_m$ = 230 °C and $T_w$ = 30 °C compared to a complete fusion bonding of the interface (right) at $T_m$ = 270 °C and $T_w$ = 100 °C.

It is hence assumed that at low process temperatures fusion bonding is only successful at a locally limited fraction of the skin-core interface. This may be attributed to inhomogenous thermal properties of the facesheets due to the different thermal conductivities and heat capacities of glass fibre and PP matrix and the inhomogenous fibre volume fraction within the cross section of the UD tapes [95]. Hence, if the interface temperature is at the edge of being sufficient for complete melting of the UD tape surface, small and locally limited variations of its thermal properties may cause successful fusion bonding at one region of the facesheet-core interface and unsuccessfull fusion bonding at others.

In order to evaluate the fracture behaviour on a microscopic scale, scanning electron microscopy images of the fractured surfaces were made. In Figure 60, a representative part of the fracture surface of a specimen after roller peel testing, manufactured with $T_m$ = 230 °C and $T_w$ = 30 °C, is analysed by means of SEM at different magnifications between 50 x and 1000 x.

Figure 60 (a) clearly depicts the two different macroscopic fracture surface features presented in Figure 59. Next to the glassy surface, an area with rough and deformed structures can be observed. Consequently, the glassy feature of the fracture surface is considered as interface fraction where no fusion bonding took place. The surface area with rough appearance is considered as the fractured surface after successful fusion bonding of CFRTP facesheet and core.

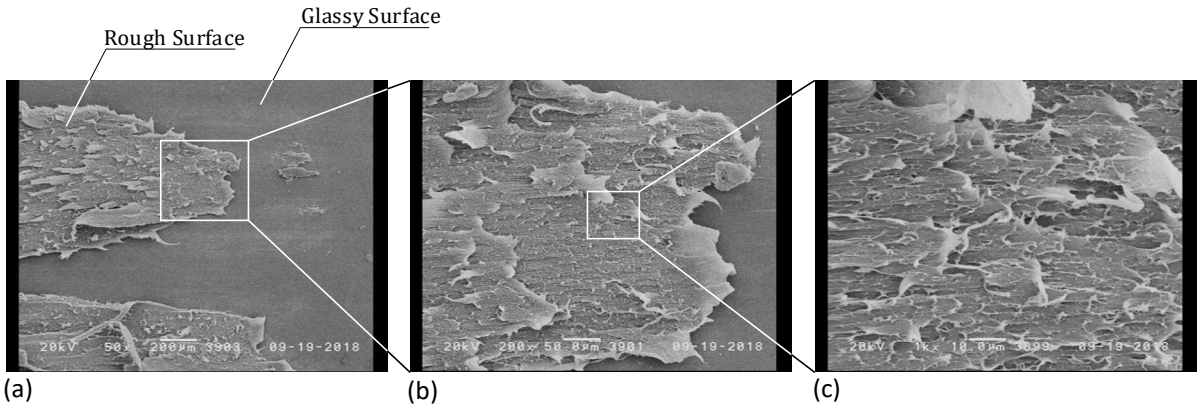


Figure 60: SEM images of the fracture surface of in-situ sandwich specimens manufactured at $T_m$ = 230 °C and $T_w$ = 30 °C after roller peel testing: 50x magnification (a), 200x magnification (b) and 1000x magnification (c).

The material-specific origin of this fracture feature, either facesheet or core, can also be determined by SEM analysis. In Figure 61, the crack onset $a$ of a roller peel test specimen is depicted.

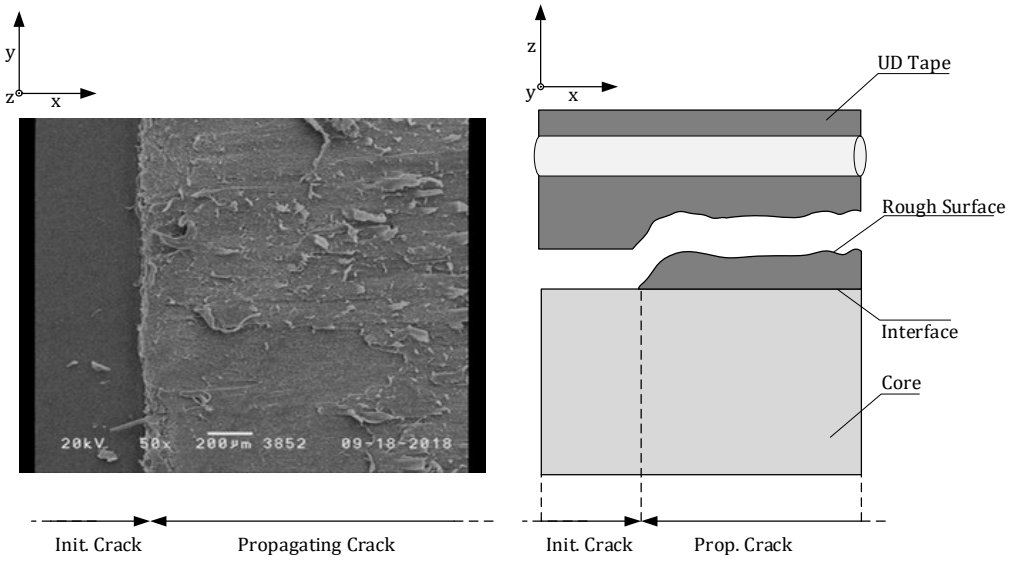


Figure 61: SEM of the initial crack zone with transfer to the RPT test zone at which the fracture surface protrudes from the initial interface between core and UD tape facesheet (left) which is schematically illustrated as cross section (right).

The glassy surface denotes the injection moulded polymer core material, which was covered by a PI foil preventing fusion bonding between CFRTP facesheet and injection moulded core. After the PI foil overlap ends, fusion bonding between the CFRTP facesheet and the polymer core took place. The RPT induced fractured surface clearly protrudes from the polymer core surface, indicating that the fractured surface is facesheet material, which is still bonded to the polymer core after testing. This suggests a good interfacial bond created during the in-situ manufacture which was similarly found by Grouve using a TTL process [16].

Higher magnifications of the fracture surface, see Figure 60 (b) and (c), show flake-shaped platelets at varying sizes between 10 and 200 µm which stand out of the surface at low angles oriented in the peel direction. Generally, these structures resemble cusps that develop at Mode II loading [289], however at larger dimensions in the present case. Figure 62 depicts the platelet and imprints in detail.

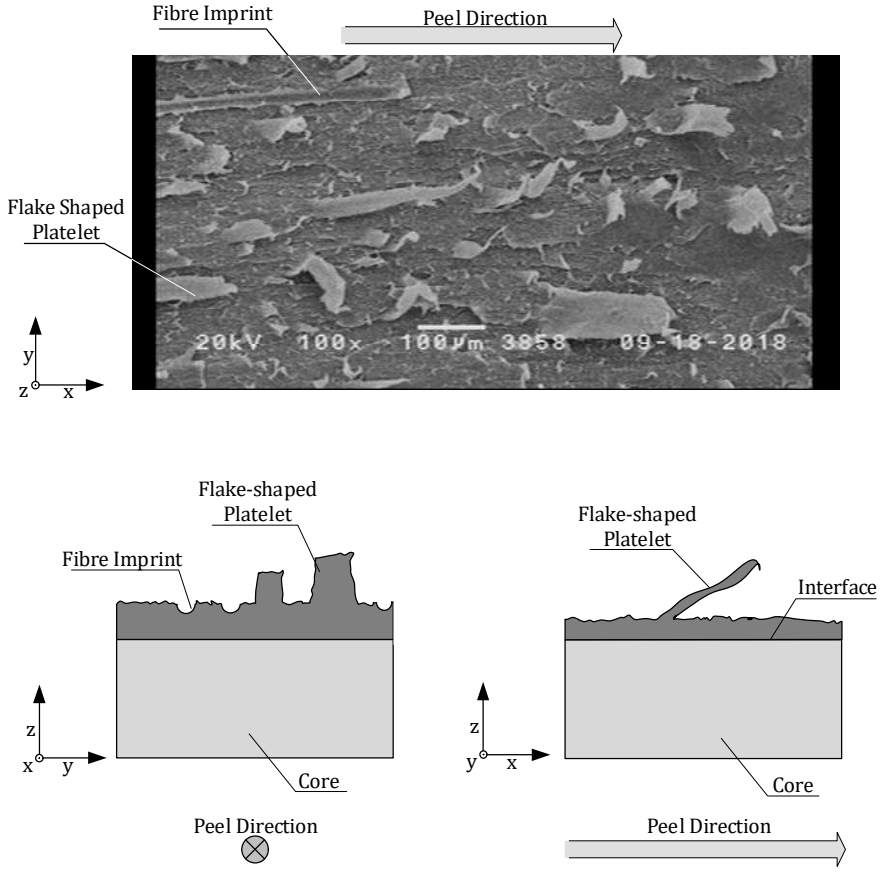


Figure 62: SEM image of the fractured surface after roller peel testing showing flake-shaped platelets protruding from the surface in peel direction (upper image). The schematic illustrations show the cross section of the sandwich specimen with the observed flake-shaped platelets and fibre imprints (lower images).

At 1000 x magnification, the fractured surface in Figure 60 reveals features of high plastic deformations such as large scale ductile drawing of the polymer material and fibrillation [289]. Fibrillation results from crack opening upon Mode I loading [289]. However, fibrils are smeared over the crack surface, resembling fracture surfaces with Mode II loading [289]. Generally, no fibre imprints can be observed.

Contrary to low process temperatures, fibre imprints are found on the fracture surface of sandwich specimens manufactured at high process temperatures. In Figure 63, the surface after roller peel testing of an in-situ CFRTP sandwich specimen manufactured at $T_m$ = 270 °C and $T_w$ = 100 °C is presented. Whilst no glassy areas can be determined in accordance with the macroscopic observation, rough surface areas with large plastic deformations are found. This feature is equivalent to the fractured surface of specimens manufactured with low process temperatures, though in the latter case it was locally limited due to the incomplete fusion bonding between core and facesheet.

Similar to specimens manufactured at low process temperatures, flake-shaped platelets can be observed again accompanied by regions with clear signs of fibre peel-off indicated by fibre imprints and fibrous residues.

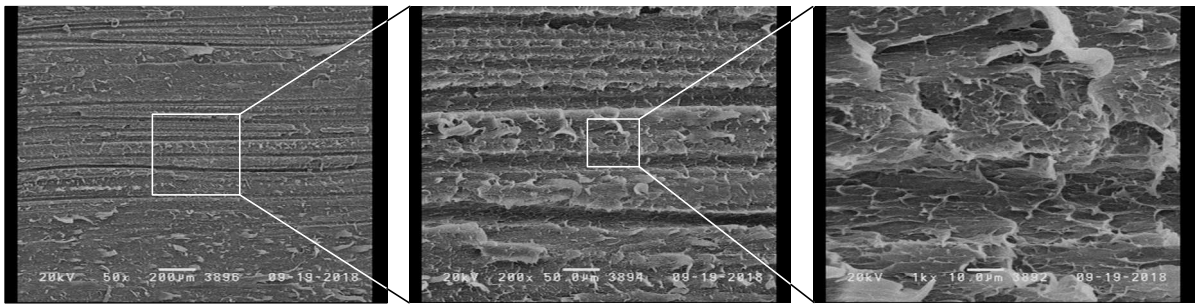


(a) (b) (c)

Figure 63: SEM images of the fracture of an in-situ sandwich specimen manufactured at $T_m$ = 270 °C and $T_w$ = 100 °C after roller peel testing: 50x magnification (a), 200x magnification (b) and 1000x magnification (c).

At higher magnifications, strong plastic deformation on micro-scale on the platelet surface and within the fibre imprints is found, see Figure 63 (c). The latter suggest that the fibre matrix adhesion of the UD tapes was good despite the nonpolar nature of polypropylene [278].

### Interface Analysis

It was shown that complete fusion bonding of the CFRTP facesheets and the injection moulded core is necessary to enable a high stress transfer between these two layers. A microscopic analysis of the interface region shall enable an understanding of the relationship of different interfacial bonding results and the respective skin-core interface morphologies. Therefore, thin cross sections of in-situ CFRTP sandwich specimens were cut using a LEICA RM2245 microtome along the x-z-plane with 50 µm thickness and subsequently analysed using an Olympus BX50 microscope.

In Figure 64, the cross section of a CFRTP sandwich specimen manufactured at $T_m$ = 230 °C and $T_w$ = 30 °C is depicted. The CFRTP facesheets appear dark, which suggests that the polymer matrix morphology within the tape is dominated by fine crystalline structures. This is assumed to be caused by the fibre reinforcement as the latter acts as strong nucleus [92, 93]. The injection moulded core shows a darker middle area, which becomes brighter in thickness direction. This indicates smaller spherulites in the middle, whereas they become larger with increasing distance to the centre. In the very vicinity of the face to core interface, the polymer core appears dark which suggests spherulites with small size. Only at a distance of more than 50 µm to the surface of the facesheet, a small number of larger spherulites can be found indicated by the typical Maltese cross. Contrary to previous studies using PA6 [95], an orientation of crystal growth or transcrystalline zone originating at the facesheet surface could not be found.

The fine spherulitic zone near the facesheet surface is considered the result of two factors. First, due to the low melt temperature of $T_m$ = 230 °C the facesheet surface exhibits only incomplete melting as shown by the fracture analysis, see Figure 59 and Figure 60, thus a mixture of solid and partially melted facesheets was achieved during in-situ injection moulding. Solid surfaces can act as strong

heterogeneous nucleus [79, 82, 83]. Hence, the crystallisation near the UD tape facesheet surface is dominated by heterogeneous primary nucleation at the partially unmelted facesheet surface. Second, the large temperature gradient of the polymer core and the comparatively cool facesheets, the latter due to the direct contact with the cooled mould at $T_w$ = 30 °C, induces a high cooling rate especially in the vicinity of the UD tape surface. This enables only a very limited time for the growth of crystallites in this interface-near region leading to smaller spherulite sizes. With increasing distance to the interface, larger radial spherulites of considerable size can develop. This leads to the assumption that the nucleation density decreases with growing distance to the facesheet surface.

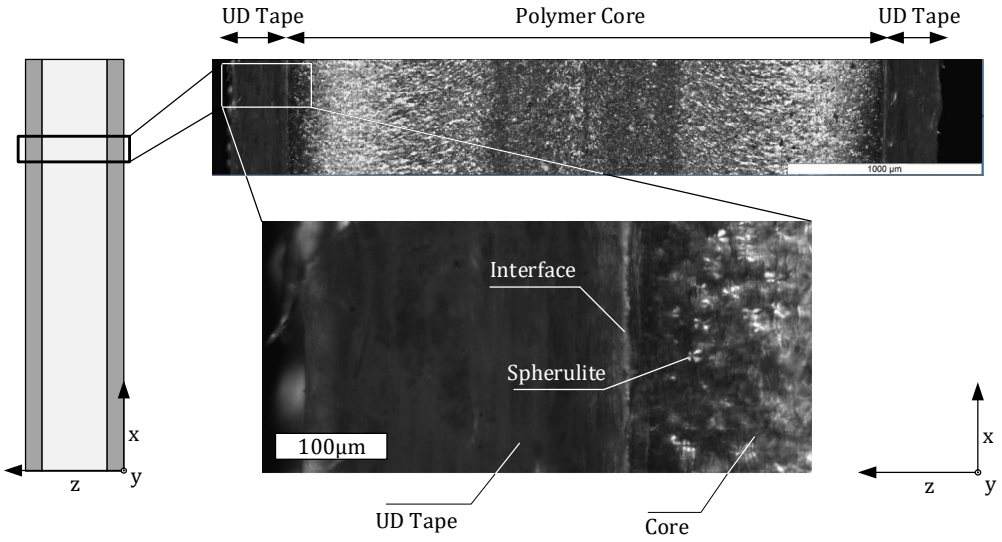


Figure 64: Image of the cross section of an in-situ sandwich specimen manufactured at $T_m$ = 230 °C and $T_w$ = 30 °C. The interface between core and UD tape facesheet is clearly observable showing fine spherulitic structures in the core near the UD tape.

In Figure 65, the cross-section of a 1UD sandwich specimen manufactured with $T_m$ = 270 °C and $T_w$ = 100 °C is depicted. In contrast to the analysed specimen with low processing temperatures, the polymer core appears much brighter and homogenous, indicating large spherulite structures all over the core cross section. The high mould temperature is assumed to lead to a slower cooling of the core, which results in increased crystal growth.

The interface region also shows distinct differences to the one observed at lower processing temperatures. Firstly, the core region at the vicinity of the UD tape surface does not appear dark, as it was found with lower melt and mould temperatures. Instead, bright and thus large crystalline structures developed which even spread across the former interface between facesheet and core. Higher magnification of the interface region shows that a clear interface between core and facesheets cannot be identified. Instead, a region is observed with no distinct separation of core and facesheets which is commonly termed interphase in contrast to the initial interface [168]. The interphase, connecting core and UD tape facesheets, is assumed to be caused by the high process temperatures, especially the high melt temperature. This enables complete melting of the CFRTP facesheet surface as shown in Figure 59 (right) and Figure 63 resulting in a reduced heterogeneous nucleating effect since the facesheet surface is not in solid state. Thus, less nuclei develop at the former interface of core and UD tape facesheet compared to lower process temperatures.

Subsequent crystal growth benefits from increased time spans at higher mould temperature combined with high melt temperatures. Moreover, nuclei are not spatially constraint by neighbouring nuclei due to the decreased nucleation density.

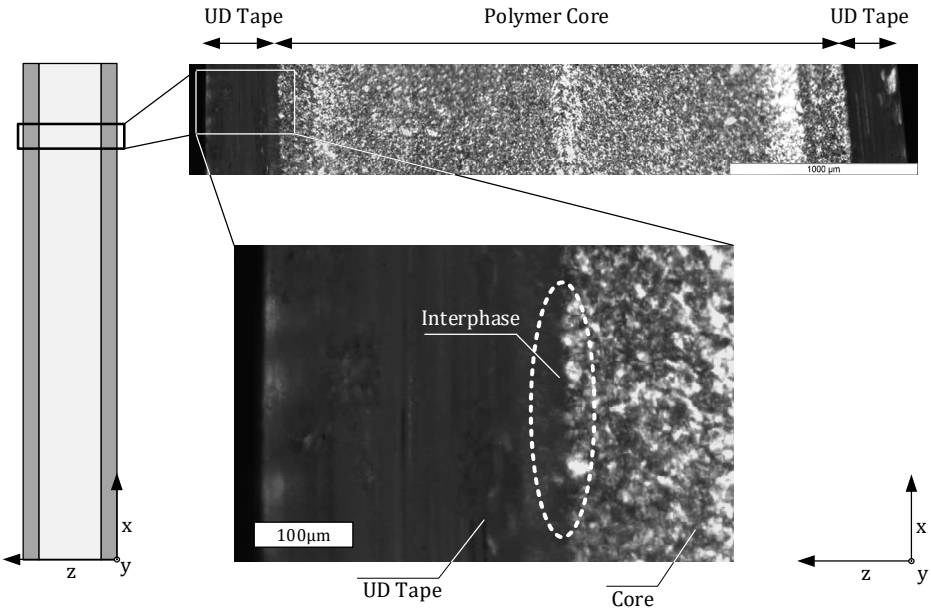


Figure 65: Image of the cross section of an in-situ sandwich specimen manufactured at $T_m$ = 270 °C and $T_w$ = 100 °C. Crystalline structures spread across at the former interface resulting in a new interphase, which is accompanied with increased interfacial bonding properties.

As a result, crystalline structures characterised by large spherulites grow across the former interface induced by the thermal gradient towards the core leading to an efficient stress transfer between core and facesheet in accordance with the findings of other authors [168, 183, 184].

### *CFRTP Facesheet Parameter Variation*

Considering the complete melting of the CFRTP facesheet as major requirement to achieve high skin-core interfacial bonding during the in-situ manufacture of CFRTP sandwich structures, the effect of different facesheet parameters shall be further evaluated. The investigated facesheet parameters comprise the facesheet thickness as well as the polymer matrix crystallinity.

#### CFRTP Facesheet Thickness

In Figure 66 the interfacial fracture toughness of sandwich structures with 1UD tape facesheets as well as 2UD laminate facesheets is presented. It can be observed that sandwich specimens with 0.6 mm thick 2UD facesheets yield significantly lower $G_I$ values than those with thinner 1UD tape facesheets with 0.33 mm tape thickness for most of the studied process temperatures. Especially at the lower end of the thermal process window, specimens with thicker 2UD facesheets yield only about 50 % of the interfacial fracture toughness of sandwich specimens with thinner 1UD facesheets at equal process temperatures. Only at elevated temperatures, beginning at $T_m$ = 270 °C and

$T_w$ = 55 °C, sandwich structures with 2UD facesheets yield $G_I$ values in the same range as sandwich specimens with 1UD facesheets.

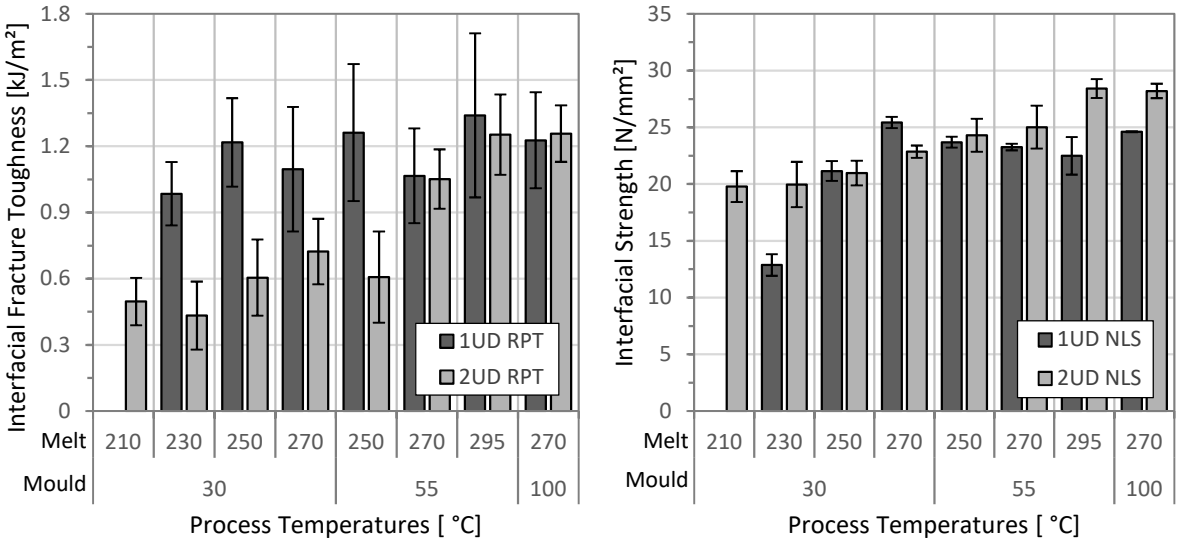


Figure 66: Interfacial bonding testing results of in-situ CFRTP sandwich specimens with varying facesheet thickness: interfacial fracture toughness (left) and interfacial strength (right).

The results of notched lap shear testing of in-situ CFRTP sandwich structures with UD CFRTP facesheets of different thickness are presented in Figure 66 (right). It must be noted that a direct quantitative comparison of CFRTP sandwich specimens with different structure such as facesheet thickness and total thickness based on notched lap shear strength results needs to be taken with care as single-lap shear based test method results are dependent on specimen geometry [213, 261]. However, a qualitative comparison of the interfacial strength development in relationship to the process temperatures is considered valid. This is supported by the observation, that RPT and NLS procedures yield similar qualitative result curves for the specific facesheet variants. While both interfacial strength and fracture toughness of in-situ CFRTP sandwich specimens with 1UD facesheets increase rapidly within a narrow process temperature span yielding a plateau of both properties, sandwich specimens with 0.6 mm thick 2UD facesheets show a steady increase of $G_I$ as well as $\tau_{NLS}$ values throughout the observed process temperature range.

The NLS results for sandwich specimens with varying facesheets thickness in Figure 66 (right) show, that contrary to sandwich specimens with thin 1UD facesheets, those with 2UD facesheets exhibit interfacial strength already at the lowest process temperature combination ($T_m$ = 210 °C and $T_w$ = 30 °C). The notched lap shear strength of 2UD sandwich structures increases approximately linearly with melt and mould temperature until $T_m$ = 295 °C and $T_w$ = 55 °C at which a maximum strength of $\tau_{NLS}$ = 28.42 N/mm² was measured.

Comparing the general interfacial bonding behaviour of in-situ injection moulded sandwich specimens with thin 1UD and thick 2UD facesheets and the polymer core, sandwich structures with thicker 2UD laminate facesheets yield significantly lower interfacial fracture toughness values especially at low to moderate process temperatures. In order to comprehend the reasons for this difference, the interface temperature profiles resulting from the combined processed temperatures

during the in-situ manufacture are evaluated since the facesheet thickness may have an effect on the resulting interface temperature leading to different interface temperatures of 1UD and 2UD sandwich structures at equal process temperatures.

The effective interface temperature between CFRTP facesheets and injection moulded polymer core resulting from the process temperatures was simulated using Autodesk Moldflow Insight 2019, according to the procedure presented in chapter 4.3. The results of interface temperature simulations for in-situ CFRTP sandwich specimens with 0.33 and 0.6 mm facesheet thickness are presented in Figure 67.

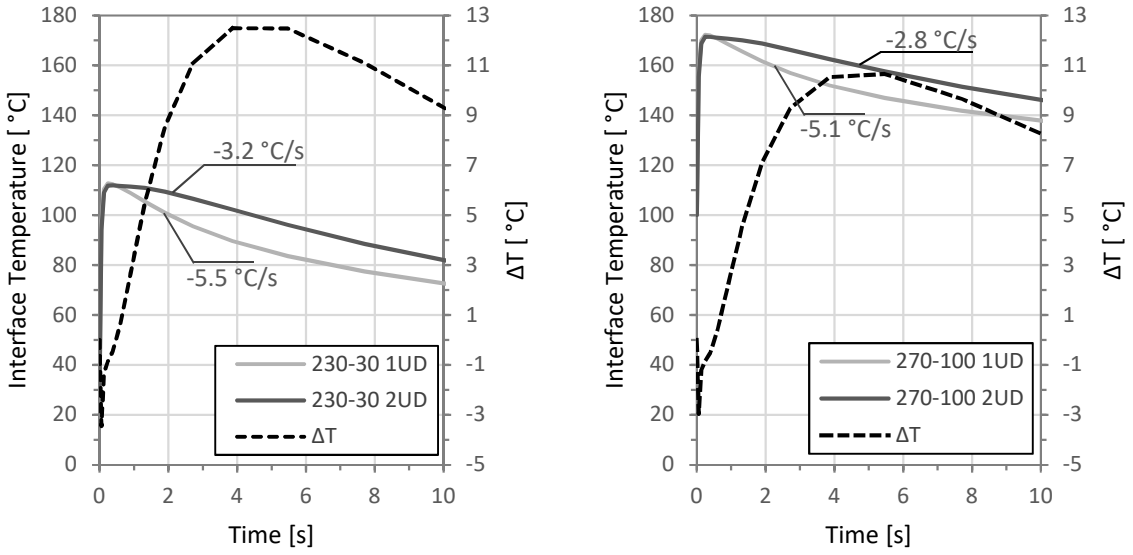


Figure 67: Simulation of the interface temperature development during the in-situ manufacture of CFRTP sandwich specimens with different facesheet thickness yields: significantly different cooling rates are found for sandwich specimens with different facesheet thickness at low process temperatures (left) as well as high process temperatures (right).

Whilst the interface peak temperature of sandwich specimens with different facesheet thicknesses is almost equal, the cooling rate during the in-situ manufacture of CFRTP sandwich structures differs. This is assumed to result from the thermal insulation effect of thicker 2UD facesheets, which act as thermal barrier to the cool mould. Thus, while the mean cooling rate in the first 5 seconds after the peak temperature is -5.5 °C/s for sandwich specimens with thin 1UD facesheets at $T_m$ = 230 °C and $T_w$ = 30 °C, it is reduced to -3.2 °C/s using facesheets with 0.6 mm thickness. Similarly, the cooling rate at higher process temperatures with $T_m$ = 270 °C and $T_w$ = 100 °C yields -5.1 °C/s and -2.8 °C/s for sandwich specimens with 1UD and 2UD facesheets respectively.

Considering the diffusion-based fusion bonding process, the reduced cooling rate has two effects. First, the peak temperature is held for a significantly longer time span, which has a strong effect on the resulting interfacial bonding. Second, the longer peak temperature time span leads in combination with the decreased cooling rate to a generally higher interface temperature within the first 30 seconds of the process. For more simulation results it is referred to Annex A. Especially within the first 10 seconds, the interface temperature difference of sandwich specimens with 0.33 and 0.6 mm facesheets can be as much as 12.7 °C in case of $T_m$ = 230 °C and $T_w$ = 30 °C. With a lower

difference of mould and melt temperature at $T_m$ = 270 °C and $T_w$ = 100 °C, the insulating effect of thicker facesheets decreases yielding a temperature difference of 10.8 °C.

Consequently, it is assumed that thicker CFRTP facesheets have a beneficial effect on resulting bonding behaviour to the sandwich core especially at lower process temperatures, since the lower cooling rate keeps the temperature at high temperatures for a longer time span. This may explain why CFRTP sandwich structures with 2UD facesheet exhibit a decent interfacial bonding between core and facesheet even at the lowest process temperature combination contrary to sandwich specimens with 1UD facesheets.

Given that the resulting peak interface temperature for in-situ sandwich structures with 0.3 mm and 0.6 mm thick UD facesheets can be considered approximately equal based on the simulation results, see Annex A, the interfacial fracture toughness for in-situ CFRTP sandwich specimens with varying facesheet thickness depending on the peak interface temperature can be evaluated. The simulated interface temperature of CFRTP facesheets with different thickness and the experimentally assessed $G_I$ values are depicted in Figure 68.

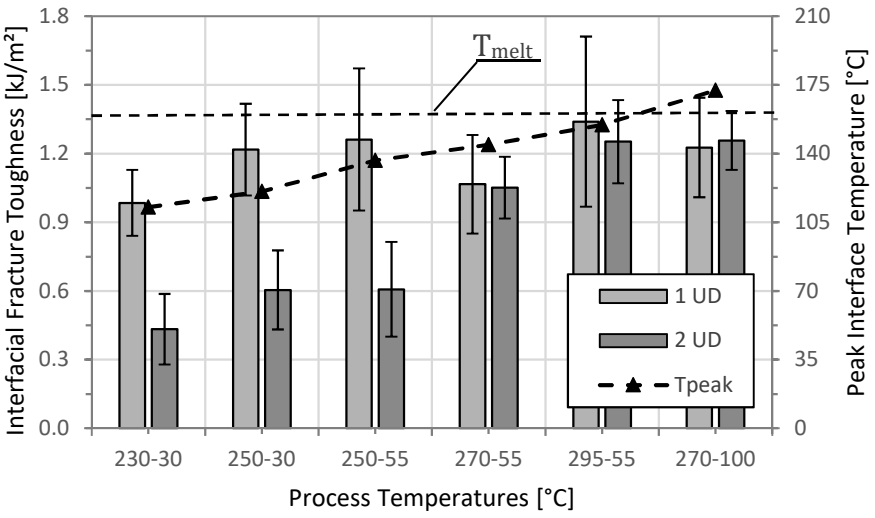


Figure 68: Comparison of interfacial fracture toughness of in-situ sandwich specimens with facesheets of different thickness with the resulting peak interface temperature during the manufacture. Sandwich specimens with 1UD facesheets yield high interfacial fracture toughness already significantly below the melting temperature of the facesheet. Using 2UD facesheets, this can only be achieved if the melting temperature of the facesheet is reached.

It can be observed that during the in-situ manufacture peak temperatures at both 1UD and 2UD facesheet surfaces do not reach the melting temperature of the UD tape material ($T_m$ = 163 °C according to DSC, see Annex B) until the maximum process temperature combination of $T_m$ = 270 °C and $T_w$ = 100 °C. However, despite the melting temperature of the facesheet was not reached, sandwich structures with thin 1UD tape facesheets already reach the aforementioned plateau value of $G_I$ at an interface temperature between $T_{peak}$ = 120.7 °C ($T_m$ = 250 °C, $T_w$ = 30 °C) and $T_{peak}$ = 136.5 °C ($T_m$ = 250 °C and $T_w$ = 55 °C). Considering the DSC results, this is 26.5 °C to 43 °C below the nominal melting temperature of the UD tapes. Contrary, sandwich specimens with thicker facesheets yield much lower $G_I$ values than those with thinner 1UD facesheets, if the melting temperature of the facesheet material is not reached. Only at an interface peak temperature near to

the melting temperature of the UD tape matrix polymer $T_{melt}$, the interfacial fracture toughness of sandwich specimens with thick 2UD facesheets yield similar values as 1UD sandwich structures.

The different bonding behaviour of 1UD and 2UD face on the polymer core after in-situ moulding shall be further evaluated using fractography analysis.

### Fracture Analysis

In Figure 69, the fracture surfaces of sandwich specimens with 0.33 mm and 0.6 mm thick UD tape facesheets at low processing temperatures ($T_m$ = 230 °C, $T_w$ = 30 °C) after roller peel testing are directly compared by means of SEM images. The fracture surfaces resemble each other in the fact, that a fusion bounding of core to facesheet took place only locally, resulting in a mixture of glassy surface and rough fusion bonded surface. At larger magnifications however, distinct differences can be observed between sandwich specimens with facesheets of different thickness. Contrary to the extensive plastic deformation observable on the fracture surface of sandwich specimens with thin 1UD tape facesheets, those with thicker 2UD facesheets result in a fracture surface that exhibits signs of brittle material behaviour indicated by relatively little plastic deformation, see Figure 70 [289]. Only a minor extent of fibrillation can be observed and no smeared micro-fibrils can be observed on the surface contrary to the surface of 1UD sandwich structures.

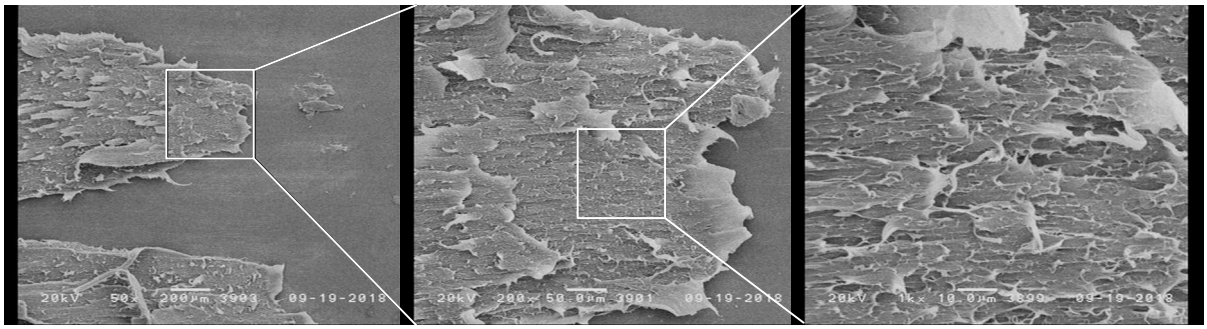


(a) (b) (c)

Figure 69: SEM images of the fracture of an in-situ sandwich specimen with as-received 1UD tape facesheets manufactured at $T_m$ = 230 °C and $T_w$ = 30 °C after RPT: 50x magnification (a), 200x magnification (b) and 1000x magnification (c).

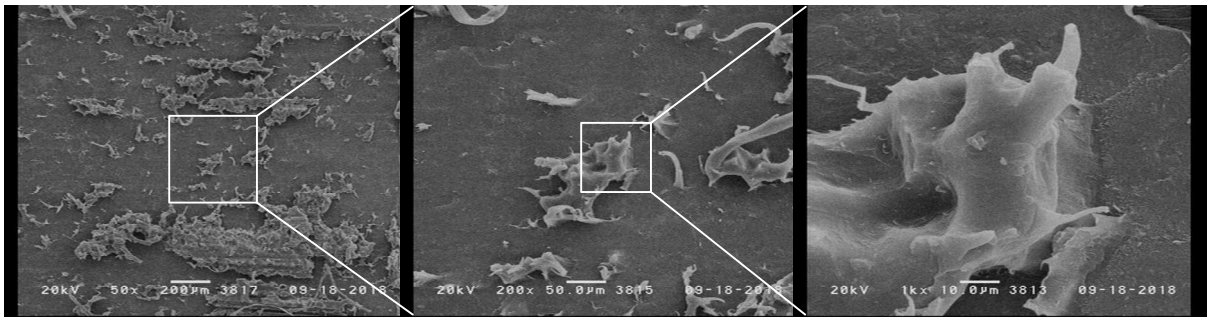


(a) (b) (c)

Figure 70: SEM images of the fracture of an in-situ sandwich specimen with thicker 2UD tape facesheets manufactured at $T_m$ = 230 °C and $T_w$ = 30 °C after RPT: 50x magnification (a), 200x magnification (b) and 1000x magnification (c).

In Figure 71, fractured surfaces of sandwich specimens manufactured using high process temperatures ($T_m$ = 270 °C, $T_w$ = 100 °C) are compared. The fracture surface of sandwich specimens with thin 1UD tape facesheet shows plastic deformations of the polymer as well as fibre imprints resulting from a peel-off of fibres from the CFRTP polymer matrix. This is a typical fractography feature found for unidirectional polymer composites during Mode I testing, especially for continuous glass fibre reinforced polymer composites [289]. Images with high magnification reveal large plastic deformation of the polymer matrix in the fibre imprints, indicating low crystallinity at the fibre-matrix interface which is beneficial for the fibre matrix adhesion [278]. In comparison, the fractured surface of sandwich specimens with thicker 2UD facesheets feature a rough structure including a large number of fibre imprints, see Figure 72. Also, fractured fibre ends with and without matrix still attached on the fibre can be observed, indicating fibre bridging during peel-off. Fibre bridging is favoured by a low fibre matrix adhesion and contributes to an increase of $G_I$ [290, 291]. A closer observation of the fibre imprints on the fracture surface indicates that only little plastic deformation during the fibre-matrix debonding occurred, suggesting a lower fibre-matrix-adhesion. Low fibre matrix adhesion indicates the presence of a higher matrix crystallinity in the vicinity of the fibre matrix interface [278].

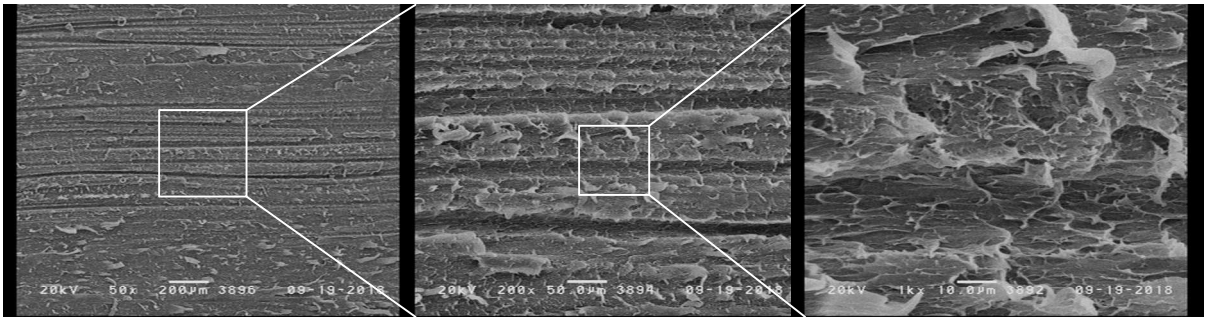

(a) (b) (c)

Figure 71: SEM images of the fracture of an in-situ sandwich specimen with as-received 1UD tape facesheets manufactured at $T_m$ = 270 °C and $T_w$ = 100 °C after RPT: 50x magnification (a), 200x magnification (b) and 1000x magnification (c).

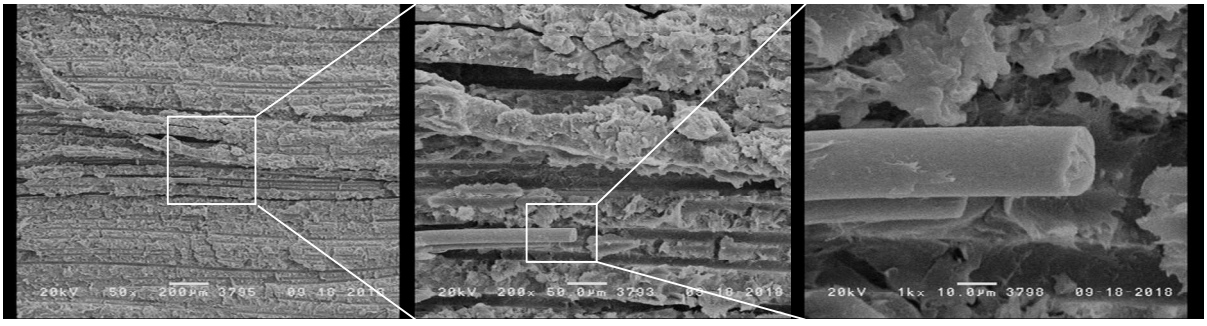

(a) (b) (c)

Figure 72: SEM images of the fracture of an in-situ sandwich specimen with thick 2UD tape facesheets manufactured at $T_m$ = 270 °C and $T_w$ = 100 °C after RPT: 50x magnification (a), 200x magnification (b) and 1000x magnification (c).

Thus, despite a more heterogeneous fracture surface and more fibre bridging, sandwich specimens with thicker UD facesheets do not yield higher interfacial fracture toughness values than in-situ CFRTP sandwich specimens with thin facesheets. The fracture surface of the CFRTP matrix polymer of

thick facesheets appears much more brittle and yields the assumption, that the degree of crystallinity of the matrix polymer of thicker 2UD facesheets is higher compared to the standard UD tape facesheets with 0.33 mm thickness, at least in the interface near region. The increased fibre bridging, typical for low fibre matrix adhesion, which correlates with higher crystalline fibre-matrix interface, also indicates this.

Considering that thicker 2UD facesheets require a consolidation step of two 1UD tape layers, it is assumed that the thermal history during consolidation alters the polymer matrix overall crystallinity. The thermal history during the manufacture of 2UD laminates via the consolidation of two 1UD tapes was therefore assessed. The unmodified 1UD tapes, in as-received condition, were first tailored according to the compression mould geometry with a length of $l_m$ = 250 mm and width $w_m$ = 250 mm. Two tailored 1UD tape sheets where placed into a hot mould where the layers were consolidated according to the material manufacturer guidelines. The thermal history during consolidation was determined by a thermocouple, integrated between the two 1UD tape sheets in the middle of the plate, see Figure 73.

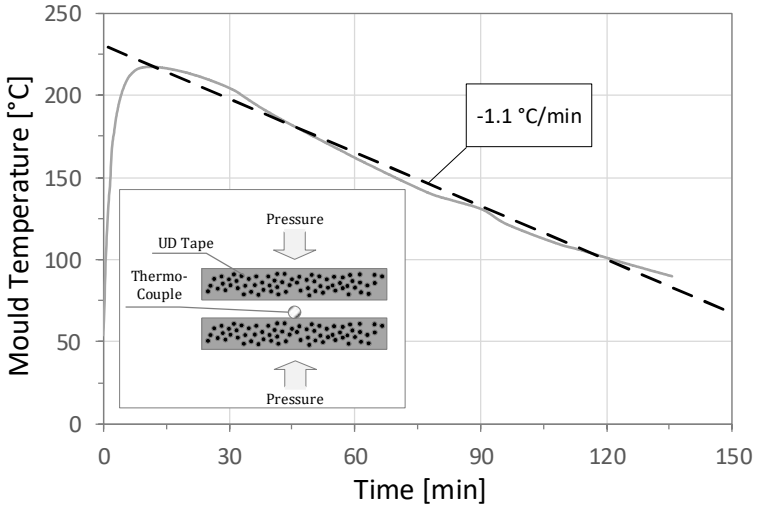


Figure 73: Temperature development at the interface between UD tape facesheets during consolidation assessed by a thermocouple: low cooling rates are observed due to a low cooling power combined with a high thermal inertia of the press.

Due to the large thermal inertia and considerably low cooling power of the press, a low cooling rate of the consolidated facesheets of $\dot{T}$ = 1.1 °C/min was determined. Subsequent DSC analysis revealed, that the reference 1UD tape, as received by the manufacturer, exhibits a degree of crystallinity of $\xi$ = 47.6 % whereas the compression moulded 2UD laminate yields a value of $\xi$ = 54.7 %. The degree of crystallinity quantified by means of DSC however must be taken with care and little differences cannot be considered significant. The determined difference between 1UD and consolidated 2UD tapes is though large enough that a significant difference of crystallinity is concluded. Consequently, it is assumed that the degree of crystallinity of the UD tape polymer matrix plays an important role with respect to the resulting skin-core bonding during the in-situ manufacture of CFRTP sandwich structures.

### CFRTP Facesheet Crystallinity

In order to evaluate the effect of the crystallinity of the facesheet matrix polymer on the interfacial fracture toughness $G_I$, facesheets with different degree of crystallinity were prepared and used for the manufacture of in-situ sandwich specimens in accordance with the procedure in chapter 5.1.3. In order to allow for a cross-correlation with 2UD facesheets, 1UD facesheets with higher crystalline fraction were prepared using the same procedure as for the manufacture of 2UD tapes. DSC measurements of all studied tapes were conducted, detailed test results can be found in Annex B. The 1UD tapes with modified high crystalline fraction (1UD-HC) were found to reach a degree of crystallinity of 55.25 % which denotes a clear increase compared to the reference 1UD tapes which yield $\xi$ = 47.6 %, see Table 9.

Table 9: Degree of crystallinity of differnet facesheets used in this study as determined via DSC (Annex B).

| Facesheet | Degree of Crystallinity | Dimension |
|---|---|---|
| 1UD | 47.6 | % |
| 1UD-HC | 55.25 | % |
| 2UD | 54.7 | % |

The interfacial fracture toughness of in-situ sandwich specimens with 1UD-HC tape facesheets is significantly lower compared to the ones with reference 1UD tape facesheets, see Figure 74 (left).

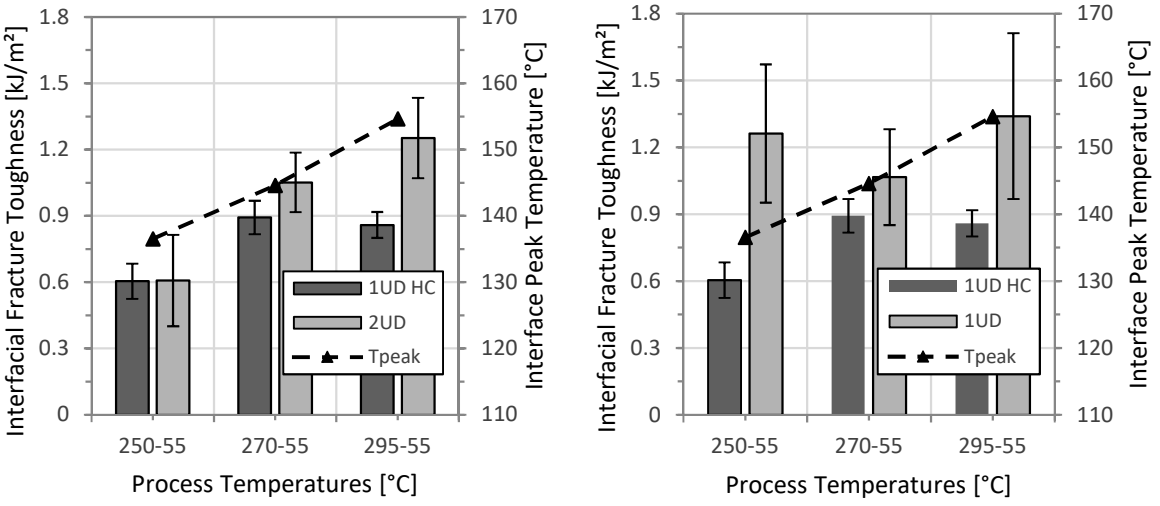


Figure 74: Interfacial fracture toughness using 1UD tapes in as-received condition (1UD) with a degree of crystallinity of $\xi$ = 47.6 % and annealed high crystalline 1UD tape facesheets (1UD-HC) with $\xi$ = 55.24 % shows a clear deterioration when using 1UD-HC (left). Sandwich specimens with similar facesheet crystallinity yield comparable interfacial fracture toughness results (right).

Especially at lower melt temperatures of $T_m$ = 250 °C, 1UD-HC facesheets bond poorly with the injected core yielding only about 50 % of the $G_I$ values compared to the reference 1UD facesheet. It is assumed that this is due to the reduced mobility of polymer chains of the high crystalline polymer matrix of the 1UD-HC tapes. This result correlates well with the findings of Boiko et al. [141] and Grouve [16]. Considering that the degree of crystallinity of the facesheets has a major effect on the resulting interfacial bonding to the core after in-situ injection moulding, the isolated effect of the facesheet thickness is evaluated using facesheets with similar degree of crystallinity but different

thickness. Figure 74 (right) shows, that in-situ CRTP sandwich specimens with both 1UD-HC tape ($\xi$ = 55.25 %) and 2UD laminate facesheets ($\xi$ = 54.7 %) yield a similar interfacial fracture toughness between face and core at low to intermediate melt temperatures. With the melt temperature increasing to $T_m$ = 295 °C, sandwich structures with 0.6 mm UD tape facesheets reach significantly higher $G_I$ values than the 0.33 mm thick variant. This was expected, as simulations have shown that thicker facesheets provide a higher thermal barrier of the interface to the mould, see Figure 67, enabling a wider time span at elevated interface temperatures that enhances the diffusion of polymer chains across the interface of core and facesheet leading to the observed increased interfacial bonding.

### Fracture Analysis

In Figure 75, the fracture surfaces of sandwich specimens after RPT are shown with 0.33 mm thick UD tape facesheets with standard (1UD) and increased degree of crystallinity (1UD-HC), both manufactured with $T_m$ = 250 °C and $T_w$ = 55 °C. The fractured surface of in-situ CFRTP sandwich specimens with reference UD tape facesheets indicates fusion bonding of core and facesheet over the entire interface area. The fracture surface shows features equivalent to fracture surfaces previously observed at 0.33 mm UD tape facesheet sandwich specimens, which is dominated by intense plastic deformation of the matrix polymer as well as fibre tracks. Fracture surfaces of sandwich specimens with high crystalline 1UD-HC tape facesheets however, show incomplete and locally limited fusion bonding of the skin-core interface.

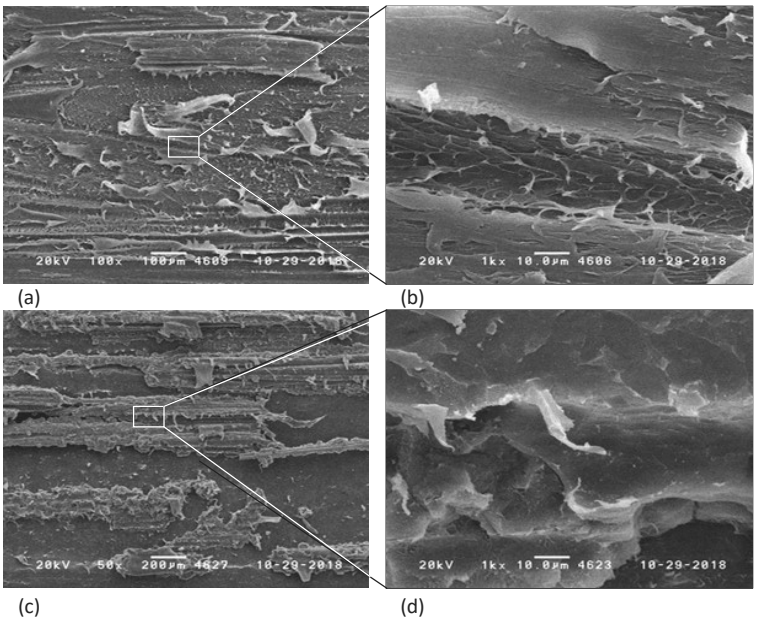


Figure 75: SEM images of fracture surface of compact polymer core sandwich specimens manufactured at $T_m$ = 250 °C and $T_w$ = 55 °C after roller peel test with high crystalline 1UD-HC facesheets at 50x (a) and 1000x magnification (b) as well as low crystalline 1UD facesheets (c) and (d).

This provides only local stress transfer from facesheet to core and provides an explanation for the low $G_I$ values compared to the sandwich specimens with reference 1UD tape facesheet, see Figure 74 (left). Also, the fractured surface of successfully fusion bonded areas shows brittle material behaviour with little signs of plastic deformation. Thus, the already limited fraction of the interface

with successful fusion bonding shows only low plasticity, in sum leading to significantly lower $G_I$ values for sandwich specimens with high crystalline 1UD-HC tape facesheets.

Considering the effect of facesheet thickness, sandwich specimens with 1UD-HC as well as 2UD facesheets yield incomplete fusion bonding at $T_m$ = 250 °C and $T_w$ = 55 °C, leading to the observed low $G_I$ values in Figure 74 (right). At $T_m$ = 295 °C both thin and thick high crystalline UD facesheets show complete fusion bonding of the whole skin-core interface, see Figure 76. However, sandwich structures with thicker facesheets yield a higher fracture toughness. SEM images show that the fractured surface of sandwich specimens with thicker 2UD facesheets exhibit the same brittle matrix polymer appearance as with 1UD-HC facesheets. However, they also show a higher amount of fibre imprints and residues of broken fibres which can be attributed to fibre bridging that increases $G_I$ [278].

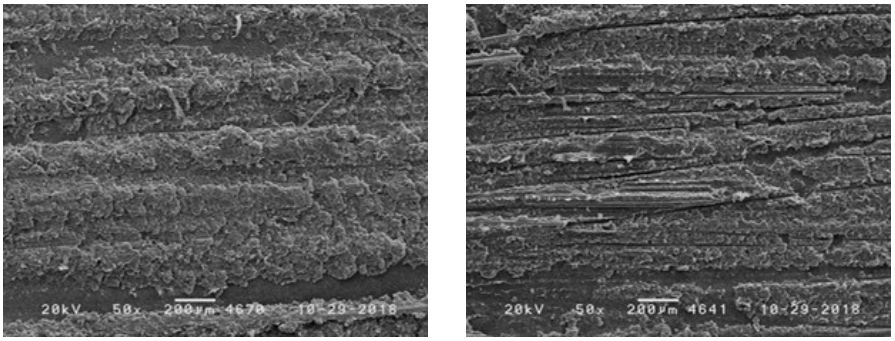


(a) (b)

Figure 76: SEM images of the fracture surface after Mode I peel test of in-situ sandwich specimens with high-crystalline UD tape facesheets with different thickness manufactured at $T_m$ = 295 °C and $T_w$ = 55 °C: 1UD-HC (a) and 2UD (b).

According to the interface temperature simulation, see Figure 67, thicker facesheets do not yield higher peak temperatures but longer time spans at which the temperature at the interface is still elevated. It is assumed that this increased time span at elevated interface temperatures leads to an improved interfacial bonding, as more time is available for the mobilisation and diffusion of polymer chains.

## 5.2. In-Situ CFRTP Sandwich Structures with Integral Foam Core

In this sub-chapter, the core of in-situ CFRTP sandwich specimen is manufactured using different foam injection moulding variants. Hereby, the effect of chemical as well as physical blowing agents on the resulting interfacial bonding between UD tape facesheets with the integral foam core during the in-situ manufacture of CFRTP sandwich specimens is investigated. In accordance with chapter 5.1, the in-situ CFRTP sandwich specimens are subject to mechanical testing as well as subsequent fracture analysis.

### 5.2.1. Specimen and Materials

The in-situ CFRTP sandwich specimen with integral foam core is depicted in Figure 77. The specimen exhibits a total length of $L$ = 220 mm, a width of $W$ = 30 mm and facesheet thickness of $t_F$ = 0.33 mm

in accordance with the specimen dimensions in chapter 5. In contrast however, the core thickness amounts to $h$ = 9.34 mm and the total specimen thickness to $H$ = 10 mm. CFRTP sandwich specimens, which are subject to roller peel testing, are equipped with a PI foil on the first 30 mm of the facesheet. This generates the initial crack length $a$ = 30 mm, equivalent to the compact core specimens in chapter 5. All materials used in this study are equal to the materials in chapter 5.1. Hence, for details of the facesheet and the core material, it is referred to Table 6.

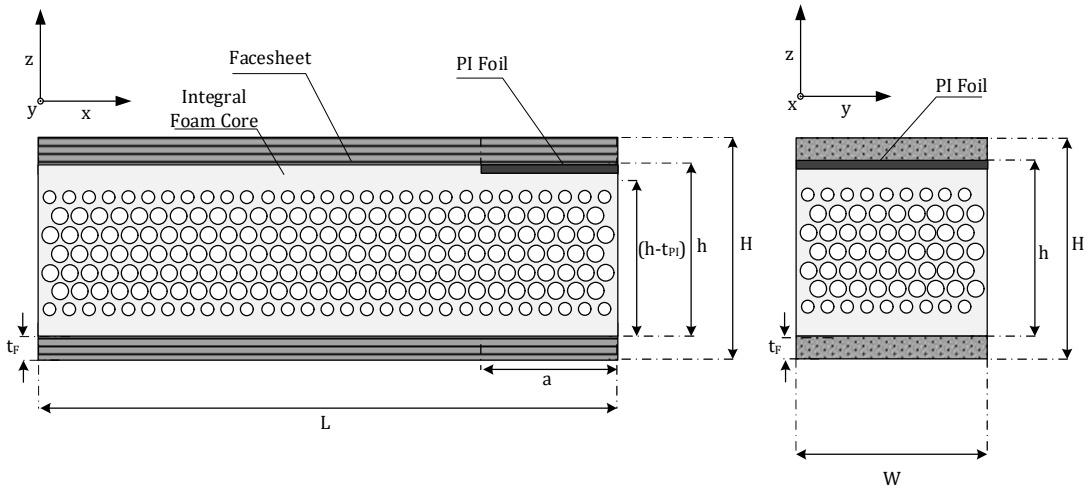


Figure 77: In-situ CFRTP sandwich specimen with integral foam cores: specimen geometry in length (left) and cross direction (right).

### 5.2.2. Design of Experiment

Pre-trials were conducted in order to evaluate the manufacturability of in-situ CFRTP foam core sandwich specimens using the process temperature parameters chosen based on the results of chapter 5.1. The findings of the latter clearly indicated that high process temperatures and interface temperatures respectively have a positive effect on interfacial bonding between facesheets and core. However, several difficulties arise during the manufacture of in-situ CFRTP sandwich structures with foam cores if high process temperatures are applied. Most importantly, cooling times for in-situ sandwich specimens with integral foam cores need to be increased due to the large polymer core volume combined with high melt and mould temperatures. The required cooling time exhibits 120 s at $T_m$ = 295 °C and $T_w$ = 55 °C whereas it must be increased to 240 s at $T_m$ = 270 and $T_w$ = 100 °C, in order to avoid a bloating of the specimen foam cores after demoulding which is known as the "post-blow-effect" [112]. Consequently the process window was limited to a maximum melt temperature of $T_m$ = 295 °C and a constant mould temperature of $T_w$ = 55 °C., see Table 10.

Table 10: Overview of the process and material parameter variation.

| Parameters | Value 1 | Value 2 | Value 3 | Dimension |
|---|---|---|---|---|
| Melt Temperature | 250 | 270 | 295 | °C |
| Mould Temperature | 55 | - | - | °C |
| Core Material | PP-H | - | - | - |
| Blowing Agent | CBA | PBA | - | - |
| Facesheet Thickness | 0.33 | - | - | mm |

Equivalent to chapter 5.1, the facesheet consists of the as-received UD tape (1UD) with a thickness of $t_F$ = 0.33 mm and a degree of crystallinity of 47.6 %. Of special interest in this chapter is the effect of a blowing agent variation on the resulting interfacial bonding of integral foam core and 1UD tape facesheets as well as the resulting flexural properties. A chemical blowing agent (Hydrocerol® ITP 822) and a physical blowing agent using the ProFoam technology will be used to create the integral foam core of the in-situ CFRTP sandwich specimens.

### 5.2.3. Manufacture of Specimens

The manufacture of in-situ CFRTP sandwich specimens with integral foam core is compliant with the manufacture of sandwich specimens with compact polymer core, see Figure 57, yet in this chapter the sandwich specimen core is manufactured using low pressure foam injection moulding with chemical as well as physical blowing agents. Using chemical blowing agents, this foam injection moulding variant does not require a change of mould design allowing the use of the same mould as well as the same injection moulding machine as for the manufacture of in-situ sandwich specimens with compact polymer cores. Hence, for further details it is referred to chapter 5.1.3. The chemical blowing agent was added to the polymer pellets using a master batch (Hydrocerol® ITP 822). The relative mass fraction of the CBA master batch was 3 wt.-% in relation to the mass of the PP pellets, which is the maximum recommended weight fraction according to the datasheet [292]. The mixture of CBA master batch with the PP-H material is inserted into the feeder of the machine. The high temperatures in the transition and metering zone of the barrel lead to the decomposition of the CBA and the release of $CO_2$, which dissolves in the polymer, melt creating a single-phase polymer-gas solution, as described in detail in chapter 2.4.1. The decomposition of the chosen CBA begins at a temperature of $T$ = 200 °C. In order to enable proper foaming, the melt temperature should exceed 230 °C, which is ensured considering the chosen process temperatures, see Table 10.

However, only chemically foamed in-situ sandwich specimens are manufactured with identical injection moulding machine and mould, as foam injection moulding with physical blowing agents using the ProFoam technology require an injection moulding machine equipped with the corresponding ProFoam modifications. Therefore, the manufacture of in-situ CFRTP sandwich specimens with PBA foam core is conducted on an Arburg injection moulding machine of the type Allrounder 470S 1000-290 with ProFoam modifications. Contrary to the CBA method, which releases $CO_2$, the ProFoam process used $N_2$ as dissolving gas. The supercritical $N_2$ is added to the pellets in the second chamber of a modified hopper at a defined pressure of 50 bar. Thereafter, the pellets are fed to the plasticizing unit.

Aside the different ways to achieve a solution of gas in the melt, the processing parameters are equal for the CBA and PBA in-situ CFRTP sandwich variants, see Table 11.

Table 11: Injection moulding process parameters using a chemical blowing agent (left) and a physical blowing agent (right).

| Process Parameter | Chemical Blowing Agent | Physical Blowing Agent | Dimension |
|---|---|---|---|
| Injection Speed | 70 | 70 | ccm/s |
| Shot Volume | 57 | 60 | ccm |
| Back Pressure | 100 | 100 | bar |
| Cooling Time | 120 | 120 | s |
| Handling Time | 8 | 8 | s |

However, different moulds need to be used for the respective variants due to compatibility issues between the different injection moulding machines used for the manufacture of in-situ sandwich specimens with chemical and physically foamed cores. The mould for the CBA based sandwich specimens is identical with the compact polymer core sandwich mould including a relatively short sprue. The mould design for the physically foamed specimens using the ProFoam technology also includes a film gate as well as the same specimen geometry, however the sprue and the cooling channels differ, see Figure 78.

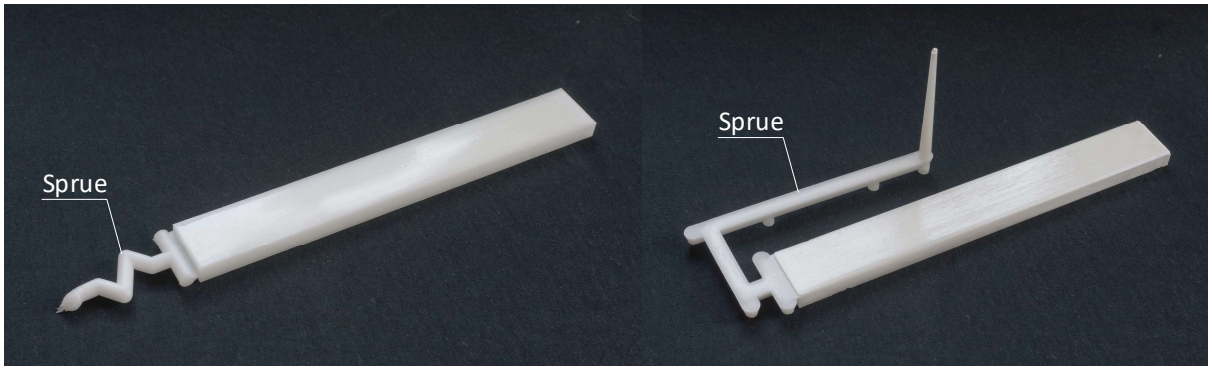


Figure 78: Comparison of the different sprue designs: in-situ CFRTP sandwich specimens using CBA (left) exhibit a shorter sprue than PBA based specimens (right) since different machines needed to be utilised.

Both chemical as well as physical blowing agent variants keep the single-phase polymer-gas solution under pressure by applying a back pressure of $p_b$ = 100 bar in order to avoid a premature release of gas. The melt is subsequently injected into the mould at an injection speed of $v$ = 70 ccm/s. Due to the dissimilar sprue, the total shot volume differs, yet the volume injected in the cavity is equal.

### 5.2.4. Results

In Figure 79 (left) the measured fracture toughness of the interface between integral foam core and UD tape facesheets is depicted in dependence of the applied melt temperatures during in-situ manufacture at a constant mould temperature of $T_w$ = 55 °C.

As discussed in chapter 5.1, increasing process temperatures generally positively affect the interfacial fracture toughness of compact polymer cores to 1UD tape facesheets. This result was also found regarding the bonding behaviour of injection moulded integral foam cores based on chemical as well as physical blowing agents and 1UD tape facesheets. In-situ CFRTP sandwich specimens with CBA based foam cores reach their lowest interfacial fracture toughness at the lowest process temperatures in accordance with PBA based foam core and with compact core sandwich specimens. Increasing $G_I$ values are measured with rising melt temperatures yielding a maximum interfacial fracture toughness of $G_I$ ≈ 1.1 kJ/m² at $T_m$ = 270 °C for both CBA and PBA based foam core sandwich structures. The interfacial fracture toughness of specimens with CBA foam core shows a minor decrease at the highest melt temperature compared to the results at lower temperatures, though a significant effect cannot be determined due to the comparatively high standard deviation. Specimens with PBA foam core however do not show a decrease of $G_I$ at $T_m$ = 295 °C.

In Figure 79 (right), the notched lap shear test results of in-situ CFRTP sandwich specimens with integral foam cores as well as compact cores are presented. The $\tau_{NLS}$ values are normalised with respect to the maximum value of the specific core type i.e. compact, CBA and PBA core in order to enable a comparison of the sandwich structures with different cores. This is because a quantitative evaluation of notched lap shear test results of specimens with different geometry is invalid [214].

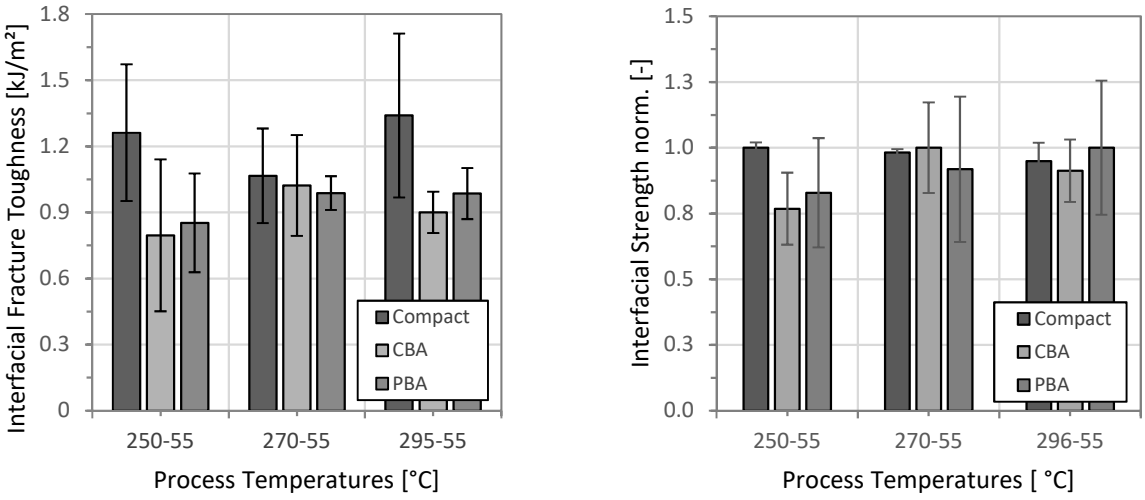


Figure 79: Comparison of interfacial bonding of in-situ sandwich specimens with solid (compact) as well as integral foam cores using chemical (CBA) and physical blowing agents (PBA): interfacial fracture toughness (left) and strength (right)

Within the studied temperature range, the $\tau_{NLS}$ remains unchanged for compact core sandwich specimens with very little variation. Sandwich specimens with CBA foam core exhibit an increase of interfacial strength of 21 % with a melt temperature rising from $T_m$ = 250 °C to $T_m$ = 270 °C. However, the interfacial strength also shows a small decrease at the highest melt temperature $T_m$ = 295 °C similarly to the measured interfacial fracture toughness in Figure 79 (left). Sandwich specimens with PBA foam core yield interfacial strength values which continuously increase by 12 % with growing melt temperature from $T_m$ = 250 °C to $T_m$ = 295 °C.

Based on the mechanical test results, the type of blowing agent does not have a significant effect on the resulting interfacial bonding between integral foam core and CFRTP facesheets though a tendency of a decreased bonding at high melt temperatures using chemical blowing agents is observed. Considering the lower standard deviation of measured $G_I$ values, integral foam core sandwich structures appear to exhibit a higher process stability than those with compact cores especially at high melt temperatures. The minor difference of fracture toughness as well as interfacial strength of sandwich structures with PBA foam cores compared to chemically foamed specimens is assumed to result from a lower interface temperature caused by the mould design differences. Due to the longer sprue channel of the mould used for the manufacture of PBA sandwich specimens, see Figure 78, the time for the melt to cool down before reaching the cavity and the CFRTP facesheet surfaces is increased. This leads to a reduced temperature at the facesheet-core interface, which is detrimental to the resulting interfacial bonding.

However, specimens with foam cores generally exhibit lower interfacial fracture toughness than those with compact cores despite the fact that in case of CBA based sandwich structures the same

machine and mould were used as for the manufacture of compact core sandwich structures. Considering that according to chapter 2.4.2 and the findings of chapter 5.1 one of the major drivers of the interfacial bond development is the interface temperature, the latter is evaluated in detail for foam and compact core in-situ CFRTP sandwich structures. In order to determine the interface temperature between UD tape facesheets and the polymer cores during the manufacture, simulations of the in-situ process were conducted based on Autodesk Moldflow Insight 2019 according to the procedure in chapter 5.1. The simulation results are depicted in Figure 80.

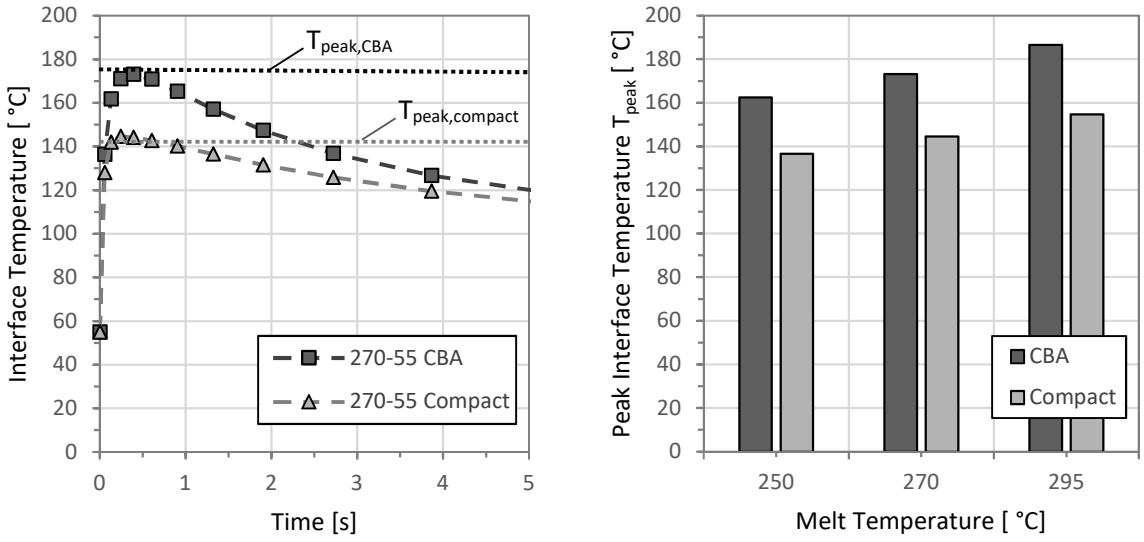


Figure 80: Comparison of the thermal simulation results of the interface temperature during in-situ manufacture of CFRTP sandwich specimens: temperature development at the interface using $T_m$ = 250 °C and $T_w$ = 55 °C (left), peak interface temperatures at different melt temperatures and constant mould temperature of $T_w$ = 55 °C (right).

It was found that the peak interface temperature $T_{peak}$ of foam core sandwich specimens is approximately 30 °C higher compared to compact core sandwich specimens for all three studied melt temperatures, see Figure 80 (right). This is attributed to the higher volume of polymer melt, which may lead to a heat accumulation until the hot centre of the injected core is sufficiently cooled down. The cooling rate is higher as well, so that after little more than 5 seconds the interface temperatures of foam core and compact cores with 1UD tape facesheets converge again according to the simulation, see Figure 80 (left). Considering the results of chapter 5.1, interface temperatures at or above the melt temperature of the UD facesheet polymer matrix should result in full bonding between compact core and 1UD facesheets. However, only incomplete macroscopic fusion bonding of the interfaces of both chemically and physically foamed sandwich specimens with the 1UD tape facesheets is observed at $T_m$ = 250 °C and $T_w$ = 55 °C despite the simulated high interface temperature of $T_{peak}$ = 162.4 °C, see Figure 81.

*Fracture Analysis*

The analysis of the fracture surface after roller peel testing via SEM shows that while in-situ sandwich specimens with 1UD tape facesheets and compact cores achieve fusion bonding of the entire facesheet-core interface, this is not the case for sandwich specimens with integral foam core. Only

locally limited fusion bonding of UD tape facesheets with the injection moulded foam core using CBA and PBA can be observed indicated by rough structures accompanied by glassy surfaces at which no fusion bonding took place, see Figure 81 (b) and (c). A closer observation of the fusion bonded areas shows signs of ductile deformation including smeared fibrils and ductile drawing which was already observed in the case of compact core sandwich structures [289]. Only at melt temperatures of $T_m$ = 270 °C and higher, the complete interface of injection moulded integral foam core and UD tape facesheet achieves interfacial bonding. This is observed for both types of blowing agents.

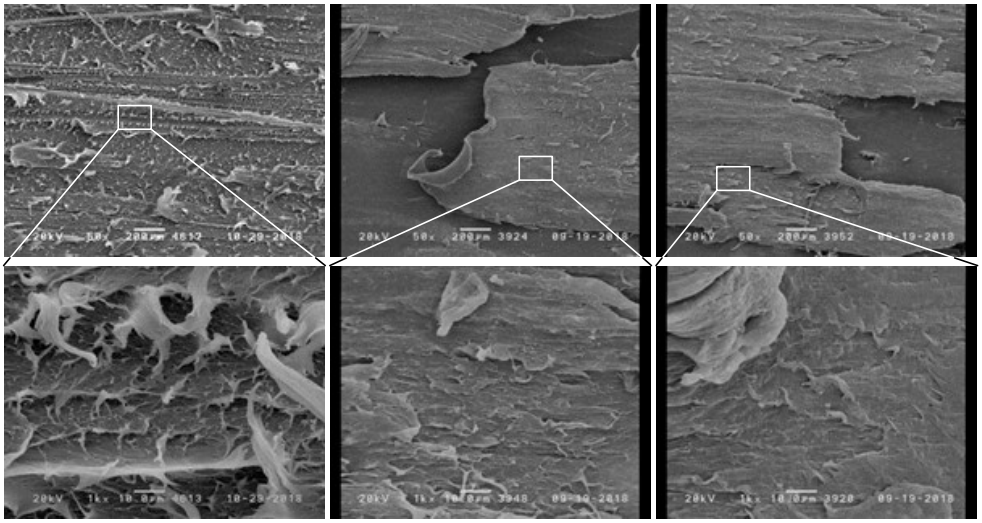

(a) (b) (c)

Figure 81: SEM images at 50x magnification (upper images) and 1000x magnification (lower images) of RPT fracture surfaces of in-situ CFRTP sandwich specimens manufactured at $T_m$ = 250 °C and $T_w$ = 55 °C: compact core sandwich specimen (a), CBA core sandwich specimen (b), PBA core sandwich specimen (c).

The microstructure on the fractured surface between integral foam cores and UD tape facesheets is again very similar compared to the fractured surfaces observed at in-situ sandwich specimens with compact polymer cores, which is typically characterised by flake-shaped platelets at low magnification, see Figure 82 top row, and intense plastic deformations at higher magnification, see Figure 82 bottom row. Thus, the achieved peak interface temperatures clearly exceed the melt temperature of the facesheet matrix polymer, which should result in maximum interfacial bonding. However, a significantly lower skin-core fracture toughness of in-situ sandwich specimens with integral foam core is achieved compared to compact core sandwich structures, despite the far higher simulated peak interface temperature between facesheet and core.

The reason for this is assumed to lie in the different cavity pressures. Considering that the cavity pressure corresponds to the applied pressure $p_{app}$ during intimate contact development, see Equation 17, a lower cavity pressure during the manufacture of in-situ sandwich structures with foam core should lead to a reduced or decelerated intimate contact development. The cavity pressure is hence insufficient to flatten the asperities of the CFRTP facesheets adequately during the process.

As interfacial bonding requires both intimate contact and healing to be complete, the lack of one process step results in low degrees of bonding, see Equation 22. Thus, even with full healing, the interfacial bonding is incomplete resulting in lower interfacial strength and fracture toughness. The assumption of an immediate intimate contact between solid substrate and overmoulded polymer

[14, 159, 163] may hence not be applicable in case of the low pressure foam injection moulding variant. A cavity pressure dependency of interfacial bonding of CFRTP substrates with overmoulded structures was also observed by Lebsack and Sauer [75, 95].

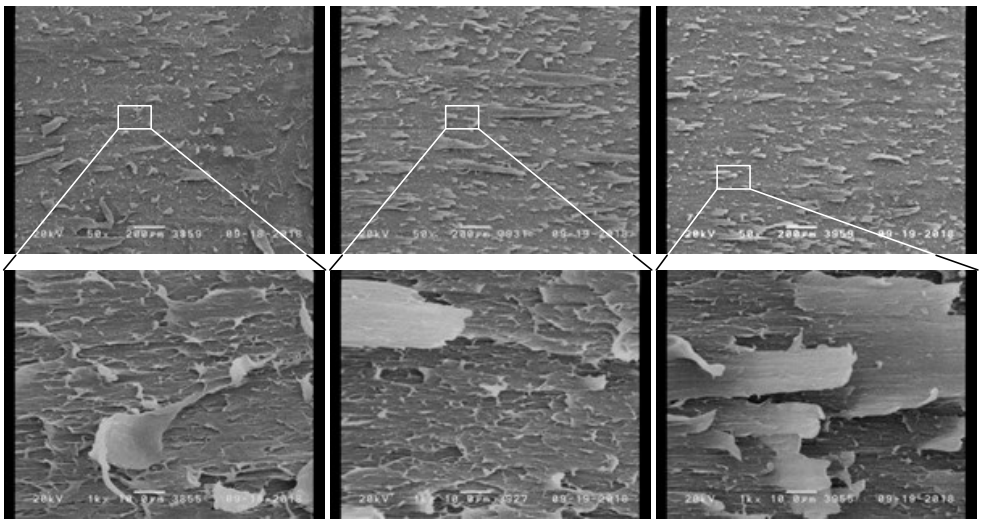

(a) (b) (c)

Figure 82: SEM images at 50x magnification (upper image) and 1000x magnification (lower image) of RPT fracture surfaces of in-situ CFRTP sandwich specimens manufactured at $T_m$ = 270 °C & $T_w$ = 55 °C: compact core sandwich specimen (a), CBA core sandwich specimen (b), PBA core sandwich specimen (c).

Another reason may be a time shift between the cavity pressure profile and interface temperature development. As only the combination of complete intimate contact and complete healing will lead to complete interfacial bonding, the time-dependency needs to be considered. If the pressure build-up in the cavity develops only after the interface temperature reached its peak, the resulting interfacial bonding is low, although the applied pressure and the interface temperature individually are high enough. Hence, only the almost simultaneous achievement of high interface temperatures and cavity pressures enable high intimate contact and subsequent healing, resulting in high interfacial bonding.

## 5.3. Discussion

A comparison of the notched lap shear test as well as the roller peel test results of in-situ CFRTP sandwich specimens showed that both tests yield similar qualitative result curves which leads to the assumption that both methods are suitable for testing the skin-core bonding of thermoplastic sandwich composites.

Furthermore, sandwich specimens with thin 1UD tape facesheets achieve interfacial bonding beginning at process temperatures as low as $T_m$ = 250 °C and $T_w$ = 30 °C. Yet at this process temperature combination, only low interfacial bonding is observed. Significantly higher interfacial bonding is found by only a minor increase of process temperatures, until a plateau value of both $G_I$ and $\tau_{NLS}$ is reached. This is accompanied by complete interfacial bonding of core and facesheet, which is verified by SEM of the fracture surfaces after roller peel testing as well as by PLM of specimen cross sections. While incomplete fusion bonding of the facesheet-core interface was revealed by a glassy fracture surface leading to lower $G_I$ and $\tau_{NLS}$ values, complete fusion bonding was indicated by a rough fracture surface and enabled a higher interfacial stress transfer. Accordingly, PLM images of specimen cross sections at the interface region showed that at lower process temperatures the initial interface between facesheet and core was still clearly recognisable suggesting that the facesheet surface was not melted. This was only achieved at higher process temperatures. PLM images also showed that after successful melting of the facesheet surface, large crystalline structures develop which extended across the former interface of core and facesheet surface. This is attributed to an increased time for crystal growth due to the high process temperatures. It is hence demonstrated that the sufficient melting of the facesheet surface and subsequent crystal growth across the former interface is associated with an increase of interfacial stress transfer, which is compliant with the findings of other authors [168, 183, 184].

A simulation of the resulting temperature at the interface between injection moulded core and 1UD tape facesheet showed that peak temperatures at the interface are up to 40 °C below the melting temperature $T_{melt}$ of the UD tape facesheets for the majority of studied process temperatures. Yet despite this low interface temperature, most process temperature combinations lead to high interfacial bonding. This result is in disagreement with other studies which assume that bonding of semi-crystalline polymer interfaces only sufficiently develops if the melting temperature is exceeded [140, 151, 182]. However, it agrees with the results of Grouve [16] as well as of Stokes-Griffin and Compston [156] who found that high interfacial strength could also be achieved below $T_{melt}$ or between $T_g$ and $T_{melt}$ respectively during TTL. Boiko et al. [141] found similar results regarding the consolidation behaviour of different combinations of amorphous and semi-crystalline polymer interfaces.

Compared to in-situ sandwich structures with thin 1UD facesheets, specimens with thicker 2UD facesheets already yield interfacial bonding at lower process temperatures ($T_m$ = 230 °C and $T_w$ = 30 °C). Similar to sandwich specimens with thin facesheets, the interfacial strength and fracture toughness increases with increasing process temperatures. However, the interfacial fracture toughness is generally much lower than with thinner facesheets. Only with the highest process temperature combinations, CFRTP sandwich specimens with thick 2UD facesheets yield similar $G_I$ values compared to those with thin 1UD facesheets.

A simulation of the resulting temperature at the interface between injection moulded core and UD tape facesheets with different thickness should clarify if different interface temperatures are the

reason for this different bonding behaviour of sandwich specimens with 1UD and 2UD facesheets. Simulation results showed that the peak temperature during the in-situ sandwich manufacture is approximately equal using 1UD and thicker 2UD facesheets (see Annex A). However, the cooling rate is significantly decreased with thicker facesheets. Considering the thicker 2UD facesheets, the assumption of the melting temperature as prerequisite for interfacial bonding however is more accurate because interfacial bonding is only high when interfacial temperatures come close to the melting temperature of the facesheet. These different results for in-situ sandwich specimens with thin and thick UD facesheets can be attributed to the crystallinity of the UD tape matrix polymer.

Based on SEM image analysis, clear differences of the fracture surfaces between sandwich specimens with 1UD and 2UD facesheets have been observed. While specimens with 1UD facesheets showed fracture surfaces with clear signs of strong plastic deformation such as fibrillation, a brittle fracture surface was found using thick 2UD facesheets. This is attributed to the thermal history of the 2UD facesheets during their manufacture via consolidation of two 1UD tapes. DSC analysis showed that the degree of crystallinity of thick 2UD facesheets increased from 47.6 % of 1UD tapes in as-received condition to 54.7 % after consolidation due to the low cooling rate (see Annex B). In order to isolate the effect of matrix crystallinity on interfacial bonding, thin 1UD facesheets have been annealed receiving high-crystalline 1UD-HC tapes with $\xi$ = 55.25 %. Subsequent RPT showed significantly decreased $G_I$ values compared to in-situ sandwich specimens with standard 1UD tapes. Hence, especially at interface temperatures below the melting temperature of the semi-crystalline matrix polymer, the interfacial bonding during in-situ moulding is distinctly reduced with increasing matrix polymer crystallinity of the UD tape facesheet.

The detrimental effect of high crystalline CFRTP facesheets on fusion bonding at interface temperatures below $T_{melt}$ of the facesheet matrix polymer is assumed to be caused by a reduced mobility of polymer chains, compliant with the findings of other authors [16, 136, 141, 178]. High crystalline UD tape facesheets exhibit a smaller fraction of amorphous structures that contribute to interfacial diffusive chain movement and entanglement below the melting temperature of the facesheet. To the contrary, increased $G_I$ values are found with low crystalline 1UD facesheets at interface temperatures below the melting temperature of the facesheet matrix. Thus, only when a sufficient fraction of the crystalline portion is melted and more polymer chains are mobilised, an pronounced interfacial polymer chain diffusion can take place.

Furthermore, sandwich specimens with thicker facesheets lead to increased interfacial fracture toughness compared to thin facesheets. This is attributed to the decreased cooling rates resulting from an increased thermal barrier effect of the thicker facesheets to the cooled mould providing more time at elevated interface temperatures for diffusive chain movement.

The effect of blowing agents on the interfacial bonding development of UD tape facesheets and integral foam core during in-situ sandwich manufacture was evaluated via roller peel test and notched lap shear test. Results show that the interfacial fracture toughness as well as interfacial strength of in-situ sandwich structures with foam cores increase with rising melt temperature, in qualitative agreement with the results of compact core structures. Compared to the latter however, foam core in-situ sandwich specimens yield lower $G_I$ values. Depending on the melt temperature, the reduction can amount to 25 %. At the lowest process temperature combination ($T_m$ = 250 °C, $T_w$ = 55 °C), SEM images of the fracture surfaces showed incomplete fusion bonding between facesheet and foam cores whereas compact cores achieved complete fusion bonding of the entire

interface. Only at elevated process temperatures, foam core sandwich structures achieve complete fusion bonding and show an identical fracture surface compared with compact core sandwich structures.

In order to find reasoning for this result, the interface temperature between UD tape facesheet and integral foam core was simulated. The simulation results showed, that the peak interface temperature of UD tape and foam core during in-situ sandwich manufacture is about 30 °C higher compared to compact core sandwich structures and exceeds the melt temperature of the UD tape facesheet at all studied process temperatures. Hence, despite the significantly higher interface temperatures, the interfacial bonding of in-situ sandwich structures with foam core is distinctly reduced compared to compact core sandwich specimens.

The lower interfacial bonding is attributed to the cavity pressure during the in-situ process using the low-pressure foam injection moulding method, as cavity pressures are typically much lower using foam injection moulding compared to common injection moulding [293]. The cavity pressure is typically below 30 bar using CBA [112] and below 50 bar using the PBA variant used in this work [294]. An insufficient development of intimate contact due to an insufficient applied pressure leads to a reduced degree of bonding despite full degree of healing, see Equation 22. This is compliant with similar findings of Sauer and Lebsack [75, 95]. Hence, the assumption of an immediate intimate contact during overmoulding [14, 159, 163] is not directly applicable if low-pressure foam injection moulding is used.

In order to overcome this issue, the high pressure foam injection moulding method is proposed for the manufacture of in-situ sandwich structures since it leads to equally high cavity pressures as injection moulding of compact components, even a short period of pack pressure is often applied in practice [47, 295]. Consequently, it is assumed that higher interfacial bonding due to an enhanced intimate contact can be achieved using this high-pressure foam injection moulding for in-situ manufacture of CFRTP sandwich structures. However, this would be accompanied with a number of challenges. Firstly, the mould complexity and cost would largely increase, as this requires a controlled increase of cavity volume (“core back”) during the process, especially if the sandwich component is geometrically complex. In this case, the core-back function may be required along all three dimensions. Furthermore, the facesheets would need to deform during the core-back movement, since the sandwich component surfaces increase. Consequently, high-pressure foam injection moulding for the in-situ manufacture of CFRTP sandwich components is only considered promising with a one-dimensional core-back technique.

In addition to the cavity pressure peak, a time shift of the pressure development in the cavity and the temperature development at the interface between foam core and UD tape facesheet during in-situ moulding may contribute to a reduced interfacial bonding. As interfacial bonding is based on the sequential process of intimate contact followed by healing, the in-situ process needs to provide a time-dependent pressure and temperature profile that provides high pressure and high temperatures at the beginning of the in-situ process for the creation of intimate contact followed by high interface temperatures for the subsequent healing of interfaces.

Based on these findings, it is assumed that the cavity pressure and more specifically its peak and correlation with time and interface temperature during the in-situ CFRTP sandwich process is the driving force of interfacial bonding development between foam core and UD tape facesheets. However, an experimental assessment of the pressure profile during in-situ moulding however would have gone beyond the scope of this work and should therefore be object of research in follow-up studies

# 6. Lightweight Design of In-Situ CFRTP Sandwich Structures

After the evaluation of mechanisms behind interfacial boding of in-situ sandwich structures in the previous chapter, this chapter puts its focus on the lightweight design of in-situ CFRTP sandwich structures reflected by the weight specific flexural behaviour, see Figure 83. Therefore, chemical as well as physical blowing agents are used to manufacture sandwich specimens with UD tape facesheets via the in-situ process. In addition, the core material is varied in order to determine the effect of particulate fillers on the foaming behaviour of the core and the resulting flexural rigidity of the sandwich structures.

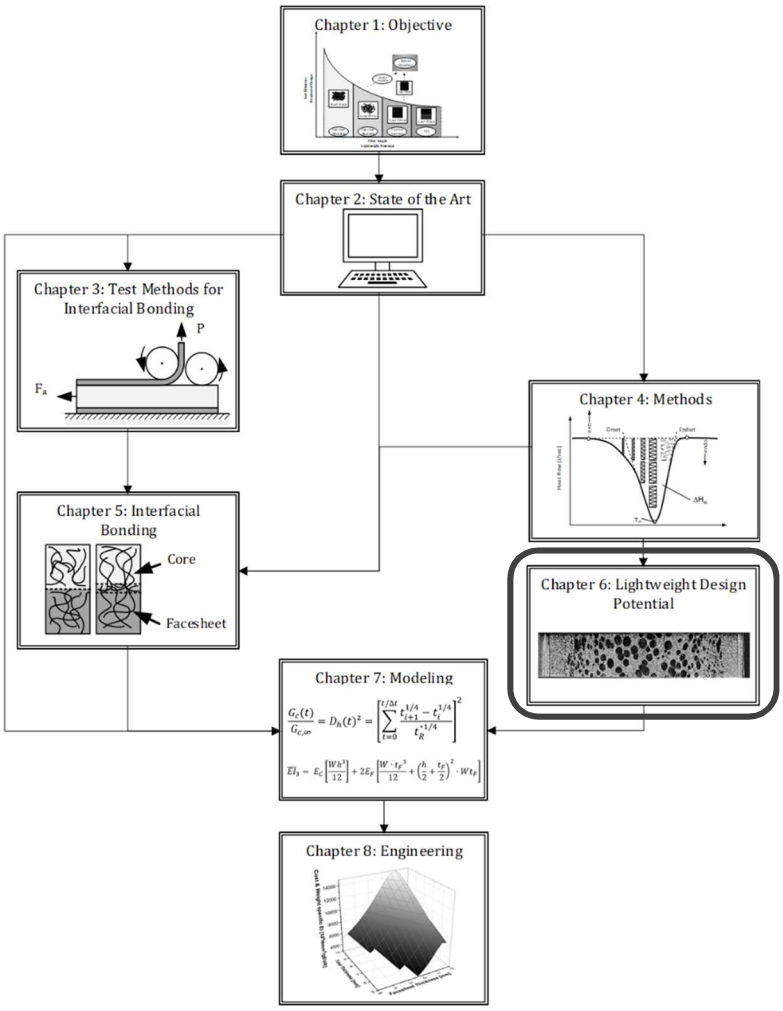


Figure 83: Systematic approach of this work: chapter 6 focuses on the lightweight design potential of in-situ CFRTP sandwich structures reflected by their flexural rigidity and correlates the results with macro- and microscopic foam morphology analysis.

Four-point bending tests shall give indication about the flexural behaviour whereas polymer analysis methods focus on the development of the foam morphology of the structural polymeric foam core and its relationship with the resulting weigh specific flexural properties.

## 6.1. Specimen and Materials

The in-situ CFRTP sandwich specimen with integral foam core is depicted in Figure 84. The specimen exhibits a total length of $L$ = 220 mm, a width of $W$ = 30 mm and facesheet thickness of $t_F$ = 0.33 mm. In accordance with the specimen dimensions in chapter 5, the core thickness amounts to $h$ = 9.34 mm and the total specimen thickness to $H$ = 10 mm.

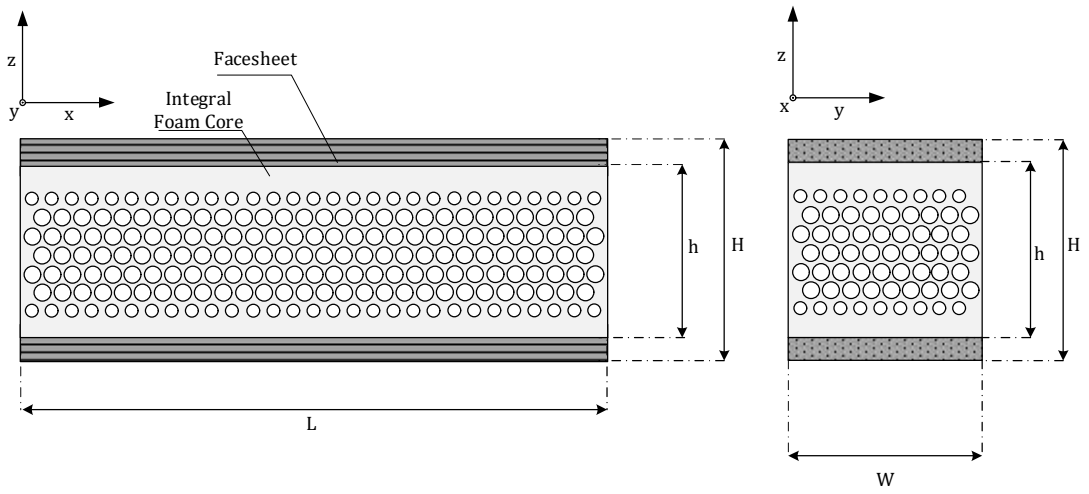


Figure 84: In-situ CFRTP sandwich specimen for flexural analysis with integral foam core: specimen geometry in length (left) and cross direction (right).

The core and facesheet materials are presented in Table 12 based on the material datasheets.

Table 12: Overview of material parameters.

| | | Core | | Facesheet | Dimension |
|---|---|---|---|---|---|
| Material | Name | Sabic® PP 576P | Sabic® 15T1020P | Celstran® CFR-TP PP GF60-13 | - |
| | Tensile Modulus | 1850 | 2600 | 25600 | N/mm² |
| Polymer | Type | PP-H | PP-H | PP | - |
| Filler | Type | - | Talcum | GF | - |
| | Content | - | 20 | 60 | wt.-% |
| | Structure | - | - | UD | - |

The UD tape facesheets used for the manufacture of CFRTP sandwich structures with integral foam cores is equivalent to the material used for the manufacture of sandwich structures in chapter 5 (Celstran® CFR-TP PP GF60-13). The core materials are a standard polypropylene homopolymer (Sabic® PP 576P) which is also equal to the core material used in chapter 5. The second core material is a 20 wt.-% talcum filled polypropylene homopolymer (Sabic® PPcompound 15T1020) which consist of the same polymer (Sabic® PP 576P) yet with the addition of the particulate filler material [296]. The talcum filled polypropylene core material was specifically chosen to study the effect of fillers on the foam morphology and flexural rigidity behaviour since fillers act as nucleus for the generation on foam cells and influence melt strength [297].

## 6.2. Design of Experiment

The process and material parameter variation is depicted in Table 13. The melt temperature is varied from $T_m$ = 250 °C to $T_m$ = 295 °C whereas the mould temperature is kept constant at $T_w$ = 55 °C.

Table 13: Experimental design.

| Parameters | Value 1 | Value 2 | Value 3 | Dimension |
|---|---|---|---|---|
| Melt Temperature | 250 | 270 | 295 | °C |
| Mould Temperature | 55 | | - | °C |
| Core Material | PP-T20 | PP-H | - | - |
| Blowing Agent | CBA | PBA | - | - |
| Facesheet Thickness | 0.33 | - | - | mm |

Of special interest in this chapter is the effect of a blowing agent variation on the resulting flexural properties. A chemical blowing agent (Hydrocerol® ITP 822) and a physical blowing agent using the ProFoam technology will be used to create the integral foam core of the in-situ CFRTP sandwich specimens.

## 6.3. Manufacture of Specimens

The manufacture of the in-situ sandwich specimens is compliant with the procedure in chapter 5.2. The process parameters are unchanged and presented in Table 14.

Table 14: Foam Injection moulding machine process parameters.

| Process Parameter | Chemical Blowing Agent | Physical Blowing Agent | Dimension |
|---|---|---|---|
| Injection Speed | 70 | 70 | ccm/s |
| Shot Volume | 57 | 60 | ccm |
| Back Pressure | 100 | 100 | bar |
| Cooling Time | 120 | 120 | s |
| Handling Time | 8 | 8 | s |

## 6.4. Results

Figure 85 gives an overview of the absolute as well as weight specific flexural rigidity, assessed by four-point bending. The weight specific flexural rigidity is calculated as the ratio of flexural rigidity to the experimentally determined specimen weight. The results are normalised with respect to the global minimum of absolute flexural rigidity and specific flexural rigidity. This reference value was achieved using PP-T20 as core material with CBA at a melt temperature of $T_m$ = 295 °C and a mould temperature of $T_w$ = 55 °C. Both absolute as well as specific flexural rigidity of in-situ sandwich specimens with 1UD tape facesheets and CBA based foam core yield lower values than those with PBA based foam cores. Moreover, CBA based sandwich specimens with PP-T20 foam core do not reach significantly higher flexural rigidities than with PP-H foam cores despite the higher Young's modulus of the core polymer used (Table 12). Compared to PP-H the specific flexural rigidity of chemically foamed sandwich specimens is even decreased if PP-T20 is used as core material.

Contrary to CBA based sandwich structures, specimens with physically foamed cores show a significant difference in absolute flexural rigidity in dependency of the core material. Compared to specimens with PP-T20 foam cores, sandwich structures with PP-H as core material reach lower values by 9 % at $T_m$ = 295 °C to 33 % at $T_m$ = 250 °C. Despite this distinct difference of absolute

flexural rigidity, the specific flexural rigidity of physically foamed sandwich specimens based on PP-H is up to 8 % higher compared to in-situ specimens with PP-T20 foam cores. Thus, in order to evaluate the specific flexural rigidity, the material and process dependent density reduction must be taken into account.

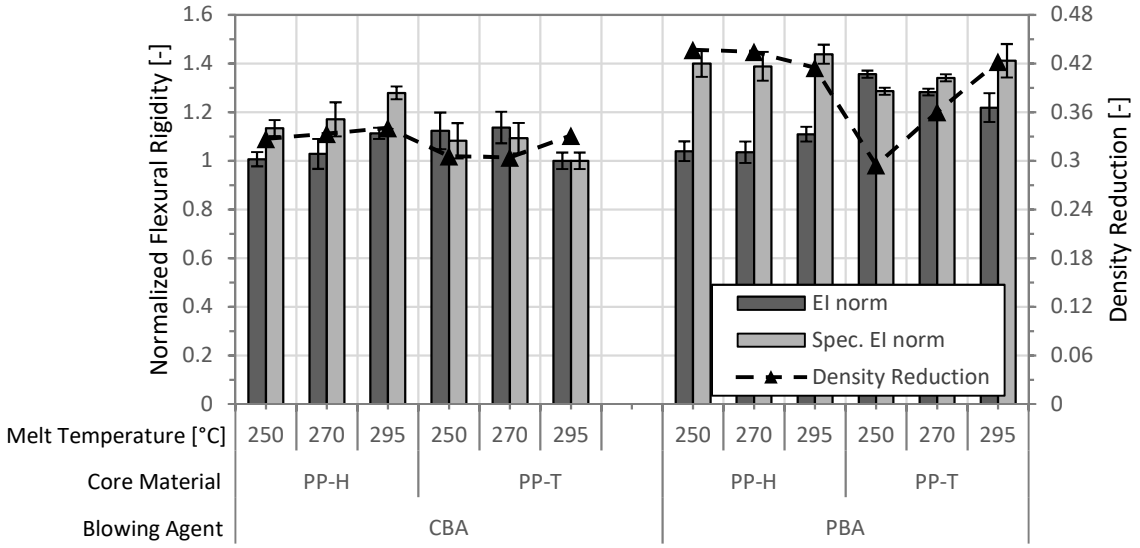


Figure 85: The density reduction, absolute and weight specific flexural rigidity of in-situ CFRTP sandwich specimens with integral foam core using CBA and PBA with unfilled PP-H as well as 20 wt.-% talcum filled PP-T20 at varying melt temperatures and $T_w$ = 55 °C. The flexural rigidity results are normalised in order to enable comparability.

Closer examination of Figure 85 shows that the variants with chemical blowing agent, both based on PP-H as well as PP-T20 core material, always achieve similar high density reductions between 30.4 % and 33.4 %. The density reduction increases slightly with rising melt temperature for both PP-H and PP-T20 core materials and thus corresponds to the general behaviour of chemically foamed thermoplastic foams [112]. Contrary to the relatively temperature insensitive density reduction of CBA integral foam core sandwich specimens, distinct differences of density reduction can be observed using the ProFoam technique and PP-T20 as core material. Physically foamed in-situ CFRTP sandwich specimens manufactured with PP-H as core material achieve very high weight reductions, which marginally vary depending on the melt temperature, similar to CBA. In contrast, PBA based PP-T20 foam core sandwich specimens and the achieved weight reduction are very sensitive to the melt temperature applied during the manufacture. Here the application of $T_m$ = 250 °C leads to a density reduction of 29 %, whereas increasing the melt temperature to $T_m$ = 295 °C yields a density reduction of 42 %. However, the absolute flexural rigidity of PBA based PP-T20 sandwich specimens decreases with rising melt temperature, which compensates the density reduction effect, leading to similar weight specific flexural rigidity values compared to physically foamed PP-H sandwich specimens.

Thus, in-situ CFRTP sandwich structures with core materials with higher Young's modulus do not necessarily result in increased weight specific or even absolute flexural rigidity of in-situ sandwich specimens with UD tape facesheets. Only a proper combination of material and process parameters appears to enable the utilisation of the full lightweight design potential of the in-situ CFRTP sandwich process. In order to evaluate the effect of the specific material and process parameter variants on flexural rigidity and the accompanied weight reduction, the lightweight design effect $LD$ is

introduced as relationship of specific flexural rigidity to absolute flexural rigidity. This related parameter allows for a comparison of in-situ sandwich structures with foam cores of different materials and their potential with respect to lightweight design. In Figure 86, the *LD* is depicted in relationship with the process parameters for the manufacture of the respective sandwich specimens.

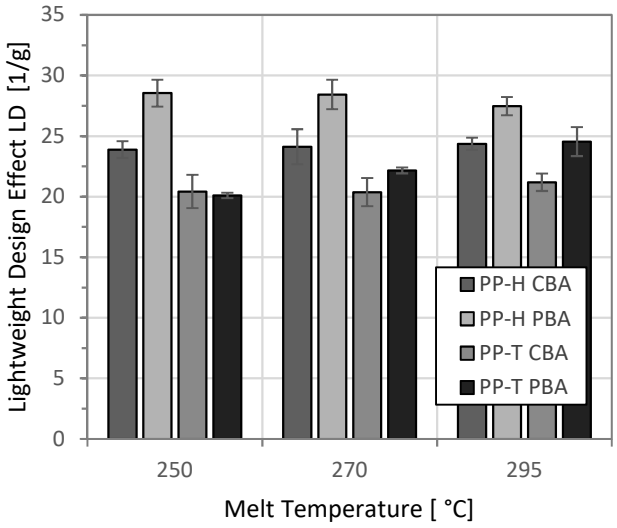


Figure 86: The lightweight design effect ($LD$) as ration of weight specific to absolute flexural rigidity shows that PBA based in-situ CFRTP sandwich structures mostly yield higher $LD$ values compared to CBA. The highest lightweight design effect is achieved combining PP-H as core material and physical blowing agents.

The increase of specific flexural rigidity in relation to the referenced absolute flexural rigidity indicated by the lightweight design effect is largest for PP-H based foam core sandwich structures. PP-T20 based specimens yield a lower $LD$ effect, however using physical blowing agents the achieved values reach the level of sandwich specimens with chemically foamed PP-H cores. This is because in case of the combination of PBA and PP-T, an increase of the $LD$ values can be observed with increasing melt temperatures contrary to all other material and blowing agent combinations.

Thus, the core material as well as the process parameters including melt temperature and type of blowing agent significantly affect both absolute as well as flexural stiffness and consequently the resulting lightweight design effect. The observed differences are assumed to result from the material and process parameter induced morphology of the integral foam core. Therefore, the foam morphology is examined on a macroscopic and microscopic scale. The macroscopic foam morphology is evaluated by means of the core skin thickness $t_s$ whereas the microscopic foam morphology is assessed by analysis of the mean cell diameter and its distribution.

### 6.4.1. Macroscopic Foam Morphology

The absolute flexural rigidity and its variation shall be evaluated by means of the respective core-skin thickness. The expression “core-skin” hereby denotes the compact polymer skin that develops in an integral polymeric foam and the CFRTP facesheets, which are used as reinforcement of the integral foam. The thickness of the core-skin depends on the material and process parameters. In order to determine the core-skin thickness, longitudinal cross sections of the sandwich specimens were

prepared using a Mutronic laboratory table saw. The manufactured cross sections were subsequently polished on a Struers Abramin grinding machine. The polished cross sections were photographed with a Nikon D300 digital reflex camera using a close-up lens. An image of a cross section is exemplarily depicted in Figure 87. It shows that the macroscopic foam morphology is dependent on the x-location along the flow length of the specimen core. At the vicinity of the injection point, the core-skin thickness is low, whereas it growths with increasing flow length.

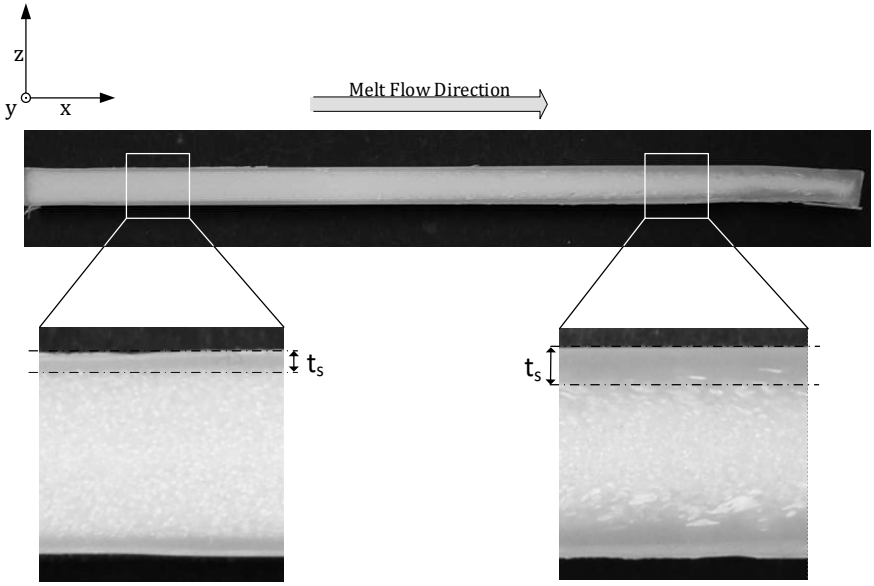


Figure 87: The analysis of the x-z-cross-section of an in-situ sandwich specimen illustrates the issue of flow length dependency of the foam morphology in accordance with [129].

The varying core-skin thickness must be attributed to when evaluating the bending behaviour of CFRTP sandwich specimens. Considering the momentum profile in the 4PB test set-up, see Figure 88, the load span $l'$ is effectively subject to the flexural rigidity evaluation.

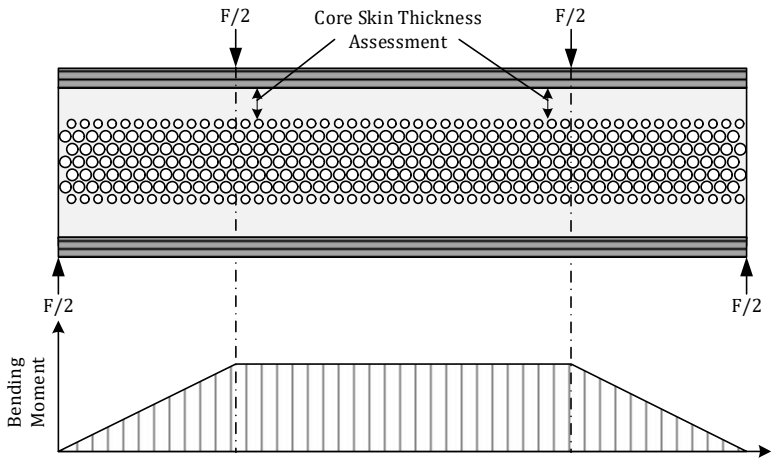


Figure 88: Qualitative illustration of the bending moment imposed by the four-point bending test set-up.

Therefore, an average skin thickness between the load applications was determined in order to assess the effect of skin thickness on the flexural behaviour. Based on reflex camera images, the core-skin thickness was quantified at two locations per specimen and at three test specimens per parameter variant using an image progressing software (ImageJ).

In Figure 89, the flexural rigidity determined by 4PB test and the respective core-skin thicknesses are presented. In-situ sandwich specimens with PP-H integral foam cores manufactured with chemical blowing agent show an increase of core-skin thickness from 0.5 to 0.7 mm with rising melt temperatures from $T_m$ = 250 °C to $T_m$ = 295 °C. This is accompanied by an increase in the resulting flexural rigidity. The measured skin thickness however exhibits a significant standard deviation. The high standard deviation is also observed for PP-T20 based sandwich specimens with integral foam cores. Considering the mean values, they show a decreasing core-skin thickness with growing melt temperatures. This observation correlates with the measured decrease of flexural rigidity. Larger core-skin thicknesses thus contribute to an increase of the flexural rigidity, which can be attributed to the larger second moment of inertia combined with the increased elastic modulus of the solid core-skins. While this was found for sandwich specimens with chemically foamed core, an evaluation of the core-skin thickness of CFRTP sandwich specimens with physically foamed core could not be made, as a clear separation of foamed core and unfoamed core-skin was not possible. The integral foam of physically foamed sandwich specimens did not exhibit a distinct macroscopic boundary between foamed core and compact core-skin, especially at elevated melt temperatures.

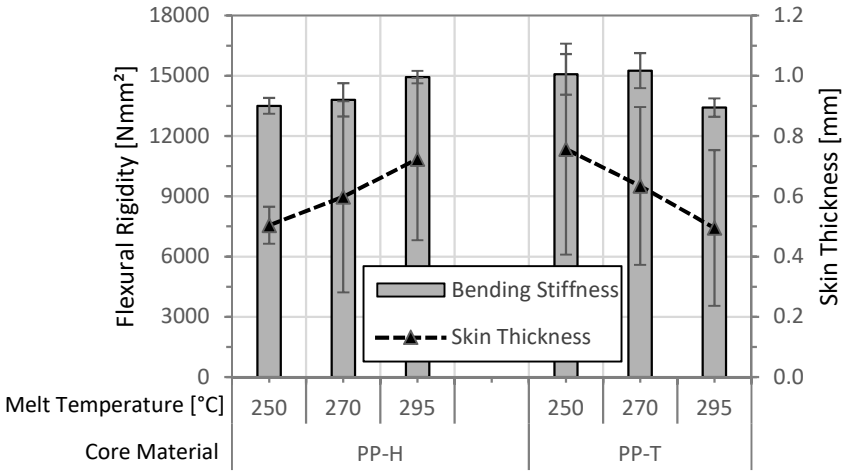


Figure 89: Correlation between absolute flexural rigidity and the measured core-skin thickness of chemically foamed in-situ CFRTP sandwich specimens with PP-H and PP-T20 core material.

The macroscopic foam morphology thus affects the absolute flexural rigidity of the in-situ CFRTP structures. The lightweight design effect however is based on the relation between absolute and specific flexural rigidity, the latter resulting from the density reduction. In order to evaluate the effect of material and process on the resulting density reduction of in-situ sandwich specimens with integral foam core, the morphology of the latter on micro scale is analysed.

### 6.4.2. Microscopic Foam Morphology

Micro computer tomography (µCT) scans of the foamed core of in-situ sandwich specimens were made using a SkyScan 1072-100 tomograph. For each test setting, a cylindrical sample was removed from a test specimen with the aid of a precision milling cutter. The cylinder was extracted at the centre of the specimen. It exhibits a diameter of 2.5 mm and a height of 10 mm, which comprised the complete thickness of the specimen. Due to the small size of the cylinder compared to the total dimension of the specimen, the foam morphology assessed via µCT cannot validly be representative for other areas of the specimen, especially due to the discussed flow length dependency of the foam morphology, see Figure 87. However, it allows for a comparison of foam morphologies at the centre of the 4PB load span and is thus considered an indication of the material and process parameter induced mean microscopic foam morphology in this specimen area.

Firstly, in-situ CFRTP sandwich structures based on chemical blowing agents are discussed. Figure 90 shows the foam morphology and density reductions of sandwich specimens with CBA integral foam core using PP-H (a) and PP-T20 (b) as core materials. With rising melt temperature from $T_m$ = 250 °C to $T_m$ = 295 °C, both PP-H and PP-T20 integral foams only show a minor increase of density reduction. While the use of PP-T20 as core material leads to a density reduction from 30.6 % to 33.1 %, it is increased using PP-H foam cores from 32.7 % to 34.1 %.

The relatively constant density reduction does not correlate with the observed cell morphology, as clear differences can be found with increasing melt temperature for both core materials. In case of PP-H, growing mean cell diameters from 172 µm at $T_m$ = 250 °C to 248 µm at $T_m$ = 295 °C are measured denoting an increase of 30 %. Sandwich specimens with PP-T20 foam cores reach mean cell diameters of 166 µm at $T_m$ = 250 °C to 222 µm at $T_m$ = 295 °C, showing a similar temperature dependent cell growth of 25 %. The smaller cell diameter of chemically foamed PP-T20 cores compared to PP-H is assumed to result from the increased nucleation density induced by the addition of the talcum particulate filler [121], compared to the CBA residues which also induce heterogeneous nucleation in the unfilled PP-H.

The significantly larger cells with increasing melt temperature should result in higher density reductions, yet the reduced cell density and expanding skin thickness compensate this effect. The reason for the general increase of cell size with growing melt temperatures is attributed to the increased diffusive mass flow according to Equation 9. Following this, the diffusion of gas depends on the diffusion coefficient and the time available for diffusion processes. The diffusion coefficient increases with growing temperatures due to Brownian motion of polymer and gas [112], moreover the high cooling time allows for a longer time span of gas diffusion. In addition to the diffusion between cells, their coalescence is facilitated with growing melt temperature as their melt strength decreases [298].

Aside the observed general increase of cell size with growing melt temperatures, a location dependent cell size is found. Specimens based on CBA exhibit a layer with a reduced number of cells in the central part of the foam core at the highest melt temperature. This results in a 5-layer structure of the integral foam core, see Figure 90 (a3) and (b3).

It is concluded that the type of core material only plays a minor part in density reduction of in-situ specimens using CBA. The same is found for the melt temperature, which only leads to a minor

change in density reduction although the cell morphology is distinctly changed with respect to mean cell size and cell size distribution.

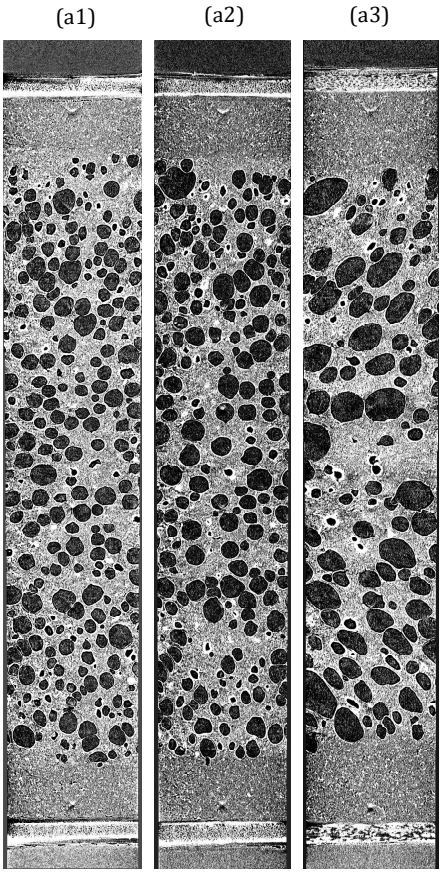


| Parameter | Value 1 | Value 2 | Value 3 | Dim. |
|---|---|---|---|---|
| Melt Temperature | 250 | 270 | 295 | °C |
| Density Reduction | 32.7 | 33.4 | 34.1 | % |
| Mean Cell Diameter | 172 | 193 | 248 | µm |

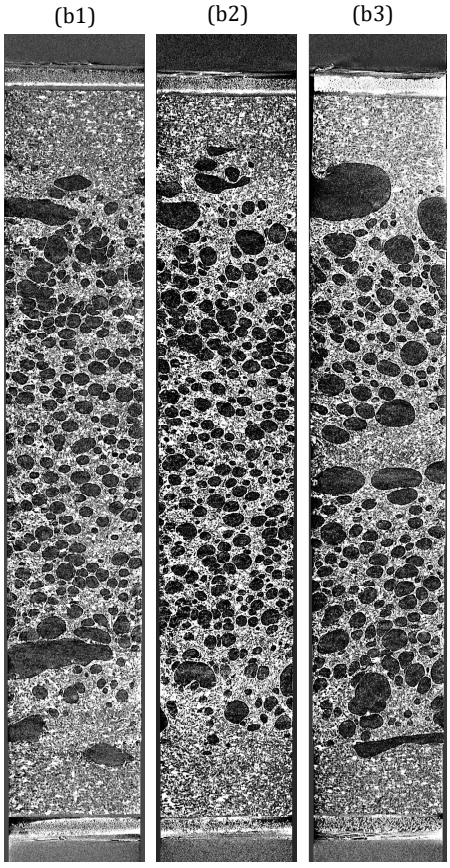


| Parameter | Value 1 | Value 2 | Value 3 | Dim. |
|---|---|---|---|---|
| Melt Temperature | 250 | 270 | 295 | °C |
| Density Reduction | 30.6 | 30.4 | 33.1 | % |
| Mean Cell Diameter | 166 | 181 | 222 | µm |

Figure 90: µCT cross section images of in-situ CFRTP sandwich specimens with chemcially foamed integral foam core [189]: (left) PP-H, (right) PP-T20. The cell diameter increases with rising melt temperature. The foam morphology shows a 5-layer structure with a small solid core area at the center of the specimen at the highest melt temperature of $T_m$ = 295 °C.

Contrary to CBA based sandwich structures, the density reduction and foam morphology of physically foamed sandwich specimens varies significantly depending on the core material and melt temperatures used, see Figure 91. The use of PP-H as core material leads to very high density reductions at all three melt temperatures ranging between 43.7 % at $T_m$ = 250 °C and 41.5 % at $T_m$ = 295 °C. The melt temperature insensitive density reduction correlates with the foam morphology based on the µCT scans of PP-H foam cores, see Figure 91 (a). The cell size only marginally varies from a mean diameter of 169 µm at $T_m$ = 250 °C to 179 µm at $T_m$ = 295 °C which is considered negligible.

Using PP-T20 as core material for in-situ sandwich specimens, similar high density reductions as PP-H based specimens can only be achieved at the highest melt temperatures of $T_m$ = 295 °C yielding 42.3 %. At $T_m$ = 250 °C the density reduction even falls below 30 % which is the lowest value of the experimental campaign. This significant difference of density reduction correlates well with the foam morphology, since the latter is distinctly affected by a change of melt temperatures especially at low

to moderate melt temperatures. The measured average pore size reduces from 184 µm at $T_m$ = 250 °C to 88 µm at $T_m$ = 270 °C, a difference of 51 %.

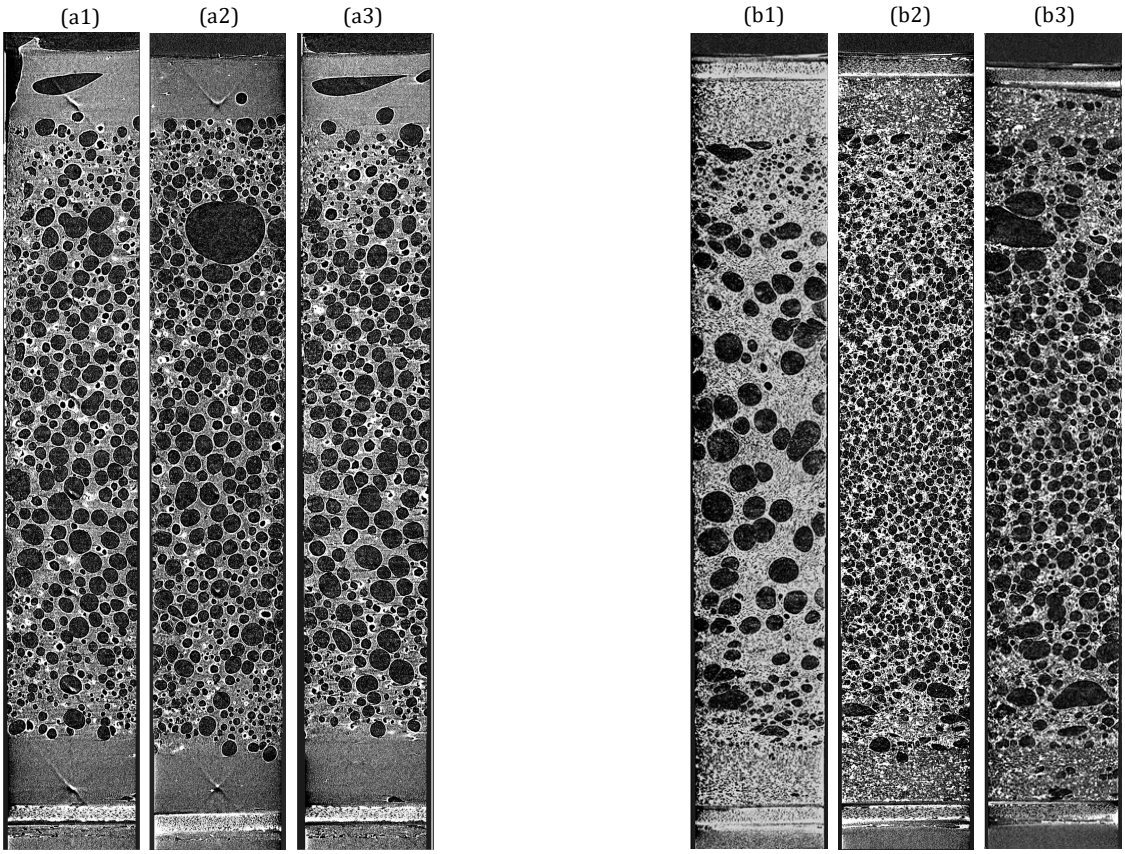


| Parameter | Value 1 | Value 2 | Value 3 | Dim. |
|---|---|---|---|---|
| Melt Temperature | 250 | 270 | 295 | °C |
| Density Reduction | 43.7 | 43.5 | 41.5 | % |
| Mean Cell Diameter | 169 | 173 | 179 | µm |

| Parameter | Value 1 | Value 2 | Value 3 | Dim. |
|---|---|---|---|---|
| Melt Temperature | 250 | 270 | 295 | °C |
| Density Reduction | 29.5 | 36.0 | 42.3 | % |
| Mean Cell Diameter | 184 | 88 | 130 | µm |

Figure 91: µCT cross section images of in-situ CFRTP sandwich specimens with physically foamed integral foam core: PP-H (left), PP-T20 (right). The foam morphology of PP-H foam cores is temperature insensitive. To the contrary, PP-T20 foam cores exhibit a distinct dependency on the melt temperature.

The difference of foam morphologies between PP-H and PP-T20 foam cores is attributed to the type of cell nucleation. Whereas physically foamed PP-H exhibits homogenous nucleation due to the lack of filler, the nucleating effect of the talcum filler is assumed to effectively lead to a significant increase of nucleation density of the PP-T20 material by the reduction of the free energy density which facilitates the development of new cell nuclei [123]. Another contributor to the different morphology may be the solubility of $N_2$ in polypropylene. With rising melt temperature, the solubility of $N_2$ is enhanced [125]. The solubility threshold of unfilled PP-H however is assumed to be already exceeded at the lowest melt temperature. Hence although it is known that large differences of foam morphologies of PP can occur in melt temperature spans as small as 4 °C [299], a further increase of melt temperature has no significant effect on the morphology and density reduction of physically foamed PP-H sandwich specimens. Consequently, physically foamed in-situ CFRTP sandwich specimens with PP-H as core material yield the best combination density reduction and process stability.

## 6.5. Discussion

The flexural behaviour of in-situ sandwich structures with UD tape facesheets and different core materials as well as blowing agents was evaluated by means of four-point bending testing. The absolute as well as the weigh specific flexural rigidity were assessed in order to evaluate the lightweight design potential using PP-H and PP-T20 as core materials. Furthermore, the effect of chemical and physical blowing agents on the flexural properties was analysed. An evaluation of the macroscopic and microscopic foam morphology should clarify its effect on the flexural behaviour of in-situ CFRTP sandwich structures.

With respect to the absolute flexural rigidity measured via 4PB, sandwich structures with PP-H and PP-T20 foam cores manufactured using chemical blowing agents yield similar absolute flexural rigidity compared with PP-T20 despite the significantly higher Young's modulus of the latter. Furthermore, the flexural rigidity is subject to moderate increase or decrease with rising melt temperature depending on the core material. The change of flexural rigidity with rising melt temperature is attributed to the thickness of the solid core-skin. A comparison of the measured mean core-skin thickness of in-situ sandwich specimens with chemically foamed integral core showed, that the increase of absolute flexural rigidity of PP-H core sandwiches with rising melt temperatures correlates with the increase of core-skin thickness. Equally, the decrease of flexural rigidity of in-situ sandwich specimens with PP-T20 as core material can be correlated with a declining thickness of the core-skin.

In contrast to CBA based in-situ sandwich structures, the use of PBA leads to a significant difference of flexural rigidity depending on the core material. Despite a small increase of flexural rigidity of sandwich specimens with PP-H foam cores with rising melt temperature, the use of PP-T20 generally leads to distinctly higher results. The largest difference was found at $T_m$ = 250 °C at which the flexural rigidity of in-situ sandwich specimens with PP-T20 foam core is about 30 % higher compared to PP-H. This was expected as the Young's modulus of PP-T20 exceeds the modulus of PP-H by 40 %, see Table 12. However, a correlation between core-skin thickness and flexural rigidity could not be assessed in case of physically foamed in-situ sandwich specimens, since a clear separation of solid skin and foamed core could not be made. This is because PBA foam cores also exhibit cells in the core-skin, which is in accordance with Altstädt [112], which hinders the macroscopic assessment of core-skin thickness.

More interesting than the shear flexural rigidity however is the weight specific flexural rigidity depending on the core material and process parameters, as the lightweight design of in-situ CFRTP sandwich structures is one of the main goals of this work. While the density reduction and accordingly the weight specific flexural rigidity of chemically foamed in-situ sandwich structures are moderate and only minor increases can be achieved with rising melt temperatures, the density reduction using PBA is significantly higher and also depends on the core material. PP-H as core material leads to the highest density reductions, ranging between 41.5 % and 43.7 %. This also leads to the highest measured weight specific flexural rigidity of the experimental campaign, despite the much lower absolute flexural rigidity compared to PP-T20. The combination of PP-T20 with physical foam injection moulding leads to sandwich structures with growing density reduction from 29.5 % to 42.3 % with an increase of melt temperature from $T_m$ = 250 °C to $T_m$ = 295 °C. Hence, the density reduction is much more dependent on the melt temperature compared to PP-H. This result could be correlated with the microscopic foam morphology analysis using µCT scans, which shows a similar result. Density reductions and microscopic foam morphology are hence closely linked, and as such the weight specific flexural rigidity since it is related to the density reduction.

In order to quantify the relative specific flexural rigidity increase, the relation of weight specific flexural rigidity and the respective absolute flexural rigidity was introduced as the lightweight design effect $\mathrm{LD}$. The highest values of $\mathrm{LD}$ are found for in-situ sandwich structures with PP-H foam cores. The use of PBA further increases the lightweight design effect by 20 % compared to CBA.

Consequently, it can be concluded that the combination of physical blowing agents with unfilled PP-H leads to the highest lightweight design effect while the latter is also considerably insensitive to the chosen process parameters, which makes the manufacture of in-situ CFRTP sandwich structures less prone to reproducibility issues. This material and process combination is hence promising for further use in the manufacture of in-situ CFRTP sandwich components.

# 7. Predictive Modelling of In-Situ CFRTP Sandwich Structures

It was shown in the previous chapters that in-situ CFRTP sandwich components can be manufactured with high interfacial bonding. Furthermore, the effects of material and process parameters on mechanical properties with respect to absolute and weight specific flexural rigidity were evaluated.

In this chapter, a methodology for the model based prediction of the interfacial bonding of CFRTP facesheets and integral polymeric foam core as well as the resulting flexural rigidity is developed in order to enable the use and application of the in-situ CFRTP sandwich manufacturing process for the conceptual development and design of new components. These models combine all findings of the previous chapters as indicated in Figure 92.

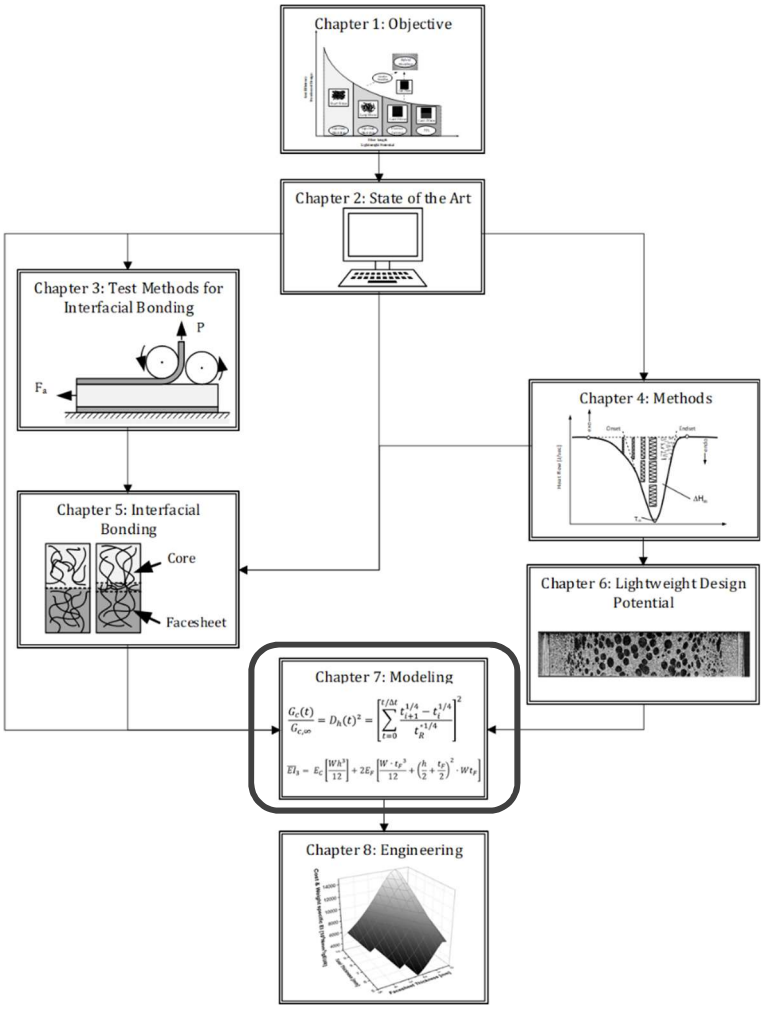


Figure 92: Systematic approach of this work: chapter 7 presents a model based approach to predict the interfacial bonding between CFRTP facesheets and foam core as well as the flexural rigidity resulting from material and process parameters.

The methodology combines two models:

- Interfacial bonding model
- Flexural rigidity model

The models require input data including the component geometry, the material properties as well as the process parameters applied for the in-situ manufacture of CFRTP sandwich specimens. The

model output is a prediction of the flexural rigidity of the sandwich component beam as well as of the interfacial bonding of CFRTP facesheet and core. The models are presented in the following chapters.

## 7.1. Interfacial Bonding Model

The interfacial bonding model consists of two consecutive separate parts. The core of the model is denoted by the calculation of the effective interfacial bonding which is executed in the fusion bonding model. The necessary input parameters for the interfacial fusion bonding model are the interface temperature profiles, which are derived from a preceding injection moulding simulation.

### 7.1.1. Fusion Bonding Model

The interfacial fusion bonding model is based on the interfacial strength development by the healing process of two miscible thermoplastic interfaces as presented in chapter 2. In order to explain the model and the resulting requirements with respect to the input parameters, the fusion bonding process described by the degree of healing is briefly presented again. Based on the non-isothermal healing model by Bastien and Gillespie [146], the resulting interfacial fracture toughness $G_c$ can be calculated as

$$\frac{G_c(t)}{G_{c,\infty}} = D_h(t)^2 = \left[\sum_{t=0}^{t/\Delta t} \frac{t_{i+1}^{1/4} - t_i^{1/4}}{t_R^{*1/4}}\right]^2 . \tag{45}$$

The non-isothermal fusion bonding process is approximated by isothermal time-steps $\Delta t = t_{i+1} - t_i$ at which the mean temperature $T^*$ of the interface must be known. The degree of healing is consequently the sum of isothermal time steps $\Delta t$ with the respective mean interface temperatures $T^*$ related to the reptation time $t_R^*(T^*)$ at these specific interface temperatures.

Therefore, the temperature dependent reptation time needs to be known. In chapter 2.4.2, methods to assess the reptation time were presented. They require either the availability of the polymer that is to be characterised or detailed knowledge about the physical behaviour of the polymer material. However, it was neither possible to obtain the pure UD tape polymer matrix material nor to gather any information that would allow for a determination of the temperature dependent reptation time. For this reason, the reptation time of the matrix polymer of another glass fibre reinforced UD tape with polypropylene matrix (UDMAX™ GPP 45-70) was used as best approximation [300]. The temperature dependent reptation time of the matrix polymer is depicted in Figure 93. The reptation time at or above the melting temperature of 163 °C [105] is in the range of a second or fraction of a second. For the core material used in this work (Sabic® PP 576P), Trippel [132] calculated a reptation time based on the Carreau approach which is about an order of magnitude lower than of the facesheet polymer matrix. According to Grouve [16] and the findings within chapter 5, fusion bonding of two interfaces is limited by the adherent with the lowest polymer chain mobility. Considering the reptation time curves and the injection moulded core as high temperature and highly amorphous melt, the solid CFRTP facesheet with semi-crystalline matrix polymer denotes the

bottleneck of interfacial bonding. The development of interfacial strength is prone to large variations if the interface temperature is near the melting temperature of the facesheet.

According to Figure 93, the reptation time abruptly increases by several orders of magnitude within a temperature range of only 10 °C below the melting temperature. This indicates how temperature-sensitive the fusion bonding process and thus the interfacial bonding development during in-situ process is. Especially at interface temperatures close to the melting temperature of the UD tape facesheet, only few degrees Celsius can result in large differences of interfacial bonding.

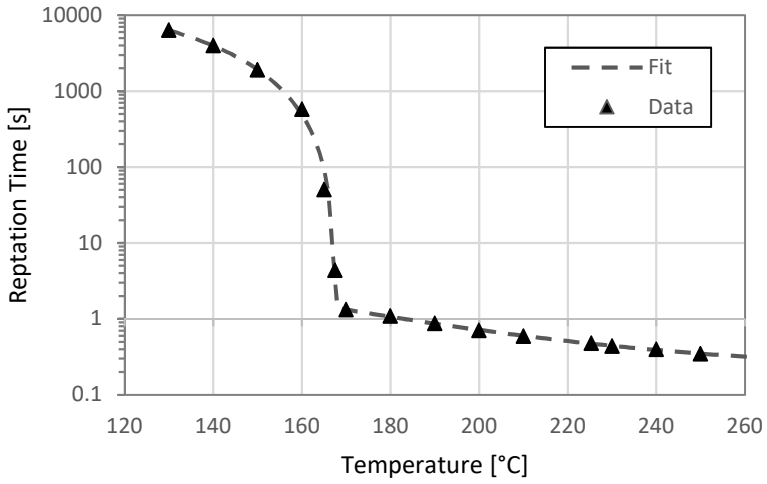


Figure 93: Reptation time curve fitted from data of Shi et al. [300].

This poses a critical requirement to the interface temperature simulation, as it consequently needs to predict the temperature very precisely especially at the vicinity of the melting temperature as small deviations may alter the result drastically and lead to incorrect bonding predictions. The interface temperature simulation is presented in the following.

### 7.1.2. Interface Temperature Simulation

The interface temperature simulation needs to predict the temperature that develops at the surface of the CFRTP facesheet resulting from the applied process parameters and materials. The simulation is based on the validated interface temperature simulation for in-situ CFRTP sandwich components presented in chapter 4. The simulation determines the surface temperature of a 3D insert during the contact with the injected polymer melt. As discussed in chapter 4, the simulation is validated by comparison with experimentally assessed interface temperature profiles of Trippel [132]. In Figure 94 the simulated as well as experimentally assessed interface temperature during in-situ moulding of a sandwich specimen with 1UD tape facesheets and chemically foamed integral foam core is depicted during the first 5 seconds of the process. Based on the reptation time curve in Figure 93, the temperature dependent time for complete fusion bonding can be less than a second if the melt temperature of the UD tape matrix polymer is exceeded. Due to this rapid process, it is essential to precisely predict not only the cooling of the interface but especially the peak temperature at the surface of the UD tape facesheets. At closer observation of Figure 94 the simulation of the peak

interface temperature during the in-situ process shows a high correlation with the experimental values. The simulated interface temperature development yields a minor underestimation with respect to the measured temperature during the process according to Trippel [132]. However, the thermocouple for the temperature assessment at the core-facesheet interface was positioned on the UD tapes and extended into the hot sandwich core.

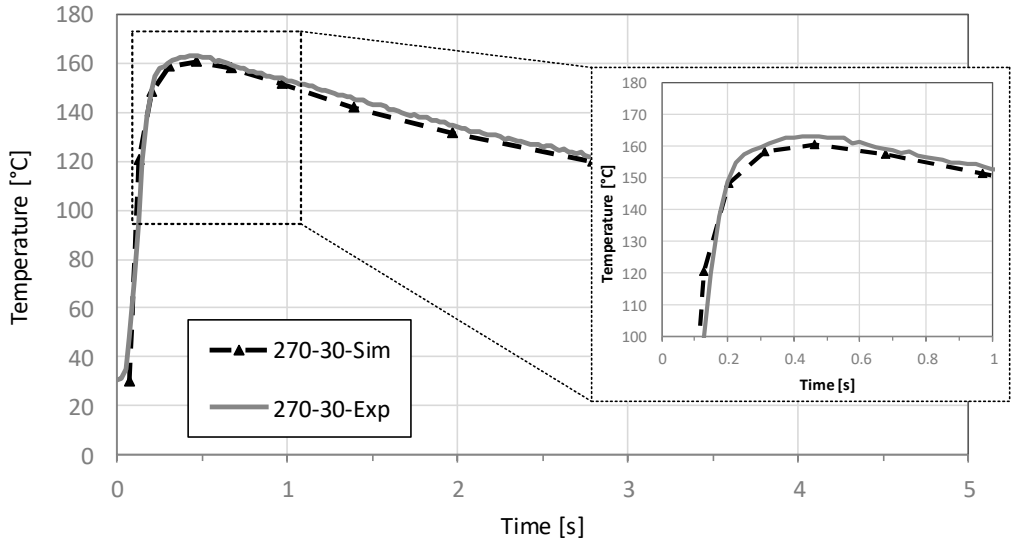


Figure 94: Comparison of simulated and experimentally assessed interface temperatures during the in-situ manufacture of CFRTP sandwich specimens. High agreement between simulation and experiment can be observed.

Despite the small diameter of the thermocouples of 0.33 mm [132], this results in a minor increase of measured temperatures compared to the temperature exactly on the facesheet surface which is simulated and which is used for the interfacial bonding prediction. Similar agreements of simulated and experimentally assessed interface temperatures were found for other process temperatures, see Annex A.

### 7.1.3. Interfacial Fracture Toughness Reference

The maximum interfacial fracture toughness of the sandwich specimen core to facesheet interface $G_{I,\infty}$ must be known for the calculation of the resulting interfacial facture toughness according to Equation 45. Therefore, CFRTP sandwich structures were manufactured based on consolidation of UD tape facesheets with the polymer core using the compression moulding process according to the classification in Figure 13. The facesheet preparation and the subsequent consolidation process is schematically depicted in Figure 95. In order to enable a direct comparison of the interfacial bonding properties of in-situ and compression moulded CFRTP sandwich specimens, it was necessary to use identical material, i.e. the same facesheet and the same CBA integral foam core. This includes using the same CBA type and amount, the same core polymer and at least a comparable integral foam core structure. These requirements regarding the validity of comparability of results led to the use of unreinforced foam injection moulded integral foam specimens as core. These integral foam components were consolidated with UD tape facesheets via the compression moulding technique in order to receive the reference CFRTP sandwich specimens as depicted in Figure 95.

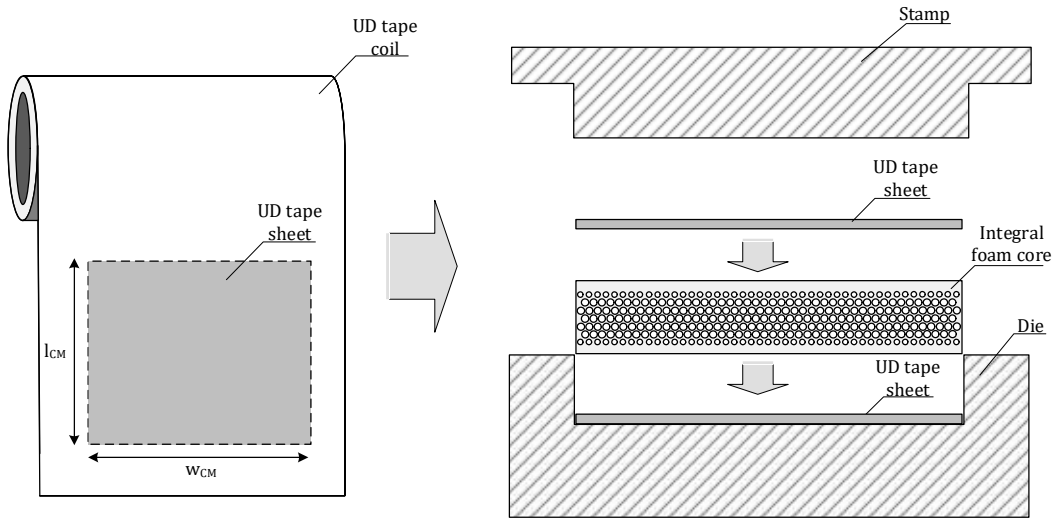


Figure 95: Schematic illustration of the manufacture of CFRTP sandwich structures via compression moulding based core-skin consolidation. The manufactured CFRTP sandwich structures are used for the subsequent determination of reference interfacial fracture toughness values $\mathbf{G}_{\mathbf{c},\infty}$.

UD tape sheets were cut from the as-received UD tape coil and tailored according to the mould size with sheet length $l_{CM}$ = 220 mm and sheet width $w_{CM}$ = 240 mm. These UD tape sheets were placed into the heated mould and covered with integral foam cores which were foam injection moulded in accordance with the process parameters used in chapter 6, however without CFRTP facesheets. The mould was closed and after equalisation of the temperatures of upper and lower press plate side, the compression moulding process was initiated according to the process parameters in Table 15.

Table 15: Process parameters during core-skin consolidation for the manufacture of reference CFRTP sandwich structures.

| | Plate Temperature | Consolidation | Cooling | Dimension |
|---|---|---|---|---|
| Target Mould Temperature | 220 | - | - | °C |
| Target Interface Temperature | - | 217 | 85 | °C |
| Pressure | 0 | 1.5 | 1.5 | bar |
| Time | 1 | 2 | 120 | min |

According to processing guidelines of the UD tape manufacturer, the applied pressure during consolidation shall be $p_{app}$ = 1.9 bar. However, this pressure resulted in an excessive compression of the foam core. Thus, a suitable consolidation pressure of 1.5 bar was determined empirically and applied during the manufacture of reference CFRTP sandwich plates. In order to enable RPT of the compression moulded CFRTP sandwich plates, the facesheets were equipped with a PI foil as initial crack before processing, equal to in-situ CFRTP sandwich specimens with injection moulded core. In order to achieve full interfacial bonding, sufficiently high interface temperatures must be reached during the process. Therefore, the interface temperature between integral foam core and UD tape facesheet was measured using a thermocouple in the middle of the sandwich plate at the interface between UD tape sheets and foam core. The mould temperature was set to 220 °C resulting in a maximum effective interfacial peak temperature $T_{peak}$ = 217.4 °C. The compression moulded sandwich plates were demoulded at an interface temperature of 85 °C. Due to the long time spans of interfacial contact at high temperatures between facesheets and core during compression moulding and considering the relatively low reptation time of polypropylene, see Figure 93, it is assumed that a full bonding foam core and UD tape facesheets is achieved. After demoulding, the compression

moulded sandwich plates were cut to the specimen geometry for the roller peel test method using a water jet-cutting machine. After storing the specimens at 23/50 standard climate for 24 h, the specimens were subsequently subject to roller peel testing in accordance with the procedure in chapter 6 in order to determine the reference $G_{I,\infty}$ value. The results are depicted in Figure 96. The calculated reference interfacial fracture toughness results to be $G_{I,\infty}$ = 1.4 kJ/m².

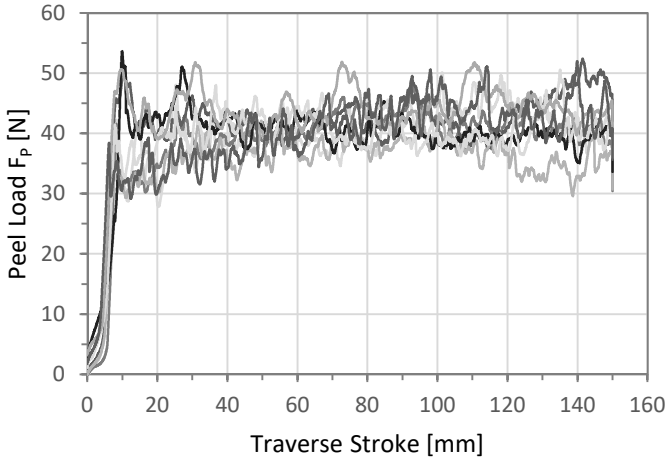


Figure 96: Resulting debonding load curves during the interfacial fracture toughness testing of the reference CFRTP sandwich structures using the roller peel test.

Combining the interface temperature prediction based on the interface temperature simulation and the interface fusion bonding model with the reference interfacial fracture toughness for CFRTP sandwich structures, the quantitative prediction of $G_I$ values for in-situ CFRTP sandwich components with different process parameters and geometry is enabled. The results will be discussed in the following.

### 7.1.4. Design of Experiments

The developed interface model shall be used for the prediction of resulting core-facesheet bonding of in-situ manufactured CFRTP sandwich structures with integral foam. The evaluation of the predicted interfacial bonding shall be conducted by comparison of predicted $G_I$ values with experimental data of roller peel test results at the respective process parameters. The experimental design is presented in Table 16.

Table 16: Overview of the process and material parameter variation.

| Parameters | Value 1 | Value 2 | Value 3 | Dimension |
|---|---|---|---|---|
| Melt Temperature | 250 | 270 | 295 | °C |
| Mould Temperature | 55 | - | - | °C |
| Core Material | PP-H | - | - | - |
| Blowing Agent | CBA | - | - | - |
| Facesheet Thickness | 0.33 | - | - | mm |

### 7.1.5. Results

In Figure 97 (left) the predicted development of interfacial bonding of in-situ foam core sandwich specimens with $T_m$ = 250 °C and $T_w$ = 55 °C based on the proposed model is presented. The degree of healing rapidly rises within the first fractions of a second of the in-situ process, resulting from the high initial interface temperatures. However, the interfacial temperature does not reach the melting temperature of the facesheet matrix according to the interface temperature simulation. After the first second of the process, the growth rate of $D_h$ is decreasing and the degree of healing stagnates at $D_h \approx 0.2$.

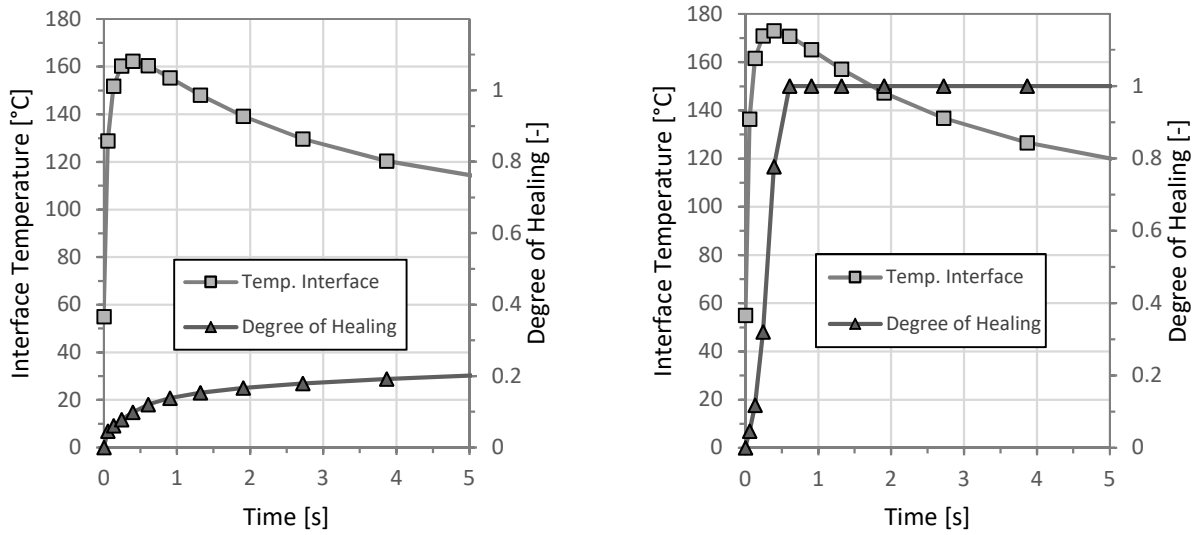


Figure 97: Simulated interface temperature and corresponding resulting degree of healing based on the fusion bonding model of Bastien and Gillespie [146]: $T_m$ = 250 °C and $T_w$ = 55 °C (left), $T_m$ = 270 °C and $T_w$ = 55 °C (right).

Increasing the melt temperature to $T_m$ = 270 °C, the resulting interface temperature between facesheet and core exceeds the melting temperature at a time span that is long enough to enable a full bonding of face and core, see Figure 97 (right). The peak interface temperature yields $T_{peak}$ = 173.1 °C. According to the model, full bonding is achieved after 0.6 s. Applying a melt temperature of $T_m$ = 295 °C, the necessary process time to enable full bonding can be even further reduced to 0.36 s.

A comparison of the development of healing in Figure 97 makes clear, that it is crucial to reach a high peak temperature at the interface between facesheet and core during the in-situ process in order to achieve full healing. According to this and the underlying healing model, the peak interface temperature must be equal or above the melting temperature of the facesheet polymer matrix. If this is achieved, the necessary time-span for the development of healing i.e. the reptation time, is generally also provided by the resulting temperature profile of the studied in-situ process. Hence, full healing develops in less than a second if the peak interface temperature is sufficiently high, due to the short reptation times of the PP matrix. If high peak temperatures cannot be reached, interfacial healing occurs at a much slower rate and full healing is usually not achieved. A lower cooling rate however contributes to prolong the times span for the development of healing at low healing rate, helping to still achieve a certain yet low interfacial bonding below melting temperature.

The healing model was applied for the prediction of interfacial fracture toughness of in-situ CFRTP sandwich structures according to Equation 45. In Figure 98 (left), the model based prediction of the degree of healing of in-situ CFRTP sandwich structures with 1UD tape facesheets and PP-H integral foam cores with chemical blowing agent related to the experimentally assessed interfacial fracture toughness is depicted. At low process temperatures using $T_m$ = 250 °C and $T_w$ = 55 °C the simulation based degree of healing underestimates the interfacial bonding of facesheets with foam injection moulded PP-H cores yielding $D_h$ = 0.28. At higher temperatures, the degree of healing reaches $D_h$ = 1 at $T_m$ = 270 °C and also at $T_m$ = 295 °C melt temperature, resulting in a plateau. Similarly, the experimentally assessed $G_I$ values also yield a plateau, indicating that the predicted degree of healing qualitatively correlates well with the experimental $G_I$ data.

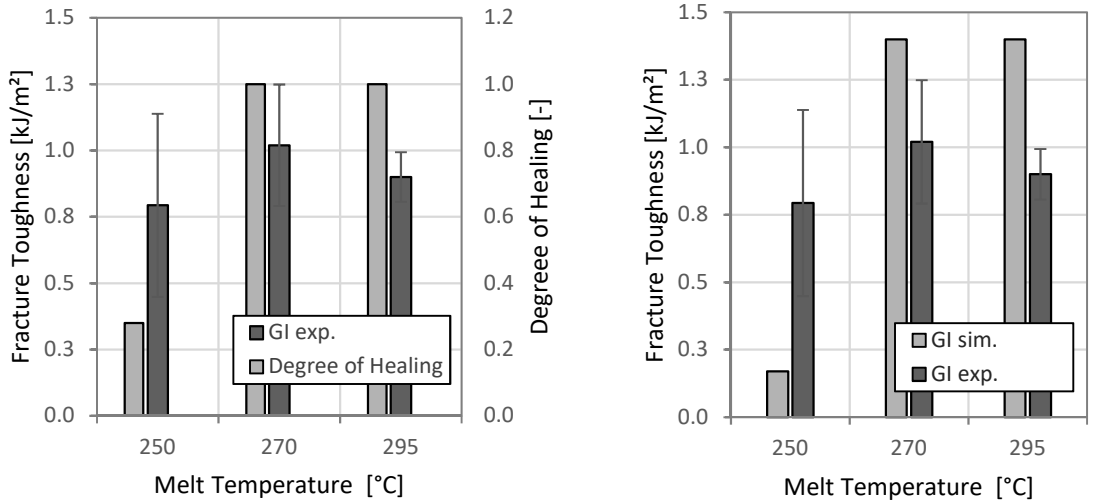


Figure 98: Comparison of the model based assessment of the degree of healing resulting from the in-situ sandwich manufacture process: the degree of healing compared to the interfacial fracture toughness yields reasonable qualitative agreement (left). The quantitative comparison of predicted and experimentally assessed interfacial fracture toughness shows an underestimation at low melt temperatures (right), which is attributed to minor inaccuracies of the interface temperature simulation of few degrees Celsius. An overestimation at elevated melt temperatures is observed, which results from the reference interfacial fracture toughness values based on sandwich specimens manufactured via the compression moulding consolidation method.

The aim of this model is to quantitatively predict the resulting interfacial fracture toughness. Therefore, the degree of healing was set in relation with the reference interfacial fracture toughness $G_{I,\infty}$ according to Equation 45. The calculated $G_I$ values are depicted in Figure 98 (right).

The predicted interfacial fracture toughness $G_{I,sim}$ at $T_m$ = 250 °C underestimates the experimentally assessed $G_{I,exp}$ value. This is attributed to the simulated temperature profile at the core-facesheet interface using a melt temperature of $T_m$ = 250 °C, giving slightly smaller simulated interface temperatures than in experiment, both near the melting temperature $T_{melt}$ of the UD tape facesheet. The effect of a small underestimation of the interface temperature resulting in a value near $T_{melt}$ can be explained by the following considerations.

Taking into account the low reptation times of PP of less than a second, only a short time span is necessary to create full healing if $T_{melt}$ is exceeded at the interface. Thus, small temperature differences can lead to large variations of interfacial healing, both regarding predicted as well as experimentally determined values. As the experimentally assessed $G_I$ value is an intermediate value

reaching $G_I$ = 0.83 kJ/m², the interface peak temperature during in-situ moulding is probably just at the vicinity of the melting temperature making the prediction of the interfacial bonding prone to large deviation of the measured values in this specific case. Consequently, if an interfacial bonding simulation is performed with PP as core as well as facesheet matrix polymer, a calculated degree of healing of below and just equal 1 respectively should be rated as critical and the corresponding process parameters should not be applied for the manufacture of in-situ CFRTP sandwich specimens.

Contrary to low process temperatures, the predicted $G_{I,sim}$ values exceed the experimentally assessed interfacial fracture toughness at $T_m$ = 270 °C and $T_m$ = 295 °C. The overestimation of $G_I$ values based on the model prediction is not attributed to the simulated peak interface temperature but to the reference $G_{I,\infty}$ values. It is assumed to result from the different techniques used for the manufacture of the respective CFRTP sandwich structures.

The reference $G_{I,\infty}$ values are determined using the facesheet-core consolidation process via compression moulding. This includes the melting of the complete UD tape facesheets as well as of the core, hence both adherent surfaces are in molten state. Especially the melting of the CFRTP facesheets enhances the creation of intimate contact, since the facesheet surface asperities are rapidly flattened due to the reduced viscosity, see Equation 17, despite a similarly low consolidation pressure compared to the low-pressure in-situ process. According to Equation 22 bonding of interfaces is a two-step process with the intimate contact as prerequisite for the diffusion of polymer chains across the interface between miscible polymer surfaces [15, 16, 156, 157]. The complete melting of both adherents is hence likely to result in higher interfacial bonding compared to the bonding process of two polymer interfaces of which one is initially solid, especially if the consolidation pressure is low. In addition, the process time of compression moulding of CFRTP sandwich reference structures was one order of magnitude higher compared to the injection moulding based in-situ process providing significantly more time for intimate contact development and healing.

Contrary to the manufacture of CFRTP sandwich specimens via skin-core consolidation, the in-situ process exhibits a process time span in the range of seconds or less at which interfacial bonding needs to be created. According to the results of chapter 5.2, this short process time might not be enough for the complete melting of the facesheet surface and the reduction of surface asperities even if the melting temperature is well exceeded. However, sufficient melting of the facesheet is necessary to reduce the surface asperities of the facesheets in order to achieve high degrees of intimate contact. Shi et al. [300] have found that the surface roughness and its reduction plays an important role when it comes to interfacial bonding of UD tapes. It is thus assumed that during in-situ manufacture of CFRTP sandwich structures the intimate contact of UD tape facesheets to the injected core is not instantly achieved contrary to the findings of other authors [14, 159, 163].

Consequently, the experimentally assessed interfacial bonding process is not well reflected using the degree of healing since the intimate contact is not necessarily always complete. This is especially true for the in-situ sandwich process based on low-pressure foam injection moulding. Models for the combined assessment of degree of healing and the degree of intimate contact yielding a degree of bonding [143, 167] might be capable of yielding better quantitative correlations of predicted interfacial bonding of in-situ sandwich specimens based on low pressure foam injection moulding. For this, however, the cavity pressure development during the process must also be simulated and the latter must be validated. In case of the high-pressure foam injection moulding, the cavity

pressure during the process is significantly higher and expected to be sufficient to immediately yield full intimate contact. This is assumed to lead to an alignment of results of the present healing model and a combined bonding model, yet with distinct advantages of the present model since it does not require the additional validated cavity pressure simulation.

## 7.2. Flexural Rigidity Model

In addition to the prediction of interfacial bonding of CFRTP facesheet and core, the material and design-dependent flexural rigidity needs to be validly predicted. In the following, different models for the characterisation of the flexural behaviour of in-situ CFRTP sandwich components are evaluated and validated by means of experimental four-point bending tests.

Based on chapter 2, different models for the prediction of flexural rigidity of in-situ CFRTP sandwich structures were developed. These allow for a characterisation of the layer structure of the sandwich composite with CFRTP facesheets and integral foam core. The calculation of the total flexural rigidity $\overline{EI}$ is based on Equation 23. With the elastic modulus $E_i$ and the second moment of inertia $I_i$ of the respective layer including foam core morphology layers i.e. foamed core and solid core-skins as well as the facesheet, the flexural rigidity yields

$$\overline{EI} = \sum_{i=1}^{n} E_i I_i. \tag{46}$$

The structural variants of the layer structure are shown in Figure 99.

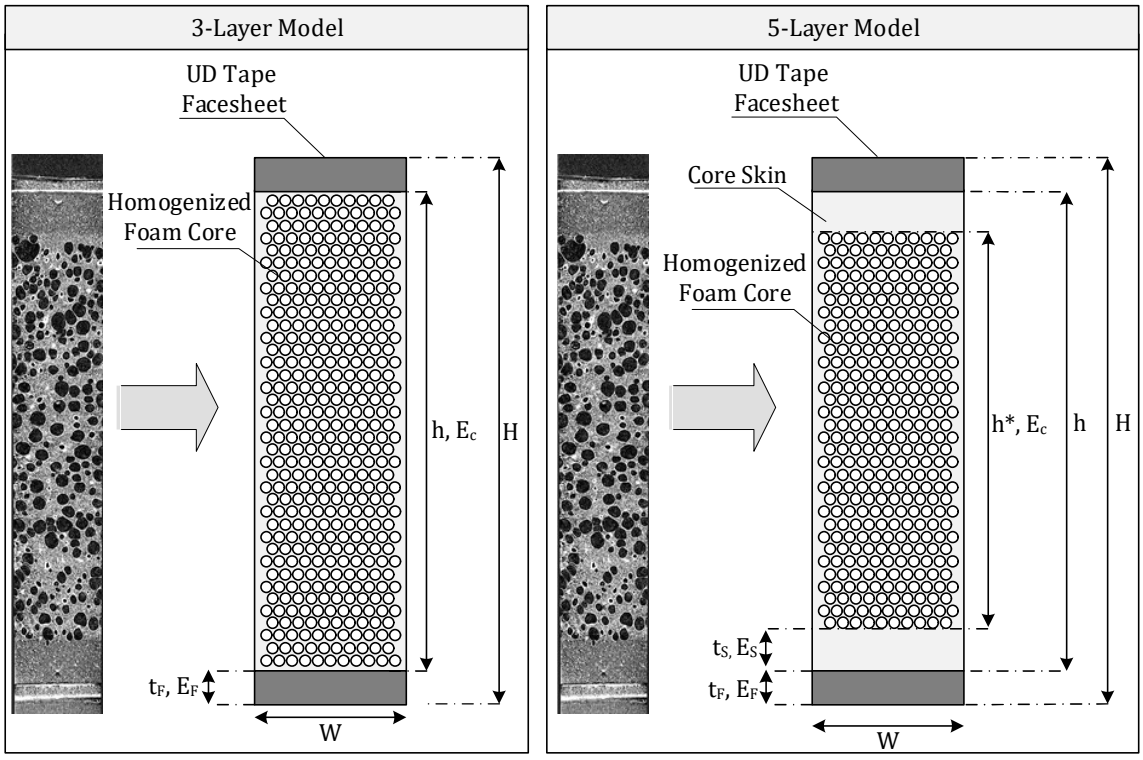


Figure 99: Schematic illustration of the different models for the structural characterisation of in-situ sandwich specimens with integral foam cores: (left) 3-layer model, (right) 5-layer model.

The structural design of the models is based on the total number of layers, which corresponds to the sum of the foam core layers and the CFRTP facesheet layers. In the 3-layer model, the integral foam core with varying macroscopic and microscopic morphology is homogenised assuming that the integral foam exhibits uniform properties over the entire thickness similar to a model first presented by Hobbs [191] yet without the introduction of the specific width $B_c$.

With the UD tape facesheet thickness $t_F$, the core thickness $h$, the width $W$, and the moduli of elasticity for the core $E_{C,3}$ and the facesheet $E_F$, the combined flexural rigidity of the 3-layer model $\overline{EI}_3$ is given as:

$$\overline{EI}_3 = E_{C,3}\left[\frac{Wh^3}{12}\right] + 2E_F\left[\frac{W \cdot {t_F}^3}{12} + \left(\frac{h}{2} + \frac{t_F}{2}\right)^2 W t_F\right]. \tag{47}$$

In order to calculate the core modulus $E_{C,3}$ according to Equation 29, the density reduction $\Delta\rho$ of the foam core must be determined. Therefore, the in-situ sandwich specimens were weighed on a precision laboratory scale after their manufacture. The mass difference $\Delta m$ of the in-situ sandwich specimens with foam core $m_{CBA}$ to the sandwich structure with solid core $m_{compact}$ yields the density reduction of the foam core of the 3-layer model with its foam core volume $V_{C,3}$ as:

$$\Delta\rho_3 = \frac{\Delta m}{V_{C,3}}, \tag{48}$$

with

$$\Delta m = m_{compact} - m_{CBA} \tag{49}$$

and

$$V_{C,3} = WLh. \tag{50}$$

Combining Equation 29 with Equation 48 leads to the Young's modulus of the foam core $E_{C,3}$ as

$$E_{C,3} = E_m\left(1 - \frac{\Delta m}{V_{C,3}}\right)^n. \tag{51}$$

The 5-layer model takes into account the formation of a thin solid skin on the integral foam core surface. The core hereby is divided into a homogenised foam middle layer and a homogenised core-skin layer. With the modulus of elasticity of the foam core $E_{C,5}$, the solid core-skins $E_S$ and the facesheets $E_F$ as well as the thickness of the foamed core $h_*$, the thickness of the solid core-skin $t_S$ and the facesheet thickness $t_F$, the total flexural rigidity of the 5 layer model $\overline{EI}_5$ yields

$$\overline{EI}_5 = E_{C,5}\left[\frac{Wh_*^3}{12}\right] + 2E_S\left[\frac{Wt_S^3}{12} + \left(\frac{h_*}{2} + \frac{t_S}{2}\right)^2 W t_S\right] + 2E_F\left[\frac{Wt_F^3}{12} + \left(\frac{h_*}{2} + t_S + \frac{t_F}{2}\right)^2 W t_F\right]. \tag{52}$$

In contrast to the 3-layer model, the 5-layer model includes the solid skins in the structural characterisation, hence the density reduction of the foamed core $\Delta\rho_5$ is increased due to the reduced foam core volume $V_{C,5}$. The thickness $t_S$ of the solid core-skin is determined by experimental

measurement according to the procedure in chapter 5. This leads to the modulus of the foamed core as

$$E_{C,5} = E_m(1 - \Delta\rho_5)^n, \tag{53}$$

with

$$\Delta\rho_5 = \frac{\Delta m}{V_{C,5}}, \tag{54}$$

and

$$V_{C,5} = WL(h - 2t_s). \tag{55}$$

The exponent $n$ in Equations 51 and 53 is an empirical value and hence needs to be adapted to the experimentally determined properties. High agreement with experimental results are achieved with $n$-values in the range $1 < n < 2$ which will thus be used for the calculation [112, 191, 197]. The correlation of the 3- and 5-layer model prediction with experimental results allows for the determination of the optimal $n$-value for the calculation of the resulting flexural rigidity of in-situ CFRTP sandwich structures depending on the respective layer model.

### 7.2.1. Design of Experiments

In order to evaluate the influence of the exponent $n$ on the accuracy of the model predictions regarding resulting flexural rigidity of CFRTP sandwich structures with different material and process parameters and thus foam morphologies, experimentally determined flexural rigidity values of chapter 6 were used as reference. The material and process parameter variation considered in this study is depicted in Table 17.

Table 17: Overview of the process and material parameter variation.

| | Value 1 | Value 2 | Value 3 | Dimension |
|---|---|---|---|---|
| Melt Temperature | 250 | 270 | 295 | °C |
| Mould Temperature | 55 | - | - | °C |
| Core Material | PP-H | PP-T20 | - | - |
| Blowing Agent | CBA | - | - | - |
| Layer-Model | 3-layer | 5-layer | - | - |
| Exponent n | 1 | 1.5 | 2 | - |

### 7.2.2. Results

The difference of flexural rigidity as predicted by the 3- and 5-layer model $\overline{EI}_{mo}$ with respect to the experimentally assessed flexural rigidity $\overline{EI}_{exp}$ indictaes the relative model deviation $\Delta\overline{EI}$ via

$$\Delta\overline{EI} = \frac{\left(\overline{EI}_{mod} - \overline{EI}_{exp}\right)}{\overline{EI}_{exp}} \cdot 100. \tag{56}$$

The results are depicted in Figure 100. The prediction of a foam core sandwich processed at melt temperatures of $T_m$ = 250 °C and $T_m$ = 270 °C yields a difference of flexural rigidity of less than 6.5 % to experimental results for both PP-H and PP-T20 based in-situ sandwich structures, depending on the n-exponent. While specimens with PP-H foam core yield a high agreement of prediction and

experiment especially using $n \geq 1.5$ with a minor overestimation, in-situ CFRT sandwich specimens with PP-T20 based foam core show the highest agreement of prediction and experimental values for $n \leq 1.5$.

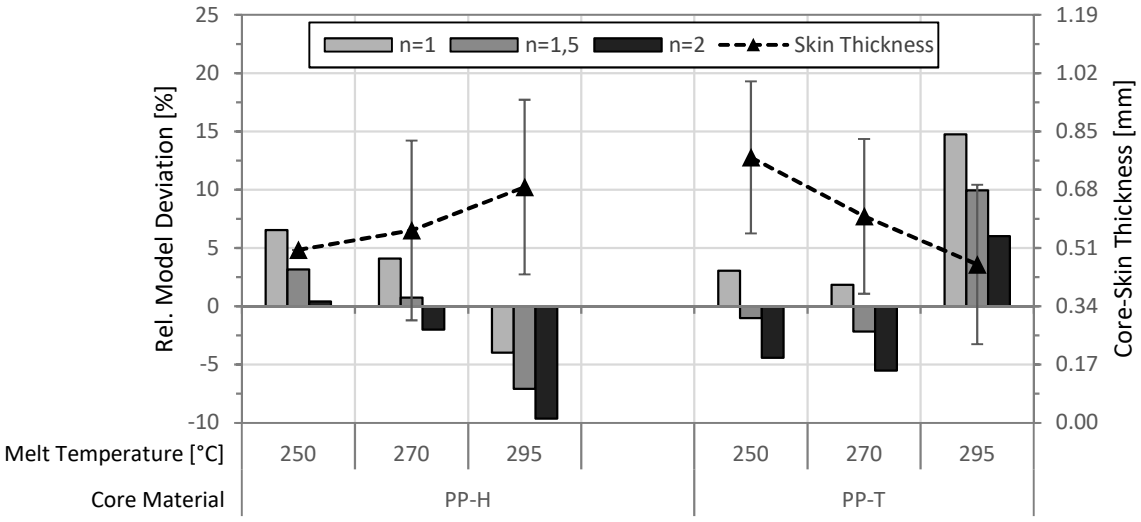


Figure 100: Comparison of the model-based prediction of the flexural rigidity of in-situ CFRTP sandwich structures manufactured using CBA with experimentally assessed values: 3-layer model.

At $T_m$ = 295 °C, the accuracy of the 3-layer model deteriorates. The flexural rigidity of sandwich structures with PP-H foam core at $T_m$ = 295 °C is predicted to be lower than actually determined in the 4PB experiment. Contrary, in-situ sandwich specimens with PP-T20 foam core are assumed to yield higher flexural rigidity values than measured at $T_m$ = 295 °C.

A similar increase of the model deviation for high melt temperatures can be observed using the 5-layer flexural rigidity model, yet only for PP-T20 foam core in-situ sandwich structures. Contrary to the findings when using CBA, the best prediction accuracy is achieved with $n$ = 2. With decreasing $n$-value the deviation bewteen prediction and experiment rises. However, the maximum difference between the results using $n$ = 1 and $n$ = 2 yields 4.3 % in case of PP-T at $T_m$ = 295 °C. Overall, the 5-layer model shows larger deviations from the experimentally determined flexural rigidity than the 3-layer model, as it generally overestimates the resulting flexural properties. Deviations between 5 to 10 % are usually observed for sandwich specimens with PP-H and PP-T20 core materials, which is still a satisfactory result. The deviation yields almost zero in case of sandwich specimens with PP-H foam cores, processed at melt temperatures of $T_m$ = 295 °C.

However, using PP-T20 as core material at equal processing temperature of $T_m$ = 295 °C, the predicted flexural rigidity is about 20 % higher than measured. Considering the profile of the core-skin thickness in Figure 100, it can be assumed that the high accuracy of flexural rigidity prediction for PP-H foam core sandwich structures of the 3-layer model at $T_m$ = 250 °C and $T_m$ = 270 °C compared to the 5-layer model results from the low core-skin thickness. The lower the core-skin thickness, the more the foam morphology resembles a homogenous foam without solid core-skins, which is assumed in the 3-layer model. The skin thickness of PP-H foam core sandwich specimens is

growing with rising melt temperature, consequently resulting in an underestimation of the flexural rigidity at $T_m$ = 295 °C using the 3-layer model. The 5-layer model by contrast almost exactly matches the experiments as it includes the core-skin thickness into the flexural rigidity calculation, see Equation 52. The reflection of the core-skin thickness in the calculation however, leads to an overestimation of flexural rigidity of PP-H specimens at $T_m$ = 250 °C and $T_m$ = 270 °C.

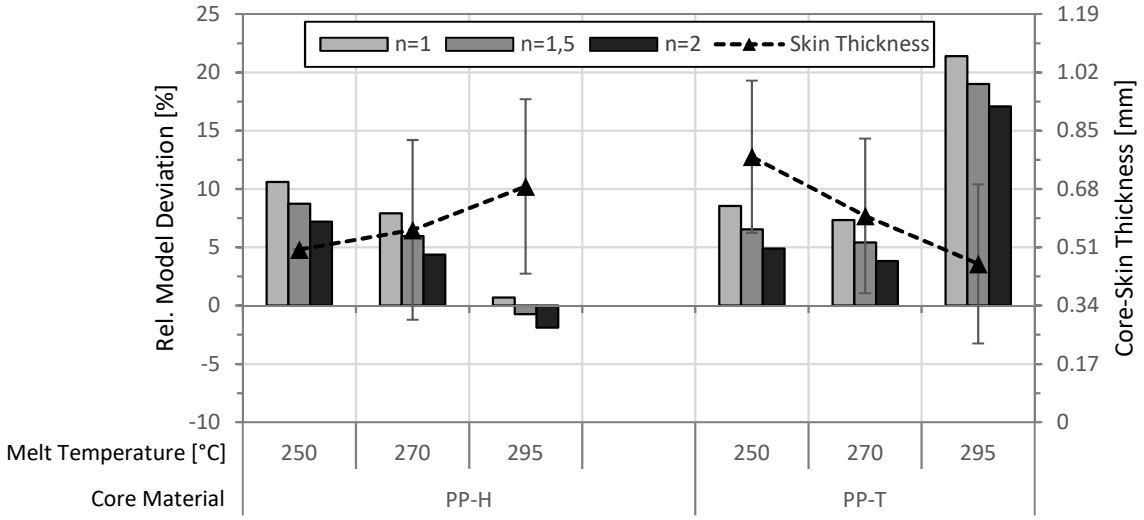


Figure 101: Comparison of model-based prediction of the flexural rigidity of in-situ CFRTP sandwich structures manufactured using CBA with experimentally assessed values: 5-layer model.

Similar results can be found with PP-T, but here the skin thickness decreases with increasing melt temperature. Despite the relatively high core-skin thickness of PP-T20 foam core sandwich specimens at $T_m$ = 250 °C and $T_m$ = 270 °C, the 3-layer model predicts the resulting flexural stiffness better than the 5-layer model, which overestimates the skin's influence on flexural rigidity. As the thickness of the core-skin decreases with rising PP-T20 melt temperature, the 3-layer model should characterise the flexural stiffness progressively well. However, at $T_m$ = 295 °C the 3-layer model overestimates the flexural stiffness, although a decrease in skin thickness would have eventually approximated a homogenous foam morphology which is represented in the 3-layer model.

It is assumed that the experimentally measured values of the flexural rigidity of in-situ CFRTP sandwich specimens with PP-T20 foam cores at high melt temperature, see Figure 85, are causative. There, the flexural rigidity decreases significantly compared to lower melt temperatures, both models thus overestimate the flexural rigidity. This experimentally determined significant drop of flexural stiffness at PP-T20 and $T_m$ = 295 °C is assumed to at least partially result from the foam morphology. In Figure 90 (right) µCT images of the specimen's foam morphology is presented. The in-situ sandwich structure based on CBA with PP-T20 foam core shows a relatively homogeneous cell size distribution over the test specimen thickness if melt temperatures of $T_m$ = 250 °C and $T_m$ = 270 °C are applied. At $T_m$ = 295 °C however, larger agglomerated cells develop at the transition of the foamed core to the solid core-skin, leading to a strong local density gradient. According to Shutov [194], this can lead to lower resulting mechanical properties of integral foams which correlates with the findings of this chapter.

Consequently, the 3-layer approach for the modelling of the flexural rigidity of in-situ sandwich structures is recommended, due to its prediction accuracy and simultaneous simplicity of application. The effect of the type of core-model on the resulting flexural rigidity of the in-situ sandwich structure however is likely to fade if the facesheet thickness increases. So far, the use of relatively thin facesheets was considered in this work and accordingly the flexural rigidity model. Nevertheless, other sandwich variants with higher relative facesheet thickness of course can be used. The contribution of the core to the total flexural rigidity of the in-situ sandwich structure depending on the relative facesheet thickness and the core material, see Figure 102, needs to be discussed.

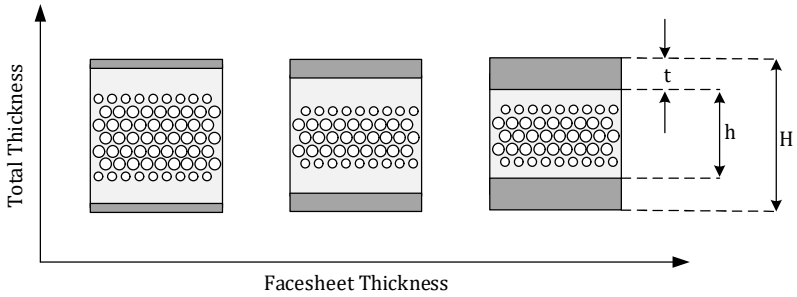


| Parameters | Value 1 | Value 2 | Value 3 | Value 4 | Value 5 | Value 6 | Dimension |
|---|---|---|---|---|---|---|---|
| Core Material | PP-H | PP-T20 | - | - | - | - | - |
| Blowing Agent | CBA | - | - | - | - | - | - |
| Facesheet Thickness h | 0.33 | 0.66 | 0.99 | 1.32 | 1.65 | 1.98 | mm |
| Total Thickness H | 10 | - | - | - | - | - | mm |
| Rel. Core Thickness h/H | 93.4 | 86.8 | 80.2 | 73.6 | 67 | 60.4 | % |

Figure 102: Design of experiment: variation of relative core thickness and core material

According to Figure 102, in-situ sandwich structures with fixed total thickness of 10 mm and varying thickness of UD tape facesheets are considered. In order to evaluate the effect of the flexural rigidity of the core in the total flexural rigidity of the in-situ sandwich structure with varying facesheet thickness, the ratio of both values is analysed. In Figure 103, it is presented in relationship of the relative core thickness $h/H$.

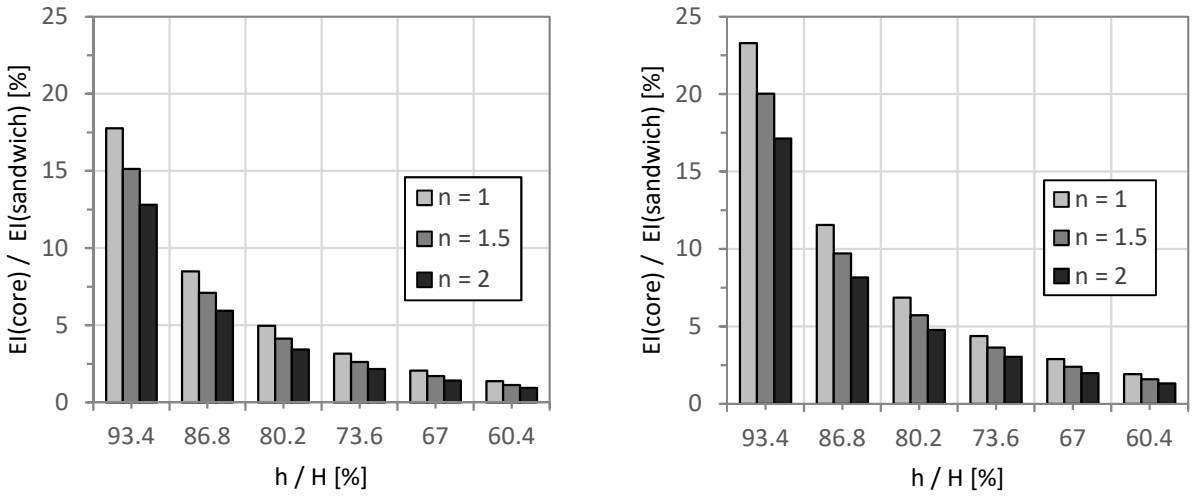


Figure 103: Relative flexural rigidity of the foam core $\mathrm{EI(core)}$ to the total flexural rigidity of the in-situ sandwich $\mathrm{EI(sandwich)}$ in relationship with the relative core thickness $\mathrm{h/H}$: an increasing facesheet thickness leads to a decrease of flexural rigidity contribution of the foam core using PP-H (left) and PP-T20 (right).

The comparison of Figure 103 left and right shows that the higher the Young's modulus of the core, the higher the contribution to the total flexural rigidity of the in-situ sandwich, which is easily comprehensive. The higher modulus of PP-T20 results in a higher relative flexural rigidity compared to PP-H, leading to 20 % compared to 15.1 %, both with $\mathrm{n}$ = 1.5.

Furthermore, it becomes evident, that the proper $\mathrm{n}$-value for the prediction of flexural rigidity of the in-situ sandwich structures is of decreasing importance with growing facesheet thickness, as the latter becomes the dominant component regarding the flexural stiffness of the whole sandwich structure. This also leads to the reduction of relative difference of flexural rigidity of the core using different $\mathrm{n}$-values. Nevertheless, especially when using thin facesheets the selection of a suitable $\mathrm{n}$-value and the contribution of the core to the total flexural rigidity must not be disregarded.

## 7.3. Discussion

A methodology for the prediction of interfacial bonding as well as flexural rigidity of in-situ CFRTP sandwich structures was presented. The model for the predictive characterisation of the interfacial bonding of UD tape facesheets and integral foam cores during the in-situ manufacture of CFRTP sandwich structures was developed based on a combined non-isothermal healing model by Bastien and Gillespie [146] and an interface temperature simulation based on Autodesk Moldflow Insight 2019. The simulation predicts the interface temperature development between UD tape facesheet and integral foam polymer core during the in-situ process. The simulation was validated based on experimental data by Trippel [132] showing very little deviation which is crucial considering the low reptation times of the UD tape polymer matrix.

The simulated interface temperature profile between UD tape facesheets and integral polymeric foam was used as input data for the non-isothermal healing model, thus enabling the prediction of the development of interfacial fracture toughness during the in-situ miniature of CFRTP sandwich structures. The interface temperature simulation showed that due to the high cooling rates, the major contribution to the development of interfacial bonding takes place within the first second, at which the hot polymer melt and the facesheet have their initial contact and the highest temperatures. At $T_m$ = 250 °C and $T_w$ = 55 °C the peak interface temperature does not reach the melt temperature of the facesheet polymer matrix, thus the degree of healing only yields $D_h$ = 0.24. An increase of melt temperature to $T_m$ = 270 °C and the accompanied increase of interface temperature leads to a full healing of the core-facesheet interface within only 0.6 s whereas a further rise of melt and interface temperature reduces the time to reach full healing to 0.36 s. Thus, according to the model and due to the high cooling rate during the in-situ process, it is essential to exceed the melting temperature of the facesheet polymer matrix, if sufficient healing shall be achieved. In case of the UD tapes used in this study, the time span at which the melting temperature needs to be exceeded only amounts to less than a second, considering the low reptation times, see Figure 93.

The model was subsequently used to quantitatively predict the interfacial fracture toughness of in-situ CFRTP sandwich structures. Therefore, reference $G_I$ values were determined based on CFRTP sandwich structures manufactured with the skin-core consolidation method based on a compression moulding process. The predicted degree of healing and the resulting predicted interfacial fracture toughness was compared to the experimental results.

The degree of healing qualitatively correlates well with the experimental $G_I$ values, despite an underestimation of bonding at $T_m$ = 250 °C. The quantitative prediction based on the reference $G_I$ values accordingly leads to an underestimation at $T_m$ = 250 °C. The significantly lower predicted values of $G_I$ at $T_m$ = 250 °C are attributed to minor undervaluation of the interface temperature simulation. The large difference of prediction and experiment results from the interface temperature, which is near the melting temperature of the facesheet. Due to the rapid change of reptation times of the PP matrix of several orders of magnitude just below the melting temperature, a minor underestimation of the interface temperature leads to a major underestimation of the corresponding reptation time. This results in the calculation of a distinctly lower degree of interfacial healing and hence interfacial fracture toughness.

Consequently, if the interface temperature simulation predicts peak values near the melting temperature of the CFRTP matrix polymer, it must be considered that the interfacial bonding prediction can be subject to large deviations from the actual experimental values due to possible simulation inaccuracies of a few degrees Celsius. Furthermore, if the simulation is used for the pre-design of an in-situ CFRTP sandwich component and the simulated interfacial temperature is near the melting temperature, it is recommended to adapt the process parameters and possibly the mould design as well in order to enable temperatures at the entire facesheet-core interface sufficiently above the melting temperature of the facesheet.

The quantitative model overestimation of interfacial fracture toughness at intermediate to high melt temperatures is attributed to the reference $G_I$ values and the respective process used for the manufacture of the reference specimens. The complete melting of UD tape facesheets as well as the core during the compression moulding skin-core consolidation of sandwich structures is presumed to lead to an increased intimate contact development. In combination with much higher interface temperatures of 217 °C and process times of one order of magnitude higher than for the in-situ manufacture of CFRTP sandwich specimens, this results in improved bonding according to Equation 22. In accordance with the results of chapter 5, the in-situ process based on low-pressure foam injection moulding does not yield complete intimate contact. The short process time accompanied by low cavity pressures is assumed insufficient to completely flatten the asperities of the UD tape facesheets and to create full intimate contact despite the findings and assumptions of other authors [14, 159, 163]. It is hence inferred. that although full healing is achieved, the imperfect intimate contact thus leads to a reduced interfacial bonding, which is compliant with Plummer et al. [139] and Shi et al. [300]. The use of the healing model to predict the bonding behaviour hence leads to deviations of the experimental results, as the intimate contact development is not considered in the model.

Combined fusion bonding models taking into account the intimate contact development are assumed to better correlate with the interfacial bonding results using the low-pressure foam injection moulding variant [143, 167]. However, these combined bonding models additionally require the pressure profile during manufacture. Hence, a simulation-based methodology for the predictive characterisation of the degree of bonding would require a validated cavity pressure simulation. An alternative promising approach would be the use of the high-pressure foam injection moulding variant in order to result in higher pressures during the in-situ manufacture of CFRTP sandwich structures. In this case, the assumption of the immediate intimate contact during the in-situ manufacture is more accurate. This is inferred to lead to an alignment of the interfacial fracture toughness prediction of the present healing model and a combined bonding model, yet with clear

advantages of the present model as an integrated and validated cavity pressure simulation can be spared which would be necessary for a combined bonding simulation.

In order to predict the flexural rigidity of in-situ CFRTP sandwich structures, different models were compared to experimental data of four-point bending test results. The models consider the integral foam core to be either fully homogenous without solid core-skin (3-layer model) or to consist of a homogenous foamed core with solid core-skins (5-layer model). The homogenised foamed core in both cases was modeled based on Equation 29 taking into account the void fraction and varying the exponent $n$ in order to adapt to the experimental results. The 5-layer model additionally required the core-skin thickness to be assessed prior to the calculation of the flexural rigidity.

Results showed that the 3-layer model with an n-value of $n$ = 1.5 yields highest correlations with experimental 4PB data. At the highest melt temperature however, the model accuracy deteriorates, especially with PP-T20 as core material. The 5-layer model yields best results with $n$ = 2. Its accuracy increases with growing core-skin thickness using PP-H, however it yields high overestimations of the flexural rigidity at high melt temperatures for PP-T20 based foam core sandwich specimens similar as the 3-layer model. It is assumed that this is due to the distinct decrease of absolute flexural rigidity which is attributed to the high local density gradient at the transition of foam core to solid skins which according to Shutov [194] leads to reduced mechanical properties. Consequently, the 3-layer model with $n$ = 1.5 is strongly recommended for modelling the flexural behaviour of in-situ CFRTP sandwich structures.

The flexural rigidity of sandwich structures is often dominated by the facesheets, hence simplified calculations neglect the contribution of the core to the total flexural rigidity of the sandwich [37]. In case of the in-situ sandwich process studied in this work, the use of very thin facesheets is generally envisaged and evaluated until now. However, the use of different layups and facesheet thicknesses may be necessary due to imposed mechanical requirements. Hence, effect of the flexural rigidity of the core on the total flexural rigidity of in-situ sandwich structures with varying facesheet thickness was evaluated.

Results show, that in a sandwich structure of 10 mm total thickness and a facesheet thickness of 0.33 mm the integral foam core based on PP-H exhibits a flexural rigidity of 17.7 to 12.8 % of the total flexural rigidity of the in-situ sandwich, depending on the n-value. Sandwich cores based on PP-T20 yield higher values between 23.3 and 17.12 %, resulting from the higher elastic moduli compared to PP-H. This significant fraction however rapidly drops to 5 %, if the facesheet thickness increases to 0.99 mm. Hence, if very thin facesheets are used in an in-situ sandwich structure, the contribution of the integral foam core to the total flexural rigidity cannot be ignored in the calculations. This demonstrates the necessity of the developed models in this work.

# 8. Pre-Design of In-Situ CFRTP Sandwich Structures in Engineering Practice

The last chapter of this work shall demonstrate the applicability of the developed models of chapter 7 on the pre-design of a new in-situ CFRTP sandwich component, see Figure 104. For this purpose, the pre-design is exemplarily conducted aiming at the substitution of a simplified reference component.

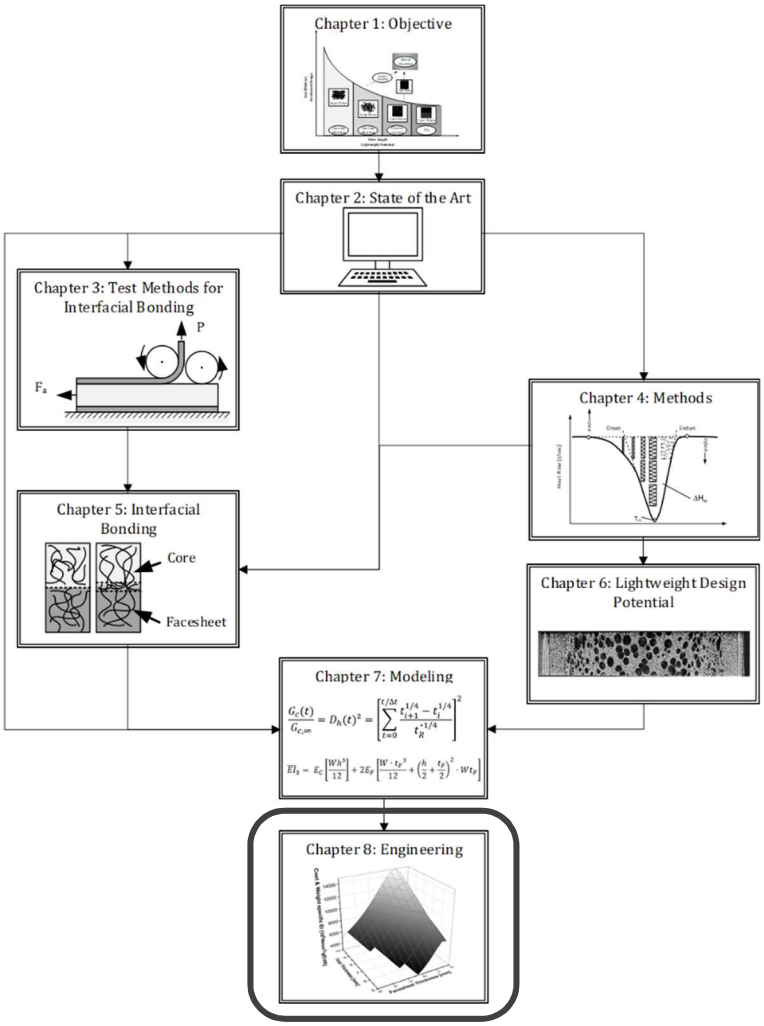


Figure 104: Systematic approach of this work: chapter 8 makes use of the developed models in chapter 7 and shall demonstrate their contribution to the pre-design of new in-situ CFTP sandwich components.

The procedure of the pre-design is schematically depicted in Figure 105. It consists of four steps:

1. Definition of requirements
2. Collecting input data
3. Optimisation of lightweight design
4. Ensuring interfacial bonding

At first, requirements must be defined that serve as constraints for the lightweight design optimisation of in-situ structures. These requirements not only include mechanical and geometrical but also cost-related targets that need to be met by the new component.

After the definition of requirements, input data is needed for the assessment of the flexural rigidity and of the interfacial bonding respectively in the last step of the procedure. The input data includes specific properties of the materials e.g. moduli and the reptation time. Using the input data, an optimisation of the in-situ component is conducted based on the variation of materials and sandwich construction. As a result, optimum in-situ sandwich structures can be determined with respect to the defined requirements and optimisation targets.

The last step of the pre-design procedure sets its focus on the interfacial bonding between CFRTP facesheet and injected foam core of in-situ CFRTP sandwich structures. For the manufacture of the latter, suitable process parameters leading to proper bonding between facesheet and core shall be determined using the interfacial bonding model. Therefore, the latter is fed with material and structural properties of the in-situ sandwich, which resulted from the lightweight design optimisation. If the predicted degree of healing deceeds a predefined lower limit, the process parameters are varied until the interfacial bonding of CFRTP facesheet and injected foam core can be ensured.

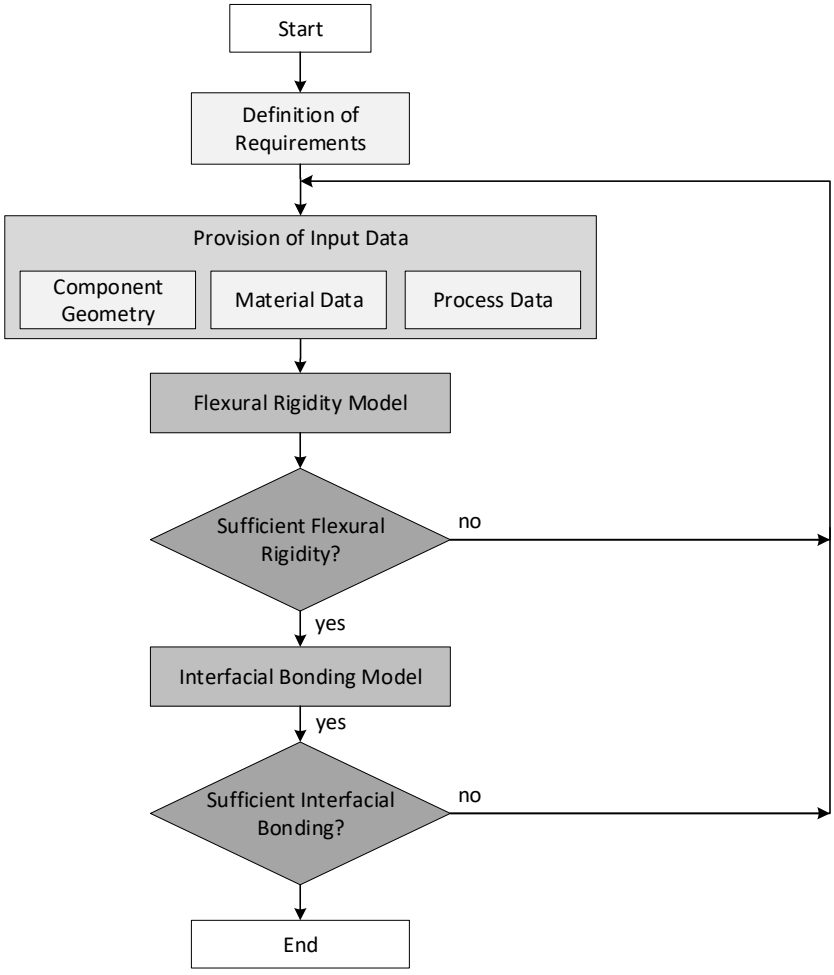


Figure 105: Schematic illustration of the predictive characterisation of in-situ CFRTP sandwich structures: the approach includes a flexural and an interfacial bonding model: application at the pre-design of an in-situ CFRTP sandwich component.

In the following, the targeted use of the developed models in engineering practice is demonstrated.

## 8.1. Definition of Requirements

The first step of the pre-design procedure is the definition of specifications and requirements, see Figure 105. The requirements and boundary conditions for the optimisation of in-situ CFRTP sandwich structures are defined by the reference component. This reference component is a steel beam with a total thickness of $H$ = 4 mm, a total length of $L$ = 220 mm and a total width of $W$ = 30 mm, see Figure 106.

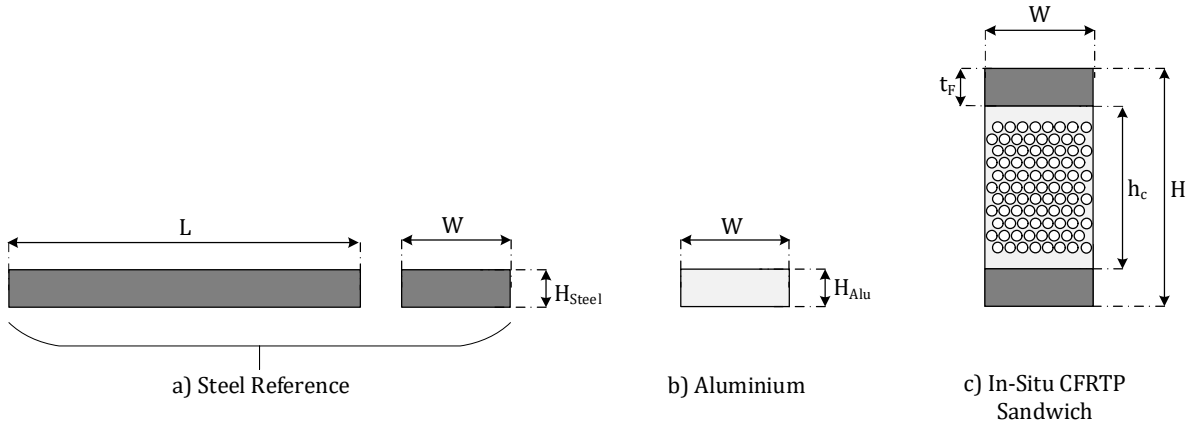


Figure 106: Schematic illustration of the compared structure variants: a steel reference (a) shall be substituted using specifically optimised in-situ CFRTP sandwich structures (c) using the models developed in this work. In addition, aluminium is also evaluated (b).

The requirements for the substitution variants are defined as follows:

- Mechanical:
  - The flexural rigidity of the reference steel beam must be achieved
- Geometrical:
  - The length and width equals the reference steel beam
  - The total thickness is limited between 5 < H < 10 mm

Based on these requirements, the flexural rigidity model shall lead to the maximum cost-efficient lightweight design. That means that with a minimum of in-situ sandwich component weight and material cost, the targeted flexural rigidity shall be reached. In addition to the in-situ CFRTP sandwich, also an aluminium variant will be part of the study since this material is frequently used for automotive lightweight design components.

## 8.2. Provision of Input Data

The collection of input data is the second step of the procedure, see Figure 105. The flexural rigidity model for in-situ sandwich components requires mechanical specifications of the core and facesheet materials as well as information about the sandwich geometry. The latter is limited due to imposed geometrical requirements, hence the geometry denotes the boundary condition for the optimisation of lightweight design.

### 8.2.1. Geometric Properties

The optimisation procedure results in the optimum combination of core thickness $h$, facesheet thickness $t_F$ and total sandwich thickness $H$ for the given optimisation target and boundary condition. In this case, the target is an optimum weight specific flexural rigidity and in addition, an optimum cost-efficient lightweight design. The boundary condition of the optimisation is imposed by a limitation of the sandwich total thickness between $5 < H < 10$ mm. Within this constraint, the facesheet thickness as well as the core thickness are variable, see Figure 107.

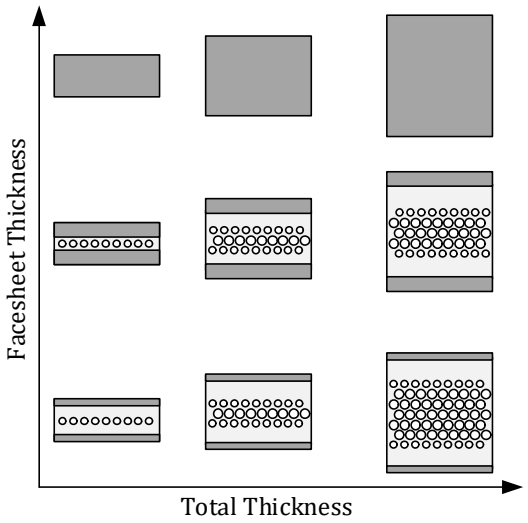


| | Total | Facesheet | | | | Dimension |
|---|---|---|---|---|---|---|
| Fibre | - | GF | GF | CF | CF | - |
| Layup | - | UD | CC | UD | CC | - |
| Thickness min. | 5 | 0.33 | 1.32 | 0.15 | 0.6 | mm |
| Thickness max. | 10 | 4.95 | 3.96 | 4.95 | 4.8 | mm |

Figure 107: Schematical illustration of the DoE and sandwich variants with varying facesheet and total thickness (left). Overview of the material variants and optimisation limits (right).

The minimum thickness of facesheets with UD layup results from the initial as-received thickness of the UD tapes. In addition to unidirectional facesheets, this optimisation also includes symmetrical cross-ply composite (CC) layups consisting of a stack of four UD layers as depicted in Figure 108.

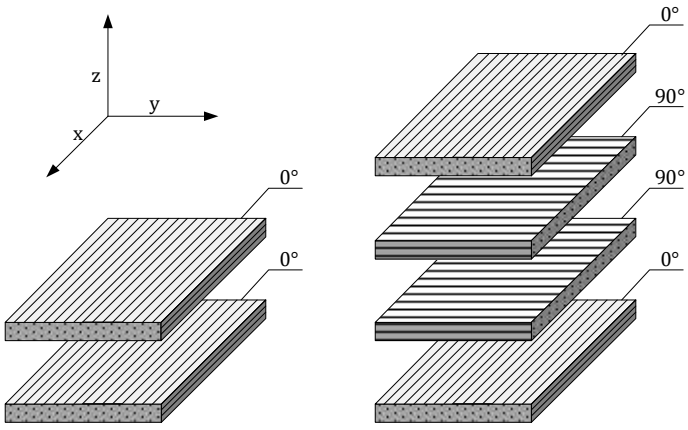


Figure 108: Schematic illustration of a unidirectional layup (left) and a symmetrical cross composite layup (right) [8].

A symmetric layup is chosen since an asymmetric stacking sequence may lead to coupling effects which are generally to be avoided [8]. The CC layup accounts for the majority of applications that

require more than one fibre orientation due to operating loads that lead to a heterogeneous stress field.

The minimum thickness of CC layups equates to four times the initial tape thickness resulting from the layup, as it is predefined that always the same number of layers are oriented in 0° and 90° direction. Of course, other layups are possible, however these shall not be considered here for the sake of simplicity and the general demonstration of the pre-design procedure of in-situ sandwich components. The maximum facesheet thickness for both UD and CC layups results from the largest number of UD layers that can be stacked to the respective layup. The theoretical maximum facesheet thickness is only limited by the boundary condition regarding the total thickness of the sandwich structure, i.e. $H$ = 10 mm. The maximum facesheet thickness within a given sandwich thickness hereby approximates a pure composite laminate without foamed core, see the top row in Figure 107 (left).

### 8.2.2. Material Properties

In Table 18, the materials and their specifications are presented. The core material is a PP-H (Sabic® PP 576P), since this leads to highest weight specific flexural rigidity based on the experimental results of chapter 6. The resulting Young's modulus of the core is calculated according to Equation 51 using an $n$-value of $n$ = 1.5. The sandwich structure was modelled using the 3-layer model, see Equation 47, since this led to the highest prediction accuracy according to chapter 7.2.

Table 18: Overview of material parameters of the UD tape sandwich facesheet and the polymer core (*data based on literature [8, 287, 301, 302], **data based on the expected commercial cost at large scale production).

| | | Core Polymer CBA | | Facesheets | | Dimension |
|---|---|---|---|---|---|---|
| Material | Trade Name | Sabic® PP 576P | Hydrocerol® ITP 822 | Celstran® CFR-TP PP GF60-13 | TAFNEX™ CF/PP | - |
| | Cost | 1.44 | 13 | 8 | 20** | €/kg |
| | Density Solid | 0.905 | 1 | 1.55 | 1.31 | g/cm³ |
| | Density Reduction | 33 | - | - | - | % |
| | Tensile Modulus Solid | 1850 | - | 25600 | 120000 | N/mm² |
| | Tensile Modulus Foam | 1258 | - | - | - | N/mm² |
| Polymer | Tensile Modulus $E_x$ | 1850 | - | 1600* | 1600 | N/mm² |
| | Poisson Ratio $\nu_{yx}$ | 0.4* | - | 0.4* | 0.4 | - |
| Fibre | Type | - | - | GF | CF | - |
| | Content | - | - | 34 | 50 | vol.-% |
| | Structure | - | - | UD | UD | - |
| | Longitudinal Tensile Modulus $E_{f,II}$ | - | - | 73000* | 240000 | N/mm² |
| | Transversal Tensile Modulus $E_{f,\perp}$ | - | - | 73000* | 28000 | N/mm² |
| | Poisson's Ratio $\nu_{f,xy}$ | - | - | 0.23* | 0.22 | - |

In this study, it is assumed that the optimised in-situ sandwich is manufactured using the low-pressure foam injection moulding variant using CBA. A density reduction of $\Delta\rho$ = 33 % is therefore assumed as this is the mean density reduction achieved in the experimental studies in this work using CBA and PP-H as core material, see Figure 90. The facesheet materials include a UD tape consisting of 34 vol.-% glass fibre reinforced polypropylene (Celstran® CFR-TP PP GF60-13), compliant with the

material used in the previous chapters, and a 50 vol.-% carbon fibre reinforced polypropylene (TAFNEX™ CF/PP) which became available in the end of the present work.

## 8.3. Lightweight Design Optimisation of in-Situ Sandwich Structures

In the next step of the procedure, the material properties are applied at the optimisation of lightweight design of in-situ CFRTP sandwich structures, see Figure 105 using the flexural rigidity model developed in this work. The model with varying foam core properties based on Equation 47 is enhanced with varying facesheet materials, thicknesses and layups. This is achieved by the introduction of the Classical Laminate Theory (CLT) for the assessment of resulting facesheet moduli $E_{F,i}$ depending on the layup. Combining the CLT with the 3-layer model leads to the flexural rigidity assessment of in-situ CFRTP sandwich structures with varying facesheet layup as

$$\overline{EI}_3 = E_{C,3}\left[\frac{Wh^3}{12}\right] + 2E_{F,i}\left[\frac{W \cdot {t_F}^3}{12} + \left(\frac{h}{2} + \frac{t_F}{2}\right)^2 W t_F\right]. \tag{57}$$

The tensile modulus of facesheets with unidirectional layup correspond to the tensile modulus of the respective UD tapes. In contrast, the elastic modulus of facesheets with CC layups $E_{F,CC}$ needs to be determined via the CLT using the facesheet material properties in Table 18. If the specific layers exhibit the same thickness $t_i$ and the same fibre volume fraction $\varphi$, the elastic modulus in lateral x- and transversal y-direction as well as the Poisson's ratios are equal [8], yielding

$$E_{F,CC} = E_x = E_y \tag{58}$$

and

$$\nu_{xy} = \nu_{yx}. \tag{59}$$

The Poisson's ratio $\nu_{xy}$ can be calculated using the Poisson's ratios of the reinforcing fibres $\nu_{f,xy}$ and of the polymer matrix $\nu_m$ [8] as

$$\nu_{xy} = \varphi\, \nu_{f,xy} + (1 - \varphi)\nu_m. \tag{60}$$

The elastic modulus $E_x$ can then be approximated with the elastic moduli of the UD tapes $E_0$ and $E_{90}$ in 0° and 90° direction respectively as well as the total thickness of the specific UD tape layers $t_0$ and $t_{90}$ and the total layup thickness $t_F$ [8, 303] via

$$E_x \cong E_0 \frac{t_0}{t_F} + E_{90} \frac{t_{90}}{t_F}. \tag{61}$$

The modulus $E_0$ corresponds to the tensile modulus of the respective UD tape material and can be found in the material datasheets. According to Puck [304] the transverse tensile modulus $E_{90}$ of a layer with unidirectional fibre orientation can be calculated using a semi-empirical approach as

$$E_{90} = \frac{E_m}{1-\nu_m^2} \cdot \frac{1+0.85\varphi^2}{(1-\varphi)^{1.25} + \frac{E_m}{(1-\nu_m^2)E_{f\perp}}\varphi}. \tag{62}$$

The tensile moduli of facesheets with different layups and materials for the present in-situ CFRTP sandwich optimisation are consequently assessed by Equation 61. The results are presented in Table 19. In addition, the properties of the steel reference as well as those of aluminium are included.

Table 19: Material parameters [305–308] (*data based on the expected commercial cost at large scale production).

| | | Reference | Variant 1 | Variant 2 | Variant 3 | Variant 4 | Variant 5 | Dimension |
|---|---|---|---|---|---|---|---|---|
| Metal | Material | Steel | Aluminium | - | - | - | - | - |
| | Tensile Modulus | 210000 | 73000 | - | - | - | - | $N/mm^2$ |
| Facesheet | Material | - | - | GF-PP | GF-PP | CF-PP | CF-PP | - |
| | Layup | - | - | CC | UD | CC | UD | - |
| | Tensile Modulus $E_x$ | | | 14799 | 25600 | 62904 | 120000 | $N/mm^2$ |
| | Material Cost | 1.75 | 4 | 8 | 8 | 20* | 20* | €/kg |
| | Density | 7.85 | 2.7 | 1.55 | 1.55 | 1.31 | 1.31 | $g/cm^3$ |

The assessed tensile moduli of the respective facesheet material and layup variant are subsequently introduced in Equation 57. By doing so, the flexural rigidity of in-situ sandwich structures with varying facesheets and compositions can be determined. The results are discussed in the following.

### 8.3.1. Optimisation Overview

In Figure 109, the weight specific flexural rigidity of in-situ CFRTP sandwich structures with PP-H integral foam core and glass fibre reinforced polypropylene (GF-PP) facesheets is presented as flexural rigidity related to the calculated specimen density. The focus is set on the relationship between different facesheet layups, facesheet thicknesses as well as total specimen thicknesses on the flexural rigidity of the in-situ CFRTP sandwich structure. In Figure 109 (left) the sandwich specimens exhibit GF-PP facesheets with unidirectional layup $(0)_n$ whereas in Figure 109 (right) a symmetric cross composite layup $(0/90)_{s,n}$ is applied.

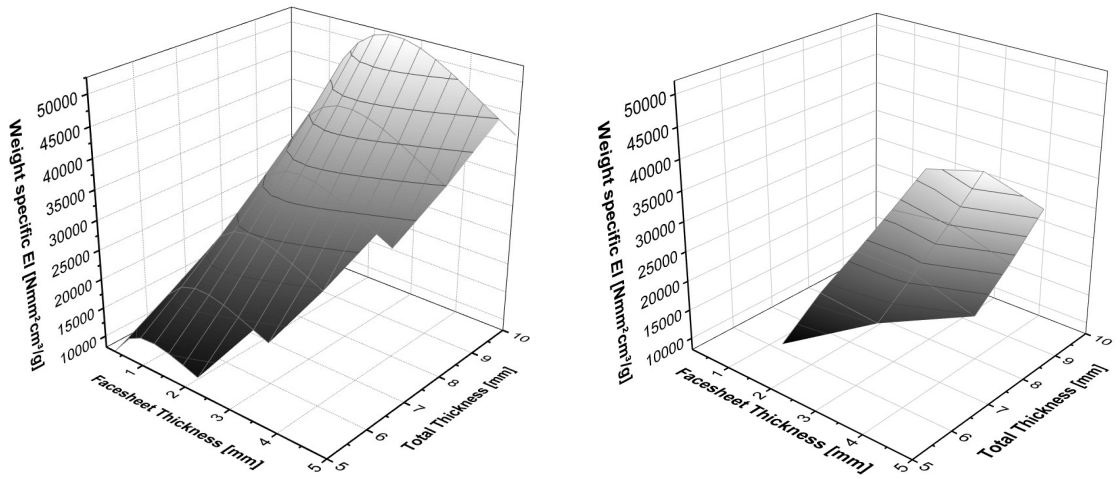


Figure 109: Weight specific flexural rigidity of in-situ CFRTP sandwich structures dependent on CFRTP facesheet thickness and total sandwich thickness: unidirectional GF-PP facesheets (left), cross-ply composite GF-PP facesheets (right).

Both facesheets layup variants yield an increasing specific flexural rigidity with growing total thickness of the sandwich components, yet also depending on the facesheet thickness. Sandwich structures using a unidirectional layup reach the highest specific flexural rigidity with a total component thickness of $H$ = 10 mm and a facesheet thickness between 2 < $t_F$ <3 mm, see Figure 109 (left). The maximum is reached at $t_F$ = 2.31 mm which corresponds to seven UD tape layers. Similarly, in-situ sandwich structures with cross-ply composite layup facesheets reach their optimum at $H$ = 10 mm and $t_F$ = 2.64 mm, which is equivalent to eight layers.

A comparison between sandwich specimens with facesheets based on a UD and CC layup clearly shows that the significantly higher tensile modulus of UD layups directly translates into the flexural rigidity of the structure. This emphasises that a stress-equivalent layup and fibre orientation of in-situ CFRTP sandwich structures always need to be considered in order to yield best mechanical results.

If the material cost is included in the optimisation, different structure combinations yield optimum values, see Figure 110. In-situ sandwich components with UD facesheets reach their maximum with facesheet thicknesses of $t_F$ = 0.99 mm whereas sandwich structures with CC facesheet layup exhibit a peak at $t_F$ = 1.32 mm, see Figure 110. These facesheet thicknesses are lower compared to the results from the optimisation with pure focus on weight specific flexural rigidity in Figure 109. This is caused by the higher material cost of the facesheets compared to the core, which ultimately leads to optima using less CFRTP material, and hence thinner facesheets. In addition, the gradient around the peak values is relatively high compared to the results for pure lightweight design. Consequently, the choice of cost-efficient structural variants is smaller and deviations from the optimum combination of total and facesheet thickness rapidly lead to a decrease of cost-efficient lightweight design.

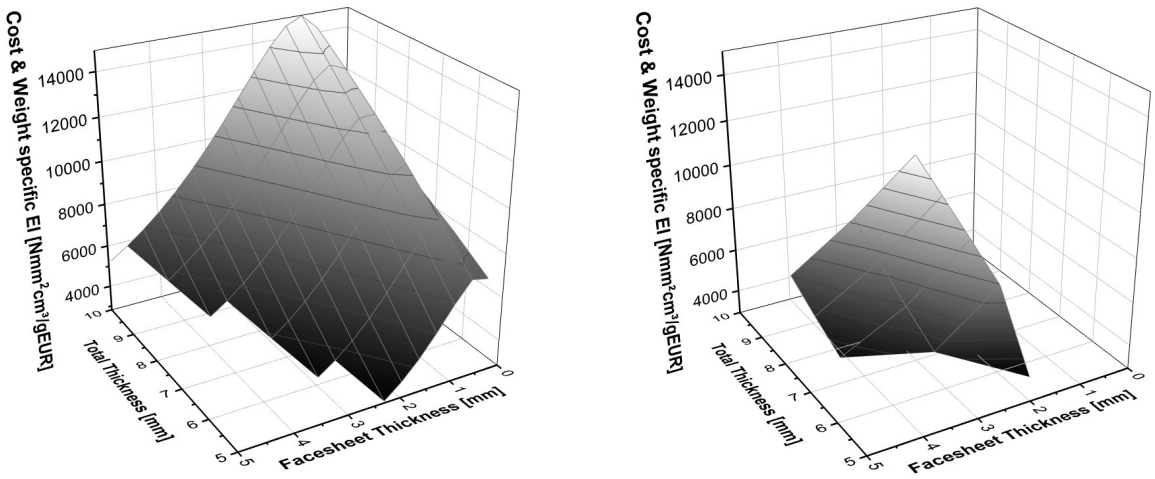


Figure 110: Cost and weight specific flexural rigidity of in-situ CFRTP sandwich structures dependent on CFRTP facesheet thickness and total sandwich thickness: unidirectional GF-PP facesheets (left), cross-ply composite GF-PP facesheets (right).

In Figure 111, the results of the flexural rigidity assessment of in-situ sandwich structures with carbon fibre reinforced polypropylene (CF-PP) facesheets are depicted. If carbon fibre reinforced facesheets are used, in-situ sandwich structures yield significantly higher weight specific flexural rigidity values compared to those with glass fibre based facesheets.

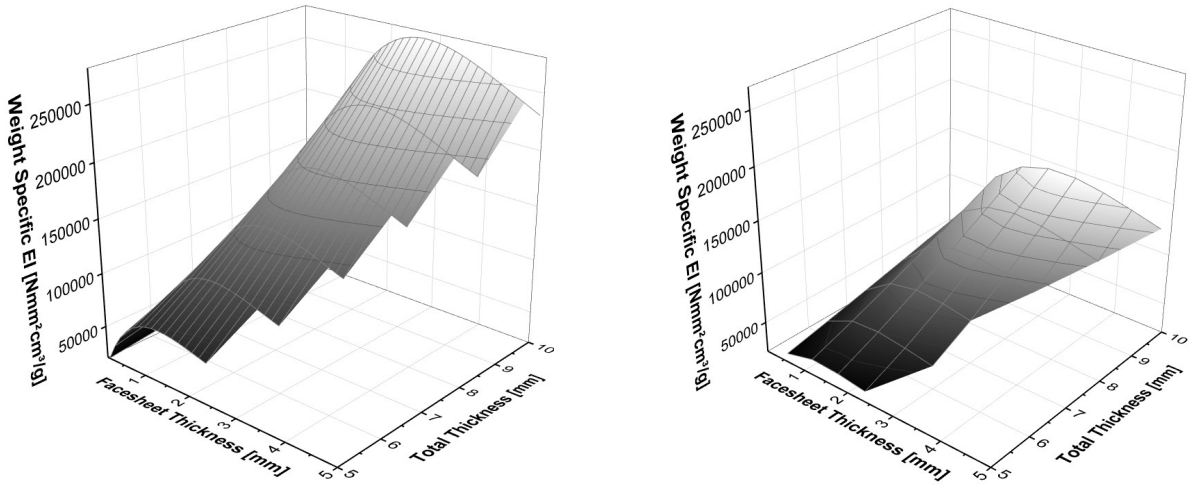


Figure 111: Weight specific flexural rigidity of in-situ CFRTP sandwich structures dependent on CFRTP facesheet thickness and total sandwich thickness: unidirectional CF-PP facesheets (left), cross-ply composite CF-PP facesheets (right).

This result can clearly be attributed to the combination of a distinctly higher elastic modulus and a lower density of the CF-PP tapes, see Table 19. Since the flexural rigidity depends linearly on the elastic modulus of the facesheet, see Equation 57, an enhancement of the latter almost equally enhances the flexural rigidity of the in-situ sandwich structure. Accordingly, the lower values found for in-situ sandwich structures with CF-PP based cross composite facesheets compared to those with unidirectional fibre orientation can be explained. The highest weight specific flexural rigidity is found using a facesheet thicknesses of $t_F$ = 2.64 mm in case of a UD layup and $t_F$ = 2.31 mm when cross composite layups are applied.

Introducing the related material cost leads to a superior cost-efficient flexural rigidity of sandwich structures with CF-PP facesheets and UD layup compared to a CC layup. Moreover, compared to GF-PP facesheets the results are evenly improved. With respect to the resulting facesheet thickness, similar qualitative results are found when compared to sandwich structures with glass fibre reinforced facesheets. The introduction of the respective material cost shifts the optimum values towards a smaller usage of facesheet material and hence thinner facesheets, see Figure 112.

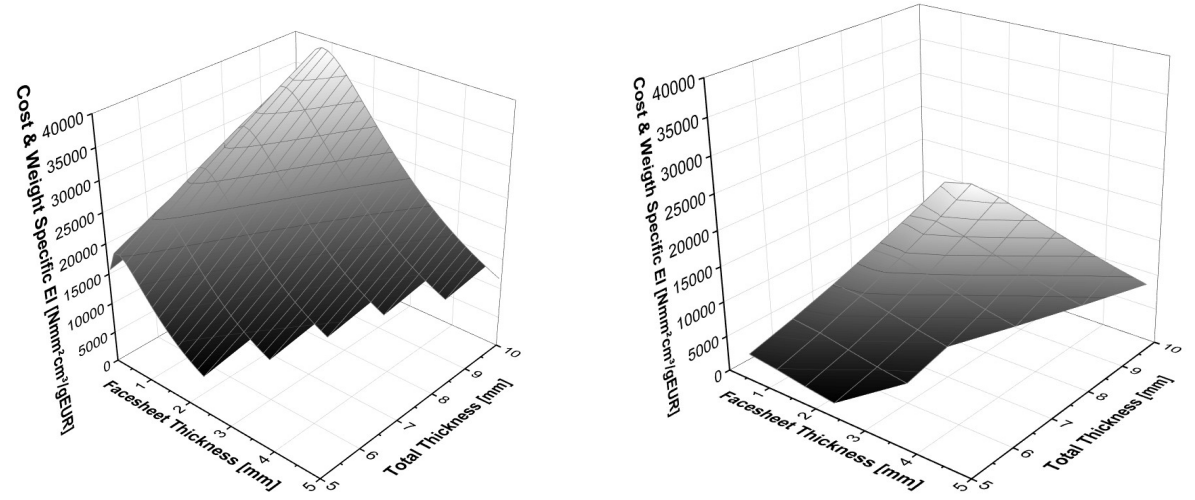


Figure 112: Cost and weight specific flexural rigidity of in-situ CFRTP sandwich structures dependent on CFRTP facesheet thickness and total sandwich thickness: unidirectional CF-PP facesheets (left), cross-ply composite CF-PP facesheets (right).

In contrast to the results in Figure 111, a facesheet thickness of $t_F$ = 0.75 mm leads to the best cost-related results in case of a UD layup and $t_F$ = 1.2 mm if the sandwich structure facesheet exhibits a cross composite layup.

Consequently, significant differences can be found depending on the optimisation target. If pure lightweight design is envisaged, different in-situ CFRTP sandwich structures will result as optimum as if the associated material cost is also considered. Furthermore, the comparison of results of sandwich structures with different facesheet materials demonstrates the potential of carbon fibre reinforced facesheets with respect to lightweight design and cost efficiency.

### 8.3.2. Optimisation Results

Based on the optimisation of in-situ CFRTP sandwich structures demonstrated in chapter 8.3.1, the optimum variants of in-situ CFRTP sandwich structures with glass and carbon fibre reinforced facesheets are determined that meet the required flexural rigidity of the reference steel beam according to chapter 8.1. The sandwich variants are compared with the reference steel sheet and the aluminium variant with respect to the component thickness, mass and cost as well as the resulting weight specific flexural rigidity, see Figure 113. The last two parameters hence reflect the cost efficiency as well as the lightweight design of the substitution variant. The results are normalised with respect to the referenced steel component.

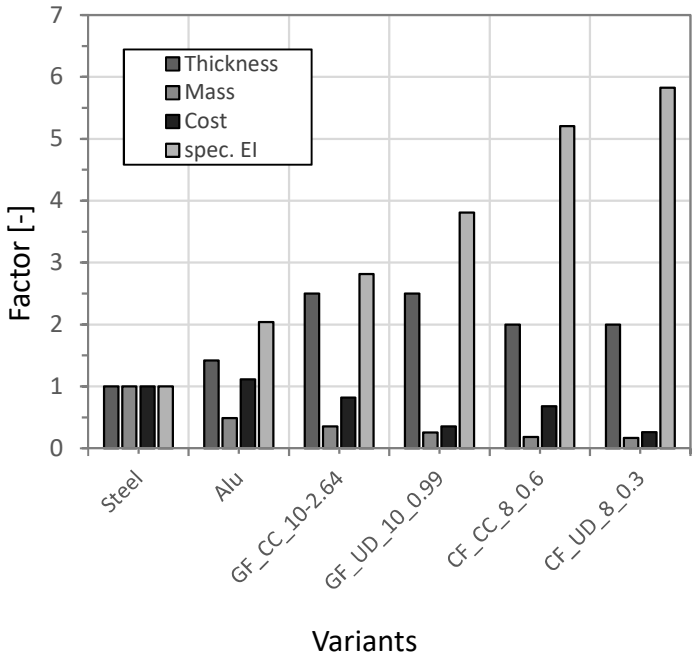


Figure 113: Comparison of the thickness, mass, component material cost and weight specific flexural rigidity of a reference steel sheet with substituting materials and structures: glass and carbon fibre reinforced in-situ CFRTP sandwich structures yield high weight specific flexural rigidity and simultaneously reduce the component cost.

Aluminium as well as the in-situ CFRTP sandwich components require a higher component thickness in order to reach the targeted flexural rigidity of the steel sheet, hence compensating for their lower elastic moduli, see Table 19. However, the component mass can be drastically reduced. The

aluminium structure mass only amounts to 48.8 % of the steel reference. Compared to the latter, CFRTP sandwich structures even exhibit only 35.2 % of the reference mass in case of glass fibre reinforced facesheets with cross-ply composite layup (GF-CC) facesheets and 25.5 % if unidirectional glass fibre reinforced facesheets are used (GF-UD). Even higher mass reductions are achieved if carbon fibre reinforced facesheets are used, leading to a relative component mass of 18.3 % and 17 % with cross-ply composite (CF-CC) and unidirectional facesheets (CF-UD), respectively.

The decrease of component mass directly translates to the weight specific flexural rigidity, which is clearly superior compared to the reference steel structure as well as compared to aluminium. In-situ sandwich components with GF-PP facesheets yield 181.8 % and 280.7 % higher weight specific flexural rigidity values compared to the steel reference. In accordance with the drastic mass reduction of carbon fibre based in-situ sandwich structures, the latter yield the highest growth of weight specific flexural rigidity reaching 420.4 % and 482.9 % using a cross-ply composite and unidirectional layup, respectively.

Hence, in-situ CFRTP sandwich structures show promising properties when it comes to lightweight design, especially using carbon fibre based facesheets. Yet, the use of carbon fibre reinforced plastic materials in cost-sensitive applications such as mass volume markets is often hindered by their material cost. The material cost per component however, based on the data in Table 19, is also reduced compared to the steel beam. The component cost reductions of in-situ CFRTP sandwich structures amount to 17.9 % and 64.73 % in case of GF-PP facesheets and 31.8 % to 73.76 % with CF-PP facesheets, despite the distinctly higher material cost of CF-PP UD tapes. The reason for the component cost reduction of in-situ sandwich structures is the efficient application of CFRTP material according to the bending induced stress field. Because of this economic application of CFRTP material, glass and carbon fibre reinforced facesheets can be applied in sandwich structures yielding very high weight specific flexural properties and cost efficiency simultaneously. The theoretically assessed values of in-situ CFRTP sandwich structures with CF-PP facesheets in Figure 113 however require experimental validation. Preliminary manufacturability tests yet confirmed that the manufacture of in-situ sandwich structures with carbon fibre reinforced UD tape facesheets is feasible using similar processing parameters as with facesheets based on glass fibres.

## 8.4. Interfacial Bonding Model

The fourth and last step in the pre-design phase is the interfacial bonding evaluation, based on the sandwich composition resulting from the flexural model, see Figure 105.

For this purpose, the degree of healing is predicted in accordance with the procedure in chapter 7.1. Since in this work the interfacial bonding model was validated with experimental values of glass fibre reinforced polypropylene facesheets, the transfer of these results to carbon fibre based facesheets is questionable. For this reason, the interfacial bonding model is only applied to the optimum in-situ CFRTP sandwich variant with GF-PP facesheets, which is the combination of unidirectional PP-GF60 facesheet layup with a thickness of $t_F$ = 0.99 mm and a total sandwich thickness of $H$ = 10 mm, see Figure 113.

The results from chapter 7.1 are applied in this procedure, hence proper interfacial bonding is achieved if the degree of healing is sufficiently above $D_h$ = 1. In this work, a margin of safety is introduced, hence a value of $D_h$ = 1.5 must be exceeded in order to ensure sufficient bonding. If this

is achieved, the respective process parameter combination can be accepted and used for the manufacture of in-situ CFRTP sandwich specimens. If the required degree of healing is not achieved, an iterative loop starts with an adjustment of process parameters, which then serve as new input for the interfacial bonding model, see Figure 105.

In Figure 114, the results of different process parameters and respective degree of healing are presented. According to the interfacial bonding model, the in-situ sandwich variant with $t_F$ = 0.99 mm and $H$ = 10 mm yields sufficient interfacial bonding if a melt temperature of $T_m$ = 270°C and a minimum mould temperature of $T_w$ = 55°C is applied. Below this process temperature combination interfacial bonding cannot be ensured according to the defined minimum required degree of healing, indicated by the dotted line in Figure 114. Above this process temperature combination, the degree of healing distinctly surpasses the degree of healing including safety margin of $D_h$ = 1.5. Hence, these process parameters can be safely applied for the manufacture of the optimised in-situ CFRTP sandwich component with proper interfacial bonding between facesheet and core.

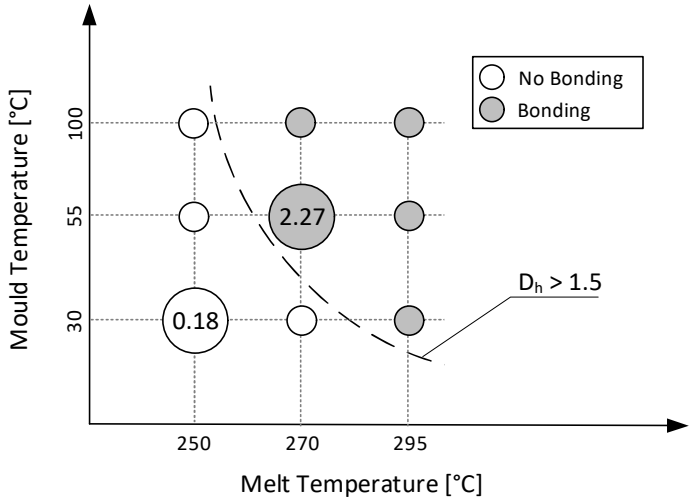


| Mould \ Melt | 250 | 270 | 295 |
|---|---|---|---|
| 100 | *0.83* | *4.53* | *5.16* |
| 55 | *0.28* | *2.27* | *3.1* |
| 30 | *0.18* | *0.22* | *2.13* |

Figure 114: Results of the interfacial bonding model applied for the evaluation of suitable process parameters for the in-situ sandwich variant, which was found most promising based on the previous flexural rigidity assessment. Process temperature combinations below the dotted line lead to insufficient bonding (left). In this evaluation the resulting degree of healing (right) is not limited to $D_h$ = 1 since it needs to exceed the defined margin of safety of 1.5. Consequently, the resulting degree of healing to safely ensure sufficient interfacial bonding is $D_h$ = 1.5.

In order to further optimise the in-situ sandwich manufacture in practice, an experimental study can use the recommended process temperatures as starting point. The process optimisation could focus on a reduction of cycle time by a reduction of the process temperature combination until a combination is reached that provides both low cycle times and a sufficient interfacial bonding. If the foaming behaviour and hence the density reduction however is also significantly affected by a process temperature change, which is the case if PBA and PP-T20 are combined, this must be considered.

## 8.5. Discussion

In this chapter, the applicability of the developed models in engineering practice was demonstrated at the substitution of a reference steel beam with in-situ CFRTP sandwich structures. Therefore, in a first step an optimisation procedure of the weight specific flexural rigidity as well as the cost-efficient lightweight design of in-situ CFRTP sandwich structures was presented, considering different CFRTP facesheet materials and layups as well as sandwich geometries. The optimisation procedure is based on the flexural rigidity model developed in this work and includes glass as well as carbon fibre reinforced polypropylene tapes as facesheet material and PP-H as core material, as the latter yields the highest lightweight design effects according to chapter 6. In the optimisation, the facesheet thickness and layup as well as the total sandwich thickness were subject to variation.

The results show that the optimisation of in-situ CFRTP sandwich structures yields different material-dependent optima regarding pure lightweight design and cost related lightweight design. Attributing to the higher material cost of CFRTP facesheets compared to the core material, an optimisation targeting cost-efficient lightweight design generally leads to thinner facesheets and hence slightly reduced mechanical properties compared to a pure focus on lightweight design. This is found for UD as well as cross composite facesheet layups, yet with different optima due to the respective tensile moduli. Also, the number of variants leading to high cost efficiency of in-situ CFRTP sandwich structures is distinctly smaller compared to a pure focus on lightweight design. Small changes of the sandwich composition hence result in significantly decreased cost efficiency and accordingly in increased component cost.

In the next step, a pre-design of an in-situ CFRTP sandwich component as substitution of a reference beam was carried out. The substitution variants were required to meet the flexural rigidity of the reference component. This should be achieved by different material and structural variants including an automotive grade aluminium alloy as well as in-situ CFRTP sandwich structures with glass as well as carbon fibre reinforced facesheets with unidirectional and cross composite layup respectively.

All substitute structures result in an increased thickness attributing to their lower elastic moduli compared to steel. While the thickness of the aluminium component leads to an increase of 42 % compared to the steel reference, glass and carbon fibre in-situ sandwich structures yield 150 % and 100 % respectively. However, the component mass can be drastically decreased using in-situ CFRTP sandwich structures by up to 74.5 % in case of glass fibre reinforced facesheets and up to 83 % when carbon fibre based facesheets are used. This leads to an equally drastic increase of weight specific flexural rigidity by 280.7 % and 482.9 % respectively, which clearly highlights the lightweight design potential of the in-situ process with optimised structure and material composition. Finally, the component material cost can also be reduced compared to the steel reference and to the aluminium variant, despite the relatively high cost of the CFRTP facesheet material. This result is attributed to the stress equivalent sandwich construction, which requires only a small amount of the costly CFRTP material in the in-situ sandwich component for the achievement of high flexural rigidities.

Consequently, it can be concluded that the developed models can be applied target-oriented at the pre-design of new in-situ sandwich components. While the flexural rigidity model allows for specific optimisations of in-situ components e.g. the cost efficiency of lightweight design, the subsequent interfacial bonding model enables to predict suitable process parameters for the manufacture of in-situ sandwich components with proper interfacial bonding. Furthermore it was demonstrate that if

the in-situ process can be controlled using the presented models, it enables the manufacture of cost-efficient lightweight design components suitable for high-volume applications.

# 9. Summary and Outlook

## 9.1. Summary

The general objective of the present work was to contribute establishing the in-situ CFRTP sandwich process as manufacturing technique for lightweight design components in high volume applications. This should be achieved by the accomplishment of three objectives. First, the critical aspect of interfacial bonding between CFRTP facesheets and the foam injection moulded core during the manufacture of in-situ sandwich structures and the underlying mechanisms needed to be determined. Second, the lightweight design of components based on the in-situ process required evaluation by correlating the weight specific flexural rigidity of in-situ sandwich specimens with material and process parameters. At last, based on the accomplishment of the previous objectives, a methodology for the prediction of interfacial bonding between UD tape facesheets and the foam injection moulded core as well as of the resulting flexural rigidity should be developed, facilitating the pre-design of new in-situ CFRTP sandwich components.

In order to evaluate the mechanisms behind the interfacial bonding development between UD tape facesheets and the injection moulded foam core during the manufacture of in-situ CFRTP sandwich specimens, an experimental campaign was conducted. In-situ sandwich specimens were manufactured using unidirectional 60 wt.-% glass fibre reinforced polypropylene tapes (UD tapes) as facesheet and a polypropylene homopolymer (PP-H) as core material. The experimental campaign comprised both compact and foamed sandwich cores to allow for an evaluation of the effect of the foaming process on the development of interfacial bonding. For the valid quantification of interfacial bonding, test methods needed to be established and systematically evaluated. Based on VDI 2225, the notched lap shear test was selected for the evaluation of interfacial strength and in addition the roller peel test for the assessment of interfacial fracture toughness. In order to determine the mechanisms governing the bonding between core and facesheet during the in-situ CFRTP sandwich process, the experimental bonding results were correlated with the applied process and material parameters. The relationship between the process- as well as material-induced interphase morphology and the interfacial bonding was assessed via SEM and PLM of the fracture surface and specimen cross section, respectively.

It was found that the selected interfacial test methods yield similar qualitative results, suggesting their valid application at the determination of interfacial bonding between CFRTP facesheets and core. Furthermore, it was ascertained that maximum bonding is already achieved at interface temperatures of up to 40 °C below the melting temperature $T_{melt}$ of the facesheet polymer matrix. In contrast, if UD tape facesheets with increased degree of crystallinity are used, the resulting interface temperatures need to reach $T_{melt}$ of the polymer matrix in order to achieve equally high bonding as sandwich specimens with standard UD tape facesheets. This is attributed to the reduced chain mobility below $T_{melt}$ of the high crystalline facesheet matrix compared to standard UD tapes with lower degree of crystallinity.

Furthermore, by doubling the facesheets thickness, higher interfacial bonding is achieved despite equally high peak interface temperatures. A thermal barrier effect of the interface towards the cooled mould is assumed to lead to a longer time span at which the interface exhibits elevated interface temperatures hence improving the bonding development. This effect also facilitates the development of interfacial bonding of sandwich specimens with high crystalline UD tape facesheets.

While these results were assessed based on the manufacture of in-situ sandwich specimens with compact core, the effect of the application of the low-pressure foam injection moulding (LP-FIM) variant on interfacial bonding was evaluated. It was found that the interfacial bonding development between foamed and compact cores and UD tape facesheets shows qualitatively the same dependency of the applied process temperatures. Sandwich specimens with foamed core however yield significantly lower absolute values than with compact core although the peak interface temperature during manufacture is approximately 30°C higher. It is assumed that the lower interfacial bonding is a result of an insufficient intimate contact due to lower cavity pressures. Hence, the incomplete intimate contact during the in-situ process using the LP-FIM technique leads to a reduced interfacial bonding despite full healing.

Consequently, it is concluded that the dominant material parameter in interfacial bonding development during the manufacture of in-situ sandwich structures is the degree of crystallinity of the polymer matrix of the UD tape facesheet. Furthermore, the interface temperature and the effective cavity pressure during the injection and foaming of the core are the most important process parameters to enable high interfacial bonding.

As second objective of this work, the lightweight design potential of in-situ CFRTP sandwich structures was evaluated. Therefore, the effect of chemical and physical blowing agents as well as PP-H and PP-T20 as core materials on the foam morphology and the resulting weight specific flexural rigidity was assessed. It was found, that the flexural rigidity correlates with the core-skin thickness, which was assessed via macroscopic foam morphology analysis based on longitudinal specimen cross sections. Furthermore, distinct differences between the effects of the blowing agents are observed. The flexural rigidity of in-situ CFRTP sandwich specimens manufactured using CBA is significantly less sensitive to temperature and material variations compared to PBA. However, higher density reductions are achieved using the latter. Accordingly, PBA-based in-situ CFRTP sandwich specimens with PP-H as core material yield the highest weight specific flexural rigidity and lightweight design effect of the experimental campaign and clearly demonstrate the lightweight design potential of this material and process combination.

As third and last objective of this work, a methodology for the predictive characterisation of in-situ CFRTP sandwich specimens was taken into focus in order to facilitate their pre-design. For this purpose, a flexural rigidity as well as an interfacial bonding model were developed, evaluated and validated by correlation with experimental results.

Two variants of the flexural rigidity model were developed based on different characterisation of the integral foam core according to its density reduction. A simplified 3-layer model assuming a homogenous foam core was compared to a 5-layer model attributing to the solid core-skin of integral foams. A comparison of model predictions and experimental results showed that the 3-layer model leads to higher conformities of the predicted flexural rigidity compared to the 5-layer model while avoiding the challenging assessment of the core-skin thickness for its calculation. The model further showed that with increasing thickness of the facesheets the latter become dominant with respect to the total flexural rigidity of in-situ sandwich specimens. However, it was demonstrated that the contribution of the core to the total flexural rigidity must not be neglected especially regarding sandwich components with thin CFRTP facesheets.

The developed novel interfacial bonding model completes the targeted methodology for the pre-design of new in-situ components. It is based on the non-isothermal healing model of Bastien and Gillespie [146] which is combined with a preceded simulation of the interface temperature development between UD tape facesheets and injected polymer foam core during the process. It was found that the major contribution to interfacial healing is achieved just upon the initial contact of CFRTP facesheet and injected polymer core due to the low reptation times of polypropylene and the rapid cooling of the interface. The comparison of results of the interfacial bonding model and the experimentally assessed interfacial fracture toughness showed good correlation, yet indicating the necessity of precise interface temperature simulations. Since the reptation time changes rapidly near $T_{melt}$ of the facesheet, the predicted degree of healing may distinctly differ from the experimental results if the simulation is inaccurate by only a few degrees Celsius. In order to avoid this, the applied process temperatures should lead to interface temperatures sufficiently above $T_{melt}$ of the CFRTP facesheet matrix in order to ensure proper bonding.

The quantitative prediction of interfacial fracture toughness showed an overestimation at moderate and high process temperatures. The observed difference between the degree of healing and the experimentally assessed interfacial fracture toughness is attributed to the incomplete intimate contact development. As interfacial bonding is the result of both intimate contact as prerequisite and subsequent healing, bonding is reduced if one of these sub-processes is incomplete. The low cavity pressure resulting from the LP-FIM variant is assumed to yield insufficient intimate contact within the limited process time, reducing the resulting interfacial bonding. The presented model however is based on the degree of healing and does not include the intimate contact for the quantitative prediction of interfacial bonding. Models for the combined assessment of degree of healing and degree of intimate contact yielding a degree of bonding may enable better quantitative correlations when LP-FIM is used. However, they require a combined pressure and temperature simulation as input and are therefore significantly more complex than the presented model. If HP-FIM is applied, it is assumed that the presented interfacial bonding methodology leads to higher quantitative correlations with experimental results.

A demonstration of applicability of the developed models in engineering practice completes the present work. A reference steel beam was exemplarily substituted by in-situ CFRTP sandwich structures providing the same flexural rigidity yet at lower component weight. After the definition of requirements and boundary conditions, necessary input data was collected including material and geometrical specifications. The applied core material was PP-H and a glass fibre as well as a carbon fibre reinforced polypropylene tape with unidirectional and cross-ply composite layup were used as facesheets.

The optimisation of lightweight design with respect to the defined requirements was conducted by a variation of the in-situ sandwich structure as well as facesheet material and layup. The optimisation showed that in-situ sandwich structures with unidirectional as well as cross-ply layups yield the highest weight specific flexural rigidity with different facesheet thicknesses. If the material cost of core and facesheet was included, this led to sandwich structures with thinner facesheets attributing to their relatively high cost. The optimised in-situ sandwich variants were compared with the steel and an aluminium variant demonstrating the anticipated mass reduction and increase of weight specific flexural rigidity. Moreover, the component material cost was distinctly reduced compared to steel, using glass and carbon fibre reinforced UD tape facesheets. This was achieved by their low

density and high weight specific mechanical properties in combination with the stress equivalent and hence efficient application of CFRTP material in the sandwich component.

After the optimisation of in-situ CFRTP sandwich specimens, the interfacial bonding model was used to find appropriate process parameters for their manufacture. Different combinations of melt and mould temperatures were found to ensure proper bonding between the facesheets and foamed core and were hence considered suitable for the manufacture of in-situ CFRTP sandwich components with optimised cost-efficient lightweight design.

## 9.2. Outlook

In follow up studies, the use of the high-pressure foam injection moulding variant should be evaluated with respect to the lightweight design and interfacial bonding of in-situ CFRTP sandwich specimens. Based on the results of this work this should lead to higher weight reductions and hence higher weight specific mechanical properties. Moreover, an increase of interfacial bonding is expected due to the higher cavity pressures. It is assumed that this would improve the conformity of the presented model for the prediction of interfacial bonding based on the degree of healing with experimental results.

Furthermore, the application of the developed models at the substitution of a reference component demonstrated the high lightweight design potential especially of in-situ sandwich structures with carbon fibre reinforced facesheets. Hence, the use of the latter in applications with highest requirements regarding weight specific mechanical properties appears very promising and should be evaluated. In addition to the use of other facesheet materials, also the polymer may be altered attributing e.g. to higher requirements with respect to working temperatures or flammability.

In this respect, the present work may serve as pattern for the evaluation and qualification of new processes and materials as well as pre-design methodologies for the in-situ CFRTP process.

# References


1. Ernstberger, U. (2018) Produktentstehung und -auslegung in der Automobilindustrie
2. Winterhagen, J. (2018) Weniger Teile, weniger Arbeit, weniger Jobs? http://www.faz.net/aktuell/technik-motor/motor/elektroautos-fordern-hersteller-und-zulieferer-heraus-14547766-p2.html. Accessed 02 May 2018
3. Neumeyer, T. (2018) Thermoplastische Sandwichstrukturen mit Partikelschaumkernen. NMB Techdays, Bayreuth
4. Mathes, V. (2018) Bringt Leichtbau bei Elektrofahrzeugen keine nennenswerten Vorteile?: Ist die E-Mobilität das Ende des Leichtbaus im PKW? Werkstoffe(3): 12–13
5. Friedrich, H. E. (ed) (2017) Leichtbau in der Fahrzeugtechnik, 2. Auflage. ATZ / MTZ-Fachbuch. Springer Vieweg, Wiesbaden
6. Königer, R. et al. (1st/2nd 2017) VORAFORCE™ RTM Resin Systems Mass Reduction for Mass Production. SICOMP Conference
7. Henning, F., Moeller, E. (eds) (2011) Handbuch Leichtbau: Methoden, Werkstoffe, Fertigung. Hanser, München
8. Schürmann, H. (2007) Konstruieren mit Faser-Kunststoff-Verbunden, 2., bearbeitete und erweiterte Auflage. VDI-Buch. Springer-Verlag Berlin Heidelberg, Berlin, Heidelberg
9. Wong J. (2017) Processing of High Performance Thermoplastic Composites, ETH Zürich, Laboartory of Composite Materials and Adaptronic Structures
10. Oechsler (2012) Hochleistungsfaserverbunde in der Großserie: It works - let‘s do it
11. Kropka, M., Muehlbacher, M., Neumeyer, T. et al. (2017) From UD-tape to Final Part – A Comprehensive Approach Towards Thermoplastic Composites. Procedia CIRP 66: 96–100. doi: 10.1016/j.procir.2017.03.371
12. Ermanni P. (2007) Composites Technologien: Version 4.0, Zürich
13. Witten E. (ed) (2014) Handbuch Faserverbundkunststoffe/Composites: Grundlagen, Verarbeitung, Anwendungen, 4. Auflage. Springer Vieweg, Wiesbaden
14. Khaled, Y., Mehdi, H. (2017) Processing of thermoplastic matrix composites through automated fiber placement and tape laying methods. Journal of Thermoplastic Composite Materials 50(2): 089270571773830. doi: 10.1177/0892705717738305
15. Sacchetti, F. (2017) Interlaminar toughness of fusion bonded thermoplastic composites
16. Grouve, W. J. B. (2012) Weld strength of laser-assisted tape-placed thermoplastic composites. Dissertation, Enschede
17. Sonmez, F. O., Akbulut, M. (2007) Process optimization of tape placement for thermoplastic composites. Composites Part A: Applied Science and Manufacturing 38(9): 2013–2023. doi: 10.1016/j.compositesa.2007.05.003
18. Bonefeld, D. (2012) Spriform: A Hybrid Technique for Serial Production of 3D Parts of Continuous Fiber Reinforced Thermoplastics, Venice, Italy
19. Bonefeld, D. et al. (2015) Großserienreif: Multiaxial verstärkte thermoplastische Composites für den Leichtbau. Kunststoffe: 190–194
20. Hufenbach, W.A., Krahl, M. (2013) Innovative Werkzeug- und Fertigungstechnologien für hybride Thermoplast-Leichtbaustrukturen. 1. Symposium lightweight SOLUTIONS Hannover
21. Häffelin, D. et al. (2017) Nicht zu bremsen: Vollkunststoff-Bremspedal mit multiaxialer Faserverstärkung im Serieneinsatz. Kunststoffe(03): 20–25

22. Bürkle, E., Wobbe, H. (2016) Kombinationstechnologien auf Basis des Spritzgießverfahrens. Carl Hanser Verlag GmbH & Co. KG, München
23. Hufenbach, W.A. (2010) Leichtbausitzschalen im Serientakt. Kunststoffe(5): 56–59
24. Tanaka, K., Fujita, Y., Katayama, T. (2015) Press and injection hybrid molding of glass fiber reinforced thermoplastics. In: Brebbia CA (ed) MATERIALS CHARACTERISATION 2015. WIT PressSouthampton, UK, pp 225–232
25. Drummer, D., Gröschel, C., Seefried, A. (2013) Organobleche durch Gasdruck direkt umformen. Kunststoffe(12)
26. Drummer, D. (2011) FIT-Hybrid: Hohlkörperverbundstrukturen im Minutentakt. Kunststoffe: 110–114
27. Kaufmann, R., Bider, T., Bürkle, E. (2011) Leichtbauteile mit Thermoplastmatrix. Kunststoffe(101): 106–109
28. BASF SE (2012) Sitzschale des Opel Astra OPC : Erstes Serienbauteil mit endlosfaser-verstärktem Composite aus Ultramid. https://www.plasticsportal.net/wa/plasticsEU~de_DE/portal/show/common/plasticsportal_news/2012/12_187. Accessed 16 Jan 2019
29. Sherman, L.M. (2012) The New Lightweights: Injection Molded 'Hybrid' Composites Spur Auto Innovation. https://www.ptonline.com/articles/the-new-lightweights-injection-molded-hybrid-composites-spur-automotive-innovation. Accessed 16 Jan 2019
30. Ottenbruch, P. (2012) Leichtbau für Pkw und Lkw. https://www.automobil-industrie.vogel.de/leichtbau-fuer-pkw-und-lkw-a-376825/index4.html
31. Wacker, M. (2006) Jacob Composite and BMW select Tepex M3 Bumper Beam. https://netcomposites.com/news/2006/september/25/jacob-composite-and-bmw-select-tepex-m3-bumper-beam/
32. Lanxess (2011) Runter mit den Pfunden: Organo-Hybridfrontend im Audi A8 reduziert Gewicht um 20 Prozent. https://automobilkonstruktion.industrie.de/karosserie-interieur/leichtbau/runter-mit-den-pfunden-3/
33. Obermann, C. (2018) Organobleche: Stückzahlen im Millionenbereich. https://www.k-zeitung.de/organobleche-stueckzahlen-im-millionenbereich/. Accessed 16 Jan 2019
34. Häffelin, D.et al. (2017) Lightweight Design on the Move: All-Plastic Brake Pedal with Multiaxial Fiber Reinforcement in Series Production. Kunststoffe(03)
35. Weidmann, F. (2017) Insulating sandwich housing structures for the thermal management of battery packs. Twelfth International Conference on Ecological Vehicles and Renewable Energies (EVER), Monaco
36. Altstädt, V. et al. (2012) Ultralitec-Verfahren: Großserientauglicher Hochleistungsleichtbau. Kunststoffe(5)
37. Wiedemann, J. (2007) Leichtbau: Elemente und Konstruktion, 3. Auflage. Klassiker der Technik. Springer-Verlag Berlin Heidelberg, Berlin, Heidelberg
38. Grünewald, J. (2018) Thermoplastic composite sandwiches for structural helicopter applications. Universität Bayreuth, Bayreuth
39. Gorbach G. et al. (2019) Mit kleinen Blasen ganz groß rauskommen: Thermoplastische Sandwichstrukturen für Großserienanwendungen. Kunststoffe(7): 38–41
40. Loypetch, N., Tröltzsch, J., Nestler, D. et al. (2019) Influence of talc in polypropylene foam cores of sandwich structures with skins made of thermoplastic prepregs. IOP Conf. Ser.: Mater. Sci. Eng. 480: 12012. doi: 10.1088/1757-899X/480/1/012012

41. Roch, A., Menrath, A., Huber, T. (2013) Faserverstärkte Thermoplaste in Sandwichbauweise. Kunststoffe(10): 183–189
42. Knöchel, J., Mühlbacher, M., Starke, J. et al. (2018) Einbaufertige Sandwichbauteile im Minutentakt. Lightweight Des 11(3): 12–17. doi: 10.1007/s35725-018-0018-y
43. VDI (1997) VDI 2225: Blatt 3 Konstruktionsmethodik - Technisch-wirtschaftliches Konstruieren - Technisch-wirtschaftliche Bewertung
44. Skawinski, O., Binetruy, C., Krawczak, P. et al. (2016) All-Thermoplastic Composite Sandwich Panels – Part I: Manufacturing and Improvement of Surface Quality. Jnl of Sandwich Structures & Materials 6(5): 399–421. doi: 10.1177/1099636204040094
45. Roch, A. (2013) Fiber-Reinforced Thermoplastics as Sandwich Construction: Lightweight Construction for Mass Production. Kunststoffe: 119–124
46. Menrath, A., Henning, F., Huber, T. et al. (2014) Foam-injected sandwich panels with continuous-reinforced facings. In: PROCEEDINGS OF PPS-29: The 29th International Conference of the Polymer Processing Society - Conference Papers. American Institute of Physics, pp 477–481
47. Roch, A. (2015) Leichtbaupotenzial langfaserverstärkter Thermoplaste (LFT) in Integralschaumbauweise hergestellt durch Schaumspritzgießen mit Dekompressionshub. Dissertation. Wissenschaftliche Schriftenreihe des Fraunhofer ICT, vol 65, KIT
48. Grünewald, J., Parlevliet, P., Altstädt, V. (2016) Manufacturing of thermoplastic composite sandwich structures. Journal of Thermoplastic Composite Materials 30(4): 437–464. doi: 10.1177/0892705715604681
49. Campbell, F. C. (op. 2010) Structural composite materials, 1st ed. ASM International, Materials Park, OH
50. Krzyżak, A., Mazur, M., Gajewski, M. et al. (2016) Sandwich Structured Composites for Aeronautics: Methods of Manufacturing Affecting Some Mechanical Properties. International Journal of Aerospace Engineering 2016(4): 1–10. doi: 10.1155/2016/7816912
51. Grünewald, J., Orth, T., Parlevliet, P. et al. (2017) Modified foam cores for full thermoplastic composite sandwich structures. Jnl of Sandwich Structures & Materials 6: 109963621770874. doi: 10.1177/1099636217708741
52. Gude, M., Just, G., Kaufhold, J. et al. (2015) Chancen und Herausforderungen im ressourceneffizienten Leichtbau für die Elektromobilität: Forelstudie. Institut für Leichtbau und Kunststofftechnik (ILK) Technische Universität Dresden, Dresden
53. Müller, I., Schmieg, H. (2003) Experimental Identification of a Surface Delamination of a Laminated Sandwich Beam. Proc. Appl. Math. Mech. 3(1): 332–333. doi: 10.1002/pamm.200310438
54. Nowacki J., Mitschang P., Neitzel M. (2001) Thermoplastische Sandwich-Strukturbauteile in einem Schritt geformt: Potenzial für Serienfertigung. Kunststoffe 91(7): 92–95
55. Akermo, M., Astrom, B. T. (2016) Experimental Investigation of Compression Molding of Glass/PP-PP Foam Core Sandwich Components. Journal of Thermoplastic Composite Materials 12(4): 297–316. doi: 10.1177/089270579901200404
56. Corvaglia, P., Passaro, A., Manni, O. et al. (2006) Recycling of PP-based Sandwich Panels with Continuous Fiber Composite Skins. j thermoplast compos 19(6): 731–745. doi: 10.1177/0892705706067918
57. Mcgarva, L. D., Åström, B. T. (2016) Insert Integration in Thermoplastic-Based Foam Core Sandwich Components. Jnl of Sandwich Structures & Materials 1(3): 214–229. doi: 10.1177/109963629900100303

58. Schreier, P. (2016) Multi Materialsysteme: Sandwich mit thermoplastischen Partikelschäumen. emobility tec(2): 58–61
59. Skawinski, O., Binetruy, C., Krawczak, P. et al. (2016) All-Thermoplastic Composite Sandwich Panels – Part II: Modelling of Bending Behaviour. Jnl of Sandwich Structures & Materials 6(5): 423–446. doi: 10.1177/1099636204040093
60. Pappadà, S., Rametta, R., Passaro, A. et al. (2010) Processing, mechanical properties, and interfacial bonding of a thermoplastic core-foam/composite-skin sandwich panel. Adv. Polym. Technol. 29(3): 137–145. doi: 10.1002/adv.20186
61. Passaro, A., Corvaglia, P., Manni, O. et al. (2004) Processing-properties relationship of sandwich panels with polypropylene-core and polypropylene-matrix composite skins. Polym Compos 25(3): 307–318. doi: 10.1002/pc.20025
62. Chen, K., Xue, P., Zhou, X. et al. (2016) Preparation and Performance of Continuous Glass Fiber Reinforced Polypropylene Composite Honeycomb Sandwich Panels. MATEC Web Conf. 67: 6082. doi: 10.1051/matecconf/20166706082
63. Bonnet, M. (2014) Kunststofftechnik: Grundlagen, Verarbeitung, Werkstoffauswahl und Fallbeispiele, 2., überarb. und erw. Aufl. Lehrbuch. Springer Vieweg, Wiesbaden
64. Schuster, T. (2014) Dreidimensionale Charakterisierung von beta-nukleierten Polypropylenrohren. Dissertation, Darmstadt
65. Jiang, J., Liu, X., Lian, M. et al. (2018) Self-reinforcing and toughening isotactic polypropylene via melt sequential injection molding. Polymer Testing 67: 183–189. doi: 10.1016/j.polymertesting.2018.03.005
66. Yu, Y., Zeng, F., Chen, J. et al. (2018) Regulating polycrystalline behavior of the β-nucleated isotactic polypropylene/graphene oxide composites by melt memory effect. Polym. Compos. 17: 109. doi: 10.1002/pc.24745
67. Tejeda, E. H., Sahagún, C. Z., González-Núñez, R. et al. (2016) Morphology and Mechanical Properties of Foamed Polyethylene-Polypropylene Blends. Journal of Cellular Plastics 41(5): 417–435. doi: 10.1177/0021955X05056959
68. Ma, L.-F., Wang, W.-K., Bao, R.-Y. et al. (2013) Toughening of polypropylene with β-nucleated thermoplastic vulcanizates based on polypropylene/ethylene–propylene–diene rubber blends. Materials & Design 51: 536–543. doi: 10.1016/j.matdes.2013.04.066
69. Du, H., Zhang, Y., Liu, H. et al. (2014) Influence of phase morphology and crystalline structure on the toughness of rubber-toughened isotatic polypropylene blends. Polymer 55(19): 5001–5012. doi: 10.1016/j.polymer.2014.08.012
70. Ohneiser, A. (2011) Kombination von Ultraschallspektroskopie und Dilatometrie zur Analyse der Strukturbildung während der Kristallisation von Polymeren unter Druck. Dissertation, Darmstadt
71. Tordjeman Ph et al. (2001) The effect of α, β crystalline structure on the mechanical properties of polypropylene. THE EUROPEAN PHYSICS JOURNAL E(4): 459–465
72. Schawe, J. E. K. (2016) Cooling rate dependence of the crystallinity at nonisothermal crystallization of polymers: A phenomenological model. J. Appl. Polym. Sci. 133(6): n/a-n/a. doi: 10.1002/app.42977
73. Frick, A., Stern, C. (2006) DSC-Prüfung in der Anwendung. Hanser, München
74. Mandelkern, L. (2004) Crystallization of Polymers. Cambridge University Press, Cambridge
75. Sauer, J. (2018) Untersuchung der Anbindungsmechanismen und Schädigungsvorgänge von kompakten Polypropylen-Sandwich-Strukturen. Master Thesis, Darmstadt
76. Hoffman, J. D. et al. (1967) Kinetics of Polymer Crystallization from Solution and the Melt. Kolloid-Zeitschri/t und Zeitschri/t /iir Polymere 231(1-2)

77. Lauritzen, J. I., Hoffman, J. D. (1959) Formation of Polymer Crystals with Folded Chains from Dilute Solution. The Journal of Chemical Physics 31(6): 1680–1681. doi: 10.1063/1.1730678
78. Lauritzen, J. I., Hoffman, J. D. (1973) Extension of theory of growth of chain-folded polymer crystals to large undercoolings. Journal of Applied Physics 44(10): 4340–4352. doi: 10.1063/1.1661962
79. Moneke, M. (2001) Die Kristallisation von verstärkten Thermoplasten während derschnellen Abkühlung und unter Druck. Dissertation, Darmstadt
80. Becker, R., Döring, W. (1935) Kinetische Behandlung der Keimbildung in übersättigten Dämpfen. Ann. Phys. 416(8): 719–752. doi: 10.1002/andp.19354160806
81. Turnbull, D., Fisher, J. C. (1949) Rate of Nucleation in Condensed Systems. The Journal of Chemical Physics 17(1): 71–73. doi: 10.1063/1.1747055
82. Kawai, T., Iijima, R., Yamamoto, Y. et al. (2002) Crystal orientation of β-phase isotactic polypropylene induced by magnetic orientation of N,N'-dicyclohexyl-2,6-naphthalenedicarboxamide. Polymer 43(26): 7301–7306. doi: 10.1016/S0032-3861(02)00690-0
83. Yan, B., Wu, H., Jiang, G. et al. (2010) Interfacial crystalline structures in injection over-molded polypropylene and bond strength. ACS Appl Mater Interfaces 2(11): 3023–3036. doi: 10.1021/am1003574
84. Lopez-Manchado, M., Biagiotti, J., Torre, L. et al. (2000) Effects of reinforcing fibers on the crystallization of polypropylene. Polym. Eng. Sci. 40
85. University of Utah Lecture 10: Homogenous Nucleation. Lecture, Salt lake City
86. National Programme on Technology Enhanced Learning (2019) Part II: Interfaces: Module 2: Nucleation of solids from their melt. https://nptel.ac.in/courses/113101003/downloads/partIII/module2.pdf
87. Atiyah, A. (2016) LECTURE 2 HOMOGENEOUS NUCLEATION, Bagdad, Iraq
88. Michel, J. C. (1999) A Quantitative Description of the Effects of Molecular Weight and Atactic Level on the Spherulite Growth Rate of Ziegler-Natta Isotactic Polypropylene. In: Imaging and Image Analysis Applications for Plastics. Elsevier, pp 43–51
89. Isayev, A. I., Catignani, B. F. (1997) Crystallization and microstructure in quenched slabs of various molecular weight polypropylenes. Polym Eng Sci 37(9): 1526–1539. doi: 10.1002/pen.11801
90. Raimo, M. (2015) On the origin of transcrystalline morphology in polymers and their composites: Re-evaluation of different views. Materials Today Communications 3: 137–140. doi: 10.1016/j.mtcomm.2015.01.003
91. Jenckel, E., Teege, E., Hinrichs, W. (1952) Transkristallisation in hochmolekularen Stoffen. Colloid Polym Sci 129(1): 19–24. doi: 10.1007/BF01802755
92. Huang, J., Xu, C., Wu, D. et al. (2017) Transcrystallization of polypropylene in the presence of polyester/cellulose nanocrystal composite fibers. Carbohydrate Polymers 167: 105–114. doi: 10.1016/j.carbpol.2017.03.046
93. Vancso, G. J., Liu, G., Karger-Kocsis, J. et al. (1997) AFM imaging of interfacial morphologies in carbon-fiber reinforced isotactic polypropylene. Colloid Polym Sci 275(2): 181–186. doi: 10.1007/s003960050069
94. Harel, H., Marom, G. (1998) On crystalline interfaces in composite materials. Acta Polymerica - ACTA POLYM 49. doi: 10.1002/(SICI)1521-4044(199810)49:10/11<583:AID-APOL583>3.0.CO;2-0
95. Lebsack, D. (2017) Untersuchung des Einflusses verschiedener Parameter auf die Anbindungsfestigkeiten thermoplastischer Faser-Kunststoff-Verbund-Sandwich-Strukturen. Master Thesis, Darmstadt

96. Quan, H., Li, Z.-M., Yang, M.-B. et al. (2005) On transcrystallinity in semi-crystalline polymer composites. Composites Science and Technology 65(7-8): 999–1021. doi: 10.1016/j.compscitech.2004.11.015
97. Lin, C. W., Ding, S. Y., Hwang, Y. W. (2001) Interfacial crystallization of isotactic polypropylene molded against the copper surface with various surface roughnesses prepared by an electrochemical process. Journal of Materials Science 36(20): 4943–4948. doi: 10.1023/A:1011848623699
98. Lin, C.W., Du, Y.C. (1999) Effect of surface topographies of PTFE and polyimide as characterized by atomic force microscopy on the heterogeneous nucleation of isotactic polypropylene. Materials Chemistry and Physics 58(3): 268–275. doi: 10.1016/S0254-0584(99)00009-7
99. Domininghaus H., Elsner P., Eyerer P. et al. (eds) (2012) Kunststoffe: Eigenschaften und Anwendungen, 8., neu bearb. und erw. Aufl. VDI-Buch. Springer, Berlin, Heidelberg
100. Hansen, D., Taskar, A. N., Casale, O.'N. (1972) Method for studying polymer crystallization in a temperature-gradient field with controlled crystal growth. J. Polym. Sci. A-2 Polym. Phys. 10(8): 1615–1619. doi: 10.1002/pol.1972.160100819
101. Barriault, R. J., Gronholz, L. F. (1955) Formation of spherulitic structure in polyhexamethylene adipamide (66 nylon). I. Structure and optical properties of spherulites at room temperature. J. Polym. Sci. 18(89): 393–403. doi: 10.1002/pol.1955.120188908
102. Eby, R. K. (1964) Diffusion in a Polymer With Lamellar Morphology, Polyethylene. Journal of Applied Physics 35(9): 2720–2724. doi: 10.1063/1.1713829
103. Grünewald, J., Parlevliet, P. P., Matschinski, A. et al. (2017) Mechanical performance of CF/PEEK–PEI foam core sandwich structures. Jnl of Sandwich Structures & Materials: 109963621771570. doi: 10.1177/1099636217715704
104. Bond Laminates (2018) Tepex® dynalite 104-RG600(x)/47% Roving Glass - PP Consolidated Composite Laminate
105. SabicFRT (2018) UDMAXTM GPP 45-70 TAPE
106. Institut für Kunststoffverarbeitung IKV (2016) Neue Produktionsanlage für UD-Tapes am IKV: Forschung zur Wechselwirkung von Tapeeigenschaften und nachfolgendem Verarbeitungsprozess. https://www.ikv-aachen.de/neuigkeiten/detailseite-neuigkeiten/news/news/detail/neue-produktionsanlage-fuer-ud-tapes-am-ikv/
107. Nestler, D., Trautmann, M., Zopp, C. et al. (2017) Continuous Film Stacking and Thermoforming Process for Hybrid CFRP/aluminum Laminates. Procedia CIRP 66: 107–112. doi: 10.1016/j.procir.2017.03.221
108. IYER S.R., DRZAL L.T. (1990) Manufacture of Powder-Impregnated Thermoplastic Composites. Journal of Thermoplastic Composite Materials(3): 325–355
109. Ho, K. K. C., Shamsuddin, S.-R., Riaz, S. et al. (2011) Wet impregnation as route to unidirectional carbon fibre reinforced thermoplastic composites manufacturing. Plastics, Rubber and Composites 40(2): 100–107. doi: 10.1179/174328911X12988622801098
110. Fraunhofer IMWS (2018) Fraunhofer PAZ and KraussMaffei Berstorff start UD tape line
111. Sewell, J., Czarnecki, T., Pflug, J. (2016) Continuous thermoplastic honeycomb sandwich panel process technology for cost optimal lightweight composites. Reinforced Plastics 60(3): 146–150. doi: 10.1016/j.repl.2016.03.002
112. Altstädt, V., Mantey, A. (2011) Thermoplast-Schaumspritzgießen. Hanser, München
113. Bürkle, E. (2014) Bauteile mit einem Schaumkern und Faserverbunddeckschichten: Leichter durch Sandwich. https://www.kunststoffe.de/specials/faserverbundwerkstoffe/bauteile-mit-einem-schaumkern-und-faserverbunddeckschichten. Accessed 13 Apr 2018

114. Luft, J. (2018) ReLei: Herstellung komplexer thermoplastischer Sandwichstrukturen für Großserienanwendungen
115. Schreier, P., Mühlbacher, M., Fafara, M. (2016) Multi-Materialsysteme im Automobil: Sandwichkonzepte auf Basis thermoplastischer Partikelschäume. https://www.plastverarbeiter.de/57293/sandwichkonzepte-auf-basis-thermoplastischer-partikelschaeume/. Accessed 07 Dec 2018
116. Raps, D., Hossieny, N., Park, C. B. et al. (2015) Past and present developments in polymer bead foams and bead foaming technology. Polymer 56: 5–19. doi: 10.1016/j.polymer.2014.10.078
117. Weidmann, F. (2015) Großserientaugliche Faserverbundtechnologien für flächige Strukturbauteile mit integrierten Funktionselementen. IGF Vorhaben
118. Hopmann, C., Sander, D. (2012) Schäume sind keine Träume: IKV präsentiert neues Verfahren auf Basis von Standardanlagen. https://industrieanzeiger.industrie.de/technik/entwicklung/schaeume-sind-keine-traeume/. Accessed 25 Dec 2018
119. Cramer, A. (2008) Analyse und Optimierung der Bauteileigenschaften beim Thermoplast-Schaumspritzgießen: Analysis and optimisation of the part properties in thermoplastic foam injection moulding. Zugl.: Aachen, Techn. Hochsch., Diss., 2007, 1. Aufl. IKV-Berichte aus der Kunststoffverarbeitung, vol 187. Mainz, Aachen
120. Doriat, C. (2015) Das Profoam-Verfahren eröffnet eine Variante des physikalischen Schäumens: Gemeinsame Granulat- und Gaszuführung. Kunststoffe(5)
121. Stange, J. (2006) Einfluss rheologischer EigenschaŌen auf das Schäumverhalten von Polypropylenen unterschiedlicher molekularer Struktur. Dissertation, Erlangen
122. Quan, H. (2000) Lösemittelfreie Herstellung von porösen polymeren Membranen durch Schaumextrusion. Dissertation, Hamburg
123. Leung, S. N. S. (2009) Mechanisms of Cell Nucleation, Growth, and Coarsening in Plastic Foaming: Theory, Simulation, and Experiment. Dissertation, Torornto
124. Vieth, W. R. (1991) Diffusion in and through polymers: Principles and applications. Hanser; Oxford Univ. Press, Munich, Vienna, New York, Barcelona, New York, Don Mills, Ontario
125. Sato, Y., Fujiwara, K., Takikawa, T. et al. (1999) Solubilities and diffusion coefficients of carbon dioxide and nitrogen in polypropylene, high-density polyethylene, and polystyrene under high pressures and temperatures. Fluid Phase Equilibria 162(1-2): 261–276. doi: 10.1016/S0378-3812(99)00217-4
126. Michaeli, W., Pfannschmidt, O., Habibi-Naini, S. (2002) Wege zum mikrozellulären Schaum: Grundlagen zu Material und Prozessführung. Kunststoffe(92): 48–51
127. Baldwin, D. F., Tate, D., Park, C. B. et al. (1994) Microcellular Plastics Processing Technology. Journal of Japan Society of Polymer Processing (SEIKEIKAKOU) Vol. 6(No.3): 187–194
128. Park, C. B., Cheung, L. K. (1997) A study of cell nucleation in the extrusion of polypropylene foams. Polym Eng Sci 37(1): 1–10. doi: 10.1002/pen.11639
129. Dong, G., Zhao, G., Guan, Y. et al. (2015) Formation mechanism and structural characteristics of unfoamed skin layer in microcellular injection-molded parts. Journal of Cellular Plastics 52. doi: 10.1177/0021955X15577149
130. Volmer, M., Weber, A. (1926) Nucleus Formation in Supersaturated Systems. Zeitschrift für physikalische Chemie 119(3-4): 277–301
131. Farcas, L. (1927) The Velocity of Nucleus Formation in Supersaturated Vapors. Zeitschrift für physikalische Chemie 125: 236

132. Trippel, S. (2018) Validierung einer Spritzgießsimulation zur Analyse des Thermoplast-Schaumspritzgießverfahrens. Master Thesis, Darmstadt
133. Spörrer, A. (2010) Leichte Integralschäume durch Schaumspritzgießen mit optmierten Werkstoffen und variothermen Werkzeugen. Dissertation, Bayreuth
134. Spörrer, A. N.J., Altstädt, V. (2007) Controlling Morphology of Injection Molded Structural Foams by Mold Design and Processing Parameters. Journal of Cellular Plastics 43(4-5): 313–330. doi: 10.1177/0021955X07079043
135. Giusti, R., Lucchetta, G. (2017) Analysis of the welding strength in hybrid polypropylene composites as a function of the forming and overmolding parameters. Polym Eng Sci 34: 948. doi: 10.1002/pen.24786
136. Lamèthe, J.F., Beauchêne, P., Léger, L. (2005) Polymer dynamics applied to PEEK matrix composite welding. Aerospace Science and Technology(Volume 9, Issue 3): 233–240
137. Tierney, J., Gillespie, J. W. (2006) Modeling of In Situ Strength Development for the Thermoplastic Composite Tow Placement Process. Journal of Composite Materials 40(16): 1487–1506. doi: 10.1177/0021998306060162
138. Jarrousse, G. (2004) Self adhesion of semi-crystalline polymers between their glass transition temperature and their melting temperature
139. Plummer, C. J. G., Bourban, P.-E., Zanetto, J.-E. et al. (2003) Nonisothermal fusion bonding in semicrystalline thermoplastics. J. Appl. Polym. Sci. 87(8): 1267–1276. doi: 10.1002/app.11528
140. Yang, F., Pitchumani, R. (2002) Healing of Thermoplastic Polymers at an Interface under Nonisothermal Conditions. Macromolecules 35(8): 3213–3224. doi: 10.1021/ma010858o
141. Boiko, Y. M., Gurin, G.R., Marikhin, V. A. et al. (2001) Healing of interfaces of amorphous and semi-crystalline poly(ethylene terephthalate) in the vicinity of the glass transition temperature. Polymer 42(21): 8695–8702. doi: 10.1016/S0032-3861(01)00406-2
142. Cole, P. J., Macosko, C. W. (2000) POLYMER-POLYMER ADHESION IN MELT-PROCESSED LAYERED STRUCTURES. Journal of Plastic Film and Sheeting 16(3): 213–222. doi: 10.1106/6N2B-V63L-32AW-4JYD
143. Butler, C. A., Mccullough, R. L., Pitchumani, R. et al. (1998) An Analysis of Mechanisms Governing Fusion Bonding of Thermoplastic Composites. Journal of Thermoplastic Composite Materials 11(4): 338–363. doi: 10.1177/089270579801100404
144. Richard P. Wool, Allen, K. W. (1995) Polymer interfaces: Structure and strength. Polym. Int. 38(3): 305–306. doi: 10.1002/pi.1995.210380314
145. Mantell, S. C., Springer, G. S. (1992) Manufacturing Process Models for Thermoplastic Composites. Journal of Composite Materials 26(16): 2348–2377. doi: 10.1177/002199839202601602
146. Bastien, L. J., Gillespie, J. W. (1991) A non-isothermal healing model for strength and toughness of fusion bonded joints of amorphous thermoplastics. Polym. Eng. Sci. 31(24): 1720–1730. doi: 10.1002/pen.760312406
147. Wool, R. P., Yuan, B.-L., McGarel, O. J. (1989) Welding of polymer interfaces. Polym. Eng. Sci. 29(19): 1340–1367. doi: 10.1002/pen.760291906
148. Kim, Y. H., Wool, R. P. (1983) A theory of healing at a polymer-polymer interface. Macromolecules 16(7): 1115–1120. doi: 10.1021/ma00241a013
149. Prager, S., Tirrell, M. (1981) The healing process at polymer-polymer interfaces. The Journal of Chemical Physics 75(10): 5194–5198. doi: 10.1063/1.441871
150. Wool, R. P., O'Connor, K. M. (1981) A theory crack healing in polymers. Journal of Applied Physics 52(10): 5953–5963. doi: 10.1063/1.328526

151. Awaja, F. (2016) Autohesion of polymers. Polymer 97: 387–407. doi: 10.1016/j.polymer.2016.05.043
152. Holschuh, R. (2014) Lokal lastgerecht verstärkte Multimaterialsysteme auf Basis von Polypropylen-Polypropylen-Hybriden. Zugl.: Kaiserslautern, Techn. Univ., Diss., 2014, Als Ms. gedr. IVW-Schriftenreihe, vol 111. Inst. für Verbundwerkstoffe, Kaiserslautern
153. Khan, M. A., Mitschang, P., Schledjewski, R. (2010) Identification of some optimal parameters to achieve higher laminate quality through tape placement process. Adv. Polym. Technol. 29(2): 98–111. doi: 10.1002/adv.20177
154. Lamèthe, J.F. (2004) Etude de l'adhésion de composites thermoplastiques semi-cristallins: Application à la mise en œuvre par soudure. Dissertation, Paris
155. Ezekoye, O. A., Lowman, C. D., Fahey, M. T. et al. (1998) Polymer weld strength predictions using a thermal and polymer chain diffusion analysis. Polym. Eng. Sci. 38(6): 976–991. doi: 10.1002/pen.10266
156. Stokes-Griffin, C. M., Compston, P. (2016) Investigation of sub-melt temperature bonding of carbon-fibre/PEEK in an automated laser tape placement process. Composites Part A: Applied Science and Manufacturing 84: 17–25. doi: 10.1016/j.compositesa.2015.12.019
157. Stokes-Griffin, C. M., Compston, P. (2014) Laser-Assisted Tape Placement of Thermoplastic Composites: The Effect of Process Parameters on Bond Strength. In: Wellnitz J, Subic A, Trufin R (eds) Sustainable Automotive Technologies 2013. Springer International Publishing, Cham, pp 133–141
158. Philip H. Dara, Alfred C. Loos (1985) Thermoplastic Matrix Composite Processing Model
159. Yang, F., Pitchumani, R. (2002) Interlaminar contact development during thermoplastic fusion bonding. Polym. Eng. Sci. 42(2): 424–438. doi: 10.1002/pen.10960
160. Woo Il Lee, Springer, G. S. (1987) A Model of the Manufacturing Process of Thermoplastic Matrix Composites. Journal of Composite Materials 21(11): 1017–1055. doi: 10.1177/002199838702101103
161. Yang, F., Pitchumani, R. (2001) A fractal Cantor set based description of interlaminar contact evolution during thermoplastic composites processing. Journal of Materials Science 36(19): 4661–4671. doi: 10.1023/A:1017950215945
162. Yang, F., Pitchumani, R. (2001) Fractal Description of Interlaminar Contact Development during Thermoplastic Composites Processing. Journal of Reinforced Plastics and Composites 20(7): 536–546. doi: 10.1106/DAEQ-L4HD-N45W-4MJR
163. Sauer, B. B., Kampert, W. G., Wakeman, M. D. et al. (2016) Screening method for the onset of bonding of molten PA6
resin layers to continuous fiber reinforced laminate sheets. Composites Science and Technology 129: 166–172. doi: 10.1016/j.compscitech.2016.04.030
164. Ageorges, C., Ye, L., Hou, M. (2001) Advances in fusion bonding techniques for joining thermoplastic matrix composites: A review. Composites Part A: Applied Science and Manufacturing 32(6): 839–857. doi: 10.1016/S1359-835X(00)00166-4
165. Gennes, P. G. de (1971) Reptation of a Polymer Chain in the Presence of Fixed Obstacles. The Journal of Chemical Physics 55(2): 572–579. doi: 10.1063/1.1675789
166. Edwards, S. F. (1967) The statistical mechanics of polymerized material. Proceedings of the Physical Society(Vol. 92): 9–16
167. Yang, F., Pitchumani, R. (2003) Nonisothermal healing and interlaminar bond strength evolution during thermoplastic matrix composites processing. Polym. Compos. 24(2): 263–278. doi: 10.1002/pc.10027

168. Kausch (2005) Mechanical strength of interfaces in thermoplastic polymers
169. Juhl, T. B., Christiansen, J. d., Jensen, E. A. (2013) Investigation on high strength laser welds of polypropylene and high-density polyethylene. J. Appl. Polym. Sci. 129(5): 2679–2685. doi: 10.1002/app.39000
170. Lamnawar, K., Maazouz, A. (2006) Rheological study of multilayer functionalized polymers: Characterization of interdiffusion and reaction at polymer/polymer interface. Rheol Acta 45(4): 411–424. doi: 10.1007/s00397-005-0062-2
171. Graessley, W. W. (1980) Some phenomenological consequences of the Doi–Edwards theory of viscoelasticity. J. Polym. Sci. Polym. Phys. Ed. 18(1): 27–34. doi: 10.1002/pol.1980.180180103
172. Bueche, F. J. (1962) Physical properties of polymers. Interscience Publishers, New York
173. Akué Asséko, A. C., Cosson, B., Lafranche, É. et al. (2016) Effect of the developed temperature field on the molecular interdiffusion at the interface in infrared welding of polycarbonate composites. Composites Part B: Engineering 97: 53–61. doi: 10.1016/j.compositesb.2016.04.064
174. Ferry, J. D. (1980) Viscoelastic properties of polymers, 3rd ed. Wiley, New York, Chichester
175. Lafranche, E., Renault, T., Krawczak, P. (2014) Effect of the Interdiffusion at the Polymer/Polymer Interface on the Flexural Properties of Over-Moulded Short Glass Fibre/Glass Fabric Reinforced PA6 Composites. KEM 611-612: 821–828. doi: 10.4028/www.scientific.net/KEM.611-612.821
176. Wu, S. (1989) Chain structure and entanglement. J. Polym. Sci. B Polym. Phys. 27(4): 723–741. doi: 10.1002/polb.1989.090270401
177. Wu, S. (1987) Entanglement, friction, and free volume between dissimilar chains in compatible polymer blends. J. Polym. Sci. B Polym. Phys. 25(12): 2511–2529. doi: 10.1002/polb.1987.090251207
178. Schell, J.S.U., Guilleminot, J., Binetruy, C. et al. (2009) Computational and experimental analysis of fusion bonding in thermoplastic composites: Influence of process parameters. Journal of Materials Processing Technology 209(11): 5211–5219. doi: 10.1016/j.jmatprotec.2009.03.008
179. Macedo, S., Lafranche, E., Martins, C. I. et al. (2016) Thin wall injection-overmoulding of polyamide 6/polypropylene multilayer parts: Influence of processing conditions on thermomechanical properties of the layer assembly. IJMPT 52(1/2): 53. doi: 10.1504/IJMPT.2016.073619
180. Eyerer, P. (ed) (2008) Polymer engineering: Technologien und Praxis ; mit 155 Tabellen. VDI. Springer, Berlin, Heidelberg
181. Awaja, F., Gilbert, M., Kelly, G. et al. (2009) Adhesion of polymers. Progress in Polymer Science 34(9): 948–968. doi: 10.1016/j.progpolymsci.2009.04.007
182. Aurrekoetxea, J., Castillo, G., Cortes, F. et al. (2006) Failure of multimaterial fusion bonding interface generated during over-injection molding/thermoforming hybrid process. J. Appl. Polym. Sci. 102(1): 261–265. doi: 10.1002/app.23696
183. Zanetto, J.-E., Plummer, C. J. G., Bourban, P.-E. et al. (2001) Fusion bonding of polyamide 12. Polym Eng Sci 41(5): 890–897. doi: 10.1002/pen.10787
184. Smith, G. D., Plummer, C. J.G., Bourban, P.-E. et al. (2001) Non-isothermal fusion bonding of polypropylene. Polymer 42(14): 6247–6257. doi: 10.1016/S0032-3861(01)00060-X
185. Tissandier, C., González-Núñez, R., Rodrigue, D. (2016) Asymmetric microcellular composites: Mechanical properties and modulus prediction. Journal of Cellular Plastics 52(4): 365–398. doi: 10.1177/0021955X14566208

186. Gosselin, R., Rodrigue, D., Riedl, B. (2006) Injection Molding of Postconsumer Wood–Plastic Composites II: Mechanical Properties. j thermoplast compos 19(6): 659–669. doi: 10.1177/0892705706067486
187. Barzegari, M. R., Rodrigue, D. (2007) The effect of density profile on the flexural properties of structural foams. Polym. Eng. Sci. 47(9): 1459–1468. doi: 10.1002/pen.20844
188. Rodrigue, D. (2008) Using Density Profiles to Predict the Flexural Modulus of Structural Polymer Foams. Journal of Cellular Plastics 44(5): 381–389. doi: 10.1177/0021955X08090986
189. Geiling, M. (2017) Untersuchung physikalischer und chemischer Schäumtechnologien für FKV-Sandwich-Verbunde im Spritzgießverfahren. Master Thesis, Darmstadt
190. Gonzalez Jr, H. (1976) Efficiency of foams in stiffness applications. Journal of Cellular Plastics 12(1): 49–58
191. Hobbs, S. Y. (1976) Predicting the flexural rigidity of thermoplastic structural foams. Journal of Cellular Plastics 12(5): 258–263
192. Gross, D. (2009) Technische Mechanik, 10., neu bearbeitete Aufl. Springer-Lehrbuch. Springer, Berlin
193. Gibson, L. J., Ashby, M. F. (2010) Cellular solids: Structure and properties, 2. ed., 1. paperback ed. (with corr.), transferred to digital print. Cambridge solid state science series. Cambridge Univ. Press, Cambridge
194. Shutov, F. A., Henrici-Olivé, G., Olivé, S. (eds) (1986) Integral/Structural Polymer Foams: Technology, Properties and Applications. Springer Berlin Heidelberg, Berlin, Heidelberg, s.l.
195. Luo, J., Stevens, R. (1999) Porosity-dependence of elastic moduli and hardness of 3Y-TZP ceramics. Ceramics International 25(3): 281–286. doi: 10.1016/S0272-8842(98)00037-6
196. Wagh, A. S., Poeppel, R. B., Singh, J. P. (1991) Open pore description of mechanical properties of ceramics. Journal of Materials Science 26(14): 3862–3868. doi: 10.1007/BF01184983
197. Moore, D. R., Couzens, K. H., Iremonger, M. J. (1974) The Deformational Behaviour of Foamed Thermoplastics. Journal of Cellular Plastics 10(3): 135–139. doi: 10.1177/0021955X7401000307
198. Carlsson, L. A., Sendlein, L. S., Merry, S. L. (1991) Characterization of Face Sheet/Core Shear Fracture of Composite Sandwich Beams. Journal of Composite Materials 25(1): 101–116. doi: 10.1177/002199839102500105
199. Carlsson, L. A. (1991) On the Design of the Cracked Sandwich Beam (CSB) Specimen. Journal of Reinforced Plastics and Composites 10(4): 434–444. doi: 10.1177/073168449101000407
200. Carlsson, L. A., Prasad, S. (1993) Interfacial fracture of sandwich beams. Engineering Fracture Mechanics 44(4): 581–590. doi: 10.1016/0013-7944(93)90100-7
201. Prasad, S., Carlsson, L. A. (1994) Debonding and crack kinking in foam core sandwich beams—I. Analysis of fracture specimens. Engineering Fracture Mechanics 47(6): 813–824. doi: 10.1016/0013-7944(94)90061-2
202. Cantwell, W. J., Davies, P. (1996) A study of skin-core adhesion in glass fibre reinforced sandwich materials. Appl Compos Mater 3(6): 407–420. doi: 10.1007/BF00133683
203. Li, Xiaoming and Carlsson, Leif A (ed) (1998) A Test Specimen for Determining The Fracture Resistance of a Facing Core Interface
204. LI, X., Carlsson, L. A. (2000) Elastic Foundation Analysis of Tilted Sandwich Debond (TSD) Specimen. Jnl of Sandwich Structures & Materials 2(1): 3–32. doi: 10.1177/109963620000200101
205. Kawashita, L. F., Moore, D. R., Williams, J. G. (2004) The develoment of a mandrel peel test for the measurement of adhesive fracture toughness of epoxy-metal laminates. The Journal of Adhesion 80(3): 147–167. doi: 10.1080/00218460490279215

206. Kawashita, L. F., Kinloch, A. J., Moore, D. R. et al. (2006) A critical investigation of the use of a mandrel peel method for the determination of adhesive fracture toughness of metal-polymer laminates. Engineering Fracture Mechanics 73(16): 2304–2323. doi: 10.1016/j.engfracmech.2006.04.025
207. Østergaard, R. C., Sørensen, B. F. (2007) Interface crack in sandwich specimen. Int J Fract 143(4): 301–316. doi: 10.1007/s10704-007-9059-4
208. Avilés, F., Carlsson, L. A. (2008) Analysis of the sandwich DCB specimen for debond characterization. Engineering Fracture Mechanics 75(2): 153–168. doi: 10.1016/j.engfracmech.2007.03.045
209. Weaver C. (2009) Evaluation of Mode I Fracture Mechanics Test Methods For Sandwich Composites. Master Thesis, Salt lake City
210. Ramantani, D. A., Moura, M.F.S.F. de, Campilho, R.D.S.G. et al. (2010) Fracture characterization of sandwich structures interfaces under mode I loading. Composites Science and Technology 70(9): 1386–1394. doi: 10.1016/j.compscitech.2010.04.018
211. Ratcliffe, J. G., Reeder, J. R. (2011) Sizing a single cantilever beam specimen for characterizing facesheet–core debonding in sandwich structure. Journal of Composite Materials 45(25): 2669–2684. doi: 10.1177/0021998311401116
212. Nettles, A. T., Gregory, E. D., Jackson, J. R. (2016) Using the Climbing Drum Peel (CDP) Test to Obtain a G IC Value for Core/Face Sheet Bonds. Journal of Composite Materials 41(24): 2863–2876. doi: 10.1177/0021998307079974
213. da Silva, L.F.M. (2006) Influence of the Adhesive, the Adherend and the Overlap on the Single Lap Shear Strength. Journal of Adhesion and Interface Vol.7(No.4)
214. Grant, L.D.R., Adams, R. D., da Silva, L. F.M. (2009) Experimental and numerical analysis of single-lap joints for the automotive industry. International Journal of Adhesion and Adhesives 29(4): 405–413. doi: 10.1016/j.ijadhadh.2008.09.001
215. Manalo, A. C. (2013) Behaviour of fibre composite sandwich structures under short and asymmetrical beam shear tests. Composite Structures 99: 339–349. doi: 10.1016/j.compstruct.2012.12.010
216. Adams, D., Bluth, Z., Braegger, R. (2013) Development and Evaluation of Fracture Mechanics Test Methods for Sandwich Composites. 2013 Technical Review, Utah
217. Feraboli P.J., KEDWARD K.T. (Nineteenth technical conference ; 2004, Hilton Hotel, Atlanta, Georgia) In Search of the True Interlaminar Shear Strength. Proceedings of the joint American Society for Composites/American Society for Testing and Materials Committee D 30. DEStech Publications, Lancaster, Pa.
218. Kadlec, M., Nováková, L., Růžek, R. (2014) An Experimental Investigation of Factors Considered for the Short Beam Shear Strength Evaluation of Carbon Fiber–reinforced Thermoplastic Laminates. J. Test. Eval. 42(3): 20120043. doi: 10.1520/JTE20120043
219. Gross, D., Seelig, T. (2007) Bruchmechanik: Mit einer Einführung in die Mikromechanik ; mit 8 Tabellen, 4., bearb. Aufl. Springer, Berlin
220. Brocks W. (ed) (2018) Plasticity and Fracture. Solid Mechanics And Its Applications. Springer International Publishing, Cham
221. Griffith, A. A. (1921) The Phenomena of Rupture and Flow in Solids. Philosophical Transactions of the Royal Society A: Mathematical, Physical and Engineering Sciences 221(582-593): 163–198. doi: 10.1098/rsta.1921.0006
222. Lubin G. (ed) (1982) Handbook of Composites. Springer US, Boston, MA

223. Cantwell W. J. (1994) A test technique for assessing core-skin adhesion in composite sandwich structures. Journal of Materials Science Letters (13): 203–205
224. Patra, A., Mitra, N. (2014) Interface fracture of sandwich composites: Influence of MWCNT sonicated epoxy resin. Composites Science and Technology 101: 94–101. doi: 10.1016/j.compscitech.2014.07.006
225. Pietrek, M., Horst, P. (2018) Determination of the fracture toughness of debonded asymmetric sandwich beams with a thin-walled skin considering plastic deformation. Engineering Fracture Mechanics 188: 217–231. doi: 10.1016/j.engfracmech.2017.08.025
226. Ozdil, F., Carlsson, L. A. (1999) Beam analysis of angle-ply laminate DCB specimens. Composites Science and Technology 59(2): 305–315. doi: 10.1016/S0266-3538(98)00069-4
227. Shah, O. R., Tarfaoui, M. (2017) Determination of mode I & II strain energy release rates in composite foam core sandwiches. An experimental study of the composite foam core interfacial fracture resistance. Composites Part B: Engineering 111: 134–142. doi: 10.1016/j.compositesb.2016.11.044
228. He, M.-Y., Bartlett, A., Evans, A. G. et al. (1991) Kinking of a Crack out of an Interface: Role of In-Plane Stress. J American Ceramic Society 74(4): 767–771. doi: 10.1111/j.1151-2916.1991.tb06922.x
229. Echtermeyer, A.T. and McGeorge, D (ed) (1998) Fracture Toughness of Core Skin Interfaces of Sandwich Materials, vol 2
230. McGarva, L. D., Åström, B. T. (1999) Experimental investigation of compression moulding of glass/PA12-PMI foam core sandwich components. Composites Part A: Applied Science and Manufacturing 30(10): 1171–1185. doi: 10.1016/S1359-835X(99)00028-7
231. Li, S., Thouless, M. D., Waas, A. M. et al. (2006) Mixed-mode cohesive-zone models for fracture of an adhesively bonded polymer–matrix composite. Engineering Fracture Mechanics 73(1): 64–78. doi: 10.1016/j.engfracmech.2005.07.004
232. Shen, Y.-o., Cantwell, W., Li, Y. (2014) Skin-core adhesion in high performance sandwich structures. J. Zheijang Univ.-Sci. 15(1): 61–67. doi: 10.1631/jzus.A1300283
233. Shivakumar, K. N., Smith, S. A. (2004) In Situ Fracture Toughness Testing of Core Materials in Sandwich Panels. Journal of Composite Materials 38(8): 655–668. doi: 10.1177/0021998304042392
234. Cantwell, W. (1999) Interfacial fracture in sandwich laminates. Composites Science and Technology 59(14): 2079–2085. doi: 10.1016/S0266-3538(99)00065-2
235. J.L. Grenestedt (1996) The Tilted Sandwich Debond Specimen. personal communication
236. LI, X., Carlsson, L. A. (1999) The Tilted Sandwich Debond (TSD) Specimen for Face/Core Interface Fracture Characterization. Jnl of Sandwich Structures & Materials 1(1): 60–75. doi: 10.1177/109963629900100104
237. LI, X., Carlsson, L. A. (2001) Fracture Mechanics Analysis of Tilted Sandwich Debond (TSD) Specimen. Journal of Composite Materials 35(23): 2145–2168. doi: 10.1106/J9XM-GFRJ-J87Q-FPLU
238. Saha, M. C., Kabir, E., Jeelani, S. (2008) Study of debond fracture toughness of sandwich composites with nanophased core. Materials Letters 62(4-5): 567–570. doi: 10.1016/j.matlet.2007.06.017
239. Zenkert, D. (1991) Strength of sandwich beams with interface debondings. Composite Structures 17(4): 331–350. doi: 10.1016/0263-8223(91)90025-T
240. Müller, M., Herák, D. (2010) Dimensioning of the bonded lap joint. Res. Agr. Eng. 56(No. 2): 59–68. doi: 10.17221/35/2009-RAE

241. Farmand-Ashtiani, E., Cugnoni, J., Botsis, J. (2013) Monitoring and characterization of the interfacial fracture in sandwich composites with embedded multiplexed optical sensors. Composite Structures 96: 476–483. doi: 10.1016/j.compstruct.2012.08.059
242. D14 Committee Test Method for Climbing Drum Peel for Adhesives
243. DIN (1982) DIN 53295: Prüfung von Kernverbunden; Trommel-Schälversuch
244. DIN (2005) DIN EN 2243-3:2006-10: Luft- und Raumfahrt - Nichtmetallische Werkstoffe - Strukturelle Klebstoffsysteme - Prüfverfahren - Teil 3: Trommelschälversuch für Wabenkernverbunde;
245. D30 Committee Test Method for Mode I Interlaminar Fracture Toughness of Unidirectional Fiber-Reinforced Polymer Matrix Composites
246. Ural, A., Zehnder, A. T., Ingraffea, A. R. (2003) Fracture mechanics approach to facesheet delamination in honeycomb: Measurement of energy release rate of the adhesive bond. Engineering Fracture Mechanics 70(1): 93–103. doi: 10.1016/S0013-7944(02)00024-3
247. He, M.-Y., Hutchinson, J. W. (1989) Kinking of a Crack Out of an Interface. J. Appl. Mech. 56(2): 270. doi: 10.1115/1.3176078
248. Glaessgen, E. H., Reeder, J. R., Sleight, D. W. et al. (2005) Debonding Failure of Sandwich-Composite Cryogenic Fuel Tank with Internal Core Pressure. Journal of Spacecraft and Rockets 42(4): 613–627. doi: 10.2514/1.5567
249. Grouve, W.J.B., Warnet, L. L., Akkerman, R. (2013) Critical assessment of the mandrel peel test for fiber reinforced thermoplastic laminates. Engineering Fracture Mechanics 101: 96–108. doi: 10.1016/j.engfracmech.2012.07.005
250. Kawashita, L. F., Moore, D. R., Williams, J. G. (2005) Comparison of Peel Tests for Metal–Polymer Laminates for Aerospace Applications. The Journal of Adhesion 81(6): 561–586. doi: 10.1080/00218460590954557
251. Grouve, W. J. B., Warnet, L., Akkerman, R. et al. (2010) Weld Strength Assessment for Tape Placement. Int J Mater Form 3(S1): 707–710. doi: 10.1007/s12289-010-0868-z
252. Grouve, W.J.B., Warnet, L. L., Rietman, B. et al. (2012) On the weld strength of in situ tape placed reinforcements on weave reinforced structures. Composites Part A: Applied Science and Manufacturing 43(9): 1530–1536. doi: 10.1016/j.compositesa.2012.04.010
253. DIN (1984) DIN 53494:1984-05: Galvanische Überzüge; Prüfung von galvanisierten Kunststoffteilen; Bestimmung der Abzugkraft(53494)
254. DIN EN (2015) DIN EN 1372:2015-06: Adhesives - Test method for adhesives for floor and wall coverings - Peel test(1372)
255. DIN (1982) DIN 53292:1982-02: Prüfung von Kernverbunden; Zugversuch senkrecht zur Deckschichtebene
256. Abali, F., Pora, A., Shivakumar, K. (2016) Modified Short Beam Shear Test for Measurement of Interlaminar Shear Strength of Composites. Journal of Composite Materials 37(5): 453–464. doi: 10.1177/0021998303037005053
257. Stokes-Griffin, C. M., Compston, P. (2015) The effect of processing temperature and placement rate on the short beam strength of carbon fibre–PEEK manufactured using a laser tape placement process. Composites Part A: Applied Science and Manufacturing 78: 274–283. doi: 10.1016/j.compositesa.2015.08.008
258. Johnson, W. S., Masters, J. E., Adams, D. F. et al. (1995) Experimental Study of Three- and Four-Point Shear Test Specimens. J. Compos. Technol. Res. 17(4): 341. doi: 10.1520/CTR10454J
259. Robert A. Heller (1968) Interlaminar Shear Stress in Sandwich Beams. SESA Fall Meeting, San Francisco

260. Ageorges, C., Ye, L., Mai, Y.-W. et al. (1998) Characteristics of resistance welding of lap-shear coupons. Part III. Crystallinity. Composites Part A: Applied Science and Manufacturing 29(8): 921–932. doi: 10.1016/S1359-835X(98)00024-4
261. Kafkalidis, M. S., Thouless, M. D. (2002) The effects of geometry and material properties on the fracture of single lap-shear joints. International Journal of Solids and Structures 39(17): 4367–4383. doi: 10.1016/S0020-7683(02)00344-X
262. Banea, M. D., da Silva, L. F. M. (2009) Adhesively bonded joints in composite materials: An overview. Proceedings of the IMechE 223(1): 1–18. doi: 10.1243/14644207JMDA219
263. Feraboli, P., Kedward, K. T. (2003) Four-point bend interlaminar shear testing of uni- and multi-directional carbon/epoxy composite systems. Composites Part A: Applied Science and Manufacturing 34(12): 1265–1271. doi: 10.1016/S1359-835X(03)00204-5
264. Whitney, J. M., Browning, C. E. (1985) On short-beam shear tests for composite materials. Experimental Mechanics 25(3): 294–300. doi: 10.1007/BF02325100
265. Composite materials handbook. SAE International on behalf of CMH-17, a division of Wichita State University, [Warrendale, Pa.] 2012
266. D14 Committee Test Method for Apparent Shear Strength of Single-Lap-Joint Adhesively Bonded Metal Specimens by Tension Loading (Metal-to-Metal)
267. D14 Committee Test Method for Determining Strength of Adhesively Bonded Rigid Plastic Lap-Shear Joints in Shear by Tension Loading
268. D14 Committee Test Method for Lap Shear Adhesion for Fiber Reinforced Plastic (FRP) Bonding
269. Kline, D. B., Wool, R. P. (1988) Polymer welding relations investigated by a lap shear joint method. Polym Eng Sci 28(1): 52–57. doi: 10.1002/pen.760280109
270. Villegas, I. F., Palardy, G. (2016) Ultrasonic Welding of Thermoplastic Composite Coupons for Mechanical Characterization of Welded Joints through Single Lap Shear Testing. J Vis Exp(108): e53592. doi: 10.3791/53592
271. Silva L. F. M. d. (ed) (2011) Handbook of adhesion technology, 1. ed. Springer
272. Volkersen O. (1938) Die Nietkraftverteilung in zugbeanspruchten Nietverbindungen mit konstanten Laschenquerschnitten. Luftfahrtforschung(15): 41–47
273. Habenicht, G. (2009) Kleben: Grundlagen, Technologien, Anwendungen, 6., aktual. Aufl. VDI-Buch. Springer, Berlin
274. Özer, H. (2018) Introductory Chapter: Structural Adhesive Bonded Joints. In: Özer H (ed) Applied Adhesive Bonding in Science and Technology. InTech
275. DIN (1998) DIN EN ISO 14125:1998: Faserverstärkte Kunststoffe - Bestimmung der Biegeeigenschaften
276. D14 Committee Test Method for Strength Properties of Adhesives in Shear by Tension Loading of Single-Lap-Joint Laminated Assemblies
277. D20 Committee Test Method for In-Plane Shear Strength of Reinforced Plastics
278. Wang, Y., Dong, Q., Liu, X. (2007) Mode 1 Interlaminar Fracture Behaviour of Continuous Glass Fibre/ Polypropylene Composites Based on Commingled Yarn. Polymers and Polymer Composites 15(3): 229–239. doi: 10.1177/096739110701500307
279. Ehrenstein, G. W., Riedel, G., Trawiel, P. (op. 2004) Thermal analysis of plastics: Theory and practice. Hanser; Hanser Gardner Publications [distributor], Munich, Cincinnati
280. DIN (2018) DIN EN ISO 11357-3:2018: Kunststoffe - Dynamische Differenz-Thermoanalyse (DSC) - Teil 3: Bestimmung der Schmelz- und Kristallisationstemperatur und der Schmelz- und Kristallisationsenthalpie
281. Polymer Microscopy. Springer New York, New York, NY 2008

282. Moneke, M. (2016) Werkstoffwissenschaften, Darmstadt
283. Mönnich, S. (2015) Entwicklung einer Methodik zur Parameteridentifikation für Orientierungsmodelle in Spritzgießsimulationen. Dissertation, Magdeburg
284. MOLDFLOW (2018) Thermal characterisation of fibre reinforced thermoplastics in MOLDFLOW INSIGHT 2019. Email
285. Clariant (2018) Foam nucleation density of Hydrocerol 822. Telephone
286. Brian Y. Lattimer, Thomas W. Goodrich, Jillian Chodak, and Christopher Cain (2009) Properties of composite materials for modeling high temperature response, Virginia Tech, Department of Mechanical Engineering
287. Celanese (2018) Celstran® CFR-TP PP GF60-13 Datenblatt
288. Ehrenstein, G. W., Pongratz, S. (2007) Beständigkeit von Kunststoffen. Carl Hanser Verlag GmbH & Co. KG, München
289. Greenhalgh, E. S. (2009) Failure analysis and fractography of polymer composites, 1. publ. Woodhead publishing in materials. CRC Press, Boca Raton, Fla.
290. Spearing, S. M., Evans, A. G. (1992) The role of fiber bridging in the delamination resistance of fiber-reinforced composites. Acta Metallurgica et Materialia 40(9): 2191–2199. doi: 10.1016/0956-7151(92)90137-4
291. Feih, S., Wei, J., Kingshott, P. et al. (2005) The influence of fibre sizing on the strength and fracture toughness of glass fibre composites. Composites Part A: Applied Science and Manufacturing 36(2): 245–255. doi: 10.1016/j.compositesa.2004.06.019
292. Clariant (2017) Datasheet: Hydrocerol® ITP 822
293. Wörndle, R., Steinbichler, G., Egger, P. et al. (2001) Thermoplastische Träume durch Schäume. Wirtschaftliches Schaumspritzgießen für individuelle Bauteileigenschaften. Kunststoffe 91: 64–67
294. Rahner S. (2017) Leichtbau leicht umgesetzt: Neuheiten beim physikalischen Schaumspritzgießen und Faser-Direkt-Compoundieren. K_PROFI(3-4): 48–49
295. Neue Materialien Bayreuth GmbH (2015) Spritzgießtechnologie @ Polymer Engineering: Verfahren, Spritzgießmaschinen und Werkzeuge
296. SABIC Europe B.V. (2017) Base polymer of SABIC® PPcompound 15T1020. Oral
297. McInerney, L. F., Kao, N., Bhattacharya, S. N. (2003) Melt strength and extensibility of talc-filled polypropylene. Polym Eng Sci 43(12): 1821–1829. doi: 10.1002/pen.10154
298. C. Lau, H., Bhattacharya, S., J. Field, G. (1998) Melt strength of polypropylene: Its relevance to thermoforming. Polym Eng Sci 38. doi: 10.1002/pen.10362
299. Yu, C., Wang, Y., Wu, B. et al. (2011) Evaluating the foamability of polypropylene with nitrogen as the blowing agent. Polymer Testing 30(8): 887–892. doi: 10.1016/j.polymertesting.2011.08.014
300. Huajie Shi (ed) (2017) CONSOLIDATION MODEL FOR OPTIMIZATION OF THERMOPLASTIC COMPOSITE LAMINATION PROCESSES
301. Mitsui Chemicals Group Mitsui Chemicals CF/PP-UD-Tape: Datasheet
302. SABIC Europe B.V. SABIC® PP 576P PP homopolymer for Injection moulding: Datasheet
303. Kepeng Qiu (2008) Analysis and optimal design of lightweight sandwich structures and materials. Dissertation, Belfort-Montbéliard
304. Puck, A. (1967) Zur Beanspruchung und Verformung von GFK-Mehrschichtenverbund-Bauelementen .: T. 1. Grundlagen d. Spannungs- u. Verformungsanalyse. T. 2. Spannungs- u. Verformungsanalyse an GFK-Wickelrohren unter Überdruck. T. 3. Versuche an Mehrschichtenverbunden. Dissertation, Berlin

305. Schultz R. (2012). Aluminum Week, Chicago
306. Berezowsky T. (2012) From Mild To High-Strength: Cost/Benefit of Automotive Steel Today. https://agmetalminer.com/2012/11/01/from-mild-to-high-strength-costbenefit-of-automotive-steel-today/
307. MacKenzie D. (2018) What would steel and aluminum tariffs mean for automobile costs, materials choice, and fuel economy? https://faculty.washington.edu/dwhm/2018/03/05/what-would-steel-and-aluminum-tariffs-mean-for-automobile-costs-materials-choice-and-fuel-economy/. Accessed 28 Nov 2019
308. Stodolsky, F., Vyas, A., Cuenca, R. et al. (1995) Life-Cycle Energy Savings Potential from Aluminum-Intensive Vehicles. In: SAE International400 Commonwealth Drive, Warrendale, PA, United States

## Supervised Theses

| Date | Author | Title | Insitute, University |
|---|---|---|---|
| 04/2015 | Wettling, J. | Middle-layer injection moulding of continuous fibre-reinforced semi-finished products | Institute for Polymer Technology, University of Applied Sciences Darmstadt |
| 11/2015 | Graupner, N.B., | Systematic investigation of the bonding quality of different facesheets to the core of a FRP sandwich structure as a function of manufacturing parameters | System Reliability, Adaptive Structures, and Machine Acoustics, Technical University Darmstadt |
| 09/2016 | Fornoff, M. | Prediction of shrinkage and warpage and the connection quality at organosheed reinforced hybrid plastic parts | Institute for Polymer Technology, University of Applied Sciences Darmstadt |
| 09/2017 | Lebsack, D. | Investigation of the influence of various parameters on the bond strength of thermoplastic composite sandwich structures | Institute for Polymer Technology, University of Applied Sciences Darmstadt |
| 10/2017 | Geiling, M. | Investigation of physical and chemical blowing agents for FRP sandwich composites based on injection moulding | Institute for Polymer Technology, University of Applied Sciences Darmstadt |
| 05/2018 | Sauer, J. | Investigation of bonding mechanisms and damage processes of compact polypropylene sandwich structures | Institute for Polymer Technology, University of Applied Sciences Darmstadt |
| 05/2018 | Friedrich, M. | Innovative joining processes and functional integration for thermoplastic FRP sandwich structures | Institute for Polymer Technology, University of Applied Sciences Darmstadt |
| 06/2018 | Wybierek, P. | Investigation of various influencing factors on spring-in and shrinkage in foam injection moulded FRP sandwich composites | Institute for Polymer Technology, University of Applied Sciences Darmstadt |
| 06/2018 | Trippel, S. | Validation of an injection molding simulation for the analysis of the thermoplastic foam injection moulding process | Institute for Polymer Technology, University of Applied Sciences Darmstadt |

# Annex A

## Interface Temperature of In-Situ CFRTP Sandwich Moulding: Simulation and Experiment

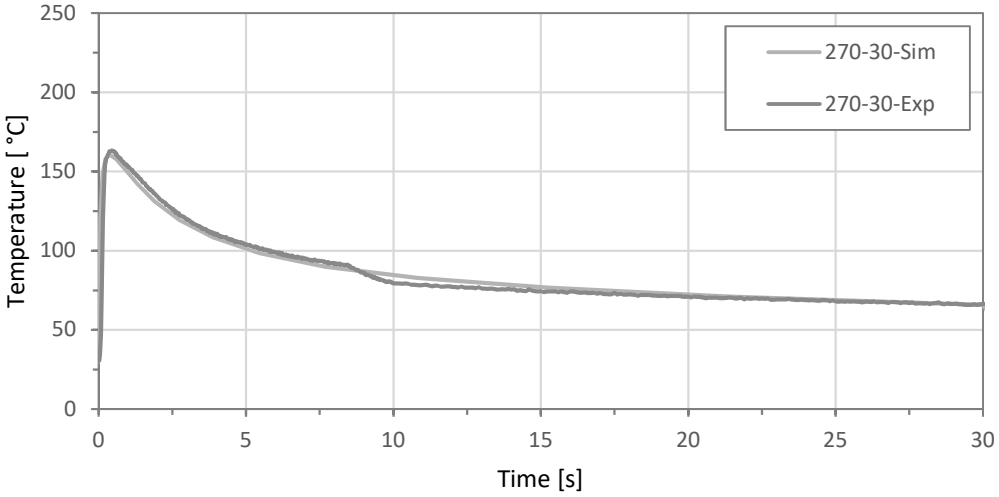


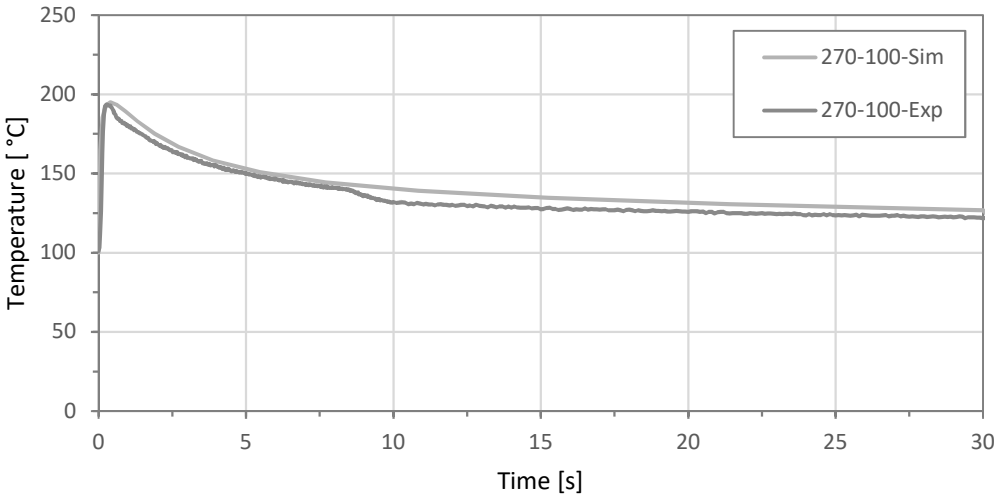

## Interface Temperature of In-Situ CFRTP Sandwich Moulding: Specimens with 1UD and 2UD Facesheets

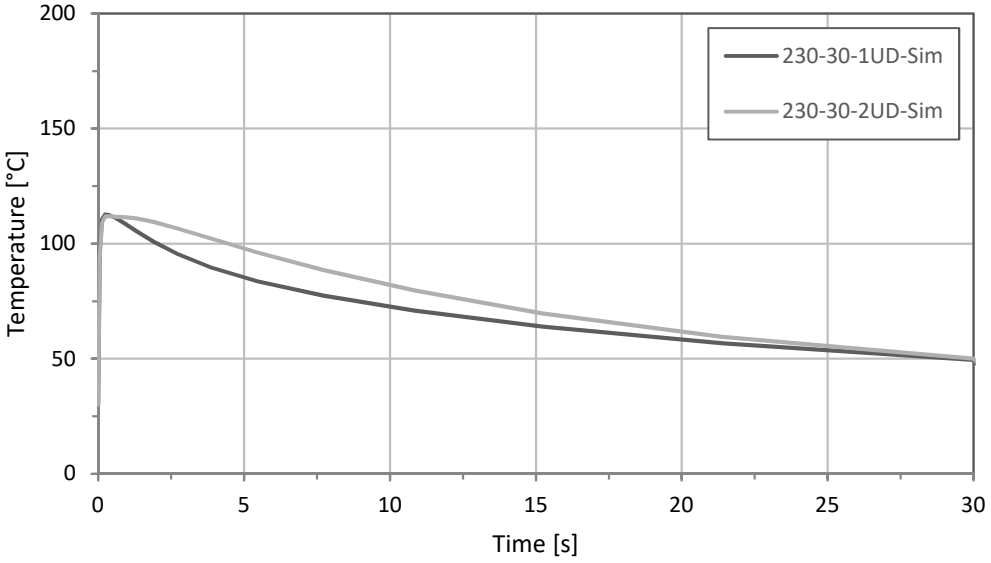


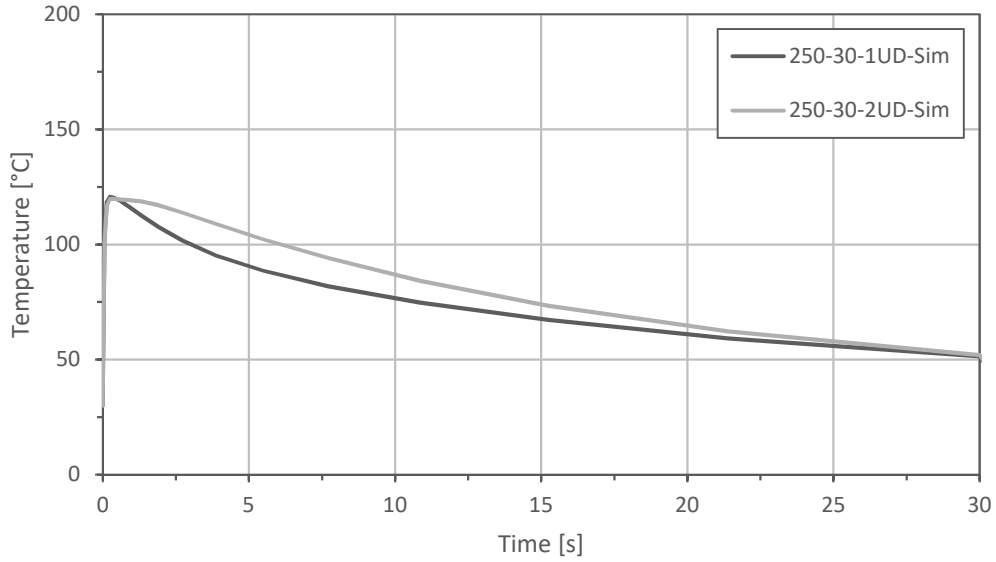

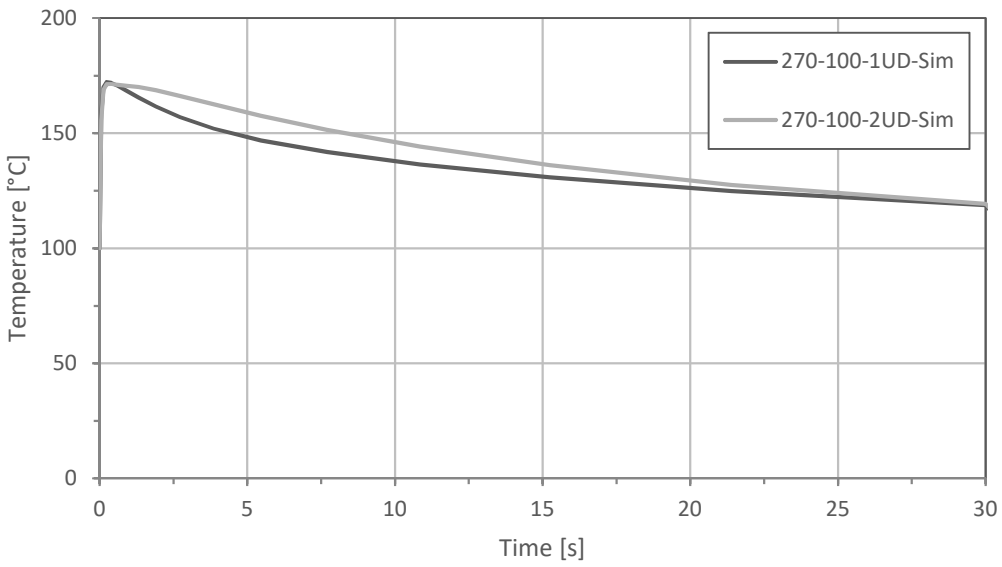
200
150
100
50
0
Temperature [°C]
0
5
10
15
20
25
30
Time [s]
270-100-1UD-Sim
270-100-2UD-Sim

# Annex B

## DSC Measurements

### DSC of as-received UD Tape Celstran® CFR-TP PP GF60-13

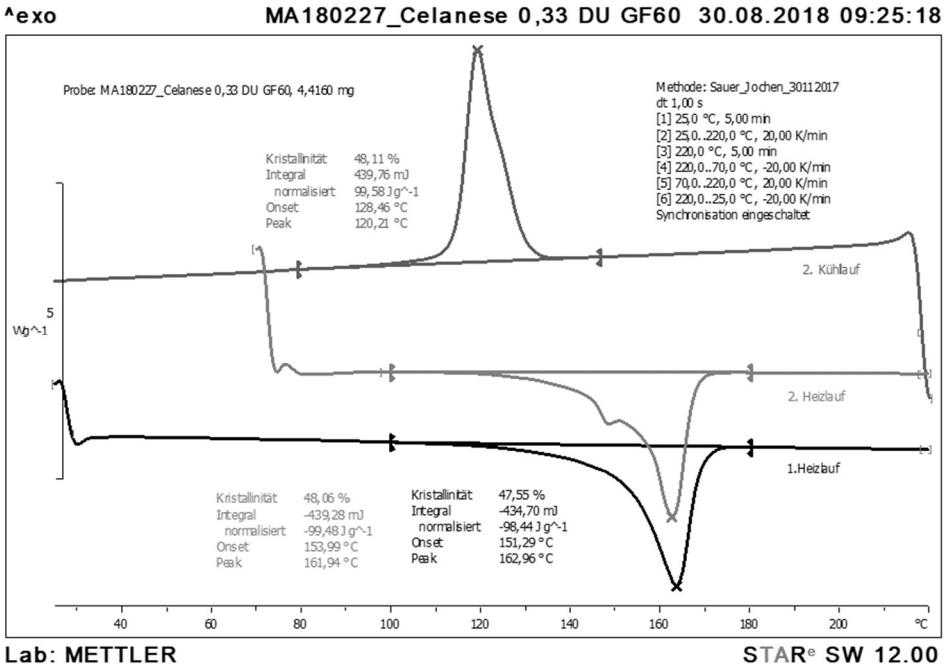


### DSC of consolidated 2UD Tape Celstran® CFR-TP PP GF60-13

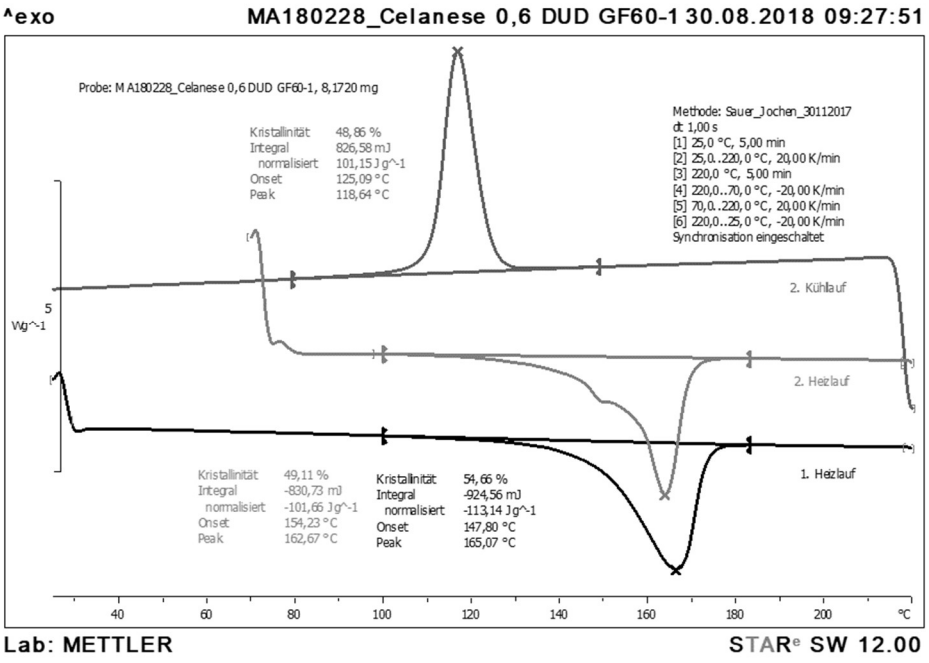

## DSC of annealed 1UD-HC Tape Celstran® CFR-TP PP GF60-13

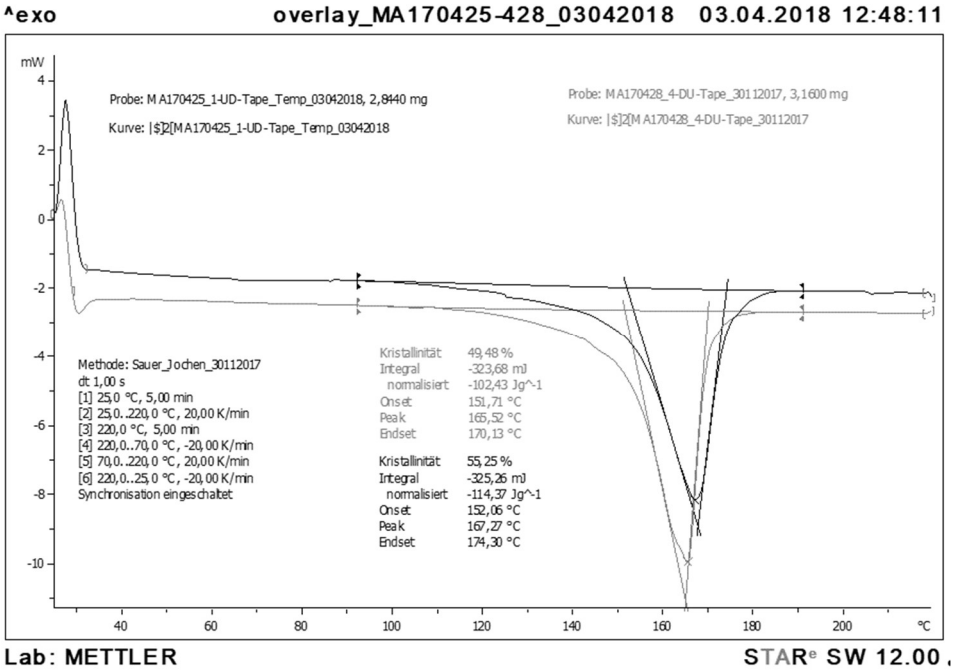

# Curriculum Vitae

## *Person*

| | |
|---|---|
| Name: | Felix Christian Weidmann |
| Date of Birth: | 25.11.1984 |
| Place of Birth: | Weinheim |

## *Academic Education*

04/2017 – 04/2020 Clausthal University of Technology (TU Clausthal), Institute of Polymer Materials and Plastic Engineering (PuK)

**Thesis:** On the in-situ manufacture of thermoplastic sandwich structures with continuous fibre reinforced facesheets and integral foam cores

**Degree**: Doctor of Engineering (Dr.-Ing.)

11/2008 – 04/2012 Technical University of Darmstadt (TU Darmstadt), Institute for Lightweight Construction and Design (KluB)

**Thesis**: Optimisation of a method for the production of fibre blends (OLaF) in a continuous process and experimental evaluation of the crack stopping effect of the fibre blends in fatigue-loaded UD glass fibre plastic samples

**Degree**: Master of Science (M.Sc.), Diplomingenieur (Dipl.-Ing.)

10/2003 – 11/2008 Technical University of Darmstadt (TU Darmstadt), Institute of Ergonomics (IAD)

**Thesis:** Execution and evaluation of driving tests to determine driver inattention based on vehicle data

**Degree**: Bachelor of Science (B.Sc.)

## *Professional Experience*

01/2018 – current Fraunhofer Institute for Structural Durability and System Reliability LBF

**Occupation**: Team Leader Thermoplastic Composite Systems

09/2012 – 12/2017 Fraunhofer Institute for Structural Durability and System Reliability LBF

**Occupation**: Research Associate

| | |
|---|---|
| 10/2013 – current | Baden-Wuerttemberg Cooperative State University (DHBW) Mosbach |
| | **Occupation:** Lecturer |
| 04/2010 – 08/2010 | Technical University of Darmstadt (TU Darmstadt), Institute for Lightweight Construction and Design (KluB) |
| | **Occupation**: Research Assistant |
| 11/2009 – 03/2010 | Canyon Bicycles GmbH |
| | **Occupation:** Internship |

### *Further Qualifications*

| | | |
|---|---|---|
| Languages: | German: | native |
| | English: | fluent |
| | French: | conversational |
| | Spanish: | basic |
| Software: | MS-Office | advanced |
| | Solid Works | advanced |
| | Citavi | advanced |
| | Moldflow | intermediate |
| | Cadmould | intermediate |
| | Python | basic |

# Publications

| # | Topic | Magazine or Platform | Author | Date | Type[1] |
|---|---|---|---|---|---|
| 1 | History and future trends of plastics in automotive industry | 2nd Summer School, Stockholm Sweden | Author | 17.10.2013 | GC |
| 2 | How to create a micro-climate around the passengers to dispense with climatizing the entire cabin" | Joint XERIC-JOSPEL-OPTEMUS EU Cluster Workshop, Bologna Italy | Author | 24.11.2016 | WS |
| 3 | Insulating sandwich housing structures for the thermal management of battery packs | Twelfth International Conference on Ecological Vehicles and Renewable Energies (EVER), Monaco | Author | 12.4.2017 | SC |
| 4 | Using a traction battery as thermal storage | ATZ worldwide January 2018, Volume 120, Issue 1, pp 62–67 | Co-Author | 2018 | A |
| 5 | Using a Traction Battery as Thermal Storage | 27th Aachen Colloquium Automobile and Engine Technology 2018 | Co-author | 09.10.2018 | SC |
| 6 | Thermisch speicherfähige Traktionsbatterie ermöglicht höhere und konstantere Reichweite | eMobilJournal 02/19 pp 104 - 109 | Author | 2019 | A |
| 7 | Functionalized thermoplastic sandwich composites within minutes | JEC Europe, Paris Nord Villepinte | Author | 12. – 14.3.2019 | TF |

[1] B: A: Magazine Article, GC: General Conference, WS: Workshop, SC: Scientific Conference, TF: Trade Fair

# Acknowledgements

Diese Arbeit entstand während meiner Tätigkeit am Fraunhofer LBF, wo ich seit Mitte 2012 als wissenschaftlicher Mitarbeiter und seit Anfang 2018 als Teamleiter beschäftigt bin.

Zunächst gilt mein Dank Herrn Professor Dr. Ziegmann, welcher mir die Möglichkeit gab an seinem Fachgebiet zu promovieren. Ohne die hervorragende fachliche sowie sehr herzliche Betreuung, wäre die vorliegende Arbeit nicht möglich gewesen. Ebenso möchte ich mich bei Herrn Professor Dr. Wieser bedanken, der die in dieser Arbeit untersuchte hybride Verfahrenstechnik erdacht und ebenso die Betreuung als zweiter Gutachter übernommen hat. Darüber hinaus möchte ich mich bei Herrn Professor Dr. Palkowski für den Vorsitz der Promotionskommission bedanken. Weiterhin möchte ich meinen Dank Herrn Professor Dr. Bein aussprechen, der es mir ermöglicht hat, im Rahmen des Projekts OPTEMUS zu promovieren sowie mich im Bereich Elektromobilität fachlich und beruflich weiterzuentwickeln. Nicht zuletzt möchte ich Herrn Professor Dr. Helmut Schürmann dankbar erwähnen, der durch vorbildliche Lehre und wissenschaftliche Betreuung mein Interesse an Faserverbunden während des Studiums weckte und mich auf einen Weg führte, auf welchem diese Arbeit womöglich nur ein Zwischenziel darstellt.

Da die vorliegende Arbeit im Rahmen des OPTEMUS Projekts entstand, möchte ich weiterhin Dr. Alois Steiner, der das Projekt wunderbar leitete, sowie Alberto Maria Merlo und dem ganzen OPTEMUS Konsortium meinen Dank aussprechen. Es war stets im positiven Sinne herausfordernd und hat mir viele schöne und interessante Erfahrungen beschert. Ich denke dabei vor allem an Bologna, aber auch an Monaco und natürlich an Turin.

Seit den Anfängen der Entwicklung und Untersuchung des In-Situ CFRTP Verfahrens, haben mich eine Vielzahl fleißiger Studenten und Studentinnen unterstützt. Dabei möchte ich mich vor allem bei Nico-Benedict Graupner bedanken, mit dem ich bis heute an dieser Verfahrenstechnik und deren Anwendung arbeite. In diesem Zusammenhang sei auch Marcel Knorr genannt, der das Dreigespann junger ambitionierter Ingenieure vervollständigte und mir vor allem bei der Korrektur der vorliegenden Arbeit eine verlässliche Hilfe und großer Rückhalt war. Weiterhin möchte ich mich bei Mandy Geiling und Daniel Lebsack bedanken, die einen großen Beitrag zum Verständnis des In-Situ Prozesses geleistet haben. Spätere Studenten-Generationen seien auch erwähnt: Jochen Sauer und Sebastian Trippel, die sich mit der Anbindung von CFRTP und überspritzten Kunststoffmassen sowie mit der Simulation des In-Situ Prozesses beschäftigten. Mit den guten Arbeiten von Marten Friedrich und Patrick-Dave Wybierek, die sich auf erweiterte Themen des In-Situ Prozess konzentrierten, schließt sich die Gruppe studentischer Arbeiten im Umfeld dieser Arbeit.

In den vergangenen Jahren habe ich auch von vielen Kollegen großartige Unterstützung erfahren, insbesondere in den Doktorandenkolloquien. Hierbei gilt mein besonderer Dank Dr. Felix Dillenberger, Markus Fornoff und Tamara van Roo, die auch in den zahlreichen Probekolloquien Ausdauer bewiesen. Auch außerhalb des erwähnten Kolloquiums wurde ich fachlich großartig von Dr. Guru Geertz sowie Alexander Klumpp unterstützt. Weiterhin war mir Axel Nierbauer wie auch Daniel Fritz bei der Erstellung von µCT-Aufnahmen und bei der Durchführung mechanischer Prüfungen eine große Hilfe. Bei der Vor- und Nachbearbeitung der Prüfkörper konnte ich mich stets auf Steffen Koch, Alexander Perez und Arno Hirschel verlassen. Die Herstellung der in-Situ Prüfkörper selbst sowie die anspruchsvolle Ermittlung der Interfacetemperaturen wäre ohne die stets offene und mitdenkende Art von Herrn Harald Dörr sowie die Arbeit und Expertise von Joachim Amberg nicht möglich

gewesen. Und nicht zuletzt gilt mein Dank Ines Roth, die mir immer den Rücken freigehalten hat sowie Alexandra Kreickenbaum, für ihr stets offenes Ohr.

Neben den fachlichen Aspekten meiner Tätigkeit am Fraunhofer LBF, soll die zwischenmenschliche Seite hier auch berechtigte Erwähnung finden. Ich bin glücklich über die großartige Kollegenschaft, welche ich in der Abteilung KB des Bereichs Kunststoffe als auch in anderen Bereichen des Instituts erfahren durfte. Dabei denke ich gerne an die Fahrradausflüge, Darmstädter Weinfeste und Rheingauer Weinlagenwanderungen sowie Boule-Feierabende mit Maike Bargmann, Dr. Alexander Knieper, Dr. Sascha Sedelmeier und Theresa Döll zurück. Ebenso sind mir die spaßigen Mittagessen mit Dr. Jan Spengler, Dr. Marcel Meub und den anderen der „alten“ Chemikerriege in dauerhaft schöner Erinnerung.

Zuletzt möchte ich Freunden und meiner Familie danken. Viele Freunde haben die Korrektur dieser Arbeit tatkräftig unterstützt, auszugsweise seien hierbei Dr. Svenja Wiechmann, Susanne Mohr, David del Valle Gois, Philipp Kappes und Bruno Pistacchio genannt. Meiner Familie, insbesondere meiner Nichte und meinen Neffen, die mich die letzten Jahre nur selten zu Gesicht bekamen, gelobe ich Besserung. Weiterhin gilt mein tiefer Dank meinem Großvater, der mir stets ein Vorbild sein wird. Er brachte uns Kindern schon früh bei, wie man das eigenartig mit Vokalen versetzte Wort „Ingenieur“ schreibt. Damit setzte er sicherlich gewollt die Grundlage für das etwa 13 Jahre später folgende Studium der Zwillinge, welches letztlich bei beiden im Dr.-Ing. mündete. Nicht nur Dank, sondern vor allem auch Hochachtung gilt meiner Mutter, die sehr viel Energie und Kapazitäten in uns drei Kinder investiert hat. Ohne Dich wäre diese Arbeit nie möglich gewesen.

Und ganz zu allerletzt verspreche ich meiner stets geduldigen und unterstützenden Lebensgefährtin Alica Maria Pohle, die mich nur als arbeitseifrigen Promovenden und Projektmanager kennt: es kann nur besser werden!

Mit meiner Promotion endet nun eine Generation von Doktoranden in dieser Abteilung und am Bereich Kunststoffe. Einige wenige Leser werden schmunzeln und verstehen, wenn ich schreibe: „Weidmann out!“.